Available online at www.sciencedirect.com
SCIENCE DIRECT®
Physics Reports 428 (2006) 259–390
PHYSICS REPORTS
www.elsevier.com/locate/physrep

Universality in few-body systems with large scattering length

Eric Braaten[a], H.-W. Hammer[b,c,*]

[a] *Department of Physics, The Ohio State University, Columbus, OH 43210, USA*
[b] *Institute for Nuclear Theory, University of Washington, Seattle, WA 98195, USA*
[c] *Helmholtz-Institut für Strahlen- und Kernphysik, Universität Bonn, 53115 Bonn, Germany*

Accepted 9 March 2006

editor: W. Weise

Abstract

Particles with short-range interactions and a large scattering length have universal low-energy properties that do not depend on the details of their structure or their interactions at short distances. In the 2-body sector, the universal properties are familiar and depend only on the scattering length a. In the 3-body sector for identical bosons, the universal properties include the existence of a sequence of shallow 3-body bound states called "Efimov states" and log-periodic dependence of scattering observables on the energy and the scattering length. The spectrum of Efimov states in the limit $a \to \pm\infty$ is characterized by an asymptotic discrete scaling symmetry that is the signature of renormalization group flow to a limit cycle. In this review, we present a thorough treatment of universality for the system of three identical bosons and we summarize the universal information that is currently available for other 3-body systems. Our basic tools are the hyperspherical formalism to provide qualitative insights, Efimov's radial laws for deriving the constraints from unitarity, and effective field theory for quantitative calculations. We also discuss topics on the frontiers of universality, including its extension to systems with four or more particles and the systematic calculation of deviations from universality.

PACS: 05.70.Jk; 31.15.Ja; 03.70.+k

Keywords: Universality; Large scattering length; Renormalization group; Three-body system; Efimov effect; Limit cycle; Discrete scale invariance; Hyperspherical formalism; Radial laws; Effective field theory

Contents

* Corresponding author. Helmholtz-Institut für Strahlen- und Kernphysik, Universität Bonn, 53115 Bonn, Germany. Tel.: +49 228 732373; fax: +49 228 733728.
E-mail addresses: braaten@mps.ohio-state.edu (E. Braaten), hammer@itkp.uni-bonn.de (H.-W. Hammer).

0370-1573/$ - see front matter © 2006 Published by Elsevier B.V.
doi:10.1016/j.physrep.2006.03.001

1. Introduction

The scattering of two particles with short-range interactions at sufficiently low energy is determined by their S-wave *scattering length*, which is commonly denoted by a. By *low energy*, we mean energy close to the scattering threshold for the two particles. The energy is sufficiently low if the de Broglie wavelengths of the particles are large compared to the range of the interaction. The scattering length a is important not only for 2-body systems, but also for few-body and many-body systems. If all the constituents of a few-body system have sufficiently low energy, its scattering properties are determined primarily by a. A many-body system has properties determined by a if its constituents have not only sufficiently low energies but also separations that are large compared to the range of the interaction. A classic example is the interaction energy per particle in the ground state of a sufficiently dilute homogeneous Bose–Einstein condensate:

$$\mathscr{E}/n \approx \frac{2\pi\hbar^2}{m} an, \tag{1}$$

where $\mathscr{E}$ and n are the energy density and number density, respectively. In the literature on Bose–Einstein condensates, properties of the many-body system that are determined by the scattering length are called *universal* [1]. The expression for the energy per particle in Eq. (1) is an example of a universal quantity. Corrections to such a quantity from the effective range and other details of the interaction are called *nonuniversal*. Universality in physics generally refers to situations in which systems that are very different at short distances have identical long-distance behavior. In the case of a dilute Bose–Einstein condensate, the constituents may have completely different internal structure and completely different interactions, but the many-body systems will have the same macroscopic behavior if their scattering lengths are the same.

Generically, the scattering length a is comparable in magnitude to the range r_0 of the interaction: $|a| \sim r_0$. Universality in the generic case is essentially a perturbative weak-coupling phenomenon. The scattering length a plays the role of a coupling constant. Universal properties can be calculated as expansions in the dimensionless combination $a\kappa$, where κ is an appropriate wave number variable. For the energy per particle in the dilute Bose–Einstein condensate, the wave number variable is the inverse of the coherence length: $\kappa = (16\pi an)^{1/2}$. The weak-coupling expansion parameter $a\kappa$ is therefore proportional to the diluteness parameter $(na^3)^{1/2}$. The order $(na^3)^{1/2}$ and $na^3 \ln(na^3)$ corrections to Eq. (1) are both universal [2]. Nonuniversal effects, in the form of sensitivity to 3-body physics, appear first in the order na^3 correction [3].

In exceptional cases, the scattering length can be much larger in magnitude than the range of the interaction: $|a| \gg r_0$. Such a scattering length necessarily requires a *fine-tuning*. There is some parameter characterizing the interactions that if tuned to a critical value would give a divergent scattering length $a \to \pm\infty$. Universality continues to be applicable in the case of a large scattering length, but it is a much richer phenomenon. We continue to define *low energy* by the condition that the de Broglie wavelengths of the constituents be large compared to r_0, but they can be comparable to $|a|$. Physical observables are called *universal* if they are insensitive to the range and other details of the short-range interaction. In the 2-body sector, the consequences of universality are simple but nontrivial. For example, in the case of identical bosons with $a > 0$, there is a 2-body bound state near the scattering threshold with binding energy

$$E_{\rm D} = \frac{\hbar^2}{ma^2}. \tag{2}$$

The corrections to this formula are parametrically small: they are suppressed by powers of r_0/a. Note the nonperturbative dependence of the binding energy on the interaction parameter a. This reflects the fact that universality in the case of a large scattering length is a nonperturbative strong-coupling phenomenon. It should therefore not be a complete surprise that counterintuitive effects can arise when there is a large scattering length.

A classic example of a system with a large scattering length is ^{4}He atoms, whose scattering length is more than a factor of 10 larger than the range of the interaction. More examples ranging from atomic physics to nuclear and particle physics are discussed in detail in Sections 2.3 and 2.4.

The first strong evidence for universality in the 3-body system was the discovery by Vitaly Efimov in 1970 of the *Efimov effect* [4],[1] a remarkable feature of the 3-body spectrum for identical bosons with a short-range interaction and a large scattering length a. In the *resonant limit* $a \to \pm\infty$, there is a 2-body bound state exactly at the 2-body

[1] Some early indications of universality were already observed in Refs. [5,6].

scattering threshold $E = 0$. Remarkably, there are also infinitely many, arbitrarily-shallow 3-body bound states with binding energies $E_{\rm T}^{(n)}$ that have an accumulation point at $E = 0$. As the threshold is approached, the ratio of the binding energies of successive states approaches a universal constant:

$$E_{\rm T}^{(n+1)}/E_{\rm T}^{(n)} \longrightarrow 1/515.03 \quad \text{as } n \to +\infty \text{ with } a = \pm\infty. \tag{3}$$

The universal ratio in Eq. (3) is independent of the mass or structure of the identical particles and independent of the form of their short-range interaction. The Efimov effect is not unique to the system of three identical bosons. It can also occur in other 3-body systems if at least two of the three pairs have a large S-wave scattering length. If the Efimov effect occurs, there are infinitely many, arbitrarily-shallow 3-body bound states in the resonant limit $a = \pm\infty$. Their spectrum is characterized by an asymptotic *discrete scaling symmetry*, although the numerical value of the discrete scaling factor may differ from the value in Eq. (3).

For systems in which the Efimov effect occurs, it is convenient to relax the traditional definition of universal which allows dependence on the scattering length only. In the resonant limit $a \to \pm\infty$, the scattering length no longer provides a scale. However, the discrete Efimov spectrum in Eq. (3) implies the existence of a scale. For example, one can define a wave number κ_* by expressing the asymptotic spectrum in the form

$$E_{\rm T}^{(n)} \longrightarrow \left(\frac{1}{515.03}\right)^{n-n_*} \frac{\hbar^2\kappa_*^2}{m} \quad \text{as } n \to +\infty \text{ with } a = \pm\infty \tag{4}$$

for some integer n_*. If the scattering length is large but finite, the spectrum of Efimov states will necessarily depend on both a and the 3-body parameter κ_*. Thus although the existence of the Efimov states is universal in the traditional sense, their binding energies are not. The dependence of few-body observables on κ_* is qualitatively different from the dependence on typical nonuniversal parameters such as the effective range. As $a \to \pm\infty$, the dependence on typical nonuniversal parameters decreases as positive powers of r_0/a, where r_0 is the range of the interaction. In contrast, the dependence on κ_* not only does not disappear in the resonant limit, but it takes a particularly remarkable form. Few-body observables are log-periodic functions of κ_*, i.e. the dependence on κ_* enters only through trigonometric functions of $\ln(\kappa_*)$. For example, the asymptotic spectrum in Eq. (4) consists of the zeroes of a log-periodic function:

$$\sin(\tfrac{1}{2}s_0 \ln[mE_{\rm T}/(\hbar^2\kappa_*^2)]) = 0, \tag{5}$$

where $s_0 \approx 1.00624$. Instead of regarding κ_* as a nonuniversal parameter, it is more appropriate to regard it as a parameter that labels a continuous family of universality classes. Thus for systems in which the Efimov effect occurs, it is convenient to relax the definition of universal to allow dependence not only on the scattering length a but also on the 3-body parameter associated with the Efimov spectrum. This definition reduces to the standard one in the 2-body system, because the 3-body parameter cannot affect 2-body observables. It also reduces to the standard definition for dilute systems such as the weakly-interacting Bose gas, because 3-body effects are suppressed by at least $na^3 \ll 1$ in a dilute system. We will refer to this extended universality simply as "universality" in the remainder of the paper.

If the problem of identical bosons with large scattering length is formulated in a *renormalization group* framework, the remarkable behavior of the system of three identical bosons in the resonant limit is associated with a renormalization group *limit cycle*. The 3-body parameter associated with the Efimov spectrum can be regarded as parameterizing the position along the limit cycle. The asymptotic behavior of the spectrum in Eq. (3) reflects a *discrete scaling symmetry* that is characteristic of a renormalization group limit cycle. In contrast to renormalization group *fixed points*, which are ubiquitous in condensed matter physics and in high energy and nuclear physics, few physical applications of renormalization group limit cycles have been found. Consequently, the renormalization group theory associated with limit cycles is largely undeveloped. The development of such a theory could prove to be very helpful for extending universality into a systematically improvable calculational framework.

Since universality has such remarkable consequences in the 2-body and 3-body sectors, we expect it to also have important implications in the N-body sector with $N \geqslant 4$. This is still mostly unexplored territory. Universality may also have important applications to the many-body problem. These applications are particularly topical, because of the rapid pace of experimental developments in the study of ultracold atoms. By cooling an atom with a large scattering length to sufficiently low temperature, one can reach a regime where universality is applicable. Fascinating many-body phenomena can occur within this regime, including Bose–Einstein condensation in the case of bosonic atoms and

superfluidity in the case of fermionic atoms. Universality has particularly exciting applications to these many-body phenomena, but they are beyond the scope of this review.

Most of this review is focused on the problem of identical bosons, because this is the system for which the consequences of universality have been most thoroughly explored. Identical bosons have the advantage of simplicity while still exhibiting the nontrivial realization of universality associated with the Efimov effect. However, we also summarize the universal results that are currently known for other few-body systems, including ones that include identical fermions. We hope this review will stimulate the further development of the universality approach to such systems.

The idea of universality in systems with a large scattering length has its roots in low-energy nuclear physics and has many interesting applications in particle and nuclear physics. Most of these applications are to systems with fortuitously large scattering lengths that arise from some accidental fine-tuning. Universality also has many interesting applications in atomic and molecular physics. There are some atoms that have fortuitously large scattering lengths, but there are also atoms whose scattering lengths can be tuned experimentally to arbitrarily large values. This makes universality particularly important in the field of atomic and molecular physics. We will therefore develop the ideas of universality using the language of atomic physics: "atom" for a particle, "dimer" for a 2-body bound state, etc.

We begin by introducing some basic scattering concepts in Section 2. We introduce the *natural low-energy length scale* and use it to define *large scattering length*. In Section 3, we describe the Efimov effect and introduce some renormalization group concepts that are relevant to the few-body problem with large scattering length. We define the *scaling limit* in which universality becomes exact and the *resonant limit* in which $a \to \pm\infty$. We point out that these limits are associated with a *renormalization group limit cycle* that is characterized by a *discrete scaling symmetry*. The simple and familiar features of universality in the problem of two identical bosons are described in Section 4. We point out that there is a trivial *continuous scaling symmetry* in the scaling limit and we calculate the leading *scaling violations* which are determined by the effective range.

In Section 5, we develop the hyperspherical formalism for three identical bosons. We use this formalism to deduce some properties of Efimov states in the resonant limit and near the atom–dimer threshold. In Section 6, we describe the most important features of universality for three identical bosons in the scaling limit. Logarithmic scaling violations reduce the continuous scaling symmetry to a discrete scaling symmetry. They also imply that low-energy 3-body observables depend not only on a but also on an additional scaling-violation parameter. We then present explicit results for 3-body observables, including the binding energies of Efimov states, atom–dimer scattering, 3-body recombination, and 3-atom scattering. We illustrate these results by applying them to the case of helium atoms, which have a large scattering length. We use universal scaling curves to illustrate the nontrivial realization of universality in the 3-body sector for identical bosons. In Section 7, we describe how the predictions from universality are modified by effects from deep 2-body bound states.

In Section 8, we describe a powerful method called effective field theory for calculating the predictions of universality. Using an effective field theory that describes identical bosons in the scaling limit, we derive a generalization of the Skorniakov–Ter-Martirosian (STM) integral equation and use it to calculate the most important low-energy 3-body observables. We also show that the renormalization of the effective field theory involves an ultraviolet limit cycle.

Sections 4–8 are focused exclusively on the problem of identical bosons. In Section 9, we discuss universality for other 3-body systems. We summarize what is known about the generalizations to distinguishable particles, fermions, unequal scattering lengths, and unequal masses. In Section 10, we discuss some of the most important frontiers of universality in few-body systems. They include power-law scaling violations such as those associated with the effective range, the N-body problem with $N \geqslant 4$, unnaturally large low-energy constants in other angular momentum channels such as P-waves, and the approach to universality in scattering models.

Some of the sections of this review could be omitted by the first-time reader. He or she should begin by reading Section 2 on *Scattering Concepts* and Sections 3.1 and 3.2 on *Renormalization Group Concepts*. The first-time reader should then read Section 4 on *Universality for Two Identical Bosons*, Sections 5.1, 5.5, and 5.6 on the *Hyperspherical Formalism*, and Section 6 on *Universality for Three Identical Bosons*. The reader who is primarily interested in systems for which there are no tightly-bound 2-body bound states could skip Section 7 on *Effects of Deep Two-body Bound States*. The first-time reader could also skip Section 8 on *Effective Field Theory*. A first pass through the review could be completed by reading Section 9 on *Universality in Other Three-body Systems*. We hope this will whet the reader's appetite for a more thorough reading of all the sections.

2. Scattering concepts

In this section, we introduce the concept of the *natural low-energy length scale* and use it to define a *large scattering length*. We also give examples of 2-body systems with large scattering lengths.

2.1. Scattering length

In order to introduce some basic concepts associated with universality in systems with a large scattering length, we begin with a brief review of scattering theory [7,8]. More thorough reviews with a focus on ultracold atoms can be found in Refs. [9,10].

The most important parameter governing the interactions of low-energy atoms is the 2-body S-wave scattering length a, which we will refer to simply as the *scattering length*. It can be defined in terms of the partial wave expansion for the scattering amplitude. Consider atoms with mass m that interact through a short-range potential. The elastic scattering of two such atoms with opposite momenta $\pm\hbar\boldsymbol{k}$ and total kinetic energy $E=\hbar^2k^2/m$ can be described by a stationary wave function $\psi(\boldsymbol{r})$ that depends on the separation vector $\boldsymbol{r}$ of the two atoms. Its asymptotic behavior as $r\to\infty$ is the sum of a plane wave and an outgoing spherical wave:

$$\psi(\boldsymbol{r}) = \mathrm{e}^{\mathrm{i}kz} + f_k(\theta)\frac{\mathrm{e}^{\mathrm{i}kr}}{r}. \tag{6}$$

This equation defines the *scattering amplitude* $f_k(\theta)$, which depends on the scattering angle θ and the wave number k. The *differential cross section* $\mathrm{d}\sigma/\mathrm{d}\Omega$ can be expressed in the form

$$\frac{\mathrm{d}\sigma}{\mathrm{d}\Omega} = |f_k(\theta) \pm f_k(\pi-\theta)|^2, \tag{7}$$

where the plus (minus) sign holds for identical bosons (fermions). If the two atoms are distinguishable, the term $\pm f_k(\pi-\theta)$ should be omitted. The elastic cross section $\sigma(E)$ is obtained by integrating over only $\frac{1}{2}$ the 4π solid angle if the two atoms are identical bosons or identical fermions and over the entire 4π solid angle if they are distinguishable.

In the low-energy limit, the scattering becomes isotropic. The scattering length a can be defined by the low-energy limit of the scattering amplitude:

$$f_k(\theta) \longrightarrow -a \quad \text{as } k\to 0. \tag{8}$$

The absolute value of the scattering length can be determined by measuring the low-energy limit of the elastic cross section:

$$\sigma(E) \longrightarrow 8\pi a^2 \quad \text{as } E\to 0. \tag{9}$$

If the atoms are distinguishable, the prefactor is 4π instead of 8π. If there are inelastic channels at $E=0$, the scattering length is complex-valued and a^2 on the right side of Eq. (9) is replaced by $|a|^2$. Determining the sign of a is more complicated, because it requires measuring an interference effect.

The *partial-wave expansion* resolves the scattering amplitude $f_k(\theta)$ into contributions from definite angular momentum quantum number L by expanding it in terms of Legendre polynomials of $\cos\theta$:

$$f_k(\theta) = \frac{1}{k}\sum_{L=0}^{\infty}(2L+1)c_L(k)P_L(\cos\theta). \tag{10}$$

If the atoms are identical bosons (fermions), only even (odd) values of L contribute to the differential cross section in Eq. (7). The coefficients in Eq. (10) are constrained by unitarity to satisfy $|c_L(k)|\leqslant 1$. The unitarity constraints can be taken into account automatically by expressing the coefficients in terms of *phase shifts* $\delta_L(k)$:

$$c_L(k) = \mathrm{e}^{\mathrm{i}\delta_L(k)}\sin\delta_L(k). \tag{11}$$

The expression for the scattering amplitude can be written as

$$f_k(\theta) = \sum_{L=0}^{\infty}\frac{2L+1}{k\cot\delta_L(k) - \mathrm{i}k}P_L(\cos\theta). \tag{12}$$

If there are inelastic channels, the phase shifts can be complex-valued with positive imaginary parts. If there are no inelastic 2-body channels, the phase shifts $\delta_L(k)$ are real-valued. The expression for the cross section integrated over the scattering angle is then

$$\sigma(E) = \frac{8\pi}{k^2} \sum_{L=0}^{\infty} (2L+1) \sin^2 \delta_L(k), \tag{13}$$

where $E = \hbar^2 k^2/m$ is the total kinetic energy of the two atoms. If the atoms are identical bosons (fermions), the sum is only over even (odd) values of L. If the atoms are distinguishable, the prefactor in Eq. (13) is 4π instead of 8π.

The *optical theorem* relates the total cross section to the forward-scattering limit ($\theta \to 0$) of the scattering amplitude:

$$\sigma^{(\text{total})}(E) = \frac{8\pi}{k} \operatorname{Im} f_k(\theta = 0). \tag{14}$$

If the atoms are distinguishable, the prefactor is 4π instead of 8π. If there are no inelastic 2-body channels, the total cross section on the left side of Eq. (14) is the elastic cross section in Eq. (13). If there are inelastic 2-body channels, the total cross section is the sum of the elastic and inelastic cross sections.

If the atoms interact through a short-range 2-body potential, then the phase shift $\delta_L(k)$ approaches zero like k^{2L+1} in the low-energy limit $k \to 0$. Thus S-wave ($L = 0$) scattering dominates in the low-energy limit unless the atoms are identical fermions, in which case P-wave ($L = 1$) scattering dominates. At sufficiently low energies, the S-wave phase shift $\delta_0(k)$ can be expanded in powers of k^2 [11]. The expansion is called the *effective-range expansion* and is conventionally expressed in the form

$$k \cot \delta_0(k) = -1/a + \tfrac{1}{2} r_s k^2 - \tfrac{1}{4} P_s k^4 + \cdots. \tag{15}$$

The first few terms define the scattering length[2] a, the S-wave *effective range* r_s, and the S-wave *shape parameter* P_s.

If the 2-body potential $V(r)$ has a long-range tail that falls off like $1/r^n$ with $n > 1$, the higher partial waves are not as strongly suppressed at low energy. For $L > (n-2)/2$, the phase shifts $\delta_L(k)$ approach 0 like k^{n-1}. Thus in the low-energy expansion of the scattering amplitude, all partial waves contribute at order k^{n-2} and beyond. For example, the interatomic potential between atoms in their ground state has a van der Waals tail that falls off like $1/r^6$. The phase shifts for $L = 0$, 1, and 2 approach 0 like k, k^3, and k^5, respectively, just as in the case of a short-range potential. However, all the phase shifts $\delta_L(k)$ for $L \geqslant 2$ approach 0 like k^5. Thus the low-energy expansion of the scattering amplitude receives contributions from all partial waves beginning at order k^4 [12].

If the potential has an attractive region that is sufficiently deep, the two atoms can form bound states. The binding energies E_2 for 2-body bound states are determined by the poles of the scattering amplitude in the upper half-plane of the complex variable k. It is convenient to define the binding wave number κ by

$$E_2 = \hbar^2 \kappa^2/m. \tag{16}$$

For S-wave bound states, the binding wave number κ is a positive real-valued solution to the equation

$$\mathrm{i}\kappa \cot \delta_0(\mathrm{i}\kappa) + \kappa = 0. \tag{17}$$

If the potential is sufficiently weak, the scattering amplitude is given by the Born approximation:

$$f_k(\theta) \approx -\frac{m}{4\pi\hbar^2} \int \mathrm{d}^3 r \mathrm{e}^{-\mathrm{i}\boldsymbol{q}\cdot\boldsymbol{r}} V(r). \tag{18}$$

The integral is a function of $|\mathbf{q}| = 2k \sin(\theta/2)$. The scattering length is linear in the potential:

$$a \approx \frac{m}{4\pi\hbar^2} \int \mathrm{d}^3 r\, V(r). \tag{19}$$

[2] We caution the reader that the opposite sign convention for the scattering length is used in some of the literature.

A simple condition for the applicability of the Born approximation to scattering with wave number k is

$$\frac{m}{4\pi\hbar^2}\left|\int \mathrm{d}^3 r \frac{\mathrm{e}^{-\mathrm{i}kr}}{r} V(r)\right| \ll 1. \tag{20}$$

In the case of a large scattering length, this condition is not satisfied and the dependence of a on $V(r)$ is highly nonlinear.

2.2. Natural low-energy length scale

At sufficiently low energies, atoms behave like point particles with short-range interactions. The length scale that governs the quantum behavior of the center-of-mass coordinate of an atom is the de Broglie wavelength $\lambda = 2\pi\hbar/p$, where p is the momentum of the atom. If the relative momentum p of two atoms is sufficiently small, their de Broglie wavelengths are larger than the spacial extent of the atoms and they are unable to resolve each other's internal structure, which is provided by their electron clouds. Their interactions will therefore be indistinguishable from those of point particles.

If the atoms interact through a short-range potential with range r_0 and if the relative momentum of the two atoms satisfies $p \ll \hbar/r_0$, then their de Broglie wavelengths prevent them from resolving the structure of the potential. In this case, the effects of the interactions would be indistinguishable from those of a local potential consisting only of contact terms proportional to the delta function $\delta^3(\boldsymbol{r} - \boldsymbol{r}')$ and derivatives of the delta function. The effects of the interaction could be reproduced with higher and higher accuracy by including higher and higher derivatives of the delta function. Equivalently, the scattering amplitude could be approximated by a truncated expansion in powers of the relative momentum. Approximations with higher and higher accuracy could be obtained by including more and more terms in the expansion.

For real atoms, the potential is not quite short-range. The interatomic potential $V(r)$ between two neutral atoms in their ground states consists of a short range potential and a long-range tail provided by the van der Waals interaction. The short-range part of the potential $V(r)$ is essentially the Born–Oppenheimer potential, which is the ground-state energy of the electron clouds when the nuclei of the atoms have a fixed separation r. For separations much larger than the size of the electron cloud of an individual atom, the interaction energy is dominated by the van der Waals interaction, which arises from the polarizability of the electron clouds. The Coulomb interaction between the polarized electron clouds produces a power-law potential that falls off asymptotically like $1/r^6$:[3]

$$V(r) \longrightarrow -\frac{C_6}{r^6} \quad \text{as } r \to \infty. \tag{21}$$

At sufficiently low energy, the interactions between atoms are dominated by the van der Waals interaction. The natural length scale associated with these interactions can be determined by assuming that the wave function has only one important length scale ℓ_{vdW} and requiring a balance between the typical kinetic and potential energies:

$$\frac{\hbar^2}{mr^2} \sim \frac{C_6}{r^6} \quad \text{at } r \sim \ell_{\mathrm{vdW}}. \tag{22}$$

The resulting length scale is called the van der Waals length:

$$\ell_{\mathrm{vdW}} = (mC_6/\hbar^2)^{1/4}. \tag{23}$$

For real atoms whose potential has a long-range van der Waals tail, the interactions can be described accurately by a local potential if their relative momentum p satisfies $p \ll \hbar/\ell_{\mathrm{vdW}}$, where ℓ_{vdW} is the van der Waals length scale given in Eq. (23). However, there is a limit to the accuracy of such a description. The scattering amplitude can be expanded in powers of the relative momentum $\boldsymbol{p}$, but at 4th order the dependence on $\boldsymbol{p}$ becomes nonpolynomial. The analogous statement in coordinate space is that for $p \ll \hbar/\ell_{\mathrm{vdW}}$, the interactions can be approximated by a local potential

[3] Retardation effects ultimately change the asymptotic power-law behavior to $1/r^7$, but this complication is not essential for our purposes.

proportional to $\delta^3(\boldsymbol{r}-\boldsymbol{r}')$ and more accurately by a potential with two terms proportional to $\delta^3(\boldsymbol{r}-\boldsymbol{r}')$ and $\nabla^2\delta^3(\boldsymbol{r}-\boldsymbol{r}')$. However, any further improvement in accuracy must take into account the nonlocal behavior of the potential. The relative errors cannot be decreased below $(p\ell_{\rm vdW}/\hbar)^4$ without taking into account the van der Waals tail of the potential explicitly. This limit will not be of much concern to us, because our primary goal will be calculations of the universal properties of low-energy atoms up to relative errors of order $p\ell_{\rm vdW}/\hbar$.

In order to define *large scattering length*, we introduce the concept of the *natural low-energy length scale* ℓ associated with an interaction potential. It is sometimes referred to as the *characteristic radius of interaction* and often denoted r_0. The natural low-energy length scale sets the natural scale for the coefficients in the low-energy expansion of the scattering amplitude $f_k(\theta)$. By dimensional analysis, the coefficient of a term proportional to k^n can be expressed as ℓ^{n+1} with a dimensionless coefficient. There is no general constraint on the magnitude of these coefficients. However, for a generic potential, one usually finds that there is a length scale ℓ such that the coefficients all have magnitudes of order 1. The absolute value of any specific coefficient can be orders of magnitude larger than 1, but this typically requires the *fine-tuning* of parameters in the potential, such as its depth or its range. We define the natural low-energy length scale ℓ by the condition that most of the coefficients of $\ell^{n+1}k^n$ in the low-momentum expansion of the scattering amplitude have magnitudes close to 1. If the magnitude $|a|$ of the scattering length is comparable to ℓ, we say that a has a *natural size*. If $|a|\gg\ell$, we call the scattering length *unnaturally large*, or just *large* to be concise. As mentioned above, this case typically requires the fine-tuning of some parameter in the potential $V(r)$. The natural low-energy length scale sets the natural scale for the other coefficients in the low-energy expansion of the scattering amplitude, such as the effective range r_s defined by Eq. (15). Even if a is large, we should expect r_s to have a natural magnitude of order ℓ. For a and r_s to both be unnaturally large would require the simultaneous fine-tuning of two parameters in the potential.

The natural low-energy length scale ℓ also sets the natural scale for the binding energies of the 2-body bound states closest to threshold. The binding energy of the shallowest bound state is expected to be proportional to $\hbar^2/m\ell^2$, with a coefficient whose magnitude is roughly one. The coefficient can be orders of magnitude smaller, but this again requires the fine-tuning of a parameter in the potential. This is precisely the same fine-tuning required to get a large positive scattering length $a\gg\ell$. This can be seen by inserting the effective range expansion in Eq. (15) into the bound-state equation in Eq. (17). If $a\gg\ell$ and if all higher coefficients in the effective-range expansion have natural sizes set by ℓ, then the bound-state equation has the approximate solution in Eq. (2). Thus a large positive scattering length can be obtained by tuning the binding energy to a value much smaller than $\hbar^2/m\ell^2$.

If a short-range potential $V(r)$ is sufficiently weak, the Born approximation in Eq. (19) is applicable and the scattering length scales like $(mV_0/\hbar^2)\ell^3$, where V_0 is the depth of the potential. On the other hand, if the potential is very strong and if there is a well-behaved limit as $V_0\to\infty$, then dimensional analysis implies that a should scale like ℓ. If $V(r)$ is completely repulsive, the scattering length a is necessarily positive and always comparable to ℓ. If $V(r)$ has regions that are attractive, the scattering length a can be positive or negative. In general, its value can be anywhere between $-\infty$ and $+\infty$, but its absolute value $|a|$ is most likely to be of order ℓ. This vague statement can be made into a more precise probabilistic statement by considering a 1-parameter deformation $V_\lambda(r)$ that allows the number of bound states in the potential to be changed, such as $V_\lambda(r)=\lambda V(r)$. The corresponding scattering length a_λ depends on λ. As λ increases from its initial value 1, the depth of the potential increases and a_λ decreases. It eventually decreases to $-\infty$ and then jumps discontinuously to $+\infty$ at the critical value λ_c at which a virtual state drops below threshold to become an additional bound state. If we continue to increase λ, a_λ will ultimately return to its original value a at some value λ_1. A uniform probability distribution for λ in the range $1<\lambda<\lambda_1$ defines a probability distribution for the scattering length a_λ. Most of the probability is concentrated in regions where $|a|$ is comparable to ℓ. The scattering length is more than an order of magnitude larger only if λ is in a narrow interval around λ_c that has a very small probability. Thus a large scattering length requires a fine-tuning of the parameter λ to the region near λ_c. In the absence of any fine-tuning, one should expect $|a|$ to be comparable to ℓ.

For an attractive short-range potential, the natural low-energy length scale ℓ is simply the *range* itself, i.e., the length beyond which the potential falls rapidly to zero. To illustrate the point that the range is the natural low-energy length scale, we consider an attractive square well with range r_0 and depth V_0 as shown in Fig. 1:

$$V(r) = -V_0, \quad r<r_0, \tag{24a}$$

$$= 0, \quad r>r_0. \tag{24b}$$

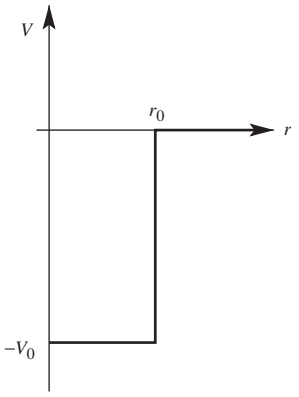

Fig. 1. Attractive square well potential with range r_0 and depth V_0.

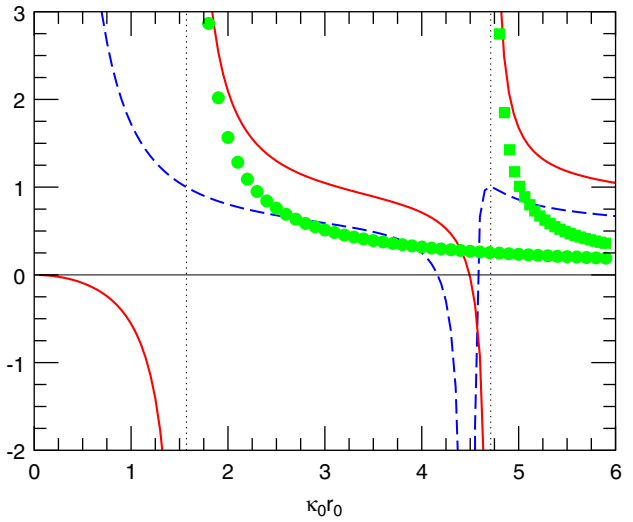

Fig. 2. Two-body observables for the attractive square-well potential. The scattering length a (solid curve), the effective range r_s (dashed curve), and the inverse binding wave numbers $(mE_2/\hbar^2)^{-1/2}$ for the first two bound states (dots and squares) in units of r_0 are shown as functions of $\kappa_0 r_0$. The vertical dotted lines are the critical values where a diverges.

The natural low-energy length scale is $\ell \approx r_0$. We will treat the depth V_0 as a parameter that can be varied to adjust the scattering length a. The scattering length and effective range are

$$a = r_0 \left[1 - \frac{\tan(\kappa_0 r_0)}{\kappa_0 r_0}\right], \tag{25a}$$

$$r_s = r_0 \left[1 - \frac{r_0^2}{3a^2} - \frac{1}{\kappa_0^2 a r_0}\right], \tag{25b}$$

where $\kappa_0 = (mV_0/\hbar^2)^{1/2}$. The binding energies $E_2 > 0$ satisfy the transcendental equation

$$(\kappa_0^2 - \kappa^2)^{1/2} \cot[(\kappa_0^2 - \kappa^2)^{1/2}] = -\kappa, \tag{26}$$

where $\kappa = (mE_2/\hbar^2)^{1/2}$ is the binding wave number. In Fig. 2, we show the scattering length a, the effective range r_s, and the inverse binding wave number $1/\kappa$ for the first two bound states as functions of the dimensionless

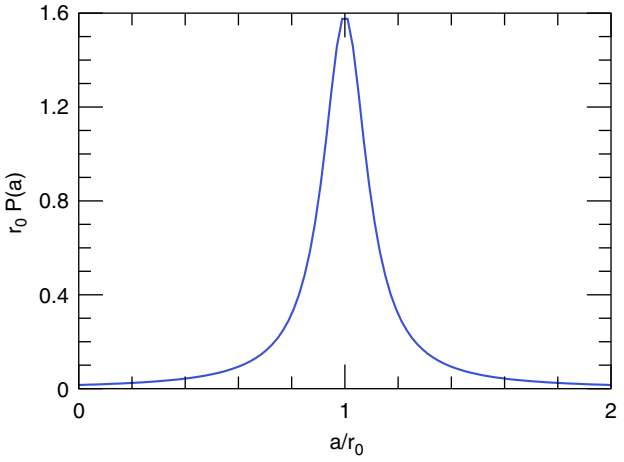

Fig. 3. Probability distribution for the scattering length a for the attractive square-well potential with $\kappa_0 r_0 = 10$.

variable $\kappa_0 r_0$. For most values of $\kappa_0 r_0$, the variables a, r_s, and $1/\kappa$ all have magnitudes of order r_0. The scattering length is unnaturally large only in narrow intervals of $\kappa_0 r_0$ near the critical values $\frac{1}{2}\pi$, $\frac{3}{2}\pi$, $\frac{5}{2}\pi$, ..., which are shown as vertical dotted lines in Fig. 2. The critical values can be reached by tuning either the depth V_0 or the range r_0 of the potential. Wherever a is unnaturally large and positive, there is a bound state with unnaturally small binding energy given approximately by Eq. (2). Note that the effective range has the natural value $r_s = r_0$ at the critical values of $\kappa_0 r_0$ where a diverges. The effective range r_s is unnaturally large only near those values of $\kappa_0 r_0$ where a vanishes, but $a^2 r_s$ has a natural value at those points.

If $\kappa_0 r_0 \gg 1$, we can use the expression in Eq. (25a) to make a simple probabilistic statement about the scattering length. A probability distribution for V_0 or r_0 will generate a probability distribution for a. If $\kappa_0 r_0 \gg \pi$, a small fractional variation in V_0 or r_0 can generate a variation in the argument of $\tan(\kappa_0 r_0)$ that extends over several periods. Any probability distribution for V_0 or r_0 that is approximately constant over intervals of $\kappa_0 r_0$ of length π will give an approximately uniform distribution for $\kappa_0 r_0$ mod π. The resulting probability distribution for a is

$$P(a)\mathrm{d}a = \frac{1}{(a - r_0)^2 + 1/\kappa_0^2} \frac{\mathrm{d}a}{\pi \kappa_0}. \tag{27}$$

The distribution is shown in Fig. 3. It peaks at $a = r_0$ and its full width at half maximum is $2/\kappa_0$. Thus the probability is concentrated near $a = r_0$ and it is sharply peaked if $\kappa_0 r_0 \gg 1$.

For atoms interacting through a short-range potential with a $1/r^6$ van der Waals tail as in Eq. (21), the natural low-energy length scale is the van der Waals length ℓ_{vdW} given in Eq. (23). To illustrate the point that ℓ_{vdW} is the natural low-energy length scale, we consider a potential that has a hard core of radius r_0 and decreases like $-C_6/r^6$ for $r > r_0$ as illustrated in Fig. 4:

$$V(r) = +\infty, \quad r < r_0, \tag{28a}$$

$$= -\frac{C_6}{r^6}, \quad r > r_0. \tag{28b}$$

The scattering length and the effective range can be calculated analytically [13,14]:

$$a = \frac{\Gamma^2(\frac{3}{4})}{\pi}(1 - \tan \Phi)\ell_{\mathrm{vdW}}, \tag{29a}$$

$$r_s = \frac{2\pi}{3\Gamma^2(\frac{3}{4})} \frac{1 + \tan^2 \Phi}{(1 - \tan \Phi)^2} \ell_{\mathrm{vdW}}, \tag{29b}$$

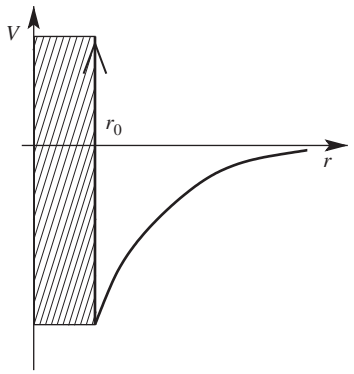

Fig. 4. Van der Waals potential with a hard-core radius r_0.

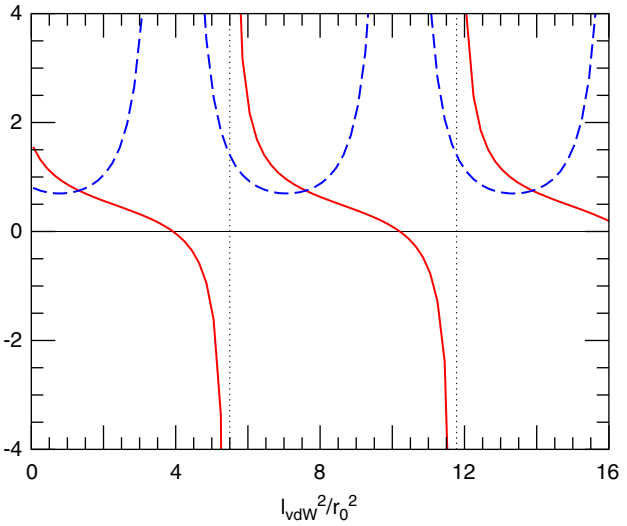

Fig. 5. Two-body scattering observables for the hard-core van der Waals potential. The scattering length a (solid curve) and the effective range r_s (dashed curve) in units of $\ell_{\rm vdW}$ are shown as functions of $\ell_{\rm vdW}^2/r_0^2$. The vertical dotted lines are the critical values where a diverges.

where the angle Φ is

$$\Phi = \frac{\ell_{\rm vdW}^2}{2r_0^2} - \frac{3\pi}{8}. \tag{30}$$

In Fig. 5, we show the scattering length a and the effective range r_s as functions of the dimensionless variable $\ell_{\rm vdW}/r_0$. For most values of $\ell_{\rm vdW}^2/r_0^2$, the scattering variables a and r_s have natural magnitudes of order $\ell_{\rm vdW}$. The scattering length is unnaturally large only in narrow intervals of $\ell_{\rm vdW}^2/r_0^2$ near the critical values $\frac{7}{4}\pi$, $\frac{15}{4}\pi$, $\frac{23}{4}\pi, \ldots$, which are shown as vertical dotted lines in Fig. 5. The critical values can be reached by fine-tuning either the strength C_6 of the long-distance potential or the hard-core radius r_0. Note that the effective range has the natural value $r_s = 1.39\ \ell_{\rm vdW}$ at the critical values of $\ell_{\rm vdW}/r_0$ where a diverges. The effective range r_s is unnaturally large only near the values of $\ell_{\rm vdW}/r_0$ at which a vanishes, but $a^2 r_s$ has a natural value at those points.

If $\ell_{\rm vdW}^2/r_0^2 \gg 2\pi$, we can use the expression in Eq. (29a) to make a simple probabilistic statement about the scattering length. A probability distribution for C_6 or r_0 will generate a probability distribution for a. If $\ell_{\rm vdW}^2/r_0^2 \gg 2\pi$, a small fractional variation in C_6 or r_0 will generate a variation in the argument of $\tan\Phi$ that extends over several periods. Any probability distribution for C_6 or r_0 that is approximately constant over intervals of $\ell_{\rm vdW}^2/r_0^2$ of length 2π will give an

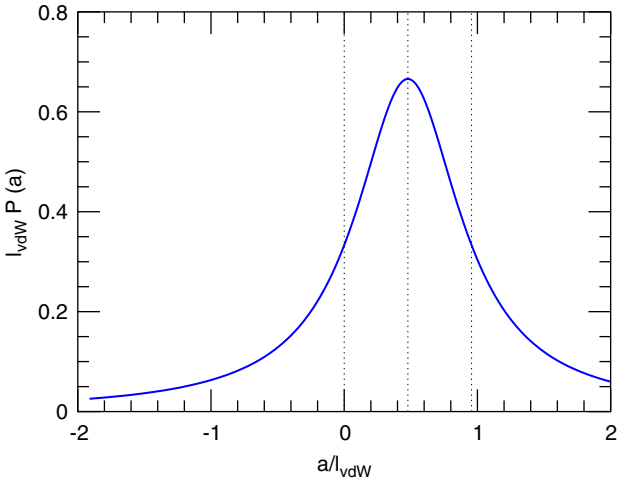

Fig. 6. Probability distribution for the scattering length a for potentials with a van der Waals tail. The vertical dotted lines separate the horizontal axis into four regions, each with probability 1/4.

approximately uniform distribution for Φ mod π. The resulting probability distribution for a is

$$P(a)\,\mathrm{d}a = \frac{1}{(a - c\ell_{\mathrm{vdW}})^2 + c^2\ell_{\mathrm{vdW}}^2}\,\frac{c\ell_{\mathrm{vdW}}\,\mathrm{d}a}{\pi}, \tag{31}$$

where $c = \Gamma^2(\frac{3}{4})/\pi \approx 0.478$. The distribution is shown in Fig. 6. It peaks at $a = c\,\ell_{\mathrm{vdW}}$ and its full width at half maximum is $2c\,\ell_{\mathrm{vdW}}$. Each of the four intervals $(-\infty, 0)$, $(0, c\,\ell_{\mathrm{vdW}})$, $(c\,\ell_{\mathrm{vdW}}, 2c\,\ell_{\mathrm{vdW}})$, and $(2c\,\ell_{\mathrm{vdW}}, +\infty)$ has probability 1/4. Note that there is a significant probability for the scattering length to be negative, but it is 3 times more likely to be positive.

2.3. Atoms with large scattering length

We have defined *large scattering length* by the condition $|a| \gg \ell$, where ℓ is the natural low-energy length scale. As illustrated in Section 2.2, a large scattering length requires the *fine-tuning* of some interaction parameter. This fine-tuning can be due to fortuitous values of the fundamental constants of nature, in which case we call it *accidental fine-tuning*, or it can be due to the adjustment of parameters that are under experimental control, in which case we call it *experimental fine-tuning*. We will give examples of atoms with both kinds of fine-tunings.

The simplest example of an atom with a large positive scattering length is the helium atom ^{4}He. The coefficient C_6 in the van der Waals potential for He is calculated in Ref. [15]. The van der Waals length defined by Eq. (23) is $\ell_{\mathrm{vdW}} \approx 10.2\,a_0$, where a_0 is the Bohr radius:

$$a_0 = 5.29177 \times 10^{-11}\,\mathrm{m}. \tag{32}$$

The equilibrium radius defined by the minimum of the interatomic potential is $r_{\mathrm{eq}} = 5.6\,a_0$ [16]. Since ℓ_{vdW} is much larger than r_{eq}, the natural low-energy length scale is ℓ_{vdW}. A pair of ^{4}He atoms has a single 2-body bound state or *dimer*, and it is very weakly bound. From a measurement of the size of the ^{4}He dimer, the scattering length has been determined to be $a = (197^{+15}_{-34})\,a_0$ [17]. This is much larger than the van der Waals length. More precise values of the scattering length can be calculated from model potentials for helium atoms. For example, the LM2M2 [18] and TTY [19] potentials have a large scattering length $a = 189\,a_0$ but a natural effective range $r_s = 14\,a_0$. The binding energy of the dimer is $E_2 = 1.31\,\mathrm{mK}$, which is much smaller than the natural low-energy scale $\hbar^2/m\ell_{\mathrm{vdW}}^2 \approx 400\,\mathrm{mK}$. We have expressed these energies in terms of the temperature unit mK. The conversion factors to electron volts and to the natural atomic energy unit $\hbar^2/m_e a_0^2$ are

$$1\,\mathrm{mK} = 8.61734 \times 10^{-8}\,\mathrm{eV} = 3.16682 \times 10^{-9}\,\hbar^2/m_e a_0^2. \tag{33}$$

Table 1
Scattering lengths and length scales for alkali atoms in units of a_0: the equilibrium radius $r_{\rm eq}$, the van der Waals length $\ell_{\rm vdW}$, the spin-singlet scattering length a_s, and the spin-triplet scattering length a_t

Atom	$r_{\rm eq}$	$\ell_{\rm vdW}$	a_s	a_t	Ref.
^{1}H	1.4	10.5	+0.3	+1.3	[21]
^{2}H	1.4	12.4	+13	−6.9	[21]
^{3}H	1.4	13.7	+35	−82	[20]
^{6}Li	5.0	62.5	+45	−2160	
^{7}Li	5.0	65.0	+34	−27.6	
^{23}Na	5.8	89.9	+19.1	+65.3	
^{39}K	7.4	129	+139.4	−37	[22]
^{40}K	7.4	130	+105	+194	
^{41}K	7.4	131	+85	+65	
^{85}Rb	8.0	164	+2800	−388	[23]
^{87}Rb	8.0	165	+90.4	+99.0	[23]
^{133}Cs	12	202	+280.3	+2405	[24]

The scattering lengths with no reference are the central values of the most precise results tabulated in Ref. [10].

The scattering length of ^{4}He atoms is large because of an *accidental fine-tuning*. The mass of the ^{4}He nucleus, the electron mass, and the fine structure constant α of QED have fortuitous values that make the potential between two ^{4}He atoms just deep enough to have a bound state very close to threshold, and therefore a large scattering length. If one of the ^{4}He atoms is replaced by a ^{3}He atom, which decreases the reduced mass by 14% without changing the interaction potential, the scattering length has the more natural value $-33a_0$.

The simplest example of an atom with a large negative scattering length is the polarized tritium atom ^{3}H [20]. The van der Waals length for ^{3}H is $\ell_{\rm vdW} = 13.7\,a_0$. The equilibrium radius defined by the minimum of the spin-triplet potential for H atoms is $r_{\rm eq} = 1.4\,a_0$. Since $\ell_{\rm vdW}$ is much larger than $r_{\rm eq}$, the natural low-energy length scale is $\ell_{\rm vdW}$. The scattering length for polarized ^{3}H atoms is the spin-triplet scattering length $a_t = -82.1\,a_0$ [20], which is much larger than the van der Waals length. Polarized tritium atoms have no 2-body bound states, but they have a single 3-body bound state with a shallow binding energy of about 4.59 mK [20].

Other examples of atoms with large scattering lengths can be found among the alkali atoms. The total spin of an alkali atom is called the *hyperfine* spin, and its quantum number is usually denoted by f. The hyperfine spin is the sum of the electronic spin, whose quantum number is $s = \frac{1}{2}$, and the nuclear spin, whose quantum number is denoted by i. The hyperfine interaction between the electronic and nuclear spins splits the ground state of the alkali atom into multiplets with hyperfine spin quantum number $f = i + \frac{1}{2}$ or $f = i - \frac{1}{2}$. We denote the individual hyperfine states by $|f, m_f\rangle$. Each of these hyperfine states has its own scattering length a_{f,m_f}, but they are all related to the spin-singlet and spin-triplet scattering lengths a_s and a_t. These scattering lengths are associated with different Born–Oppenheimer potentials with the same van der Waals tail. A compilation of the scattering lengths a_s and a_t for alkali atoms is given in Table 1. The scattering lengths for the isotopes of hydrogen were calculated in Refs. [21,20]. The scattering lengths for some of the heavier alkali were determined in Refs. [22–24]. The remaining scattering lengths are the central values of the most precise measurements tabulated in Ref. [10]. Note that 1/4 of the scattering lengths are negative, which is exactly what is expected for a random sample of potentials with van der Waals tails.

The coefficients C_6 in the van der Waals potentials for alkali atoms have been calculated in Ref. [15] for H and Li, and in Ref. [25] for the heavier alkali atoms. In Table 1, we list the corresponding van der Waals length $\ell_{\rm vdW}$ for each of the alkali atoms. We also give the equilibrium radius $r_{\rm eq}$, which is the radius of the minimum in the potential between two atoms in the spin-triplet channel. It provides an estimate of the range of the short-distance part of the potential. We see in Table 1 that the van der Waals length $\ell_{\rm vdW}$ is much larger than $r_{\rm eq}$ for all the alkali atoms. Thus the van der Waals length defined by Eq. (23) is the natural low-energy length scale for the alkali atoms. The alkali atoms in Table 1 provide several examples of atoms with large scattering lengths. The spin-triplet scattering lengths a_t for ^{6}Li and for ^{133}Cs and the spin-singlet scattering length a_s for ^{85}Rb are all more than an order of magnitude larger than the corresponding van der Waals scales $\ell_{\rm vdW}$. For these atoms, nature has provided a fortuitous fine-tuning of the potential and the mass of the atoms to give a large scattering length. The fine-tuning is illustrated by the facts that ^{7}Li, whose

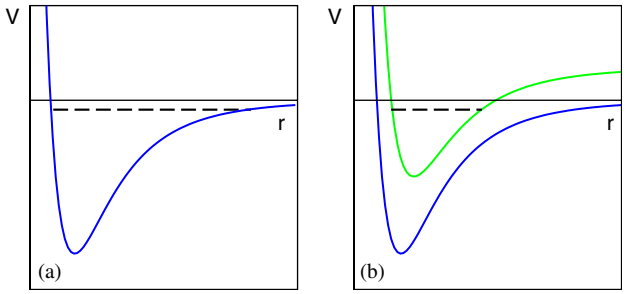

Fig. 7. Mechanisms for generating a large scattering length by tuning a bound state (dashed line) to the scattering threshold for the open channel. At a shape resonance (a), the bound state is in the potential for the open channel. At a Feshbach resonance (b), the bound state is in the potential for a weakly-coupled closed channel.

mass is 17% larger than that of ^{6}Li, has a natural value for a_t and that ^{87}Rb, whose mass is 2.3% larger than that of ^{85}Rb, has a natural value for a_s.

The mechanism for generating a large scattering length that involves tuning the depth or range of the potential is called a *shape resonance* and is illustrated in Fig. 7. With this mechanism, only the *open channel* defined by the scattering particles plays an important role. Another mechanism for generating a large scattering length is a *Feshbach resonance* [26]. This requires a second *closed channel* in which scattering states are energetically forbidden that is weakly coupled to the open channel. The closed channel might consist of particles in different spin states from those in the open channel. If the interaction potential $V(r)$ for the open channel asymptotes to 0 as $r \to \infty$, the interaction potential for the closed channel asymptotes to a positive value that is large compared to the energy scale of the particles in the open channel. Thus the only states in the closed channel that are energetically accessible are bound states. The weak coupling between the channels allows transitions between pairs of particles in the two channels. A large scattering length for particles in the open channel can be generated by tuning the depth of the potential for the closed channel to bring one of its bound states close to the threshold for the open channel, as illustrated in Fig. 7. The resulting enhancement of the scattering of particles in the open channel is a Feshbach resonance.

Feshbach resonances in alkali atoms can be created by tuning the magnetic field [27,28]. In this case, the open channel consists of a pair of atoms in a specific hyperfine state $|f, m_f\rangle$. The closed channel consists of a pair of atoms in different hyperfine states with a higher scattering threshold. The weak coupling between the channels is provided by the hyperfine interaction. Since different hyperfine states have different magnetic moments, a magnetic field can be used to vary the energy gap between the scattering thresholds and bring a bound state in the closed channel into resonance with the threshold of the open channel. The resulting enhancement of the scattering of particles in the open channel is a Feshbach resonance. The scattering lengths in Table 1 are in the absence of a magnetic field. The scattering lengths generally vary slowly with the magnetic field B. However, if B is varied through a Feshbach resonance for a particular hyperfine state, the scattering length changes dramatically as illustrated in Fig. 8. It increases or decreases to $\pm\infty$, jumps discontinuously to $\mp\infty$, and then returns to a value close to its original off-resonant value. If the Feshbach resonance is narrow, the scattering length near the resonance has the approximate form

$$a(B) \approx a_{\rm bg} + \frac{c_{\rm res}}{B - B_{\rm res}}, \tag{34}$$

where $a_{\rm bg}$ is the off-resonant scattering length, $B_{\rm res}$ is the location of the Feshbach resonance, and $c_{\rm res}$ controls the width of the resonance. In this case, the magnetic field provides an experimental fine-tuning parameter that can be used to make $|a|$ arbitrarily large. In particular, the scattering length can be made larger than the natural low-energy scale $\ell_{\rm vdW}$.

The use of a Feshbach resonance to produce a large scattering length in alkali atoms was first demonstrated in experiments with Bose–Einstein condensates of ^{23}Na atoms [29] and with cold gases of ^{85}Rb atoms [30,31]. For ^{23}Na atoms, the spin-singlet and spin-triplet scattering lengths a_s and a_t given in Table 1 have natural values, so all the hyperfine spin states $|f, m_f\rangle$ have natural scattering lengths a_{f,m_f} at $B = 0$. However, they diverge at values of B that depend on the hyperfine state $|f, m_f\rangle$. For example, $a_{1,-1}$ has Feshbach resonances near $B_{\rm res} = 853$ G and near $B_{\rm res} = 907$ G. For ^{85}Rb atoms, the spin-triplet scattering length a_t is a factor 2.4 larger than the natural scale $\ell_{\rm vdw}$, and

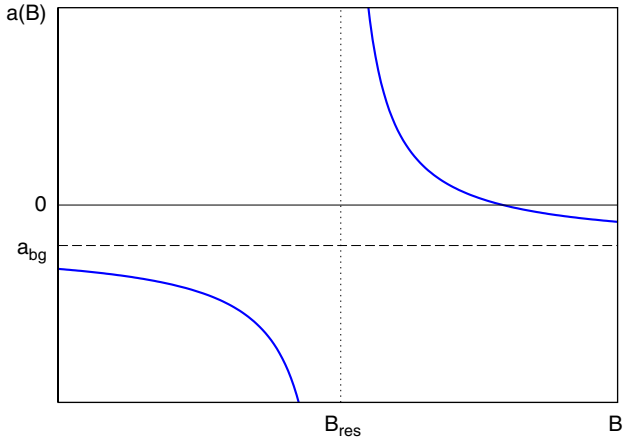

Fig. 8. The scattering length a as a function of the magnetic field B near a Feshbach resonance with $a_{\rm bg} < 0$ and $c_{\rm res} > 0$.

the spin-singlet scattering length a_s is very large. Thus most of the hyperfine spin states have relatively large scattering lengths a_{f,m_f} at $B = 0$. However, a_{f,m_f} can be made arbitrarily large by tuning the magnetic field to a Feshbach resonance. For example, $a_{2,-2}$ has a Feshbach resonance near $B_{\rm res} = 155\,\mathrm{G}$.

2.4. Particles and nuclei with large scattering length

Systems with large scattering length also arise in particle and nuclear physics. In all the subatomic systems described below, the large scattering length arises from an accidental fine-tuning of the parameters in the underlying theory.

The simplest example of a particle with a large scattering length is the neutron. The neutron is a spin-$\frac{1}{2}$ fermion. Neutrons with opposite spins can scatter in the S-wave channel. The scattering length and the effective range are $a = -18.5\,\mathrm{fm}$ and $r_s = 2.8\,\mathrm{fm}$. The low-energy interactions between two neutrons can be described by a short-range potential that is generated by the exchange of pions. The natural low-energy length scale is the range of the one-pion-exchange potential: $\ell_\pi \approx \hbar/m_\pi c = 1.4\,\mathrm{fm}$. The effective range for neutron-neutron scattering is comparable to this natural low-energy length scale, but the absolute value of the scattering length is larger by more than an order of magnitude.

The best known example of a system in nuclear physics with a large scattering length is the proton–neutron system. The proton (p), like the neutron (n), is a spin-$\frac{1}{2}$ fermion. Nuclear forces respect an approximate SU(2) isospin symmetry that mixes protons and neutrons. It is therefore useful to regard protons and neutrons as distinct isospin states of a single particle called the *nucleon* (denoted by N). Isospin symmetry is broken by electromagnetic effects, which generate the Coulomb force between protons, and by small effects associated with the difference between the masses of the up and down quarks. Because of isospin symmetry, there are two independent S-wave scattering lengths that govern the low-energy scattering of nucleons. We can take them to be the spin-singlet and spin-triplet np scattering lengths a_s and a_t, which correspond to NN scattering in the isospin-triplet ${}^1S_0$ and isospin-singlet ${}^3S_1$ channel, respectively. The spectroscopic notation ${}^{2s+1}L_j$ encodes the angular momentum quantum numbers for total spin (s), orbital angular momentum ($L = S, P, D, \ldots$ for $L = 0, 1, 2, \ldots$), and total angular momentum (j). The scattering lengths and effective ranges are $a_s = -23.76\,\mathrm{fm}$ and $r_s = 2.75\,\mathrm{fm}$ in the spin-singlet channel and $a_t = 5.42\,\mathrm{fm}$ and $r_t = 1.76\,\mathrm{fm}$ in the spin-triplet channel. The effective ranges are both comparable to the natural low-energy length scale $\ell_\pi \approx 1.4\,\mathrm{fm}$. However, the scattering length a_s is much larger than ℓ_π and a_t is at least significantly larger. The *deuteron* is an isospin-singlet ${}^3S_1$ pn bound state with binding energy $E_d = 2.225\,\mathrm{MeV}$. This issignificantly smaller than the natural low-energy scale $m_\pi^2 c^2/m_N = 21\,\mathrm{MeV}$, and fairly close to the universal prediction $\hbar^2/ma_t^2 = 1.4\,\mathrm{MeV}$ of Eq. (2). Thus we can identify the deuteron as the shallow bound state associated with the large positive spin-triplet scattering length.

Two low-energy protons interact through both the nuclear force and the Coulomb force. Isospin symmetry implies that, in the absence of the Coulomb force, the scattering length and effective range would have the same values a_s and

r_s as for the spin-singlet np system. Thus the pp scattering length is large. Unfortunately, universal effects in the pp system are complicated by the long-range Coulomb potential.

Another example of a large scattering length in nuclear physics is the $\alpha\alpha$ system [32], where α stands for the ^{4}He nucleus. The scattering length and the effective range for $\alpha\alpha$ scattering are estimated to be $a \approx 5$ fm and $r_s \approx 2.5$ fm. The scattering length is significantly larger than the natural low-energy length scale $\ell_\pi \approx 1.4$ fm set by one-pion exchange. The unstable ^{8}Be nucleus is known to be clustered into two α particles, and the ground state energy of ^{8}Be lies only about 0.1 MeV above the $\alpha\alpha$ threshold. This energy is much smaller than the natural energy scale $m_\pi^2 c^2/m_\alpha \approx 5.3$ MeV, and comparable in magnitude to the universal prediction $-\hbar^2/m_\alpha a^2 \approx -0.4$ MeV of Eq. (2). The difference can be partly attributed to the Coulomb repulsion of the doubly-charged α particles. As a consequence, the ground state of ^{8}Be can be interpreted as a shallow $\alpha\alpha$ resonance resulting from the large scattering length. Universal effects in the $\alpha\alpha$ system are complicated not only by the long-range Coulomb force between the α particles, but also by the fact that the scattering length is not terribly large.

A new example of a system with large scattering length has recently emerged in particle physics. In 2003, the Belle collaboration discovered a new hadronic resonance that decays into $J/\psi\ \pi^+\pi^-$, where J/ψ is the lowest spin-triplet charmonium state [33]. Its mass is $3872.0 \pm 0.6(\text{stat}) \pm 0.5(\text{syst})\ \text{MeV}/c^2$ and its total width is less than $2.3\ \text{MeV}/c^2$ at the 90% confidence level. The nature of this state, which was tentatively named $X(3872)$, has not yet been determined. However, its mass is extremely close to the threshold $3871.2 \pm 0.7\ \text{MeV}/c^2$ for decay into the charm mesons D^0 and $\bar{D}^{*0}$ or $\bar{D}^0$ and D^{*0}. This suggests that it might be a $D^0\bar{D}^{*0}/\bar{D}^0 D^{*0}$ molecule [34]. The natural scale for the binding energy of such a molecule is $m_\pi^2 c^2/(2\mu) \approx 10\ \text{MeV}/c^2$, where μ is the reduced mass of the D^0 and $\bar{D}^{*0}$. The mass measurement indicates that its binding energy is -0.8 ± 1.1 MeV. Since this is much smaller than the natural scale, the $D^0\bar{D}^{*0}$scattering length must be much larger than the natural length scale $\ell_\pi \approx 1.4$ fm. If the $X(3872)$ is indeed a $D^0\bar{D}^{*0}/\bar{D}^0 D^{*0}$ molecule, then it has universal properties that are determined by the unnaturally large scattering length [35,36].

3. Renormalization group concepts

In this section, we introduce some concepts that arise naturally if the problem of atoms with large scattering length is formulated within a renormalization group framework. We introduce the *resonant* and *scaling* limits, and explain how the nontrivial realization of universality in the 3-body sector is related to *renormalization group limit cycles*.

3.1. Efimov effect

The *Efimov effect* is a remarkable phenomenon that can occur in the 3-body sector for nonrelativistic particles if at least two of the three pairs of particles has a large scattering length. It was discovered by Efimov in 1970 [4]. The Efimov effect is very well-established theoretically, but there is as yet no convincing experimental evidence for this effect.

The *Thomas effect* is closely related to the Efimov effect, but it was discovered much earlier in 1935 [37]. Thomas considered particles interacting through a 2-body potential with depth V_0 and range r_0 that supported a single bound state with binding energy E_2. Thomas studied the *zero-range limit* defined by $r_0 \to 0$ and $V_0 \to \infty$ with E_2 fixed. Using a simple variational argument, he showed that the binding energy $E_{\rm T}$ of the deepest 3-body bound state diverges to ∞ in the zero-range limit. Thus the spectrum of 3-body bound states is unbounded from below. The counterintuitive conclusion is that a 2-body potential that is only attractive enough to support a single 2-body bound state can nevertheless produce 3-body bound states with arbitrarily large binding energies.

The zero-range limit considered by Thomas produces a large scattering length $a \gg r_0$. The binding energy of the 2-body bound state in this limit is given by Eq. (2). The binding energy of the deepest 3-body bound state produced by the variational argument scales like $\hbar^2/mr_0^2$, and thus diverges as $r_0 \to 0$. The importance of the Thomas effect is limited by the fact that the binding energy and other properties of this deepest 3-body bound state may depend on the details of the interaction potential.

In 1970, Efimov pointed out that when $|a|$ is sufficiently large compared to the range r_0 of the potential, there is also a sequence of 3-body bound states whose binding energies are spaced roughly geometrically in the interval between $\hbar^2/mr_0^2$ and $\hbar^2/ma^2$. As $|a|$ is increased, new bound states appear in the spectrum at critical values of a that differ by

multiplicative factors of e^{π/s_0}, where s_0 depends on the statistics and the mass ratios of the particles. In the case of identical bosons, s_0 is the solution to the transcendental equation

$$s_0 \cosh \frac{\pi s_0}{2} = \frac{8}{\sqrt{3}} \sinh \frac{\pi s_0}{6}. \tag{35}$$

Its numerical value is $s_0 \approx 1.00624$, so $e^{\pi/s_0} \approx 22.7$. As $|a|/r_0 \to \infty$, the asymptotic number of 3-body bound states is

$$N \longrightarrow \frac{s_0}{\pi} \ln \frac{|a|}{r_0}. \tag{36}$$

In the limit $a \to \pm\infty$, there are infinitely many 3-body bound states with an accumulation point at the 3-body scattering threshold. A formal proof of the Efimov effect was subsequently given by Amado and Nobel [38,39]. The Thomas and Efimov effects are closely related. The deepest 3-body bound states found by Thomas's variational calculation can be identified with the deepest Efimov states [40].

The importance of the Efimov effect is that the sequence of 3-body bound states he discovered have universal properties that are insensitive to the details of the 2-body potential at short distances. The simplest such property is that in the resonant limit in which there are infinitely many arbitrarily-shallow 3-body bound states, the ratio of the binding energies of the successive bound states approaches a universal number as the threshold is approached:

$$E_{\rm T}^{(n+1)}/E_{\rm T}^{(n)} \longrightarrow e^{-2\pi/s_0} \quad \text{as } n \to +\infty \text{ with } a = \pm\infty. \tag{37}$$

In the case of identical bosons, the universal number has the value 1/515.03. This implies that the asymptotic behavior of the spectrum in the resonant limit has the form

$$E_{\rm T}^{(n)} \longrightarrow (e^{-2\pi/s_0})^{n-n_*} \hbar^2 \kappa_*^2/m \quad \text{as } n \to +\infty \text{ with } a = \pm\infty \tag{38}$$

for some integer n_* and some parameter κ_* with dimensions of wave number. If we chose a different integer n_*, the value of κ_* would change by some power of e^{π/s_0}. Thus κ_* is defined by Eq. (38) only up multiplicative factors of e^{π/s_0}.

In subsequent papers, Efimov showed that universality is a general feature of the 3-body problem in the scaling limit. It does not require the resonant limit $a = \pm\infty$, but occurs whenever the scattering length is large. In two brilliant papers in 1971 and 1979 [41,42], Efimov derived a number of universal results on low-energy 3-body observables for three identical bosons. A remarkable example is a universal formula for the atom–dimer scattering length [42]:

$$a_{\rm AD} = (b_1 - b_0 \tan[s_0 \ln(a\kappa_*) + \beta])a, \tag{39}$$

where b_0, b_1, and β are universal numbers and κ_* is the 3-body parameter defined by the asymptotic behavior of the spectrum of Efimov states in the resonant limit given in Eq. (38). The universal numbers b_0 and b_1 were first calculated by Simenog and Sinitchenko [43]. These and other universal results for the 3-body system consisting of three identical bosons are presented in Section 6. The expression (39) for $a_{\rm AD}$ in Eq. (39) is universal in the sense that it holds for all identical bosons, independent of the short-range interactions that generate the large scattering length, provided that the shallow dimer is the only 2-body bound state. If there are additional deep 2-body bound states, the universal expression for $a_{\rm AD}$ is more complicated and is given in Section 7.

3.2. The resonant and scaling limits

We have defined a large scattering length to be one that satisfies $|a| \gg \ell$, where ℓ is the natural low-energy length scale. The corrections to the universal behavior are suppressed by powers of $\ell/|a|$. There are two obvious limits in which the size of these corrections decreases to zero:

- the *resonant limit*: $a \to \pm\infty$ with ℓ fixed,
- the *scaling limit*: $\ell \to 0$ with a fixed.

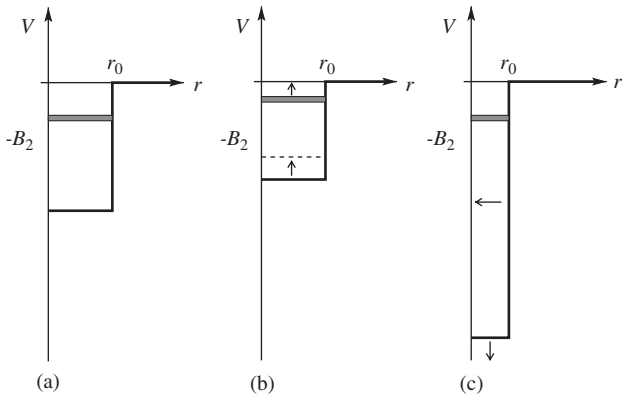

Fig. 9. (a) A square well potential with a single shallow bound state, (b) a potential with the same range r_0 that is approaching the resonant limit $E_2 \to 0$, and (c) a potential with the same binding energy E_2 as in (a) that is approaching the scaling limit $r_0 \to 0$.

In either limit, the leading corrections to the universal behavior are suppressed by powers of $\ell/|a|$. It will sometimes also be useful to consider systems in which the resonant and scaling limits are achieved simultaneously: $a = \pm\infty$ and $\ell = 0$.

The *resonant limit* is also sometimes called the *unitary limit*, because in this limit the S-wave contribution to the cross section at low energy saturates its unitarity limit $\sigma^{(L=0)} \leqslant 8\pi/k^2$. The resonant limit can often be approached by tuning a single parameter. This parameter could be the depth of the interatomic potential, or an overall rescaling of the potential: $V(r) \to \lambda V(r)$. As illustrated in Fig. 9(b), the parameter must be tuned to a critical value for which there is a 2-body bound state exactly at the 2-body threshold. In the case of a Feshbach resonance, the resonant limit can be approached by tuning the magnetic field. Since $a = \pm\infty$ in the *resonant limit*, one might expect that the natural low-energy length scale ℓ is the only important length scale at low energies. This is true in the 2-body sector. However, the Efimov effect reveals that there is another length scale in the 3-body sector. In the resonant limit, there are infinitely many, arbitrarily-shallow 3-body bound states with a spectrum of the form in Eq. (38). The parameter κ_* defined by Eq. (38) can be interpreted as the approximate binding wave number of the Efimov state labelled by the integer n_*.

The *scaling limit* is also sometimes called the *zero-range limit*. We prefer "scaling limit" because it emphasizes the renormalization aspects of the problem. This terminology seems to have been first used in Ref. [44]. The scaling limit may at first seem a little contrived, but it has proved to be a powerful concept. It can be defined by specifying the phase shifts for 2-body scattering. In the scaling limit, the S-wave phase shift $\delta_0(k)$ has the simple form

$$k \cot \delta_0(k) = -1/a, \tag{40}$$

and the phase shifts $\delta_L(k)$ for all higher partial waves vanish. To approach the scaling limit typically requires tuning multiple parameters in the interatomic potential. For example, as illustrated in Fig. 9(c), it can be reached by simultaneously tuning the range of the potential to zero and its depth to ∞ in such a way that the binding energy of the shallowest 2-body bound state remains fixed. In the scaling limit, the scattering length a sets the scale for most low-energy observables. It is the only length scale in the 2-body sector. However, as we shall see, in the 3-body sector, observables can also have logarithmic dependence on a second scale. In the scaling limit, there are infinitely many arbitrarily-deep 3-body bound states with a spectrum of the form [45,46]

$$E_{\rm T}^{(n)} \longrightarrow (e^{-2\pi/s_0})^{n-n_*} \frac{\hbar^2\kappa_*^2}{m} \quad \text{as } n \to -\infty \text{ with } \ell = 0. \tag{41}$$

Thus the spectrum is characterized by a parameter κ_* with dimensions of wave number.

The scaling limit may appear to be pathological, because the spectrum of 3-body bound states in Eq. (41) is unbounded from below. However, the deep 3-body bound states have a negligible effect on the low-energy physics of interest. The pathologies of the scaling limit can be avoided simply by keeping in mind that the original physical problem before taking the scaling limit had a natural low-energy length scale ℓ. Associated with this length scale is an energy scale $\hbar^2/m\ell^2$ that we will refer to as the *natural ultraviolet cutoff*. Any predictions involving energies comparable to or larger

than the natural ultraviolet cutoff are artifacts of the scaling limit. Thus when we use the scaling limit to describe a physical system, any predictions involving energies $|E| \gtrsim \hbar^2/m\ell^2$ should be ignored.

In spite of its pathologies, we shall take the scaling limit as a starting point for describing atoms with large scattering length. We will treat the deviations from the scaling limit as perturbations. Our motivation is that when the scattering length is large, there are intricate correlations between 3-body observables associated with the Efimov effect that can be easily lost by numerical approximations. By taking the scaling limit, we can build in these intricate correlations exactly at high energy. Although these correlations are unphysical at high energy, this does not prevent us from describing low-energy physics accurately. It does, however, guarantee that the intricate 3-body correlations are recovered automatically in the resonant limit $a \to \pm\infty$.

In the 2-body sector, the scaling limit is associated with a *continuous scaling symmetry* that consists of rescaling the scattering length a, the coordinate $\boldsymbol{r}$, and the time t by appropriate powers of a positive number λ:

$$a \longrightarrow \lambda a, \quad \boldsymbol{r} \longrightarrow \lambda \boldsymbol{r}, \quad t \longrightarrow \lambda^2 t. \tag{42}$$

The scaling of the time by the square of the scaling factor for lengths is natural in a nonrelativistic system. Under the continuous scaling symmetry, 2-body observables, such as binding energies and cross sections, scale with the powers of λ implied by dimensional analysis. This continuous scaling symmetry is a trivial consequence of the fact that a is the only length scale that remains nonzero in the scaling limit. For real atoms, the scaling limit can only be an approximation. There are *scaling violations* that break the scaling symmetry. In the 2-body sector, the most important scaling violations come from the S-wave effective range r_s, which give corrections to the scaling limit that scale as $r_s/|a|$. All other scaling violations in the 2-body sector give corrections that scale as higher powers of $\ell/|a|$. Scaling violations that give corrections that scale as powers of $\ell/|a|$ can be treated as perturbations to the scaling limit.

We will see that in the 3-body sector, there are *logarithmic scaling violations* that give corrections that scale as $\ln(|a|/\ell)$. Logarithmic scaling violations do not become less important as one approaches the scaling limit, and therefore cannot be treated as perturbations. The origin of the logarithmic scaling violations is that the 3-body problem in the scaling limit is singular at short distances. In the 3-body sector, the scaling limit is characterized not only by the scattering length a, but also by a second parameter that sets the scale for the logarithmic corrections. A convenient choice for this parameter is the wave number κ_* defined by the spectrum of Efimov states in the resonant limit, which is given in Eq. (38). Low-energy observables are log-periodic functions of κ_*. Simple observables that do not depend on any kinematic variables must have the form a raised to a power determined by dimensional analysis multiplied by a periodic function of $\ln(|a|\kappa_*)$.

The 3-body sector in the scaling limit has a trivial continuous scaling symmetry defined by Eqs. (42) together with $\kappa_* \to \lambda^{-1}\kappa_*$. However, because of the log-periodic form of the logarithmic scaling violations, it also has a nontrivial *discrete scaling symmetry*. There is a discrete subgroup of the continuous scaling symmetry that remains an exact symmetry in the scaling limit. The discrete scaling symmetry is

$$\kappa_* \longrightarrow \kappa_*, \quad a \longrightarrow \lambda_0^n a, \quad \boldsymbol{r} \longrightarrow \lambda_0^n \boldsymbol{r}, \quad t \longrightarrow \lambda_0^{2n} t, \tag{43}$$

where n is an integer, $\lambda_0 = e^{\pi/s_0}$, and $s_0 = 1.00624$ is the solution to the transcendental equation in Eq. (35). Under this symmetry, 3-body observables scale with the powers of λ_0^n implied by dimensional analysis. This discrete scaling symmetry will be discussed in Section 6.1. Note that the discrete scaling symmetry transformation leaves the 3-body parameter κ_* fixed. By combining the trivial continuous scaling symmetry with the discrete scaling symmetry given by Eqs. (43), we can see that κ_* is only defined modulo multiplicative factors of λ_0.

When we approximate a physical system by the idealized scaling limit, it is important to have an estimate for the size of the corrections. The logarithmic scaling violations must be taken into account without approximation in the scaling limit. The next most important scaling violations come from the effective range r_s, which we expect to have a natural value of order ℓ. The leading correction is linear in r_s. For an observable that does not involve any kinematic variables, the only other scales are the scattering length a and κ_*. Since the dependence on κ_* can only be logarithmic, our estimate of the fractional corrections to the scaling limit is $r_s/|a|$. For an observable involving energy E, the energy provides an alternative scale, so there can also be corrections that scale as $(m|E|/\hbar^2)^{1/2} r_s$. For observables involving energy $|E| \sim \hbar^2/ma^2$, this reduces to our previous estimate $r_s/|a|$. For observables involving energies that are comparable to the natural ultraviolet cutoff $\hbar^2/m\ell^2$, our estimate of the fractional correction is 100%.

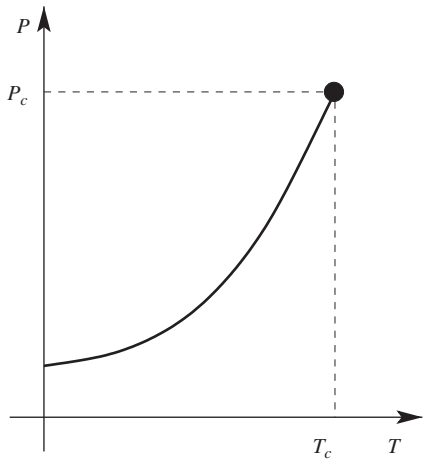

Fig. 10. The pressure P versus the temperature T for a liquid–gas system with a critical point at (T_c, P_c).

3.3. Universality in critical phenomena

Universality refers to the fact that physical systems that are completely different at short distances can in certain limits exhibit identical behavior at long distances. The classic examples of universality are condensed matter systems near the critical point where a line of first order phase transitions end [47]. Low-energy atoms with large scattering length a also exhibit universal behavior that is insensitive to the details of their interactions at separations small compared to a. Their universal behavior is more complex than the more familiar examples provided by critical phenomena in condensed matter physics. Before considering atoms with large scattering lengths, we first recall some simple examples of universality in critical phenomena.

One of the most familiar systems in which critical phenomena can occur is a substance with liquid and gas phases. The thermodynamic state of the system is determined by the temperature T and the pressure P. As illustrated in Fig. 10, the liquid and gas phases are separated by a line in the T–P plane. As this line is crossed, the substance undergoes a *phase transition*: a discontinuous change from a liquid with density $\rho_{\rm liq}(T)$ to a gas with density $\rho_{\rm gas}(T)$. The phase transition line typically ends at some point (T_c, P_c), and this endpoint is called the *critical point*. At higher temperatures and pressures, the transition between liquid and gas is smooth. Just beyond the critical point, there is a rapid cross-over between liquid and gas. At much higher temperatures, the transition is gradual.

Near the critical point (T_c, P_c), the liquid–gas system exhibits *universal behavior*. An example is the behavior of the coexistence curves $\rho_{\rm liq}(T)$ and $\rho_{\rm gas}(T)$ near the critical point. At $T = T_c$, they are both equal to the critical density ρ_c. As $T \to T_c$ from below, the deviations of $\rho_{\rm liq}(T)$ and $\rho_{\rm gas}(T)$ from ρ_c have a power-law behavior:

$$\rho_{\rm liq}(T) - \rho_c \longrightarrow +A(T_c - T)^{\beta}, \tag{44a}$$

$$\rho_{\rm gas}(T) - \rho_c \longrightarrow -A(T_c - T)^{\beta}. \tag{44b}$$

The coefficient A varies widely from substance to substance, but the *critical exponent* β is a universal number. It has the same value $\beta = 0.325$ for all liquid–gas systems. Thus substances that are completely different on the atomic level have the same universal behavior near their critical points.

Another familiar example of a system in which critical phenomena can occur is a ferromagnetic material with one easy axis of magnetization. The thermodynamic state of the system is determined by its temperature T and the magnetic field B. When $B = 0$, the magnetization M can be positive or negative. As illustrated in Fig. 11, the $M < 0$ and $M > 0$ regions are separated by a phase transition line on the $B = 0$ axis. As this line is crossed, the magnetization changes discontinuously from $-M_0(T)$ to $+M_0(T)$. The phase transition line ends at a critical temperature T_c. Above that temperature, the transition from negative to positive magnetization is smooth. Near the critical point $(T = T_c, B = 0)$, the system exhibits universal behavior. An example is the behavior of the discontinuity $M_0(T)$ near the critical point.

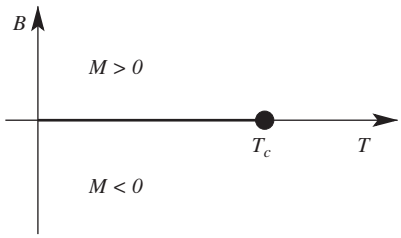

Fig. 11. The magnetic field B versus the temperature T for a ferromagnetic material with one easy axis of magnetization and a critical point at $(T_c, B = 0)$.

As $T \to T_c$ from below, M_0 has a power-law behavior:

$$M_0(T) \longrightarrow A'(T_c - T)^{\beta}. \tag{45}$$

The coefficient A' varies widely from substance to substance, but the critical exponent β is a universal number. Remarkably, it has the same value $\beta = 0.325$ as for liquid–gas systems. Thus even systems that bear as little resemblance to each other as a liquid–gas system and a ferromagnetic can exhibit the same universal behavior near a critical point, provided we make an appropriate mapping between the thermodynamic variables.

An important feature of critical phenomena is that these systems exhibit *scaling behavior* in the *critical region* [47]. There is some correlation length ξ that diverges at the critical point. In the liquid–gas system, ξ is the correlation length for density fluctuations. In the ferromagnet, it is the correlation length for spin fluctuations. The critical region is defined by $\xi \gg \ell$, where ℓ is the natural length scale for these correlations, which is the typical separation of the atoms. The rate at which the correlation length diverges as the critical point is approached is characterized by a critical exponent. For example, its dependence on the temperature has the form

$$\xi(T) \longrightarrow C|T - T_c|^{-\nu}, \tag{46}$$

where ν is a critical exponent. In the liquid–gas system or in the ferromagnet, this critical exponent is $\nu = 0.63$. In the critical region, the correlation length ξ is the only important length scale at long distances. The deviations of other observables from their critical values scale like powers of ξ. These powers typically differ from the values suggested by dimensional analysis, so they are called *anomalous dimensions*. For example, the deviations in Eqs. (44) and (45) have anomalous dimensions β/ν.

The modern understanding of universality in critical phenomena is based on the *renormalization group*. The basic ideas of renormalization group theory are described in Ken Wilson's Nobel lectures [48]. An excellent overview of this subject has been given more recently by Michael Fisher [47]. The crucial concept is that of a *renormalization group* (*RG*) *transformation* on a Hamiltonian $\mathscr{H}$ that eliminates short-distance degrees of freedom while keeping long-distance observables invariant. If all degrees of freedom with length scale shorter than $1/\Lambda$ have been eliminated, we refer to Λ as the ultraviolet cutoff. It is convenient to expand the Hamiltonian in terms of a suitable basis of operators $\mathscr{O}_n$:

$$\mathscr{H} = \sum_n g_n \mathscr{O}_n. \tag{47}$$

This allows the Hamiltonian to be represented by a point $\boldsymbol{g} = (g_1, g_2, \ldots)$ in the infinite-dimensional space of coupling constants. If the ultraviolet cutoff Λ can be treated as a continuous variable, the RG transformation defines a flow in the space of coupling constants that can be expressed as a differential equation:

$$\Lambda \frac{\mathrm{d}}{\mathrm{d}\Lambda} \boldsymbol{g} = \boldsymbol{\beta}(\boldsymbol{g}), \tag{48}$$

The *beta function* $\boldsymbol{\beta}(\boldsymbol{g})$ is in general a complicated nonlinear function of the coupling constants. If we start from a generic Hamiltonian $\mathscr{H}_0$ with coupling constants $\boldsymbol{g}_0$, the RG flow will carry it along a path called an *RG trajectory* that leads in the *infrared limit* $\Lambda \to 0$ to a very complicated Hamiltonian that describes the long-distance physics in terms of the long-distance degrees of freedom only.

Wilson pointed out that the scale-invariant behavior at long distances that is characteristic of critical phenomena can arise from RG flow to a *fixed point* in the infrared limit $\Lambda \to 0$. A fixed-point Hamiltonian $\mathscr{H}_*$ is one that does not change with Λ. Its coupling constant $\boldsymbol{g}(\Lambda)$ satisfies

$$\boldsymbol{g}(\Lambda) = \boldsymbol{g}_*, \tag{49}$$

where $\boldsymbol{g}_*$ is a solution to $\boldsymbol{\beta}(\boldsymbol{g}_*) = 0$. Since the Hamiltonian $\mathscr{H}_*$ remains invariant as one varies the ultraviolet cutoff Λ that specifies the length scale of the short-distance degrees of freedom that have been eliminated, the Hamiltonian $\mathscr{H}_*$ must describe a scale-invariant system. Associated with a fixed point $\boldsymbol{g}_*$, there is typically a *critical subspace* of points that flow asymptotically to $\boldsymbol{g}_*$ as $\Lambda \to 0$. If the initial Hamiltonian $\mathscr{H}_0$ is carefully tuned to a point in this subspace, it will flow along a *critical trajectory* that asymptotically approaches the fixed point $\mathscr{H}_*$ in the infrared limit $\Lambda \to 0$. The tuning of macroscopic variables to a critical point corresponds at the microscopic level to the tuning of the coupling constants to the critical trajectory. The universality of critical phenomena can be explained by the fact that critical trajectories can flow to the same infrared fixed point from widely separated regions of the space of Hamiltonians. Thus systems that are completely different at the microscopic level can have the same long-distance behavior.

Since a Hamiltonian $\mathscr{H}$ on the critical trajectory flows to the fixed point $\mathscr{H}_*$ in the infrared limit $\Lambda \to 0$, that Hamiltonian must be characterized by asymptotic scale invariance in the infrared limit. Critical phenomena are associated with fixed points of the RG flow. In the neighborhood of a fixed point, the RG flow given by Eq. (48) can be linearized:

$$\Lambda \frac{\mathrm{d}}{\mathrm{d}\Lambda} \boldsymbol{g} \approx B(\boldsymbol{g} - \boldsymbol{g}_*), \tag{50}$$

where B is a linear operator. The eigenvalues of the operator B are called the *critical exponents* of the operators associated with the corresponding eigenvectors of B. Operators with positive, zero, and negative critical exponents are called *relevant*, *marginal*, and *irrelevant*, respectively. As the ultraviolet cutoff Λ increases, the coupling constants of relevant operators increase and the system flows away from the fixed point. Thus, in order for the system to flow to the fixed point in the ultraviolet limit, the coupling constants of the relevant operators must be tuned to their critical values. The critical exponent β in Eqs. (44) and (45) and the critical exponent ν in Eq. (46) are related in a simple way to the critical exponents of appropriate operators in the Hamiltonian.

RG fixed points are central to the modern understanding of critical phenomena and they play an important role in many other problems in condensed matter physics. They also play a central role in the Standard Model of elementary particle physics, and in many of the proposed extensions of the Standard Model, such as grand unified theories. The many applications in condensed matter physics, high energy physics, and nuclear physics have provided a strong driving force for the development of the renormalization group theory associated with RG fixed points.

3.4. Renormalization group limit cycles

The RG flow defined by Eq. (48) can in general have a very complicated topology. A fixed point is only the simplest possible topological feature. A more complicated possibility is a *limit cycle*, in which the RG trajectory flows forever around a closed loop. A limit cycle is a family $\mathscr{H}_*(\theta)$ of Hamiltonians that is closed under the RG flow and can be parameterized by an angle θ that runs from 0 to 2π. The Hamiltonian makes a complete circuit around the limit cycle every time the ultraviolet cutoff Λ changes by some multiplicative factor λ_0. The parameter θ can be chosen so that the RG flow on the limit cycle $\boldsymbol{g}_*(\theta)$ is just a linear increase in θ with $\ln \Lambda$. Thus if the coupling constant at some initial cutoff Λ_0 is $\boldsymbol{g}(\Lambda_0) = \boldsymbol{g}_*(\theta)$, its value for a general cutoff is

$$\boldsymbol{g}(\Lambda) = \boldsymbol{g}_*(\theta + 2\pi \ln(\Lambda/\Lambda_0)/\ln(\lambda_0)). \tag{51}$$

Note that the coupling constant is invariant under a discrete scale transformation of the ultraviolet cutoff Λ with discrete scaling factor λ_0.

The possibility of RG limit cycles was first discussed by Wilson in a pioneering paper that proposed applying the renormalization group to the strong interactions of elementary particle physics [49]. The fundamental theory of the strong interactions was not yet known at that time, but Wilson suggested that it ought to be a relativistic quantum field theory whose coupling constants are governed by the renormalization group. Experiments on deeply-inelastic lepton–nucleon scattering had revealed evidence for scaling behavior in the strong interactions at high energy. Wilson

suggested that such simple high-energy behavior could be explained by simple behavior of the RG flow in the *ultraviolet limit* $\Lambda \to \infty$. The simplest possibility is RG flow to an ultraviolet fixed point. The next simplest possibility is RG flow to an *ultraviolet limit cycle*. The fundamental field theory of the strong interactions called Quantum Chromodynamics (QCD) was subsequently developed. QCD has a single coupling constant $\alpha_s(\Lambda)$ with an *asymptotically free* ultraviolet fixed point: $\alpha_s(\Lambda) \to 0$ as $\Lambda \to \infty$ [50,51]. Thus ultraviolet limit cycles are not relevant to QCD.[4]

As pointed out by Wilson, one of the signatures of an RG limit cycle is *discrete scale invariance*. If the ultraviolet cutoff is decreased by the factor λ_0, the Hamiltonian $\mathscr{H}_*(\theta_0)$ flows around the limit cycle and returns to $\mathscr{H}_*(\theta_0)$. This implies that if degrees of freedom with length scales less than $1/\Lambda$ have been eliminated and if one further eliminates all degrees of freedom with length scales between $1/\Lambda$ and λ_0/Λ, the dynamics of the system is unchanged. This is possible only if the system has a discrete scaling symmetry under $\boldsymbol{r} \to \lambda_0^n \boldsymbol{r}$ for all n. The discrete scale invariance implies that long-distance observables can have a periodic dependence on the logarithm of the variable that characterizes the critical region [49]. An example of such a periodic dependence on the logarithm of a is provided by Efimov's expression for the atom–dimer scattering length in Eq. (39). Discrete scale invariance may also arise in other contexts that are as varied as turbulence, sandpiles, earthquakes, and financial crashes [53].

In contrast to RG fixed points, the development of the renormalization group theory associated with RG limit cycles is still in its infancy. This situation is partly due to the lack of compelling examples. However, new examples of RG limit cycles have recently begun to emerge. A very simple example of a renormalization group limit cycle occurs in the quantum mechanics of a particle in a $1/r^2$ potential. This example is described in Section 8.2. Glazek and Wilson have presented a discrete Hamiltonian system whose renormalization involves a limit cycle [54,55]. The spectrum of this model has some features in common with the 3-body spectrum of identical bosons, so it will be discussed in detail later in this section. LeClair, Roman, and Sierra have constructed a generalization of a reduced Hamiltonian for Cooper pairs in a superconductor whose renormalization involves a limit cycle [56]. The gap equation for this model has multiple solutions related by a discrete scaling symmetry.

LeClair, Roman, and Sierra have also discovered a (1+1)-dimensional quantum field theory whose renormalization involves a limit cycle [57–59]. The model is a perturbation of a conformal field theory with an SU(2) current algebra by a current–current interaction. The current–current interaction has three independent coupling constants. For generic values of the coupling constants, the S-matrix is a log-periodic function of the energy. There are infinitely many resonances, with masses and widths related by a discrete scaling symmetry. The discrete scaling symmetry is the signature of an RG limit cycle. The conformal field theory is an interacting quantum field theory that corresponds to a nontrivial RG fixed point. At a generic point in the three-dimensional space of coupling constants for the current–current interaction, the RG flow is log-periodic. As the ultraviolet cutoff is decreased by the discrete scaling factor, the coupling constants flow out to infinity in one direction, flow back from infinity from another direction, and return to their original values.

Leclair, Roman, and Sierra have used the colorful phrase *Russian doll renormalization group* to describe RG limit cycles [56,57]. The name refers to a traditional souvenir from Russia consisting of a set of hollow wooden dolls that can be nested inside each other. An example is shown in Fig. 12. The scaling factors between each doll and the next smaller one are all approximately equal.

We now discuss the discrete Hamiltonian model of Glazek and Wilson [54,55] in some detail. The Hamiltonian H_N for the $(N+1)$-state model is an $(N+1) \times (N+1)$ matrix with entries

$$\langle m|H_N|n\rangle = b^{(m+n)/2}\epsilon(I_{mn} - g_N S_{mn} - \mathrm{i}h_N A_{mn}), \quad m, n = 0, 1, \ldots, N, \tag{52}$$

where $b > 1$ is dimensionless, $\epsilon > 0$ has units of energy, I is the identity matrix, S is the symmetric matrix all of whose entries are $+1$, and A is the antisymmetric matrix all of whose entries above the diagonal are $+1$. We can interpret ϵ as an infrared cutoff and $\Lambda = b^N\epsilon$ as an ultraviolet cutoff.

The Glazek–Wilson model has two coupling constants: g_N and h_N. In the noninteracting case $g_N = h_N = 0$, the model has a geometric spectrum of energy eigenvalues: $E_n = b^n\epsilon$, $n = 0, 1, \ldots, N$. We can define a continuum limit by taking $N \to \infty$, $b \to 1$ and $\epsilon \to 0$ with $\Lambda = b^N\epsilon$ fixed. In this limit, the energy spectrum of the noninteracting model is a continuum of positive-energy states with energies $0 < E < \Lambda$ as illustrated in Fig. 13(a).

[4] There is, however, a possibility that QCD in the few-nucleon sector has an infrared limit cycle at critical values of the quark masses that are not far from their physical values [52].

Fig. 12. Nesting Russian dolls with a discrete scaling factor of about 1.3.

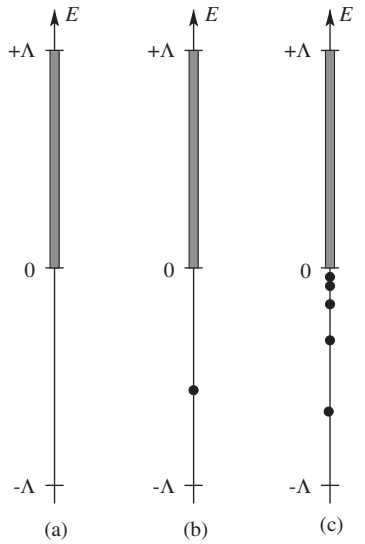

Fig. 13. Energy spectrum for the continuum limit of the Glazek–Wilson model in three cases: (a) the noninteracting model with $g = h = 0$; (b) the interacting model with $h = 0$; and (c) the interacting model with discrete scaling factor $\lambda_0 = 2$. A shaded band represents a continuum of positive energy states, while a dot represents a discrete negative-energy state. In case (c), there are infinitely many negative energy states with an accumulation point at $E = 0$.

In the interacting case in which g_N and h_N are nonzero, the energy spectrum is more interesting [54]. In addition to positive eigenvalues, the Hamiltonian H_N has negative eigenvalues that are exponential in $1/g_N$. Thus the interaction terms are nonperturbative. In the continuum limit, there is a continuum of positive-energy states with energies $0 < E < \Lambda$. If $h_N = 0$, there is a single negative eigenvalue in the continuum limit as illustrated in Fig. 13(b). If $h_N \neq 0$, there are multiple negative eigenvalues as illustrated in Fig. 13(c).

One way to study the model is using the renormalization group. An RG transformation that integrates out the state $|N\rangle$ is obtained by constructing a Hamiltonian H_{N-1} for the states $|n\rangle$, $n = 0, 1, \ldots, N-1$, that reproduces the low-energy eigenvalues E_n of H_N that satisfy $|E_n| \ll \Lambda$. Remarkably the Hamiltonian H_{N-1} has the same form as H_N in Eq. (52),

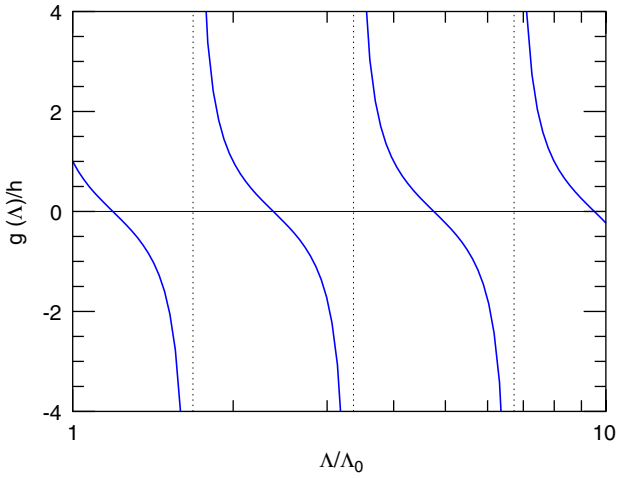

Fig. 14. The behavior of $g(\Lambda)/h$ as a function of Λ/Λ_0 for the case $g(\Lambda_0)/h = 1$ and $\lambda_0 = 2$.

except that I, S, and A are $N \times N$ matrices. The coupling constants g_{N-1} and h_{N-1} in H_{N-1} are

$$g_{N-1} = \frac{g_N + h_N^2}{1 - g_N}, \quad h_{N-1} = h_N. \tag{53}$$

Since $h = h_N$ remains fixed under the RG transformation, its subscript is unnecessary. After p iterations of the RG transformation, the coupling constant g_{N-p} is given by

$$\arctan(g_{N-p}/h) = \arctan(g_N/h) + p \arctan h. \tag{54}$$

This implies that if the cutoff is decreased by a factor of b^p such that $p \arctan h = n\pi$, where n is an integer, the coupling constant g_{N-p} returns to its original value g_N. This implies that the low-energy behavior of the system is characterized by as asymptotic discrete scaling symmetry with discrete scaling factor

$$\lambda_0 = b^{\pi/\arctan(h)}. \tag{55}$$

When the continuum limit is taken, it is convenient to take $h \to 0$ along with $b \to 1$ in such a way that λ_0 remains fixed. In this case, the positive-energy spectrum approaches a continuum while the negative-energy spectrum remains discrete with an accumulation point at $E = 0$ as illustrated in Fig. 13(c). As the accumulation point is approached, the ratio of adjacent negative energy levels approaches λ_0. The spectrum is characterized by an asymptotic discrete scaling symmetry with discrete scaling factor λ_0. In the continuum limit, g becomes a function of the ultraviolet cutoff Λ, and the discrete RG transformation in Eq. (54) becomes a continuous RG flow:

$$\arctan \frac{g(\Lambda)}{h} = \arctan \frac{g(\Lambda_0)}{h} - \frac{\pi}{\ln \lambda_0} \ln \frac{\Lambda}{\Lambda_0}. \tag{56}$$

The coupling constant $g(\Lambda)$ is a periodic function of $\ln(\Lambda)$. Thus the renormalization of $g(\Lambda)$ is governed by a limit cycle with a discrete scaling factor λ_0. The behavior of $g(\Lambda)$ is illustrated in Fig. 14 for the case $g(\Lambda_0)/h = 1$ and $\lambda_0 = 2$. As Λ decreases, $g(\Lambda)$ increases eventually to $+\infty$, jumps discontinuously to $-\infty$, and then continues increasing. The discontinuous behavior of the coupling constant is easy to understand. When the ultraviolet cutoff is decreased to a value Λ, not only are positive energy states with energies $E > \Lambda$ removed from the spectrum, but negative energy eigenvalues with $E_n < -\Lambda$ are also removed. The discontinuous change in $g(\Lambda)$ from $+\infty$ to $-\infty$ occurs when Λ is decreased through $|E_n|$, where E_n is a negative eigenvalue. The discontinuous change in $g(\Lambda)$ is necessary to compensate for the effects at low energy of the discrete state with negative energy E_n that has been removed from the spectrum.

3.5. Universality for large scattering length

The universal low-energy behavior of atoms with large scattering length has many features in common with critical phenomena. The scattering length a plays a role analogous to the correlation length ξ. The region of large scattering length $|a| \gg \ell$ is analogous to the critical region, and the resonant limit where a diverges is analogous to the critical point. In the critical region, $|a|$ is the most important length scale for low-energy observables. It would be the only important length scale if it were not for the logarithmic scaling violations associated with short-distance singularities in the 3-body sector in the scaling limit. These logarithmic scaling violations make the universal behavior of atoms with large scattering length richer and more complex in some ways than standard critical phenomena.

We now give a few specific examples of universality in atoms with large scattering length. In the 2-body sector, the universal predictions are very simple. They are described in detail in Section 4. The simplest example is that for positive a, there is a shallow 2-body bound state that we call the *dimer* whose binding energy in the scaling limit is given by Eq. (2). In the 3-body sector, the universal predictions are more complex. They are described in detail in Section 6. The simplest example comes from the asymptotic behavior of the spectrum of Efimov states in the resonant limit given in Eq. (3). This spectrum has an asymptotic discrete scaling symmetry with discrete scaling factor e^{π/s_0}. Another example is the universal expression for the atom–dimer scattering length in Eq. (39). The scaling behavior $a_{\rm AD} \sim a$ expected from dimensional analysis is violated by the logarithmic dependence of the coefficient on a. Thus there are logarithmic scaling violations. A remarkable feature of the coefficient is that it is a log-periodic function of a that is invariant under the discrete scaling symmetry in Eq. (43). This discrete scaling symmetry is a signature of a RG limit cycle.

The connection between the Efimov effect and RG limit cycles was first realized in Ref. [60]. The connection was made manifest by Bedaque, Hammer, and van Kolck in their formulation of the problem of identical bosons in terms of effective field theory [61,62], although they did not use the phrase "limit cycle" initially. Their effective-field-theory formulation will be described in Section 8. Some renormalization group aspects of the limit cycle in the 3-body problem with large scattering length were discussed in Refs. [63–66].

We will sketch briefly how one could approach the problem of low energy atoms with large scattering length from a renormalization group perspective. Our starting point is a Hamiltonian $\mathscr{H}_0$ that describes identical bosons interacting through a short-range 2-body potential $V_0(r)$. We imagine constructing a renormalization group transformation that eliminates the interaction energy for configurations in which the atoms approach to within a short distance $1/\Lambda$ while leaving low-energy observables invariant. The low-energy observables include the binding energies and scattering amplitudes for states for which the total energy per atom in any isolated cluster of N atoms satisfies $|E|/N \ll \hbar^2\Lambda^2/m$, where $E = 0$ is the energy of atoms at rest with infinite separations. In the 2-body sector, the resulting interaction between atoms can be described by a potential $V(r;\Lambda)$ that agrees with $V_0(r)$ at long distances $r \gg 1/\Lambda$ but vanishes at short distances $r \ll 1/\Lambda$. At intermediate distances $r \sim 1/\Lambda$, the potential $V(r;\Lambda)$ must be adjusted so that it gives the same spectrum as $V_0(r)$ for 2-body bound states with binding energies $E_2 \ll \hbar^2\Lambda^2/m$ and the same scattering phase shifts $\delta_\ell(k)$ as $V_0(r)$ for wave numbers $k \ll \Lambda$. In the 3-body sector, the potential $V(r;\Lambda)$ will compensate for the absence of interaction energy for configurations in which one pair of atoms has a small separation $r_{12} \ll 1/\Lambda$ and the third atom is well-separated from the pair. However, it will not completely compensate for the absence of interaction energy for configurations in which all three atoms have small separations $r_{ij} \ll 1/\Lambda$. To compensate for these configurations, it will be necessary to include a 3-body potential $V(\boldsymbol{r}_1, \boldsymbol{r}_2, \boldsymbol{r}_3; \Lambda)$ that vanishes when any pair of atoms has a small separation $r_{ij} \ll 1/\Lambda$. In the region where all three atoms have intermediate separation $r_{ij} \sim 1/\Lambda$, the potential must be adjusted so that 3-body observables with low energies satisfying $|E| \ll \hbar^2\Lambda^2/m$ agree with those for the original Hamiltonian with the 2-body potential $V_0(r)$ only. Similarly, to compensate for the absence of interaction energy for N-body configurations in which all atoms have separations $r_{ij} \ll 1/\Lambda$, it is necessary to include an N-body potential $V(\boldsymbol{r}_1, \boldsymbol{r}_2, \ldots, \boldsymbol{r}_N; \Lambda)$ that is adjusted to make low-energy N-body observables agree with those of the original Hamiltonian.

Thus the RG flow corresponding to decreasing Λ carries the original Hamiltonian defined by the 2-body potential $V_0(r)$ into a larger space of Hamiltonians defined by N-body potentials for all N. We suggest that the RG flow must have a limit cycle in this larger space of Hamiltonians. In the resonant limit, the spectrum of Efimov states satisfies Eq. (38). It has an asymptotic scaling symmetry with scaling factor $\lambda_0 = e^{\pi/s_0}$. It is therefore plausible that tuning to the resonant limit corresponds to tuning the 2-body potential $V_0(r)$ to the critical trajectory for an infrared limit cycle in the space of Hamiltonians defined by short-range N-body potentials for all N. As the momentum scale Λ is

decreased, 3-body bound states with binding energies $E_T > \hbar^2\Lambda^2/m$ are eliminated from the spectrum. The spectrum of the remaining 3-body bound states approaches closer and closer to the corresponding state in a spectrum with an exact discrete scaling symmetry:

$$E_T^{(n)} = (e^{-2\pi/s_0})^{n-n_*}\hbar^2\kappa_*^2/m \quad \text{for all } n \text{ with } a = \pm\infty,\ \ell = 0. \tag{57}$$

Such a spectrum is characteristic of an RG limit cycle.

The resonant ($a \to \pm\infty$) and scaling ($\ell \to 0$) limits have simple interpretations in terms of the renormalization group limit cycle. In the subspace of Hamiltonians defined by 2-body potentials $V_0(r)$, there is a subspace of potentials that lie on critical trajectories that flow asymptotically to the limit cycle in the infrared limit. The resonant limit corresponds to tuning the potential to one of these critical trajectories. The RG flow will then carry the Hamiltonian asymptotically to the limit cycle as $\Lambda \to 0$. One of the signatures of the infrared limit cycle is that there are infinitely many arbitrarily-shallow 3-body bound states with an asymptotic discrete scaling symmetry as in Eq. (38). The scaling limit corresponds to tuning the potential $V_0(r)$ to a critical trajectory that flows asymptotically to the limit cycle in the ultraviolet limit. One of the signatures of the ultraviolet limit cycle is that there are infinitely many, arbitrarily-deep 3-body bound states with an asymptotic discrete scaling symmetry as in Eq. (41). Taking the resonant limit and the scaling limit simultaneously corresponds to tuning the Hamiltonian to the limit cycle itself. A signature of the limit cycle is the exact discrete scaling symmetry in Eq. (57).

4. Universality for two identical bosons

In this section, we describe the universal aspects of the 2-body problem for identical bosons with large scattering length. We exhibit a trivial scaling symmetry that relates the 2-body observables for different values of the scattering length. We also discuss the leading scaling violations associated with the effective range.

4.1. Atom–atom scattering

One of the universal 2-body observables is the cross section for low-energy atom–atom scattering. By low energy, we mean energies $E = \hbar^2k^2/m$ much smaller than the natural ultraviolet cutoff $\hbar^2/m\ell^2$, which means that the wave number satisfies $k \ll 1/\ell$. The partial wave expansion in Eq. (12) expresses the scattering amplitude in terms of phase shifts $\delta_L(k)$. The natural magnitude for the coefficients in the low-energy expansion of $k\cot\delta_L(k)$ is ℓ raised to the power required by dimensional analysis. In the scaling limit, all these coefficients vanish with the exception of the scattering length. The S-wave phase shift $\delta_0(k)$ is given in Eq. (40). The scattering amplitude in Eq. (12) reduces to

$$f_k(\theta) = \frac{1}{-1/a - ik}, \tag{58}$$

and the differential cross section in Eq. (7) is

$$\frac{d\sigma_{AA}}{d\Omega} = \frac{4a^2}{1 + a^2k^2}. \tag{59}$$

The cross section is obtained by integrating over the solid angle 2π. The differential cross section in Eq. (59) is shown in Fig. 15. For very low wave numbers $k \ll 1/|a|$, it reduces to the constant $4a^2$. For wave numbers $k \gg 1/|a|$, it has the scale-invariant form $4/k^2$, which saturates the upper bound from partial-wave unitarity in the $L = 0$ channel.

The wave function for atom–atom scattering states at separations $r \gg \ell$ is also universal. The stationary wave function in the center-of-mass frame for two atoms in an $L = 0$ state with energy $E = \hbar^2k^2/m$ is

$$\psi_{AA}(\boldsymbol{r}) = \frac{1}{kr}\sin[kr + \delta_0(k)]. \tag{60}$$

For all other angular momentum quantum numbers L, the phase shifts vanish in the scaling limit. The wave function associated with the scattering of two identical bosons with wave numbers $\pm\boldsymbol{k}$ is

$$\psi_{AA}(\boldsymbol{r}) = \cos(\boldsymbol{k}\cdot\boldsymbol{r}) - \frac{1}{1/a + ik}\,\frac{e^{ikr}}{r}. \tag{61}$$

Projecting onto $L = 0$ by averaging over the angles of $\boldsymbol{r}$, we recover the wave function in Eq. (60) up to a phase.

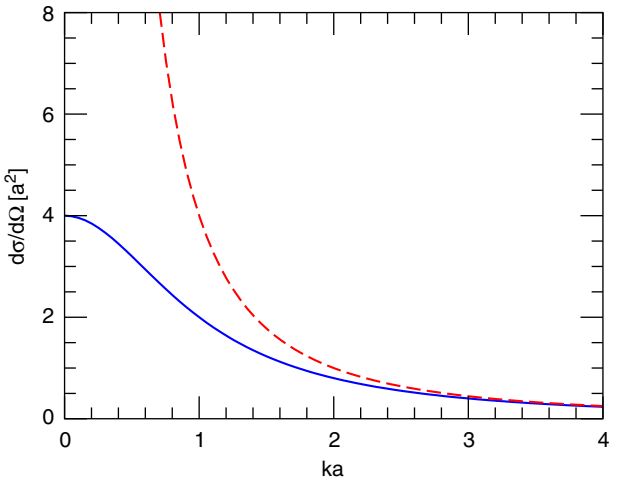

Fig. 15. Differential cross section for atom–atom scattering as a function of ka (solid line). The dashed line is the unitarity bound $4/k^2$.

4.2. The shallow dimer

Another universal observable is the spectrum of shallow 2-body bound states. By a *shallow bound state*, we mean one with binding energy $E_{\rm D}$ much smaller than the natural ultraviolet cutoff $\hbar^2/m\ell^2$. The spectrum of shallow 2-body bound states is very simple. For $a<0$, there are no shallow bound states. For $a>0$, there is a single shallow bound state, which we will refer to as the *shallow dimer*, or simply as the *dimer* for brevity. The binding energy $E_{\rm D}$ of the dimer can be deduced by inserting the expression for the phase shift in Eq. (40) into the bound-state equation (17):

$$E_{\rm D} = \frac{\hbar^2}{ma^2}. \tag{62}$$

The wave function of the dimer at separations $r \gg \ell$ is also universal. The unnormalized coordinate-space wave function is

$$\psi_D(\boldsymbol{r}) = \frac{1}{r} e^{-r/a}, \tag{63}$$

where $r = |\boldsymbol{r}|$ is the separation of the two atoms. The normalized probability distribution for the separation r of the atoms in the shallow dimer is shown in Fig. 16. The size of the dimer is roughly a. A quantitative measure of the size is the mean-square separation of the atoms:

$$\langle r^2 \rangle = a^2/2. \tag{64}$$

The momentum-space wave function for the dimer is

$$\psi_D(\boldsymbol{k}) = \frac{4\pi}{k^2 + 1/a^2}, \tag{65}$$

where $\boldsymbol{k}$ is the relative wave number of the two atoms. Thus the typical scale of the relative wave number is $1/a$.

4.3. Continuous scaling symmetry

The simple expressions for the cross-section in Eq. (59) and the binding energy in Eq. (62) depend only on the scattering length. The fact that low-energy observables depend only on a single parameter a with dimensions of length can be expressed formally in terms of a continuous scaling symmetry. Under this symmetry, the scattering length a and kinematic variables such as the energy E are scaled by appropriate powers of a positive real number λ:

$$a \longrightarrow \lambda a, \quad E \longrightarrow \lambda^{-2} E. \tag{66}$$

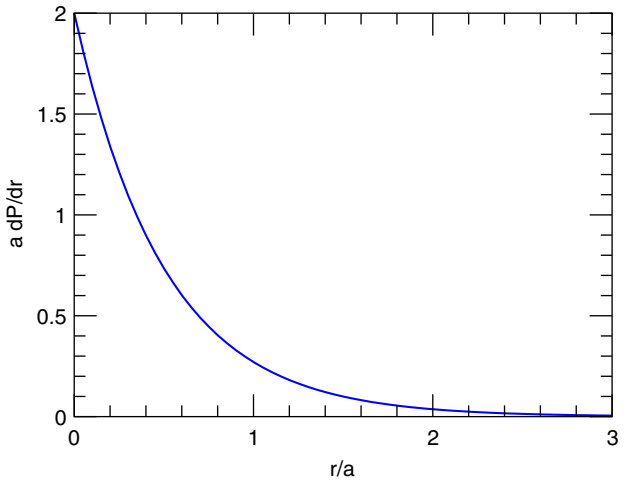

Fig. 16. Normalized probability distribution $\mathrm{d}P/\mathrm{d}r$ for the separation r of the atoms in the shallow dimer as a function of r/a.

Under this symmetry, observables, such as the dimer binding energy E_{D} or the atom–atom cross section σ_{AA}, scale with the powers of λ suggested by dimensional analysis.

The scaling symmetry strongly constrains the dependence of the observables on the scattering length and on kinematic variables. As a simple example, consider the dimer binding energy, which scales as $E_{\mathrm{D}} \to \lambda^{-2} E_{\mathrm{D}}$. The scaling symmetry constrains its dependence on the scattering length:

$$E_{\mathrm{D}}(\lambda a) = \lambda^{-2} E_{\mathrm{D}}(a). \tag{67}$$

This implies that E_{D} is proportional to $1/a^2$, in agreement with the explicit formula in Eq. (62). As another example, consider the atom–atom cross section, which scales as $\sigma_{\mathrm{AA}} \to \lambda^2 \sigma_{\mathrm{AA}}$. The scaling symmetry constrains its dependence on the scattering length and the energy:

$$\sigma_{\mathrm{AA}}(\lambda^{-2} E; \lambda a) = \lambda^2 \sigma_{\mathrm{AA}}(E; a). \tag{68}$$

The explicit expression for the differential cross section in Fig. (59) is consistent with this constraint.

The set of all possible low-energy 2-body states in the scaling limit can be represented as points (a^{-1}, K) on the plane whose horizontal axis is $1/a$ and whose vertical axis is the wave number variable

$$K = \mathrm{sign}(E)(m|E|/\hbar^2)^{1/2}. \tag{69}$$

It is convenient to also introduce polar coordinates consisting of a radial variable H and an angular variable ξ defined by

$$1/a = H \cos\xi, \quad K = H \sin\xi. \tag{70}$$

We choose ξ to be 0 on the positive a axis and to have a discontinuity with values $\pm\pi$ on the negative a^{-1} axis. In terms of these polar coordinates, the scaling symmetry given by Eqs. (66) is simply a rescaling of the radial variable: $H \to \lambda^{-1} H$.

The a^{-1}–K plane for the 2-body system in the scaling limit is shown in Fig. 17. The possible states are atom–atom scattering states and the shallow dimer. The quadrants in which there are atom–atom scattering states are labelled AA. The threshold for atom–atom scattering states is indicated in Fig. 17 by the hatched area. The shallow dimer lies along the ray $\xi = -\frac{1}{4}\pi$, which is indicated by the heavy line labelled D. A given physical system has a specific value of the scattering length, and so is represented by a vertical line. Changing a corresponds to sweeping the line horizontally across the page. The continuum of atom–atom scattering states is represented by the points on the vertical line that lie in the upper-half plane. If $a > 0$, there is also a discrete bound state (the shallow dimer) lying on the intersection of the vertical line with the ray $\xi = -\frac{1}{4}\pi$. The resonant limit corresponds to tuning the vertical line to the K axis.

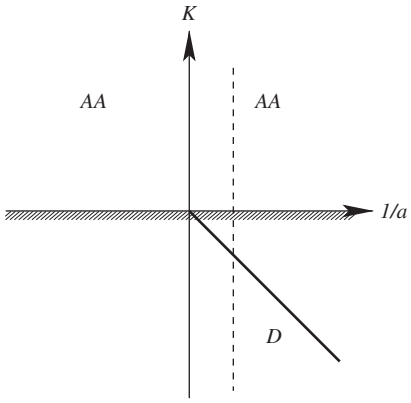

Fig. 17. The a^{-1}–K plane for the 2-body problem. The allowed region for atom–atom scattering states are the two quadrants labelled AA. The heavy line labelled D is the shallow dimer. The cross-hatching indicates the 2-atom threshold.

4.4. Scaling violations

The scaling symmetry given by Eqs. (66) is reflected in the scaling behavior of the universal expressions for 2-body observables. The differential cross section in Eq. (59) scales like a^2 with a coefficient that is a function of ka. The dimer binding energy in Eq. (62) scales like a^{-2}. If the natural low-energy length scale ℓ is nonzero, there are scaling violations that give corrections to the universal expressions that decrease as powers of $\ell/|a|$ when $a \to \pm\infty$.

The leading scaling violations decrease as a single power of $\ell/|a|$. They come from the S-wave effective range r_s defined by the effective-range expansion in Eq. (15). We can deduce the leading scaling violations to the differential cross section by truncating the effective-range expansion in Eq. (15) after the k^2 term:

$$k \cot \delta_0(k) = -1/a + \tfrac{1}{2} r_s k^2. \tag{71}$$

This approximation to the 2-body problem is called the *effective-range theory* [11,67,68]. The expression for the differential cross section in Eq. (7) then becomes

$$\frac{\mathrm{d}\sigma}{\mathrm{d}\Omega} = \frac{4a^2}{(1 - \frac{1}{2} r_s a k^2)^2 + a^2 k^2}. \tag{72}$$

If $k \ll 1/|r_s|$, this can be expanded in powers of r_s:

$$\frac{\mathrm{d}\sigma}{\mathrm{d}\Omega} = \frac{4a^2}{1 + a^2 k^2} \left(1 + \frac{r_s}{a} \frac{a^2 k^2}{1 + a^2 k^2} + \frac{r_s^2}{a^2} \frac{a^4 k^4 (3 - a^2 k^2)}{4(1 + a^2 k^2)^2} + \cdots \right). \tag{73}$$

The leading term is the universal expression in Eq. (59). For $k \sim 1/|a|$, the next-to-leading term is suppressed by $r_s/|a|$. For small wave numbers $k \ll 1/|a|$, there is an additional suppression factor of $(ka)^2$.

We can study the leading scaling violations to the binding energy of the shallow dimer by inserting the truncated effective-range expansion in Eq. (71) into Eq. (17). The binding energy equation then reduces to a quadratic equation:

$$-1/a - \tfrac{1}{2} r_s \kappa^2 + \kappa = 0. \tag{74}$$

A positive real-valued solution κ to the binding energy equation corresponds to a bound state with binding energy $E_2 = \hbar^2 \kappa^2 / m$. The two solutions to the quadratic equation (74) are

$$\kappa^{(\pm)} = \left(1 \pm \sqrt{1 - 2 r_s / a} \right) \frac{1}{r_s}. \tag{75}$$

Assuming that the scattering length is large, the two solutions are both real-valued. The asymptotic solutions in the limit $|r_s| \ll |a|$ are

$$\kappa^{(+)} \longrightarrow 2/r_s, \tag{76a}$$

$$\kappa^{(-)} \longrightarrow 1/a. \tag{76b}$$

The solution $\kappa^{(+)}$ is positive and corresponds to a deep bound state if $r_s > 0$, while $\kappa^{(-)}$ is positive and corresponds to a shallow bound state if $a > 0$.

If $a > 0$, the binding energy for the shallow bound state is obtained by inserting the solution $\kappa^{(-)}$ in Eq. (75) into Eq. (16):

$$E_2^{(-)} = \frac{\hbar^2}{mr_s^2}\left(1 - \sqrt{1 - 2r_s/a}\right)^2. \tag{77}$$

In the limit $|r_s| \gg a$, this reduces to the universal expression in Eq. (62). The expansion of the binding energy in powers of the effective range is

$$E_2^{(-)} \approx \frac{\hbar^2}{ma^2}\left(1 + \frac{r_s}{a} + \frac{5r_s^2}{4a^2} + \cdots\right). \tag{78}$$

Thus the leading scaling violation is linear in r_s/a.

One can study higher-order scaling violations by considering the effects of higher-order terms in the low-momentum expansion of the scattering amplitudes. If the k^4 term in the effective-range expansion in Eq. (15) has a natural coefficient $P_s \sim \ell^3$, the corresponding correction to the universal differential cross section in Eq. (59) is suppressed by a factor $k^4 a \ell^3$, which is of order $(\ell/a)^3$ if $k \sim 1/|a|$. For identical bosons, there is no P-wave ($L = 1$) term in the partial wave expansion. The leading contribution to the differential cross section from higher partial waves $L \geqslant 2$ comes from interference with the $L = 0$ term and is suppressed by a factor $(k\ell)^{2L}\ell/|a|$, which is of order $(\ell/a)^{2L+1}$ for $k \sim 1/|a|$. Thus the scaling violations of order ℓ/a and ℓ^2/a^2 in the differential cross section are completely determined by the effective range r_s and are given in Eq. (73). The correction to the dimer binding energy in Eq. (62) from a k^4 term in the effective-range expansion in Eq. (15) is suppressed by ℓ^3/a^3. Thus the scaling violations of order ℓ/a and ℓ^2/a^2 in the dimer binding energy are completely determined by the effective range r_s and are given in Eq. (78).

If $r_s > 0$, the solution $\kappa^{(+)}$ in Eq. (75) to the binding energy equation (74) corresponds to a deep (tightly-bound) diatomic molecule with binding energy

$$E_2^{(+)} \approx 4\hbar^2/(mr_s^2). \tag{79}$$

Its binding energy is of order $\hbar^2/m\ell^2$. By considering higher orders terms in the low-momentum expansion of $k \cot \delta_0(k)$, such as the k^4 term in Eq. (15), one can easily show that there can be other contributions to the binding energy of order $\hbar^2/m\ell^2$. Thus there is nothing universal about the expression for the binding energy $E_2^{(+)}$, or even the existence of that deep bound state. It is simply an artifact of the model defined by truncating the effective-range expansion after the k^2 term in Eq. (15).

4.5. Theoretical approaches

Historically, the idea of universality has its roots in nuclear physics. Early on, it was realized that the deuteron is large compared to the range of the nuclear force. Similarly, the spin-singlet S-wave scattering length of two nucleons was found to be large compared to the range. Starting in the 1930's, these observations lead to the development of various theoretical approaches to exploit this separation of length scales. In the following, we will give a brief overview of these techniques. For a more detailed discussion, see Ref. [69].

The *boundary condition method* was first used by Bethe and Peierls [70–72]. For short-range interactions, the two-particle wave function is governed by the free Schrödinger equation, except for particle separations of the order of the range or less. The effect of the interactions at short distances can be taken into account through a boundary condition

on the wave function as the separation vector $\boldsymbol{r}$ goes to zero:

$$\psi(\boldsymbol{r}) \longrightarrow C\left(\frac{1}{r}-\frac{1}{a}\right) \quad \text{as } r \to 0, \tag{80}$$

where C is a constant. Together with the free Schrödinger equation for large r, Eq. (80) determines the long-distance wave function completely. Note that the scattering wave function in Eq. (60) and the dimer wave function in Eq. (63) satisfy the boundary condition in Eq. (80) with $C=-a/(1+a^2k^2)^{1/2}$ and $C=1$, respectively.

An alternative way to introduce a boundary condition on the wave function is the *pseudopotential method* [72,73]. It involves replacing the potential $V(r)$ in the Schrödinger equation by a *pseudopotential* that acts on the wave function $\psi(\boldsymbol{r})$ for the separation vector of the two particles as

$$V(r)\psi(\boldsymbol{r}) = \frac{4\pi\hbar^2 a}{m}\delta^3(\boldsymbol{r})\frac{\partial}{\partial r}(r\psi(\boldsymbol{r})). \tag{81}$$

The Schrödinger equation with this pseudopotential is equivalent to the free Schrödinger equation for $\boldsymbol{r}\neq 0$ supplemented by the boundary condition

$$\lim_{r\to 0} r^2\frac{\partial}{\partial r}\psi(\boldsymbol{r}) = a\lim_{r\to 0}\frac{\partial}{\partial r}(r\psi(\boldsymbol{r})). \tag{82}$$

This boundary condition is equivalent to that in Eq. (80).

A third method to exploit universality in the two-body problem is the *effective-range expansion* [11,67,68], which was already discussed in Section 4.4. For short-range potentials, $k\cot\delta_0(k)$ is an analytic function of the energy E and it can therefore be expanded as a power series in k^2 as in Eq. (71). Truncating this expansion after the energy-independent scattering length term $-1/a$ is equivalent to the boundary condition and pseudopotential methods discussed above. The description of the phase shifts can be improved by including higher order terms in the effective-range expansion.

The *effective field theory* method, which is discussed in detail in Section 8, is another method that can be used to exploit universality [74,75]. All three methods discussed above can be related within an effective field theory for short-range forces [69]. In particular, the effective-range expansion is reproduced order by order in k^2 within an effective field theory with contact interactions. (See Section 8.) Effective field theory is particularly convenient for calculating corrections to universality systematically and for calculating the effects of electromagnetic and weak interactions for charged particles.

5. Hyperspherical formalism

In this section, we introduce hyperspherical coordinates, develop the hyperspherical formalism for the low-energy 3-body problem, and use it to derive the Efimov effect. We will start out with the general formalism, but later focus on the sector with zero total angular momentum.

5.1. Hyperspherical coordinates

The universal aspects of the 3-body problem can be understood most easily by formulating it in terms of *hyperspherical coordinates*. A good introduction to hyperspherical coordinates and a thorough review of the hyperspherical formalism is given in a recent review article by Nielsen et al. [76].

In order to define hyperspherical coordinates, we first introduce Jacobi coordinates. A set of Jacobi coordinates consists of the separation vector $\boldsymbol{r}_{ij}$ between a pair of atoms and the separation vector $\boldsymbol{r}_{k,ij}$ of the third atom from the center-of-mass of the pair. For atoms of equal mass, the Jacobi coordinates are

$$\boldsymbol{r}_{ij} = \boldsymbol{r}_i - \boldsymbol{r}_j, \quad \boldsymbol{r}_{k,ij} = \boldsymbol{r}_k - \tfrac{1}{2}(\boldsymbol{r}_i + \boldsymbol{r}_j). \tag{83}$$

In Fig. 18, we illustrate one of the three possible sets of Jacobi coordinates. The *hyperradius* R is the root-mean-square separation of the three atoms:

$$R^2 = \tfrac{1}{3}(r_{12}^2 + r_{23}^2 + r_{31}^2) = \tfrac{1}{2}r_{ij}^2 + \tfrac{2}{3}r_{k,ij}^2. \tag{84}$$

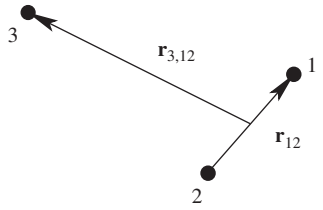

Fig. 18. One of the three possible sets of Jacobi coordinates defined in Eqs. (83).

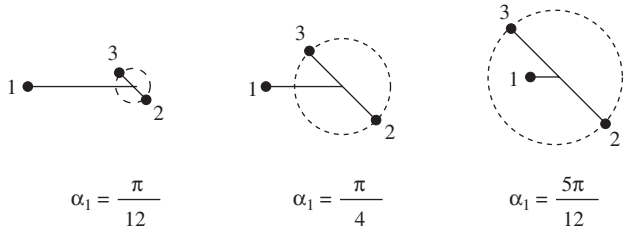

Fig. 19. Three-body configurations with the same hyperradius R but different hyperangles: $\alpha_1 = \pi/12$, $\pi/4$, and $5\pi/12$. Any configuration with atoms 2 and 3 at the endpoints of a diameter of the dashed circle will have the same values of R and α as the one shown.

The hyperradius is small only if all three atoms are close together. It is large if any single atom is far from the other two. The *Delves hyperangle* [77] α_k is defined by

$$\alpha_k = \arctan\left(\frac{\sqrt{3}r_{ij}}{2r_{k,ij}}\right), \tag{85}$$

where (i, j, k) is a permutation of $(1, 2, 3)$. The range of the hyperangle α_k is from 0 to $\frac{1}{2}\pi$. It is near 0 when atom k is far from atoms i and j, and it is near $\frac{1}{2}\pi$ when atom k is near the center of mass of atoms i and j. The magnitudes of the separation vectors can be expressed as

$$r_{ij} = \sqrt{2}R\sin\alpha_k, \quad r_{k,ij} = \sqrt{3/2}R\cos\alpha_k. \tag{86}$$

Examples of 3-body configurations with the same hyperradius R but different hyperangles are illustrated in Fig. 19. The definition in Eq. (85) expresses the hyperangle α_k in terms of the Jacobi coordinates $\boldsymbol{r}_{ij}$ and $\boldsymbol{r}_{k,ij}$ defined in Eqs. (83). The other two hyperangles can also be expressed as functions of those Jacobi coordinates:

$$\sin^2\alpha_i = \tfrac{1}{4}\sin^2\alpha_k + \tfrac{3}{4}\cos^2\alpha_k + \tfrac{1}{2}\sqrt{3}\sin\alpha_k\cos\alpha_k\hat{\boldsymbol{r}}_{ij}\cdot\hat{\boldsymbol{r}}_{k,ij}, \tag{87}$$

where (i, j, k) is a permutation of $(1, 2, 3)$. For fixed α_k, the range of α_i is

$$|\tfrac{1}{3}\pi - \alpha_k| < \alpha_i < \tfrac{1}{2}\pi - |\tfrac{1}{6}\pi - \alpha_k|. \tag{88}$$

The consistency with Eq. (87) can be verified by applying the function $\sin^2$ to each term. Using Eq. (87), we can also derive the simple identity

$$\sin^2\alpha_1 + \sin^2\alpha_2 + \sin^2\alpha_3 = \tfrac{3}{2}. \tag{89}$$

The volume element for the Jacobi coordinates can be written

$$d^3r_{ij}d^3r_{k,ij} = \frac{3\sqrt{3}}{4}R^5\,\mathrm{d}R\sin^2(2\alpha_k)\,\mathrm{d}\alpha_k\,\mathrm{d}\Omega_{ij}\,\mathrm{d}\Omega_{k,ij}, \tag{90}$$

where $\mathrm{d}\Omega_{ij}$ and $\mathrm{d}\Omega_{k,ij}$ are the differential solid angles for the unit vectors $\hat{\boldsymbol{r}}_{ij}$ and $\hat{\boldsymbol{r}}_{k,ij}$.

The Schrödinger equation for the stationary wave function $\Psi(\boldsymbol{r}_1, \boldsymbol{r}_2, \boldsymbol{r}_3)$ of three atoms with mass m interacting through a potential V is

$$\left(-\frac{\hbar^2}{2m} \sum_{i=1}^{3} \nabla_i^2 + V(\boldsymbol{r}_1, \boldsymbol{r}_2, \boldsymbol{r}_3) \right) \Psi = E\Psi. \tag{91}$$

If the interaction potential V is translation invariant, it depends only on 6 independent coordinates. The wave function Ψ in the center-of-mass frame also depends on only 6 independent coordinates. A convenient choice consists of the hyperradius R, one of the hyperangles α_k, and the unit vectors $\hat{\boldsymbol{r}}_{ij}$ and $\hat{\boldsymbol{r}}_{k,ij}$. We will refer to the five dimensionless variables $(\alpha_k, \hat{\boldsymbol{r}}_{ij}, \hat{\boldsymbol{r}}_{k,ij})$ as hyperangular variables and denote them collectively by Ω. When expressed in terms of hyperspherical coordinates, the Schrödinger equation for the wave function in the center-of-mass frame reduces to

$$\left(T_R + T_{\alpha_k} + \frac{\Lambda_{k,ij}^2}{2mR^2} + V(R, \Omega) \right) \Psi = E\Psi, \tag{92}$$

where T_R is the hyperradial kinetic energy operator,

$$T_R = -\frac{\hbar^2}{2m} \left[\frac{\partial^2}{\partial R^2} + \frac{5}{R} \frac{\partial}{\partial R} \right] \tag{93a}$$

$$= \frac{\hbar^2}{2m} R^{-5/2} \left[-\frac{\partial^2}{\partial R^2} + \frac{15}{4R^2} \right] R^{5/2}, \tag{93b}$$

T_{α_k} is the kinetic energy operator associated with the hyperangle α_k,

$$T_\alpha = -\frac{\hbar^2}{2mR^2} \left[\frac{\partial^2}{\partial \alpha^2} + 4\cot(2\alpha) \frac{\partial}{\partial \alpha} \right] \tag{94a}$$

$$= \frac{\hbar^2}{2mR^2} \frac{1}{\sin(2\alpha)} \left[-\frac{\partial^2}{\partial \alpha^2} - 4 \right] \sin(2\alpha), \tag{94b}$$

and $\Lambda_{k,ij}^2$ is a generalized angular momentum operator:

$$\Lambda_{k,ij}^2 = \frac{\boldsymbol{L}_{ij}^2}{\sin^2\alpha_k} + \frac{\boldsymbol{L}_{k,ij}^2}{\cos^2\alpha_k}. \tag{95}$$

The operators $\boldsymbol{L}_{ij}$ and $\boldsymbol{L}_{k,ij}$ are the conventional angular momentum operators associated with the vectors $\boldsymbol{r}_{ij}$ and $\boldsymbol{r}_{k,ij}$, respectively.

A convenient way to solve the Schrödinger equation in hyperspherical coordinates is to use the *adiabatic hyperspherical representation*. For each value of R, the wave function $\Psi(R, \Omega)$ is expanded in terms of a complete set of hyperangular functions $\Phi_n(R, \Omega)$:

$$\Psi(R, \Omega) = R^{-5/2} \sum_n f_n(R) \Phi_n(R, \Omega). \tag{96}$$

The functions $\Phi_n(R, \Omega)$ are solutions to a differential eigenvalue equation in the hyperangular variables:

$$[T_{\alpha_k} + \Lambda_{k,ij}^2/(2mR^2) + V(R, \Omega)] \Phi_n(R, \Omega) = V_n(R) \Phi_n(R, \Omega). \tag{97}$$

The hyperradius R is treated as a parameter and the eigenvalue $V_n(R)$ is a function of that parameter. It can be interpreted as an effective potential for the channel associated with the hyperangular function Φ_n. The orthonormality condition on the hyperangular functions can be written as

$$\int \mathrm{d}\Omega \, \Phi_n(R, \Omega)^* \Phi_m(R, \Omega) = \delta_{nm}, \tag{98}$$

where the hyperangular integral is

$$\int d\Omega = \int_0^{(1/2)\pi} d\alpha_k \sin^2(2\alpha_k) \int d\Omega_{ij} \int d\Omega_{k,ij}. \tag{99}$$

Upon using the orthonormality condition to project onto Φ_n, the Schrödinger equation (92) reduces to a coupled set of eigenvalue equations for the hyperradial functions $F_n(R)$:

$$\left[\frac{\hbar^2}{2m}\left(-\frac{\partial^2}{\partial R^2}+\frac{15}{4R^2}\right)+V_n(R)\right] f_n(R) + \sum_m \left[2U_{nm}(R)\frac{\partial}{\partial R}+W_{nm}(R)\right] f_m(R) = E f_n(R), \tag{100}$$

where $U_{nm}(R)$ and $W_{nm}(R)$ are coupling potentials defined by

$$U_{nm}(R) = -\frac{\hbar^2}{2m}\int d\Omega\, \Phi_n(R,\Omega)^* \frac{\partial}{\partial R}\Phi_m(R,\Omega), \tag{101a}$$

$$W_{nm}(R) = -\frac{\hbar^2}{2m}\int d\Omega\, \Phi_n(R,\Omega)^* \frac{\partial^2}{\partial R^2}\Phi_m(R,\Omega). \tag{101b}$$

The off-diagonal coupling potentials generally fall off more rapidly at large distances than the hyperspherical potentials by a factor of $1/R^2$ [76]. In the low-energy limit, the off-diagonal terms in Eq. (100) are therefore small compared to the diagonal terms. If the off-diagonal terms are neglected, the set of eigenvalue equations decouple:

$$\left[\frac{\hbar^2}{2m}\left(-\frac{\partial^2}{\partial R^2}+\frac{15}{4R^2}\right)+V_n(R)+2U_{nn}(R)\frac{\partial}{\partial R}+W_{nn}(R)\right] f_n(R) = E f_n(R). \tag{102}$$

This approximation is called the *adiabatic hyperspherical approximation*. It was first introduced by Macek in 1968 [78]. In many cases, the diagonal coupling terms are also small compared to the hyperspherical potential $V_n(R)$. The eigenvalue equations then reduce to radial Schrödinger equations in the hyperspherical potentials. One advantage to keeping the diagonal coupling potentials is that the adiabatic hyperspherical approximation is then a variational approximation [79].

5.2. Low-energy Faddeev equation

One disadvantage of the 3-body Schrödinger equation is that it does not take advantage of simplifications associated with configurations consisting of a 2-body cluster that is well-separated from the third atom. The *Faddeev* equations are an equivalent set of equations that exploit these simplifications. We will use the Faddeev equations together with a restriction to total angular momentum zero and some further approximations that can be justified at low energy to reduce the 3-body problem to a set of coupled integro-differential equations in one variable, the hyperradius R. We follow closely the treatment of Fedorov and Jensen in Ref. [80].

We make the simplifying assumption that the potential V can be expressed as the sum of three 2-body potentials, each of which depends only on the separation r_{ij} of a pair of atoms:[5]

$$V(\boldsymbol{r}_1,\boldsymbol{r}_2,\boldsymbol{r}_3) = V(r_{12}) + V(r_{23}) + V(r_{31}). \tag{103}$$

We use the same symbol V for the total potential and the 2-body potential, distinguishing them by the context and by the number of arguments. The assumption in Eq. (103) is milder than it appears, because even if the potential includes intrinsically 3-body terms at short distances, their universal effects at low-energy can be reproduced by a sum of pair-wise terms.

The *Faddeev equations* are a set of equations that generate solutions to the 3-body Schrödinger equation of the form [82]

$$\Psi(\boldsymbol{r}_1,\boldsymbol{r}_2,\boldsymbol{r}_3) = \psi^{(1)}(\boldsymbol{r}_{23},\boldsymbol{r}_{1,23}) + \psi^{(2)}(\boldsymbol{r}_{31},\boldsymbol{r}_{2,31}) + \psi^{(3)}(\boldsymbol{r}_{12},\boldsymbol{r}_{3,12}). \tag{104}$$

[5] One could also include an intrinsically 3-body potential at the cost of a small complication in the formalism. See, e.g., Ref. [81].

The Faddeev equations are

$$\left(T_R + T_{\alpha_1} + \frac{\Lambda_{1,23}^2}{2mR^2}\right)\psi^{(1)} + V(r_{23})(\psi^{(1)} + \psi^{(2)} + \psi^{(3)}) = E\psi^{(1)}, \tag{105}$$

together with the two equations obtained by cyclicly permuting the subscripts and superscripts (1, 2, 3). If $\psi^{(1)}$, $\psi^{(2)}$, and $\psi^{(3)}$ are solutions to this set of equations, then their sum is a solution to the Schrödinger equation (92). If we set $\psi^{(2)} = \psi^{(3)} = 0$ and take $\psi^{(1)}$ to be a function of $\boldsymbol{r}_{23}$ only, the Faddeev equation (105) reduces to the 2-body equation for atoms 2 and 3. Thus the Faddeev wave function $\psi^{(1)}$ can naturally take into account the correlations between atoms 2 and 3 at large hyperradius R when they are both far away from atom 1. Note that nontrivial solutions $\psi^{(1)}$, $\psi^{(2)}$, and $\psi^{(3)}$ of the Faddeev equations can give the trivial solution $\psi^{(1)} + \psi^{(2)} + \psi^{(3)} = 0$ to the Schrödinger equation. Such solutions of the Faddeev equations are called *spurious solutions*.

We restrict our attention to states with total angular momentum quantum number $L = 0$. For a discussion of higher angular momenta, see Refs. [76,83]. We also make an additional simplifying assumption about the form of the wave function. The Faddeev wave function $\psi^{(1)}(\boldsymbol{r}_{23}, \boldsymbol{r}_{1,23})$ can be decomposed into spherical harmonics for the unit vectors $\hat{\boldsymbol{r}}_{23}$ and $\hat{\boldsymbol{r}}_{1,23}$:

$$\psi^{(1)}(\boldsymbol{r}_{23}, \boldsymbol{r}_{1,23}) = \sum_{l_x,m_x}\sum_{l_y,m_y} f^{(1)}_{l_x m_x, l_y m_y}(R, \alpha_1) Y_{l_x m_x}(\hat{\boldsymbol{r}}_{23}) Y_{l_y m_y}(\hat{\boldsymbol{r}}_{1,23}), \tag{106}$$

where l_x, m_x and l_y, m_y are the quantum numbers associated with orbital angular momentum in the 23 and 1, 23 subsystems, respectively. Our simplifying assumption is that the expansion in Eq. (106) is dominated by the $l_x = l_y = 0$ term. Thus we neglect any orbital angular momentum of the subsystems ij or k, ij. This is not an essential assumption, but it greatly simplifies the formalism by avoiding sums over the angular momentum quantum numbers l_x, m_x and l_y, m_y. For a general treatment of the problem including subsystem angular momentum, see Ref. [76]. The simplifying assumption of neglecting subsystem angular momentum is motivated by the general suppression of higher orbital angular momentum at low energies. Ignoring subsystem angular momentum is a better approximation for the Faddeev equations than for the Schrödinger equation. In the Faddeev equations, the coupling between different angular momenta for the subsystems enters only at second order in the 2-body potential V [76], while it enters at first order for the Schrödinger equation.

Given the simplifying assumption of neglecting subsystem angular momentum, the Schrödinger wave function in Eq. (104) for three identical particles reduces to

$$\Psi(\boldsymbol{r}_1, \boldsymbol{r}_2, \boldsymbol{r}_3) = \psi(R, \alpha_1) + \psi(R, \alpha_2) + \psi(R, \alpha_3). \tag{107}$$

The Faddeev equations for the pairwise potential in Eq. (103) then reduce to a particularly simple set of Faddeev equations:

$$(T_R + T_{\alpha_1} - E)\psi(R, \alpha_1) + V(\sqrt{2}R\sin\alpha_1)[\psi(R, \alpha_1) + \psi(R, \alpha_2) + \psi(R, \alpha_3)] = 0, \tag{108}$$

together with the two equations obtained by cyclicly permuting α_1, α_2, and α_3. We can reduce these three equations to a single equation by exploiting the fact that the averages of $\psi(R, \alpha_2)$ and $\psi(R, \alpha_3)$ over the angular variables $\hat{\boldsymbol{r}}_{23}$ and $\hat{\boldsymbol{r}}_{1,23}$ can be expressed as an integral operator acting on $\psi(R, \alpha_1)$:

$$\langle\psi(R, \alpha_2)\rangle_{\hat{\boldsymbol{r}}_{23},\hat{\boldsymbol{r}}_{1,23}} = \langle\psi(R, \alpha_3)\rangle_{\hat{\boldsymbol{r}}_{23},\hat{\boldsymbol{r}}_{1,23}} = \frac{2}{\sqrt{3}}\int_{|(1/3)\pi-\alpha_1|}^{(1/2)\pi-|(1/6)\pi-\alpha_1|} \frac{\sin(2\alpha')}{\sin(2\alpha_1)}\psi(R, \alpha')\,\mathrm{d}\alpha'. \tag{109}$$

The resulting integro-differential equation for $\psi(R, \alpha)$ is

$$(T_R + T_\alpha - E)\psi(R, \alpha) = -V(\sqrt{2}R\sin\alpha)\left[\psi(R, \alpha) + \frac{4}{\sqrt{3}}\int_{|(1/3)\pi-\alpha|}^{(1/2)\pi-|(1/6)\pi-\alpha|} \frac{\sin(2\alpha')}{\sin(2\alpha)}\psi(R, \alpha')\,\mathrm{d}\alpha'\right]. \tag{110}$$

We will refer to this equation as the *low-energy Faddeev equation*.

A convenient way to solve this equation is to use a *hyperspherical expansion*. For each value of R, the wave function $\psi(R,\alpha)$ is expanded in a complete set of functions $\phi_n(R,\alpha)$ of the hyperangle α:

$$\psi(R,\alpha) = \frac{1}{R^{5/2}\sin(2\alpha)} \sum_n f_n(R)\phi_n(R,\alpha). \tag{111}$$

The divergence of the prefactor $1/\sin(2\alpha)$ at the endpoints $\alpha = 0$ and $\frac{1}{2}\pi$ imposes boundary conditions that $\phi_n(R,\alpha)$ must vanish at the endpoints. The functions $\phi_n(R,\alpha)$ are solutions to an integro-differential eigenvalue equation in the single variable α:

$$\left[-\frac{\partial^2}{\partial\alpha^2} - \lambda_n(R)\right]\phi_n(R,\alpha) = -\frac{2mR^2}{\hbar^2}V(\sqrt{2}R\sin\alpha)\left[\phi_n(R,\alpha) + \frac{4}{\sqrt{3}}\int_{|(1/3)\pi-\alpha|}^{(1/2)\pi-|(1/6)\pi-\alpha|}\phi_n(R,\alpha')\,\mathrm{d}\alpha'\right]. \tag{112}$$

The hyperradius R is treated as a parameter and the eigenvalue $\lambda_n(R)$ is a function of that parameter. The eigenvalues $\lambda_n(R)$ in Eq. (112) define channel potentials for the hyperradial variable:

$$V_n(R) = [\lambda_n(R) - 4]\frac{\hbar^2}{2mR^2}. \tag{113}$$

Note that since the operator on the right side of Eq. (112) is not hermitian, hyperangular functions $\phi_m(R,\alpha)$ and $\phi_n(R,\alpha)$ with distinct eigenvalues $\lambda_m(R)$ and $\lambda_n(R)$ need not be orthogonal functions of α. Their inner products define a matrix $G_{nm}(R)$ that depends on R:

$$G_{nm}(R) = \int_0^{(1/2)\pi}\mathrm{d}\alpha\,\phi_n^*(R,\alpha)\phi_m(R,\alpha). \tag{114}$$

By inserting the expansion in Eq. (111) into the low-energy Faddeev equation (110), projecting onto $\phi_n^*(R,\alpha)$, and then multiplying by the inverse of the matrix $G_{nm}(R)$, we obtain a coupled set of eigenvalue equations for the hyperradial wave functions $f_n(R)$:

$$\left[\frac{\hbar^2}{2m}\left(-\frac{\partial^2}{\partial R^2} + \frac{15}{4R^2}\right) + V_n(R)\right]f_n(R) + \sum_m\left[2P_{nm}(R)\frac{\partial}{\partial R} + Q_{nm}(R)\right]f_m(R) = Ef_n(R), \tag{115}$$

where the coupling potentials $P_{mn}(R)$ and $Q_{mn}(R)$ are defined by

$$P_{nm}(R) = -\frac{\hbar^2}{2m}\sum_k G_{nk}^{-1}(R)\int_0^{(1/2)\pi}\mathrm{d}\alpha\,\phi_k^*(R,\alpha)\frac{\partial}{\partial R}\phi_m(R,\alpha), \tag{116a}$$

$$Q_{nm}(R) = -\frac{\hbar^2}{2m}\sum_k G_{nk}^{-1}(R)\int_0^{(1/2)\pi}\mathrm{d}\alpha\,\phi_k^*(R,\alpha)\frac{\partial^2}{\partial R^2}\phi_m(R,\alpha). \tag{116b}$$

The set of radial equations (115) looks similar to the set of radial equations (100) for the adiabatic hyperspherical representation of the 3-body Schrödinger equation. The difference is that the channel potentials $V_n(R)$ in Eq. (115) are obtained by solving integro-differential eigenvalue equations in only one variable, while the channel potentials $V_n(R)$ in Eq. (100) are obtained by solving differential eigenvalue equations in five hyperangular variables. The reduction in the number of variables came from our simplifying assumption of neglecting subsystem angular momenta.

If all the eigenvalues $\lambda_n(R)$ were independent of R, then the hyperangular functions $\phi_n(R)$ obtained by solving Eq. (112) would be independent of R and the coupling potentials $P_{mn}(R)$ and $Q_{mn}(R)$ defined by Eqs. (116) would vanish. Thus in regions of R in which all the eigenvalues $\lambda_n(R)$ vary sufficiently slowly with R, the coupling potentials $P_{mn}(R)$ and $Q_{mn}(R)$ can be neglected. The adiabatic hyperspherical approximation [78] consists of neglecting the off-diagonal coupling terms in Eq. (115), in which case the eigenvalue equations decouple. If the diagonal coupling terms in Eq. (115) are also neglected, the equations reduce to radial Schrödinger equations for each of the hyperspherical potentials:

$$\left[\frac{\hbar^2}{2m}\left(-\frac{\partial^2}{\partial R^2} + \frac{15}{4R^2}\right) + V_n(R)\right]f_n(R) \approx Ef_n(R). \tag{117}$$

If the 2-body potential $V(r)$ vanishes, the integro-differential eigenvalue equation (112) reduces to a simple differential eigenvalue equation that is easy to solve. The eigenvalues are independent of R:

$$\lambda_n(R) = 4(n+1)^2, \quad n = 0, 1, 2, \ldots. \tag{118}$$

The corresponding eigenfunctions are

$$\phi_n(R, \alpha) = \sin[2(n+1)\alpha]. \tag{119}$$

The corresponding hyperspherical potentials are

$$V_n(R) = 4n(n+2)\frac{\hbar^2}{2mR^2}. \tag{120}$$

If the 2-body potential $V(r)$ is short-ranged, there are two regions in which the integro-differential eigenvalue equation (112) for the angular function $\Phi_n(R, \alpha)$ can be solved analytically. One region is $R \sin\alpha$ large enough that the $V(R\sin\alpha)$ term is small compared to $\lambda_n(R)$. In this case, we can neglect the R^2V term and the equation reduces to

$$\left[-\frac{\partial^2}{\partial\alpha^2} - \lambda_n(R)\right]\phi_n^{(\mathrm{hi})}(R, \alpha) \approx 0. \tag{121}$$

The solution that vanishes at the upper endpoint $\alpha = \pi/2$ is

$$\phi_n^{(\mathrm{hi})}(R, \alpha) \approx \sin\left[\lambda_n^{1/2}(R)\left(\frac{\pi}{2} - \alpha\right)\right]. \tag{122}$$

The other region for which Eq. (112) can be solved analytically is $R\sin\alpha$ small enough that $\lambda_n(R)$ is small compared to the $V(R\sin\alpha)$ term. In this case, we can neglect λ_n. In the region $\alpha \ll 1$, the equation reduces to

$$\left[-\frac{\partial^2}{\partial\alpha^2} + \frac{2mR^2}{\hbar^2}V(\sqrt{2}R\alpha)\right]\phi_n^{(\mathrm{lo})}(R, \alpha) \approx -\frac{2mR^2}{\hbar^2}V(\sqrt{2}R\alpha)\frac{8\alpha}{\sqrt{3}}\phi_n^{(\mathrm{hi})}\left(R, \frac{\pi}{3}\right). \tag{123}$$

The general solution to this inhomogeneous equation is the sum of a particular solution and the general solution to the homogeneous equation. A particular solution is

$$\phi_n^{(\mathrm{lo})}(R, \alpha) = -\frac{8\alpha}{\sqrt{3}}\phi_n^{(\mathrm{hi})}\left(R, \frac{\pi}{3}\right). \tag{124}$$

The homogeneous equation can be expressed in the form

$$\left[-\frac{\hbar^2}{2mR^2}\frac{\partial^2}{\partial\alpha^2} + V(\sqrt{2}R\alpha)\right]\phi_n^{(\mathrm{lo})}(R, \alpha) \approx 0. \tag{125}$$

This is identical to the radial Schrödinger equation for a pair of particles with zero energy interacting through the 2-body potential $V(r)$, where $r = \sqrt{2}R\alpha$. If we denote the zero-energy solution by $\psi_0(r)$, the most general solution to Eq. (123) is

$$\phi_n^{(\mathrm{lo})}(R, \alpha) \approx A(R)\psi_0(\sqrt{2}R\alpha) - \frac{8\alpha}{\sqrt{3}}\phi_n^{(\mathrm{hi})}\left(R, \frac{\pi}{3}\right), \tag{126}$$

where $A(R)$ is an arbitrary function of R.

5.3. Hyperspherical potentials

Thus far, we have made no assumptions about the potential $V(\boldsymbol{r}_1, \boldsymbol{r}_2, \boldsymbol{r}_3)$ except that it is a sum of three pair potentials as in Eq. (103). We now apply the low-energy Faddeev equation in Eq. (110) to the problem of a 2-body potential with large scattering length $|a| \gg \ell$. Zhen and Macek have used a variational approach to obtain approximate equations for the

channel eigenvalues [84]. The integro-differential eigenvalue equation can also be reduced to an exact transcendental equation for $\lambda_n(R)$. We follow closely the derivation of Fedorov and Jensen in Ref. [80].

The hyperangular functions $\Phi_n(R,\alpha)$ have the approximate solutions given in Eqs. (122) and (126) in appropriate regions of R and α. In the case of large scattering length, the high-α solution in Eq. (122) holds for $R\sin\alpha \gg \ell$. The low-α solution in Eq. (126) holds for $\alpha \ll 1$ and $R\alpha \gg \ell$. For $R\alpha \gg \ell$, the zero-energy solution $\psi_0(r)$ that appears in Eq. (126) is simply the limit as $k \to 0$ of the atom–atom scattering solution given in Eq. (60):

$$\psi_0(r) = r - a, \tag{127}$$

where a is the scattering length. Upon inserting $\psi_0(\sqrt{2}\alpha R)$ into Eq. (126), we see that the extrapolation of the high-α solution in Eq. (122) to the region $\alpha \ll 1$ is compatible with the low-α solution in Eq. (126). Matching their values at $\alpha = 0$, we determine the unknown function of R that appears in Eq. (126):

$$A(R) = -\sin\left[\lambda^{1/2}(R)\frac{\pi}{2}\right]\frac{1}{a}. \tag{128}$$

Equating the derivatives with respect to α at $\alpha = 0$, we obtain the matching equation that determines the channel eigenvalues $\lambda_n(R)$[6]:

$$\cos\left(\lambda^{1/2}\frac{\pi}{2}\right) - \frac{8}{\sqrt{3}}\lambda^{-1/2}\sin\left(\lambda^{1/2}\frac{\pi}{6}\right) = \sqrt{2}\lambda^{-1/2}\sin\left(\lambda^{1/2}\frac{\pi}{2}\right)\frac{R}{a}. \tag{129}$$

This equation was first derived by Efimov [41]. There are infinitely many solutions for the channel eigenvalues $\lambda_n(R)$ at each value of R. The corresponding hyperangular wave functions are

$$\phi_n(R,\alpha) = \sin\left[\lambda_n^{1/2}(R)\left(\frac{\pi}{2} - \alpha\right)\right]. \tag{130}$$

This solution does not satisfy the boundary condition $\phi_n(R,\alpha) \to 0$ as $\alpha \to 0$, because the zero-energy solution in Eq. (127) is accurate only for $R\alpha \gg \ell$. Thus the solution in Eq. (130) is not accurate in the region $R\alpha \sim \ell$. It is, however, accurate enough to calculate quantities that are sufficiently insensitive to short distances.

The consistency equation (129) for the channel eigenvalues has the constant solution $\lambda(R) = 16$, but it is unphysical. The hyperangular wave function in Eq. (130) is $\phi(R,\alpha) = \sin(4\alpha)$. The resulting Faddeev wave function in Eq. (111) is proportional to $\cos(2\alpha)$. This is a spurious solution to the low-energy Faddeev equation, because the corresponding Schrödinger wave function given by Eq. (107) is the trivial solution $\Psi = 0$. This follows from the identity

$$\cos(2\alpha) = -\frac{4}{\sqrt{3}}\int_{|(1/3)\pi-\alpha|}^{(1/2)\pi-|(1/6)\pi-\alpha|}\frac{\sin(2\alpha')}{\sin(2\alpha)}\cos(2\alpha')\,d\alpha'. \tag{131}$$

The physical channel eigenvalues $\lambda_n(R)$ can be obtained by solving Eq. (129) numerically. The lowest three eigenvalues for $a > 0$ and the lowest three eigenvalues for $a < 0$ are shown as functions of $R/|a|$ in Fig. 20. For $R \ll |a|$, the eigenvalues approach constants independent of a. The limiting behavior of the lowest eigenvalue as $R \to 0$ is

$$\lambda_0(R) \longrightarrow -s_0^2\left(1 + 1.897\frac{R}{a}\right), \tag{132}$$

where $s_0 = 1.00624$ is the solution to the transcendental equation (35). The limiting value of the second lowest eigenvalue as $R \to 0$ is

$$\lambda_1(R) \longrightarrow 19.94. \tag{133}$$

The limiting behavior of the lowest eigenvalue as $R \to \infty$ is

$$\lambda_0(R) \longrightarrow 4\left(1 - \frac{12}{\sqrt{2}\,\pi}\frac{|a|}{R}\right) \quad (a < 0), \tag{134a}$$

$$\longrightarrow -\frac{2R^2}{a^2}\left(1 + \frac{8\sqrt{2}\,a}{\sqrt{3}\,R}e^{-\sqrt{2}\,\pi R/3a}\right) \quad (a > 0). \tag{134b}$$

[6] In Ref. [80], Fedorov and Jensen used the opposite sign convention for the scattering length. They also made an error that resulted in the omission of the factor of $\sqrt{2}$ on the right side of Eq. (129).

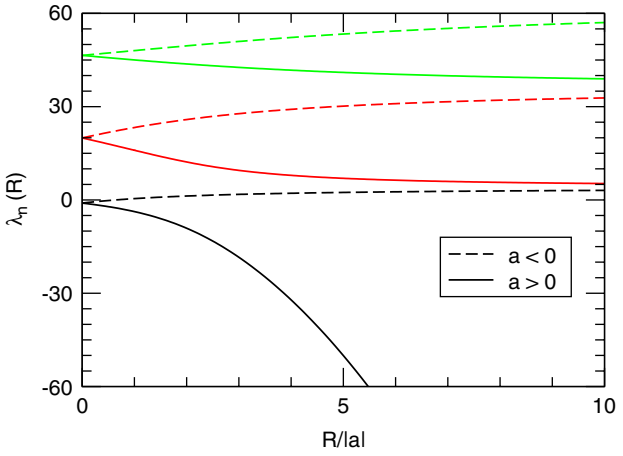

Fig. 20. The three lowest channel eigenvalues $\lambda_n(R)$ for $a > 0$ (solid lines) and for $a < 0$ (dashed lines).

The limit of the second lowest eigenvalue as $R \to \infty$ is

$$\lambda_1(R) \longrightarrow 36 \quad (a < 0), \tag{135a}$$
$$\longrightarrow 4 \quad (a > 0). \tag{135b}$$

For $n \geqslant 2$, the limits of the eigenvalues as $R \to \infty$ are

$$\lambda_n(R) \longrightarrow 4(n+2)^2 \quad (a < 0), \tag{136a}$$
$$\longrightarrow 4(n+1)^2 \quad (a > 0). \tag{136b}$$

With the exception of $\lambda_0(R)$ in the case $a > 0$, the limiting values in Eqs. (134)–(136) are among those for free particles given in Eq. (118).

We have simplified the derivation of the matching equation for the channel eigenvalues by ignoring the orbital angular momentum of the subsystem consisting of the two atoms in a pair or the subsystem consisting of a pair and a third atom. The lowest channel eigenvalue with nonzero subsystem orbital angular momentum comes from one unit of angular momentum in the subsystem consisting of a pair and a third atom. This corresponds to the $l_x = 0, l_y = 1$ term in the angular momentum decomposition of the Faddeev wave function in Eq. (106). The matching equation for general values of the angular momentum quantum number l_y is given in Ref. [76]. The matching equation for $l_y = 1$ is [76]

$$\sin\left(\lambda^{1/2}\frac{\pi}{2}\right) + \frac{1}{3}\lambda^{1/2}\,{}_2F_1\left(\frac{1}{2}(3+\lambda^{1/2}),\ \frac{1}{2}(3-\lambda^{1/2}),\ \frac{5}{2};\ \frac{1}{4}\right) = -\frac{\sqrt{2}\,\lambda^{1/2}}{\lambda - 1}\cos\left(\lambda^{1/2}\frac{\pi}{2}\right)\frac{R}{a}. \tag{137}$$

The limiting value of the lowest eigenvalue as $R \to 0$ is

$$\lambda(R) \longrightarrow 8.201. \tag{138}$$

The limiting behavior of the lowest eigenvalue as $R \to \infty$ is

$$\lambda(R) \longrightarrow 25 \quad (a < 0), \tag{139a}$$
$$\longrightarrow -2R^2/a^2 \quad (a > 0). \tag{139b}$$

The lowest eigenvalue for $l_x = 0, l_y = 1$ is always lower than the second lowest eigenvalue for $l_x = l_y = 0$. Thus the neglect of subprocess orbital angular momentum is not useful as a quantitative approximation.

The hyperspherical potential $V_n(R)$ associated with the eigenvalue $\lambda_n(R)$ is given in Eq. (113). The lowest three hyperspherical potentials for $a > 0$ and for $a < 0$ are shown in Fig. 21. For either sign of a, the lowest hyperspherical potential $V_0(R)$ is negative for all r and all the others are positive for all R.

As $R \to \infty$, all the hyperspherical potentials asymptote to the 3-atom threshold $E = 0$, with the exception of $V_0(R)$ in the case $a > 0$. We can interpret the asymptotic configurations in the channels that asymptote to $E = 0$ as 3-atom

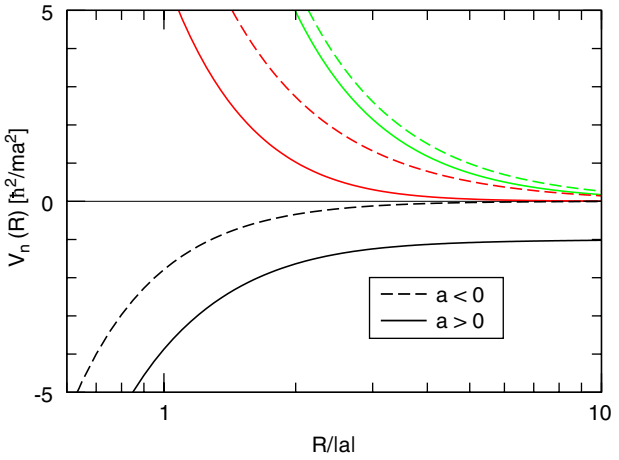

Fig. 21. The three lowest hyperspherical potentials $V_n(R)$ scaled by $\hbar^2/ma^2$ for $a > 0$ (solid lines) and for $a < 0$ (dashed lines).

scattering states. For $a > 0$, the lowest hyperspherical potential $V_0(R)$ asymptotes to $-\hbar^2/ma^2$, which is the dimer binding energy. We can interpret the asymptotic configuration in this channel as an atom–dimer scattering state. As $R \to 0$, the hyperspherical potentials asymptote to $1/R^2$ potentials with different coefficients:

$$V_n(R) \longrightarrow [\lambda_n(0) - 4]\frac{\hbar^2}{2mR^2}, \quad R \ll |a|. \tag{140}$$

The $1/R^2$ potential is attractive for the lowest channel $n = 0$ and repulsive for all the other channels. We obtain scale-invariant $1/R^2$ potentials, because we have taken the scaling limit $\ell \to 0$. For finite ℓ, the hyperspherical potentials have the scale-invariant form in Eq. (140) only in the region $\ell \ll R \ll |a|$. At short distances $R \sim \ell$, they may be very complicated.

In the adiabatic hyperspherical approximation, the coupling potentials are ignored and the equations for the hyperradial wave functions $f_n(R)$ reduce to Eq. (117). This is a good approximation only at limiting values of R. It is a good approximation in the limit $R \ll |a|$, because all the eigenvalues $\lambda_n(R)$ approach constant values and the hyperangular functions $\phi_0(R, \alpha)$ become independent of R. The coupling potentials in Eqs. (116) are therefore suppressed by the derivatives with respect to R. The adiabatic hyperspherical approximation is also a good approximation in the limit $R \gg |a|$. In the case $a < 0$, this is again because all the eigenvalues approach constant values in the limit. In the case $a > 0$, this argument does not apply to the coupling potentials $P_{n0}(R)$ and $Q_{n0}(R)$, because the lowest eigenvalue $\lambda_0(R)$ diverges to $-\infty$ as $R \to \infty$ as shown in Eq. (134b). The hyperangular wave function $\phi_0(R, \alpha)$ for the lowest channel is a hyperbolic function of a real argument. For $R \gg a$, it provides an exponential factor $\exp[\sqrt{2}R/a((\pi/2) - \alpha)]$ that ensures that the wave function has support only in the region $\alpha \sim a/R$. But for all the other channels, $\lambda_n^{1/2}(R)$ approaches an even integer as $R \to \infty$, according to Eqs. (135b) and (136b). Thus $\phi_n(R, \alpha = 0)$ approaches zero as $R \to \infty$. These zeroes provide suppression of the coupling potentials $P_{n0}(R)$and $Q_{n0}(R)$, which guarantees that the adiabatic hyperspherical approximation is also a good approximation in the limit $R \gg |a|$.

5.4. Boundary condition at short distances

The behavior of the hyperradial wave functions $f_n(R)$ at very small hyperradius $R \sim \ell$ is determined by the 2-body potential $V(r)$ at short distances $r \sim \ell$. In the scaling limit $\ell \to 0$, the information about short distances is lost and it may need to be reintroduced through boundary conditions on the hyperradial wave functions.

In the scaling limit, the channel eigenvalues $\lambda_n(R)$ are the solutions to Eq. (129). For $R \ll |a|$, the eigenvalues approach constant values $\lambda_n(0)$, so the adiabatic hyperspherical approximation in Eq. (117) is justified. The hyperradial

eigenvalue equation (117) then reduces in the region $R \ll |a|$ to

$$\frac{\hbar^2}{2m}\left[-\frac{\partial^2}{\partial R^2} + \frac{\lambda_n(0) - 1/4}{R^2}\right] f_n(R) = E f_n(R). \tag{141}$$

This looks like the radial Schrödinger equation for a particle in a $1/R^2$ potential, with the strength of the potential determined by $\lambda_n(0)$. As illustrated in Fig. 21, in the region $R \ll |a|$, all the channel potentials with the exception of $V_0(R)$ are repulsive $1/R^2$ potentials. The hyperspherical wave functions $f_n(R)$ for $n \geqslant 1$ therefore decrease exponentially as $R \to 0$, and no boundary conditions are required. In contrast, the potential $V_0(R)$ is an attractive $1/R^2$ potential for $R \ll |a|$:

$$V_0(R) \approx -(4 + s_0^2)\frac{\hbar^2}{2mR^2}, \quad R \ll |a|. \tag{142}$$

This potential is too singular as $R \to 0$ for the hyperradial equation (141) to have well-behaved solutions. Having taken the scaling limit $\ell \to 0$, we have lost information about the boundary condition at $R \to 0$ provided by the 2-body potential $V(r_{ij})$ at short distances. If the solution $f(R)$ to the complete problem with the correct boundary condition at $R \to 0$ was known, it could be matched onto the solution of Eq. (141) simply by choosing a hyperradius R_0 where Eq. (141) is accurate and demanding that the logarithmic derivatives $R_0 f'(R_0)/f(R_0)$ match at that point. Thus the correct treatment of the problem at short-distances is equivalent to choosing a matching point R_0 and specifying the dimensionless number $R_0 f'(R_0)/f(R_0)$.

The matching point R_0 can be chosen to lie in the scale-invariant region $\ell \ll R_0 \ll |a|$. If we also choose $R_0 \ll (m|E|/\hbar^2)^{-1/2}$, the energy eigenvalue E in Eq. (141) can be neglected relative to the channel potential, and the hyperradial equation reduces to

$$\frac{\hbar^2}{2m}\left[-\frac{\partial^2}{\partial R^2} - \frac{s_0^2 + 1/4}{R^2}\right] f_0(R) \approx 0. \tag{143}$$

This equation has solutions that behave like powers of R. The most general solution is

$$f_0(R) \approx A R^{1/2 + i s_0} + B R^{1/2 - i s_0}, \quad R \ll |a|, 1/\kappa, \tag{144}$$

where A and B are constants. The ratio B/A is a complex number that could be determined by matching to the solution of the problem at short distances $R \sim \ell$. If $|A| < |B|$, there is a net flow of probability into the short-distance region. As will be discussed in detail in Section 7, such a flow of probability is possible if there are deep (tightly-bound) diatomic molecules. In the absence of such deep bound states, we must have $|A| = |B|$ and the solution in Eq. (144) can be written as

$$f_0(R) \approx A R^{1/2} \sin[s_0 \ln(\kappa R) + \alpha], \tag{145}$$

where α is a constant and the factor of $\kappa = (m|E|/\hbar^2)^{1/2}$ in the argument of the logarithm is inserted to make it dimensionless. The phase α is determined by matching to the solution of the problem at long distances $R \sim |a|$. It depends on a and on the energy E. Since α is dimensionless, it can depend only on the dimensionless combination κa, and on the signs of E and a. Computing the logarithmic derivative of the solution in Eq. (145) and evaluating it at the matching point, we obtain

$$R_0 \frac{f_0'(R_0)}{f_0(R_0)} = \frac{1}{2} + s_0 \cot[s_0 \ln(\kappa R_0) + \alpha]. \tag{146}$$

Inside the argument of the cotangent, the dependence on R_0 can be separated from the dependence on E and a. This implies that the wave function at distances $R \gg \ell$ depends only on a particular function of the matching point R_0 and the logarithmic derivative $R_0 f'(R_0)/f(R_0)$:

$$\Lambda_0 = \frac{1}{R_0} \exp\left\{\frac{1}{s_0}\operatorname{arccot}\left[\frac{1}{s_0}\left(R_0 \frac{f_0'(R_0)}{f_0(R_0)} - \frac{1}{2}\right)\right]\right\}. \tag{147}$$

The parameter Λ_0 has dimensions of wave number. We refer to it as a scaling-violation parameter, because logarithmic scaling violations can affect low-energy observables only through their dependence on this parameter.[7]

We can interpret the matching point R_0 as a short-distance cutoff. Configurations with smaller hyperradii R need not be taken into account explicitly. Instead their effects on the physics at longer distances are taken into account through the value of $R_0 f'(R_0)/f(R_0)$. All low-energy observables in the 3-body sector are determined either by specifying the short-distance cutoff R_0 and the dimensionless number $R_0 f'(R_0)/f(R_0)$ or, alternatively, by specifying the scaling-violation parameter Λ_0 defined by Eq. (147). This phenomenon of a dimensionless short-distance parameter and a short-distance cutoff being equivalent to a dimensionful long-distance parameter is known as *dimensional transmutation*. It is a familiar feature of quantum chromodynamics, the quantum field theory that describes the strong interactions [50,51]. The theory has a single parameter: the strong coupling constant α_s. It can be specified by giving its value $\alpha_s(\Lambda)$ when the theory is defined with a large momentum cutoff Λ. When the coupling constant is small, its dependence on the cutoff can be calculated using perturbation theory. It satisfies a differential renormalization group equation:

$$\Lambda \frac{\partial}{\partial \Lambda} \alpha_s(\Lambda) = -\frac{33 - 2n_f}{6\pi} \alpha_s^2(\Lambda), \tag{148}$$

where n_f is the relevant number of quark flavors. This equation implies that the parameter $\Lambda_{\rm QCD}$ defined by

$$\Lambda_{\rm QCD} = \Lambda \exp\left[\frac{-6\pi}{(33 - 2n_f)\alpha_s(\Lambda)}\right] \tag{149}$$

is independent of Λ. The theory can therefore be defined equally well by specifying the cutoff Λ and the dimensionless parameter $\alpha_s(\Lambda)$ or alternatively by specifying the scaling-violation parameter $\Lambda_{\rm QCD}$ generated by dimensional transmutation. Similarly, the low-energy theory for the 3-body problem with large 2-body scattering length can be defined by specifying a, the cutoff R_0, and the dimensionless parameter $R_0 f'(R_0)/f(R_0)$ or alternatively by specifying a and the scaling-violation parameter Λ_0 generated by dimensional transmutation.

The logarithmic scaling violations in QCD can be interpreted as the result of an *anomaly* in the scaling symmetry. An anomaly in this context refers to the violation of a symmetry by quantum effects. The classical field equations for QCD have a scaling symmetry in the limit in which the masses of all the quarks are set to zero. But this symmetry is broken by the effects of quantum field fluctuations at short distances. The logarithmic scaling violations associated with the Efimov effect can be interpreted as the result of an anomaly in a scaling symmetry [85]. The scaling symmetry appears if the scaling limit and the resonant limit are taken simultaneously. The symmetry is broken by quantum fluctuations at small hyperradii in the 3-body channel.

5.5. *Efimov states in the resonant limit*

The Efimov effect is the existence of infinitely many 3-body bound states with an accumulation point at the 3-atom threshold in the resonant limit $a \to \pm\infty$. A derivation of the Efimov effect within the hyperspherical formalism was first given by Macek [86]. We proceed to derive the Efimov effect and deduce some of the properties of the Efimov states in the resonant limit.

In the resonant limit, the adiabatic hyperspherical approximation is accurate at all finite values of R. In particular, it is accurate for bound states for which hyperradial wave functions $f_n(R)$ fall exponentially as $R \to \infty$. Since the $n = 0$ channel is the only attractive one, it is the only one that supports bound states. The channel eigenvalue is $\lambda_0(R) = -s_0^2$, so the Schrödinger wave function in the center-of-mass frame reduces to

$$\Psi(\boldsymbol{r}_1, \boldsymbol{r}_2, \boldsymbol{r}_3) = R^{-5/2} f_0(R) \sum_{i=1}^{3} \frac{\sinh[s_0((\pi/2) - \alpha_i)]}{\sin(2\alpha_i)}. \tag{150}$$

[7] An equivalent scaling-violation parameter Λ_* was introduced in Refs. [61,62] through the renormalization prescription for an effective field theory.

Since the channel eigenvalue $\lambda_0(R) = -s_0^2$ is a constant, the adiabatic hyperspherical approximation is justified. The equation for the hyperradial wave function $f_0(R)$ in Eq. (141) reduces to

$$\frac{\hbar^2}{2m}\left[-\frac{\partial^2}{\partial R^2} - \frac{s_0^2 + 1/4}{R^2}\right] f_0(R) = E f_0(R). \tag{151}$$

The boundary condition at short distances is specified by a matching point R_0 and the logarithmic derivative $R_0 f_0'(R_0)/f_0(R_0)$. Alternatively, if R_0 is in the scale-invariant region, the boundary condition can be specified by the 3-body parameter Λ_0 defined by Eq. (147).

If an Efimov state has binding energy $E_{\rm T}$, a binding wave number κ can be defined by

$$E_{\rm T} = \frac{\hbar^2\kappa^2}{m}. \tag{152}$$

The solution to the hyperradial equation (117) that decreases exponentially as $R \to \infty$ is

$$f_0(R) = R^{1/2} K_{{\rm i}s_0}(\sqrt{2}\kappa R), \tag{153}$$

where $K_{{\rm i}s_0}(z)$ is a Bessel function with imaginary index. The boundary condition at short distances determines the discrete spectrum of binding energies $E_{\rm T}^{(n)}$. In the region $\kappa R \ll 1$, the solution in Eq. (153) reduces to

$$f_0(R) \longrightarrow -(\pi/[s_0 \sinh(\pi s_0)])^{1/2} R^{1/2} \sin[s_0 \ln(\kappa R) + \alpha_0], \tag{154}$$

where the angle α_0 is

$$\alpha_0 = -\frac{1}{2} s_0 \ln 2 - \frac{1}{2} \arg \frac{\Gamma(1 + {\rm i}s_0)}{\Gamma(1 - {\rm i}s_0)}. \tag{155}$$

Inserting the solution in Eq. (154) into Eq. (147), the equation for Λ_0 reduces to

$$s_0 \ln(\Lambda_0 R_0) = \operatorname{arccot}\left(\cot[s_0 \ln(\kappa R_0) + \alpha_0]\right). \tag{156}$$

The solutions for κ can be written as

$$\kappa^{(n)} = (e^{-\pi/s_0})^{n-n_0} e^{-\alpha_0/s_0} \Lambda_0, \tag{157}$$

where n_0 is an arbitrary integer that arises from the choice of the branch of the cotangent in Eq. (147). The resulting expression for the spectrum $E_{\rm T}^{(n)}$ of the Efimov states in the resonant limit can be expressed in the form

$$E_{\rm T}^{(n)} = (e^{-2\pi/s_0})^{n-n_*} \frac{\hbar^2\kappa_*^2}{m}, \tag{158}$$

where κ_* is the binding wave number for the Efimov state labeled by $n = n_*$. The spectrum in Eq. (158) is geometric, with the binding energies of successive Efimov states having the ratio $e^{2\pi/s_0} \approx 515.03$. The relation between κ_* and Λ_0 can be expressed in a form that does not involve the integers n_0 and n_*:

$$s_0 \ln(\kappa_*) = s_0 \ln(\Lambda_0) - \alpha_0 \mod \pi. \tag{159}$$

The relation between these parameters is defined only up to multiplicative factors of $e^{\pi/s_0} \approx 22.7$, because their definitions involve the arbitrary integers n_0 in Eq. (157) and n_* in Eq. (158).

The probability distribution ${\rm d}P/{\rm d}R$ for the hyperradius R in an Efimov state in the resonant limit is proportional to $f_0(R)^2$, where $f_0(R)$ is given in Eq. (153). The normalized probability distributions for three successive Efimov states are shown in Fig. 22. A quantitative measure of the size of a 3-body bound state is the expectation value of R^2. For an Efimov state in the resonant limit, this expectation value is

$$\langle R^2 \rangle = \frac{\int_0^\infty {\rm d}R\, R^2 f_0^2(R)}{\int_0^\infty {\rm d}R\, f_0^2(R)}. \tag{160}$$

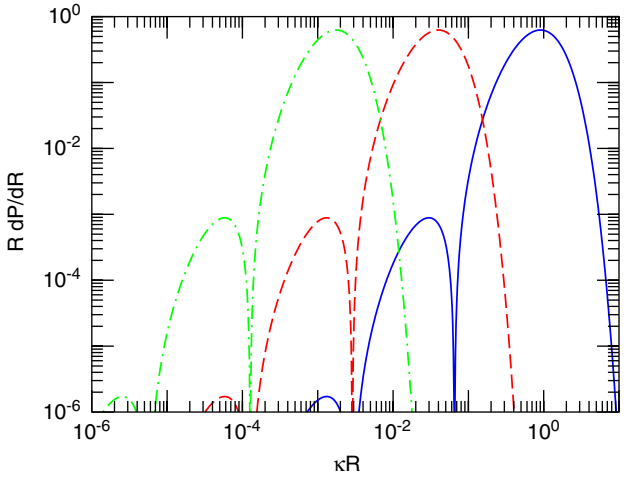

Fig. 22. The normalized probability distributions $R\,\mathrm{d}P/\mathrm{d}R$ for three successive Efimov states in the resonant limit as functions of $\ln(\kappa R)$, where κ is the binding wave number of the shallowest of the three states.

Inserting the hyperradial wave function in Eq. (153), we obtain

$$\langle R^2\rangle^{(n)} = \frac{2(1+s_0^2)}{3}(\kappa^{(n)})^{-2}. \tag{161}$$

Using the expression for κ for the nth Efimov state from Eq. (157), the mean-square hyperradius is

$$\langle R^2\rangle^{(n)} = (e^{2\pi/s_0})^{n-n_*}\frac{2(1+s_0^2)}{3}\kappa_*^{-2}. \tag{162}$$

Thus the root-mean-square hyperradius for each successively shallower Efimov state is larger than the previous one by $e^{\pi/s_0} \approx 22.7$.

The simple geometric spectrum of Efimov states given in Eq. (158) is obtained only if we take the scaling ($\ell \to 0$) and resonant ($a \to \pm\infty$) limits simultaneously. If we stay in the resonant limit but do not take the scaling limit $\ell \to 0$, the 3-body spectrum will be bounded from below. There will be a deepest Efimov state that can be labeled by $n = 0$ and whose binding energy is comparable to the natural ultraviolet cutoff:

$$E_{\mathrm{T}}^{(0)} \sim \frac{\hbar^2}{m\ell^2}. \tag{163}$$

There will also be power-law scaling violations that give corrections to the binding energies. The leading corrections scale as $\kappa^{(n)}\ell$, where $\kappa^{(n)}$ is the binding wave number of the Efimov state, so they go to zero as the binding energy $E_{\mathrm{T}}^{(n)}$ of the Efimov state goes to 0. Thus the Efimov spectrum satisfies

$$E_{\mathrm{T}}^{(n)} \longrightarrow (e^{-2\pi/s_0})^{n-n_*}\frac{\hbar^2\kappa_*^2}{m} \quad \text{as } n \to \infty \text{ with } a = \pm\infty. \tag{164}$$

There are infinitely many arbitrarily-shallow Efimov states, with an accumulation point at zero energy and an asymptotic discrete scaling symmetry with discrete scaling factor $e^{\pi/s_0} \approx 22.7$.

The parameter κ_* defined by Eq. (164) can be used as the 3-body parameter as an alternative to Λ_0. These parameters differ by a multiplicative factor that consists of a numerical constant and an arbitrary integer power of e^{π/s_0}. An advantage of κ_* is that it is defined in terms of physical observables. It is defined for any system with a large scattering length a and with a short-distance tuning parameter that can be used to tune the system to the resonant limit $a \to \pm\infty$. One can determine κ_* from calculations of the Efimov spectrum at a sequence of scattering lengths that approach the resonant limit. The definition does not depend on any calculational framework. In contrast, Λ_0 is defined in Eq. (147)

in terms of the Schrödinger wave function in hyperspherical coordinates. It cannot be determined so straightforwardly in some other frameworks, such as effective field theory.

The 2-body parameter a can be defined very simply in terms of physical observables. According to Eq. (59), a^2 is simply the limiting value of $\mathrm{d}\sigma/\mathrm{d}\Omega$ as the energy approaches zero. The sign of a is determined by whether or not there is a bound state with binding energy given by Eq. (36). The 3-body parameter κ_* is defined by a limiting procedure that involves tuning a to $\pm\infty$. However, it can also be determined approximately from the measurement of a single physical observable, such as the binding energy $E_{\rm T}^{(N)}$ of the Efimov state closest to threshold. One might be tempted to specify the theory by the physical observables a and $E_{\rm T}^{(N)}$ instead of a and κ_*. The disadvantage of this choice is that there are no other 3-body observable that can be expressed in a simple form in terms of a and $E_{\rm T}^{(N)}$. As we shall see in Section 6, the 3-body parameter κ_* has the advantage that there are some 3-body observables that are given by simple analytic expressions in terms of a and κ_*.

5.6. Efimov states near the atom–dimer threshold

While there are infinitely many Efmov trimers in the resonant limit $a = \pm\infty$, there are only finitely many for any finite value of a. Thus for almost all of these states, there must be a critical positive value of a at which the bound state appears below the atom–dimer threshold and a critical negative value of a at which it disappears through the 3-atom threshold. Efimov states near the atom–dimer threshold can be understood intuitively as 2-body systems composed of an atom and a dimer.

We will denote the critical value of a at which the Efimov state appears below the atom–dimer threshold by a_*. For a near a_*, the existence of an Efimov trimer close to threshold produces resonant enhancement of atom–dimer scattering. Thus the atom–dimer scattering length $a_{\rm AD}$ must diverge as $a \to a_*$. From Efimov's universal formula for $a_{\rm AD}$ in Eq. (39), we can see that a_* must satisfy $s_0 \ln(a_*\kappa_*) + \beta = (n + \frac{1}{2})\pi$, where n is an integer, and that the behavior of $a_{\rm AD}$ as a approaches a_* from above must be

$$a_{\rm AD} \approx \frac{b_0 a_* a}{s_0(a - a_*)}. \tag{165}$$

Thus if $a - a_*$ is small compared to a_*, the atom–dimer scattering length is large compared to a.

We can exploit the universality of the 2-body systems with large scattering lengths to deduce some properties of the shallowest Efimov state when it is close to the atom–dimer threshold. In this case, the 2-body system consists of an atom of mass m and a dimer of mass $2m$. We denote the binding energy of the shallowest Efimov state by $E_{\rm T}^{(N)}$. The analog of the universal formula in Eq. (62) is obtained by replacing the reduced mass $m/2$ of the atoms by the reduced mass $2m/3$ of the atom and dimer. Thus the binding energy relative to the 3-atom threshold can be approximated by

$$E_{\rm T}^{(N)} \approx E_{\rm D} + \frac{3\hbar^2}{4m a_{\rm AD}^2}. \tag{166}$$

The errors in this approximation scale as $(a - a_*)^3$.

We can also use universality to deduce the wave function of the Efimov trimer in the limit $a_{\rm AD} \gg a$. The Schrödinger wave function can be expressed as the sum of three Faddeev wave functions as in Eq. (104). In the limit $r_{1,23} \gg r_{23}$, the first Faddeev wave function should have the form

$$\psi^{(1)}(\boldsymbol{r}_{23}, \boldsymbol{r}_{1,23}) \approx \psi_{\rm AD}(r_{1,23})\,\psi_{\rm D}(r_{23}), \tag{167}$$

where $\psi_{\rm D}(r)$ is the dimer wave function given in Eq. (63) and $\psi_{\rm AD}(r)$ is the analogous universal wave function for a shallow bound state consisting of two particles with large positive scattering length $a_{\rm AD}$:

$$\psi_{\rm AD}(r) = \frac{1}{r} e^{-r/a_{\rm AD}}. \tag{168}$$

Expressed in terms of hyperspherical coordinates, this Faddeev wave function has the form

$$\psi(R, \alpha_1) \longrightarrow \frac{2}{\sqrt{3}R^2 \sin(2\alpha_1)} \exp\left(-\frac{\sqrt{2}R\sin\alpha_1}{a} - \frac{\sqrt{3}R\cos\alpha_1}{\sqrt{2}a_{\rm AD}}\right). \tag{169}$$

Most of the support of the probability density $|\Psi|^2$ is concentrated in the region in which the hyperradius is very large, $R \sim a_{\rm AD}$, and one of the three hyperangles is very small, $\alpha_i \ll 1$. The mean-square hyperradius can be calculated easily when $a_{\rm AD} \gg a$:

$$\langle R^2 \rangle^{(N)} \approx \tfrac{1}{3} a_{\rm AD}^2. \tag{170}$$

This result can be obtained more easily simply by using the universal atom–dimer wave function in Eq. (168) and the approximate expression $R^2 \approx \frac{2}{3} r^2$ for the hyperradius.

The dependence of the Faddeev wave function in Eq. (169) on the hyperangle α_1 is compatible with the expression for the hyperangular wave function in Eq. (130) that was derived from the hyperangular eigenvalue equation. Using the asymptotic expression in Eq. (134b) for the lowest channel eigenvalue $\lambda_0(R)$, the first Faddeev wave function in the region $R \gg a$ is predicted to have the form

$$\psi(R, \alpha_1) \approx R^{-5/2} f_0(R) \frac{\sinh[((\pi/2) - \alpha_1)\sqrt{2} R/a]}{\sin(2\alpha_1)}. \tag{171}$$

In both Eqs. (169) and (171), the leading dependence on α_1 for $R \gg a$, aside from the factor $1/\sin(2\alpha_1)$, comes from an exponential factor $\exp(-\sqrt{2} R\alpha_1/a)$. We can read off an approximate expression for the hyperradial wave function $f_0(R)$ by comparing Eqs. (169) and (171):

$$f_0(R) \approx \frac{4}{\sqrt{3}} R^{1/2} \exp\left(-\frac{\pi}{2}\sqrt{2} R/a - \left(\frac{3}{2}\right)^{1/2} R/a_{\rm AD} \right). \tag{172}$$

6. Universality for three identical bosons

In this section, we describe the universal aspects of the 3-body problem for three identical bosons with large scattering length in the simple case where the effects of deep 2-body bound states are negligible. The changes in the universal properties due to the effects of deep 2-body bound states are described in Section 7.

6.1. Discrete scaling symmetry

In the 2-body problem in the scaling limit, the continuous scaling symmetry in Eq. (66) is a trivial reflection of the fact that the scattering length a is the only scale in the problem. There is also a continuous scaling symmetry for the 3-body problem in the sectors with total angular momentum quantum number $L \geqslant 1$. However, in the $L = 0$ sector, there are logarithmic scaling violations that introduce a second scale. A convenient choice for the second scale is the wave number κ_* defined in Eq. (38) by the spectrum of Efimov states in the resonant limit. We can of course define a trivial continuous scaling symmetry by rescaling κ_* as well as a. Remarkably, however, there is also a nontrivial discrete scaling symmetry in which κ_* is held fixed while a and kinematic variables, such as the energy E, are scaled by appropriate integer powers of the discrete scaling factor $\lambda_0 = e^{\pi/s_0} \approx 22.7$:

$$\kappa_* \longrightarrow \kappa_*, \quad a \longrightarrow \lambda_0^m a, \quad E \longrightarrow \lambda_0^{-2m} E, \tag{173}$$

where m is any integer. Under this symmetry, observables such as binding energies and cross sections, scale with the integer powers of λ_0 suggested by dimensional analysis.

The discrete scaling symmetry strongly constrains the dependence of the observables on the parameters a and κ_* and on kinematic variables. For example, the scaling of the atom–dimer cross section is $\sigma_{\rm AD} \to \lambda_0^{2m} \sigma_{\rm AD}$. The discrete scaling symmetry constrains its dependence on a, κ_*, and the energy E:

$$\sigma_{\rm AD}(\lambda_0^{-2m} E; \lambda_0^m a, \kappa_*) = \lambda_0^{2m} \sigma_{\rm AD}(E; a, \kappa_*), \tag{174}$$

for all integers m. At $E = 0$, the cross section is simply $\sigma_{\rm AD} = 4\pi |a_{\rm AD}|^2$, where $a_{\rm AD}$ is the atom–dimer scattering length. The constraint in Eq. (174) implies that $a_{\rm AD}$ must have the form

$$a_{\rm AD} = f(2s_0 \ln(a\kappa_*))\, a, \tag{175}$$

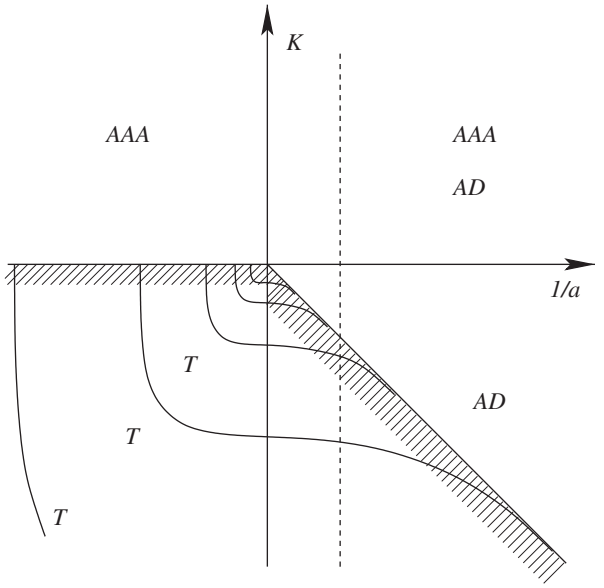

Fig. 23. The a^{-1}–K plane for the 3-body problem. The allowed regions for 3-atom scattering states and atom–dimer scattering states are labelled AAA and AD, respectively. The heavy lines labeled T are three of the infinitely many branches of Efimov states. The cross-hatching indicates the threshold for scattering states. The axes labelled $1/a$ and K are actually $H^{1/4}\cos\xi$ and $H^{1/4}\sin\xi$.

where $f(x)$ is a periodic function with period 2π. As another example, the binding energies of the Efimov trimers scale as $E_{\rm T}^{(n)} \to \lambda_0^{-2m} E_{\rm T}^{(n)}$. The constraints of the discrete scaling symmetry are more intricate in this case, because it maps each branch of the Efimov spectrum onto another branch. The dependence of the binding energies on a and κ_* must satisfy

$$E_{\rm T}^{(n)}(\lambda_0^m a, \kappa_*) = \lambda_0^{-2m} E_{\rm T}^{(n-m)}(a, \kappa_*). \tag{176}$$

This implies that the binding energies for $a > 0$ have the form

$$E_{\rm T}^{(n)}(a, \kappa_*) = F_n(2s_0 \ln(a\kappa_*))\frac{\hbar^2\kappa_*^2}{m}, \tag{177}$$

where the functions $F_n(x)$ satisfy

$$F_n(x + 2m\pi) = (e^{-2\pi/s_0})^m F_{n-m}(x). \tag{178}$$

The functions $F_n(x)$ must also have smooth limits as $x \to \infty$:

$$F_n(x) \to (e^{-2\pi/s_0})^{n-n_*} \quad \text{as } x \to \infty. \tag{179}$$

In the 3-body problem, it is again convenient to introduce the energy variable K defined by Eq. (69). For a given value of κ_*, the possible low-energy 3-body states in the scaling limit can be identified with points in the (a^{-1}, K) plane. It is also convenient to introduce the polar coordinates H and ξ defined by Eqs. (70). The discrete scaling transformation in Eqs. (173) is simply a rescaling of the radial variable with κ_* and ξ fixed: $H \to \lambda_0^{-m} H$.

The a^{-1}–K plane for three identical bosons in the scaling limit is shown in Fig. 23. The possible states are 3-atom scattering states, atom–dimer scattering states, and Efimov trimers. The regions in which there are 3-atom scattering states and atom–dimer scattering states are labelled AAA and AD, respectively. The threshold for scattering states is indicated by the hatched area. The Efimov trimers are represented by the heavy lines below the threshold, some of which are labelled T. There are infinitely many branches of Efimov trimers, but only a few are shown. They intercept the vertical axis at the points $K = -(e^{-\pi/s_0})^{n-n_*}\kappa_*$. Although we have labelled the axes $a^{-1} = H\cos\xi$ and $K = H\sin\xi$, the curves for the binding energies in Fig. 23 actually correspond to plotting $H^{1/4}\sin\xi$ versus $H^{1/4}\cos\xi$. This effectively

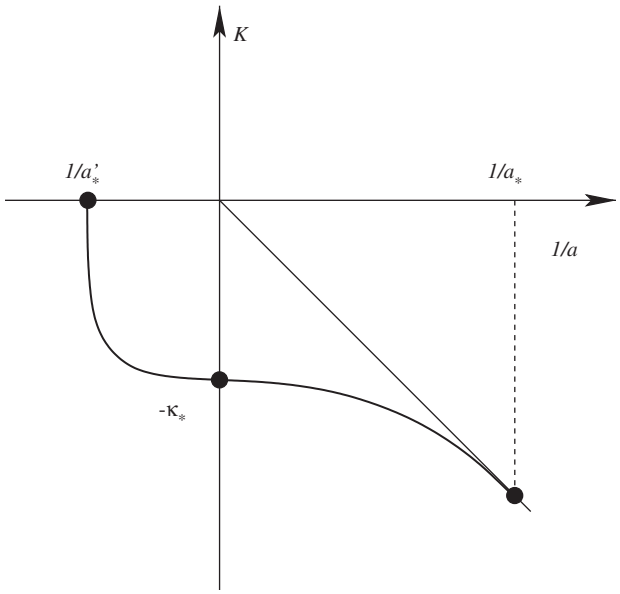

Fig. 24. The energy variable K for the branch of Efimov trimers labelled by $n = n_*$ as a function of $1/a$. In the resonant limit, the binding wave number is κ_*. The branch disappears through the atom–dimer threshold at $a = a_*$ and through the 3-atom threshold at $a = a'_*$.

reduces the discrete symmetry factor 22.7 down to $22.7^{1/4} = 2.2$, allowing a greater range of a^{-1} and K to be shown in the figure. A given physical system has a specific value of the scattering length, and so is represented by a vertical line. The points on the vertical line above the scattering threshold represent the continuum of 3-atom and atom–dimer scattering states. The intersections of the vertical line with the lines labelled T represent Efimov trimers. Changing a corresponds to sweeping the vertical dashed line in Fig. 23 horizontally across the page. The resonant limit corresponds to tuning the vertical line to the K axis.

Changing $1/a$ continuously from a large positive value to a large negative value corresponds to the vertical dashed line in Fig. 23 sweeping from right to left across the $1/a = 0$ axis. New Efimov trimers continue to appear at the atom–dimer threshold at positive critical values of $1/a$ that differ by multiples of $e^{\pi/s_0} \approx 22.7$ until there are infinitely many at $1/a = 0$. For $a < 0$, as $1/a$ increases in magnitude, the Efimov trimers disappear one by one through the 3-atom threshold at negative critical values of $1/a$ that differ by multiples of e^{π/s_0}. We will focus on the specific branch of Efimov trimers labelled by the integer $n = n_*$, which is illustrated in Fig. 24. At some positive critical value $a = a_*$, this branch of Efimov trimers appears at the atom–dimer threshold: $E_{\rm T}^{(n_*)} = E_{\rm D}$. As $1/a$ decreases, its binding energy $E_{\rm T}^{(n_*)} - E_{\rm D}$ relative to the atom–dimer threshold increases but its binding energy $E_{\rm T}^{(n_*)}$ relative to the 3-atom threshold decreases monotonically. As $1/a \to 0$, the binding energy approaches a well-defined limit: $E_{\rm T}^{(n_*)} \to \hbar^2\kappa_*^2/m$. As $1/a$ continues to decrease through negative values, $E_{\rm T}^{(n_*)}$ continues to decrease monotonically. Finally, at some negative critical value $a = a'_*$, it disappears through the 3-atom threshold.

The most obvious consequence of changing the parameter κ_* by a multiplicative factor λ is to multiply each branch of the Efimov trimers in Fig. 23 by a factor λ without changing their shapes. If the factor λ is increased to $e^{\pi/s_0} \approx 22.7$, each branch of the Efimov trimers is mapped onto the next branch. Not only is the Efimov spectrum identical for $\lambda = 1$ and λ_0, but all other 3-body observables are as well. Thus in the scaling limit the distinct 3-body systems can be labeled by a, which can range from $-\infty$ to $+\infty$, and by κ_*, which is positive and ranges over an interval whose endpoints differ by a multiplicative factor of $\lambda_0 \approx 22.7$.

6.2. Efimov's radial law

In addition to the discrete scaling symmetry, Efimov derived some powerful constraints on 3-body observables that he called the *radial law* [42]. When expressed in terms of the polar variables H and ξ defined by Eqs. (70),

an observable is proportional to H^p, where the power p is determined by dimensional analysis and the coefficient depends on the dimensionless variables H/κ_* and ξ. Efimov's radial law strongly constrains the dependence of the observables on H/κ_* and allows the calculation of 3-body observables to be reduced to the calculation of a few universal functions of ξ.

The range of the hyperradius R includes two important length scales: the short-distance scale ℓ and the long-distance scale $|a|$. There are therefore 4 important regions of R, and it is useful to give names to each of these regions:

- the *short-distance region* $R \sim |l|$,
- the *scale-invariant region* $\ell \ll R \ll |a|$,
- the *long-distance region* $R \sim |a|$,
- the *asymptotic region* $R \gg |a|$.

The only states whose wave functions can have significant support in the asymptotic region are 3-atom scattering states and atom–dimer scattering states. The amplitudes for the incoming scattering states to evolve into outgoing scattering states are given by the S-matrix. Efimov's radial law strongly constrains the dependence of the S-matrix on the radial variable H. It follows from the approximate scale-invariance of the 3-body problem at length scales R in the scale-invariant region together with the conservation of probability in both the short-distance and long-distance regions.

The simplest states whose wave functions have significant support in the asymptotic region are atom–dimer scattering states. In the center-of-mass frame, such a state can be labelled by the wave number $\boldsymbol{k}$ of the dimer. If we project onto a state with orbital angular momentum quantum number $L = 0$, the asymptotic form of the Faddeev wave function for energy $E = -E_{\rm D} + 3\hbar^2k^2/4m$ is the product of the dimer wave function $\psi_{\rm D}(r_{23}) = \psi_{\rm D}(\sqrt{2}R\sin\alpha)$, which is given in Eq. (63), and a scattering wave function in the variable $r_{1,23} = \sqrt{3/2}R\cos\alpha$:

$$\psi_{\rm AD}(R,\alpha) \longrightarrow \frac{e^{-\sqrt{2}R\sin\alpha/a}}{R^2\sin(2\alpha)}\left(C e^{{\rm i}\sqrt{3/2}\,kR\cos\alpha} + D e^{-{\rm i}\sqrt{3/2}\,kR\cos\alpha}\right), \tag{180}$$

where C and D are arbitrary coefficients. The terms with the coefficients C and D represent outgoing and incoming atom–dimer scattering states, respectively.

The other states whose wave functions have significant support in the asymptotic region are 3-atom scattering states. Such a state can be labeled by the wave numbers $\boldsymbol{k}_1$, $\boldsymbol{k}_2$, and $\boldsymbol{k}_3$ of the three atoms. In the center-of-mass frame, the wave numbers satisfy $\boldsymbol{k}_1 + \boldsymbol{k}_2 + \boldsymbol{k}_3 = 0$ and the energy is $E = \hbar^2(k_1^2 + k_2^2 + k_3^2)/2m$. If we further constrain the 3-atom state to have a very low energy E, total orbital-angular-momentum quantum number $L = 0$, and no subsystem angular momentum, the asymptotic wave function becomes relatively simple. We can identify a very low-energy 3-atom scattering state with a state in the lowest hyperspherical potential in Fig. 21 that asymptotes to 0 as $R \to \infty$. This is the lowest potential $V_0(R)$ if $a < 0$ and the second lowest potential $V_1(R)$ if $a > 0$. In either case, the eigenvalue $\lambda_n(R)$ asymptotes to 4. The corresponding hyperangular wave function is $\phi(R,\alpha) = \sin(2\alpha)$. Thus the asymptotic Faddeev wave function is independent of α. The solution to the hyperradial equation in Eq. (117) with $V_n = 0$ can be expressed in terms of Bessel functions. The asymptotic form of the Faddeev wave function for a 3-atom scattering state with total energy $E = \hbar^2\kappa^2/2m$ is

$$\psi_{\rm AAA}(R,\alpha) \longrightarrow \frac{1}{R^2}[F J_2(\kappa R) + G J_{-2}(\kappa R)], \tag{181}$$

where F and G are arbitrary coefficients. The terms with the coefficients F and G represent outgoing and incoming 3-atom scattering states, respectively.

The evolution of an incoming scattering state to an outgoing scattering state is described by a 2×2 symmetric unitary matrix with entries $S_{\rm AD,AD}$, $S_{\rm AD,AAA} = S_{\rm AAA,AD}$, and $S_{\rm AAA,AAA}$. These S-matrix elements are nontrivial only in those regions of the $a^{-1} - K$ plane where the corresponding asymptotic states are kinematically allowed. In the quadrant $0 < \xi < \frac{1}{2}\pi$, both AAA and AD are allowed. In the quadrant $\frac{1}{2}\pi < \xi < \pi$, only AAA is allowed, so $S_{\rm AAA,AAA}$ is the only nontrivial S-matrix element. In the wedge $-\frac{1}{4}\pi < \xi < 0$, only AD is allowed, so $S_{\rm AD,AD}$ is the only nontrivial S-matrix element. Finally, in the wedge $-\pi < \xi < -\frac{1}{4}\pi$, neither AAA nor AD is allowed so the S-matrix is completely trivial.

An essential ingredient in the derivation of Efimov's radial law is the approximate scale invariance of the 3-body system for hyperradius R in the scale-invariant region $\ell \ll R \ll |a|$. In this region, the equation for the hyperradial wave function reduces to Eq. (143). If R is sufficiently deep into the scale-invariant region, the energy eigenvalue can be neglected. The most general solution in Eq. (144) then has the simple form

$$f(R) = R^{1/2}[A\mathrm{e}^{\mathrm{i}s_0 \ln(HR)} + B\mathrm{e}^{-\mathrm{i}s_0 \ln(HR)}], \tag{182}$$

where H is an arbitrary variable with dimensions of wave number. The Faddeev wave function in Eq. (171) is therefore

$$\psi_{\mathrm{hw}}(R, \alpha) = \frac{\sinh[((\pi/2) - \alpha_1)R/a]}{R^2 \sin(2\alpha_1)}[A\mathrm{e}^{\mathrm{i}s_0 \ln(HR)} + B\mathrm{e}^{-\mathrm{i}s_0 \ln(HR)}], \tag{183}$$

where A and B are arbitrary coefficients. The terms with the coefficients A and B represent an outgoing hyperradial wave and an incoming hyperradial wave, respectively.

In the short-distance region $R \sim \ell$, the wave function becomes very complicated. However, as shown by Efimov, we can get surprisingly strong constraints on the S-matrix just by using the conservation of probability. Efimov assumed implicitly that the 2-body problem had no deep bound states with binding energies of order $\hbar^2/m\ell^2$ or larger. Thus the 2-body potential supports no bound states at all if $a < 0$ and only the shallow bound state with binding energy $E_{\mathrm{D}} = \hbar^2/ma^2$ if $a > 0$. If there were any deep 2-body bound states, some of the probability in an incoming hyperradial wave could flow in to short distances and then emerge through scattering states of an atom and a deep 2-body bound state. Given the assumption that there are no deep 2-body bound states, the probability in the incoming hyperradial wave must be totally reflected at short distances. Thus the amplitudes A and B of the incoming and outgoing hyperradial waves in Eq. (182) must be equal in magnitude, so they must satisfy

$$A = -\mathrm{e}^{2\mathrm{i}\theta_*}B \tag{184}$$

for some angle θ_*. The hyperradial wave function must therefore have the form

$$f(R) \approx \sqrt{HR}\sin[s_0 \ln(cHR) + \theta_*], \tag{185}$$

where c is an arbitrary constant and the angle θ_* is determined by the boundary condition on $f(R)$ at short distances. The angle θ_* can equally well be specified by giving the value of the logarithmic derivative $R_0 f'(R_0)/f(R_0)$ at a point R_0 in the scale-invariant region. It can be expressed as

$$\theta_* = -s_0 \ln(cHR_0) + \operatorname{arccot}\left[\frac{1}{s_0}\left(R_0\frac{f'(R_0)}{f(R_0)} - \frac{1}{2}\right)\right]. \tag{186}$$

All the dependence on H is in the logarithmic term. We can write this expression in the more compact form

$$\theta_* = -s_0 \ln(cH/\Lambda_0), \tag{187}$$

where Λ_0 is the 3-body parameter introduced in Eq. (38).

In the long-distance region $R \sim |a|$, the solution for the wave function again becomes very complicated. However, no matter how complicated the wave function, it must conserve probability. Thus if we identify the asymptotic states at distances $R \ll |a|$ and $R \gg |a|$, the evolution of the wave function through the long-distance region $R \sim |a|$ can be described by a unitary matrix. We denote the asymptotic states with probability flowing into the long-distance region $R \sim |a|$ by kets $|i\ \text{in}\rangle$, $i = 1, 2, 3$, and the asymptotic states with probability flowing out of that region by kets $|i\ \text{out}\rangle$, $i = 1, 2, 3$. The probability can flow into this region either from the scale-invariant region $R \ll |a|$, where the states are hyperradial waves with Faddeev wave function given by Eq. (183), or from the asymptotic region $R \gg |a|$, where the states are 3-atom or atom–dimer scattering states, with asymptotic Faddeev wave functions given by Eqs. (180) or (181), respectively. We will denote the states associated with hyperradial waves by $|1\ \text{in}\rangle$ and $|1\ \text{out}\rangle$, the asymptotic atom–dimer scattering state by $|2\ \text{in}\rangle$ and $|2\ \text{out}\rangle$, and the 3-atom scattering states by $|3\ \text{in}\rangle$ and $|3\ \text{out}\rangle$. It is convenient to normalize these states so that their probability fluxes are all the same. The states associated with the Faddeev wave functions in Eqs. (183), (180), and (181) can be expressed as

$$|\mathrm{hw}\rangle = A|1\ \text{in}\rangle + B|1\ \text{out}\rangle, \tag{188a}$$

$$|\mathrm{AD}\rangle = C|2\ \text{out}\rangle + D|2\ \text{in}\rangle, \tag{188b}$$

$$|\mathrm{AAA}\rangle = F|3\ \text{out}\rangle + G|3\ \text{in}\rangle. \tag{188c}$$

Note that the outgoing hyperradial wave is an incoming asymptotic state $|1\ \text{in}\rangle$ as far as the long-distance region $R \sim |a|$ is concerned. The amplitudes for the incoming asymptotic states to evolve through the long-distance region into the outgoing asymptotic states is described by a unitary 3×3 matrix s:

$$s_{ij} = \langle i\ \text{out}|\hat{U}|j\ \text{in}\rangle, \tag{189}$$

where $\hat{U}$ is the evolution operator that evolves a wave function through the long-distance region $R \sim |a|$ over an arbitrarily large time interval. Time-reversal invariance implies that s is a symmetric matrix.

The matrix s depends on the interaction potential only through the scattering length a. It is also a function of the energy variable K defined in Eq. (69). Because the matrix s_{ij} is dimensionless, it can depend on the variables K and a only through the dimensionless combination Ka or equivalently the angular variable ξ defined in Eq. (70). In general, the symmetric unitary 3×3 matrix s_{ij} is determined by 6 real-valued functions of ξ, but it has a much simpler form in some angular regions. In the region $\frac{1}{2}\pi < \xi < \pi$, there are no AD scattering states so the only nontrivial entries of s_{ij} are for indices 1 and 3. Thus s_{ij} reduces to a symmetric unitary 2×2 matrix that is described by three real-valued functions of ξ. In the region $-\frac{1}{4}\pi < \xi < 0$, there are no AAA scattering states so the only nontrivial entries of s_{ij} are for indices 1 and 2. Thus s_{ij} again reduces to a 2×2 matrix and is described by only three real-valued functions of ξ. In the region $-\pi < \xi < -\frac{1}{4}\pi$ where both AAA and AD scattering states are forbidden, s_{ij} reduces to a 1×1 matrix which is described by a single real-valued function of ξ.

We now proceed to write down Efimov's radial law for the S-matrix for low-energy atom–dimer and 3-atom scattering. We consider only the lowest hyperspherical channels, so the S-matrix at a given value of the energy $E > 0$ is a 2×2 matrix. The S-matrix elements can be expressed in terms of the elements of s as follows:

$$S_{\text{AD,AD}} = s_{22} + s_{21}\frac{1}{1 - \mathrm{e}^{2\mathrm{i}\theta_*}s_{11}}\mathrm{e}^{2\mathrm{i}\theta_*}s_{12}, \tag{190a}$$

$$S_{\text{AD,AAA}} = s_{23} + s_{21}\frac{1}{1 - \mathrm{e}^{2\mathrm{i}\theta_*}s_{11}}\mathrm{e}^{2\mathrm{i}\theta_*}s_{13}, \tag{190b}$$

$$S_{\text{AAA,AAA}} = s_{33} + s_{31}\frac{1}{1 - \mathrm{e}^{2\mathrm{i}\theta_*}s_{11}}\mathrm{e}^{2\mathrm{i}\theta_*}s_{13}. \tag{190c}$$

In each case, the first term on the right side is due to reflection from the long-distance region. If we expand the second term as a power series in s_{11}, we can identify the nth term as the contribution from transmission through the long-distance region and reflection from the short-distance region followed by n reflections from the long-distance region and from the short-distance region before the final transmission through the long-distance region to the asymptotic region. Note that in the regions of ξ for which either AAA or AD asymptotic states are forbidden, the form of s_{ij} implies correctly that $S_{\text{AD,AAA}} = 0$. Efimov's radial law provides very strong constraints on the dependence of the S-matrix elements on the radial variable H, which enters only through the angle θ_* given in Eq. (187). It also constrains the dependence on the angular variable ξ, which is the argument of the symmetric unitary matrix s_{ij}. It implies that the calculation of the S-matrix elements for all energies and all values of the parameters a and κ_* can be reduced to the calculation of a few universal functions of ξ.

6.3. Binding energies of Efimov states

The binding energy for each Efimov state is a function of a and κ_*. The simplest application of Efimov's radial law is to reduce the calculation of the binding energies for all the Efimov states to the calculation of a single universal function of ξ.

Efimov states have binding energies that are less than the natural ultraviolet cutoff $\hbar^2/m\ell^2$. The only adiabatic hyperspherical potential that is attractive in the region $R \gg \ell$ is the lowest one. This potential has a scale-invariant region where the general solution is the sum of an outgoing hyperradial wave and an incoming hyperradial wave as in Eq. (182). Bound states occur at energies for which the waves reflected from the scaling region $R \sim |a|$ come into resonance with the waves reflected from the short-distance region $R \sim \ell$. The resonance condition is simply

$$\exp(2\mathrm{i}\theta_*)s_{11} = 1. \tag{191}$$

Note that this is precisely the condition for the vanishing of the denominators in the three radial laws in Eqs. (190).

In the region $-\pi < \xi < -\frac{1}{4}\pi$, the asymptotic states AAA and AD are kinematically forbidden. Thus we can set $s_{22} = s_{33} = 1$ and $s_{12} = s_{13} = s_{23} = 0$. The only nontrivial entry of the matrix is s_{11}. The unitarity of the matrix implies

$$s_{11} = \exp(\mathrm{i}\Delta(\xi)), \tag{192}$$

where $\Delta/2$ is the phase shift of a hyperradial wave that is reflected from the long-distance region. Combining this with the resonance condition in Eq. (191), we get

$$2\theta_* + \Delta(\xi) = 0 \mod 2\pi. \tag{193}$$

Using the expression for θ_* in Eq. (187) and the definitions for H and ξ in Eq. (70), we obtain Efimov's equation for the binding energies:

$$E_{\mathrm{T}} + \frac{\hbar^2}{ma^2} = (e^{-2\pi/s_0})^{n-n_*} \exp[\Delta(\xi)/s_0] \frac{\hbar^2\kappa_*^2}{m}, \tag{194}$$

where the angle ξ is defined by

$$\tan\xi = -(mE_{\mathrm{T}}/\hbar^2)^{1/2} a. \tag{195}$$

Note that the left side of Eq. (194) is proportional to the radial variable H^2. For each integer n, there is a solution $E_{\mathrm{T}}^{(n)}$ to Eq. (194) that is continuous over a range of $1/a$ that includes 0. Thus the binding energy behaves smoothly as the scattering length a passes through $\pm\infty$. We have absorbed the constant c in Eq. (187) into the function $\Delta(\xi)$ so that it satisfies $\Delta(-\frac{1}{2}\pi) = 0$. Once the universal function $\Delta(\xi)$ has been calculated, the binding energies for all the Efimov states for any values of a and κ_* can be obtained by solving Eq. (194). The equation is the same for different Efimov states except for the factor of $(e^{-2\pi/s_0})^n$ on the right side. In the resonant limit $a \to \pm\infty$, $\xi \to -\frac{1}{2}\pi$ and $\Delta(\xi) \to 0$, so Eq. (194) reduces to Eq. (164). It therefore predicts that the Efimov states have a geometric spectrum in the resonant limit.

There have been many calculations of the binding energies of the Efimov states by solving the Schrödinger equation for various 2-body potentials. In principle, the function $\Delta(\xi)$ could be mapped out by carrying out such calculations for many different sequences of potentials that are approaching the scaling limit. The function $\Delta(\xi)$ can be calculated more directly using the renormalized zero-range model [44] or using effective field theory [61,62], because these methods allow the range to be set to zero so that one can carry out calculations directly in the scaling limit. In Ref. [87], the effective field theory of Refs. [61,62] was used to calculate the binding energy E_{T} of the first few Efimov trimers numerically as a function of a and a 3-body parameter Λ_* that is defined by the renormalization prescription for an effective field theory. The parameter Λ_* differs from κ_* by a multiplicative factor that consists of a numerical constant and an arbitrary integer power of e^{π/s_0}. The relation can be expressed as

$$s_0 \ln(\Lambda_*) \approx s_0 \ln(2.61\,\kappa_*) \mod \pi. \tag{196}$$

Calculations of the trimer binding energies can be used to determine $\Delta(\xi)$ over the entire range of ξ. Simple parametrizations were constructed that give good approximations for the function $\Delta(\xi)$ in three subsets of the interval $-\pi < \xi < -\frac{1}{4}\pi$:

$$\xi \in \left[-\frac{3\pi}{8}, -\frac{\pi}{4}\right] : \Delta = 6.04 - 9.63x + 3.10x^2, \tag{197a}$$

$$\xi \in \left[-\frac{5\pi}{8}, -\frac{3\pi}{8}\right] : \Delta = 2.12y + 1.97y^2 + 1.17y^3, \tag{197b}$$

$$\xi \in \left[-\pi, -\frac{5\pi}{8}\right] : \Delta = -0.89 + 0.28z + 0.25z^2, \tag{197c}$$

where the expansion parameters are

$$x = (-\tfrac{1}{4}\pi - \xi)^{1/2}, \tag{198a}$$

$$y = \tfrac{1}{2}\pi + \xi, \tag{198b}$$

$$z = (\pi + \xi)^2 \exp[-1/(\pi + \xi)^2]. \tag{198c}$$

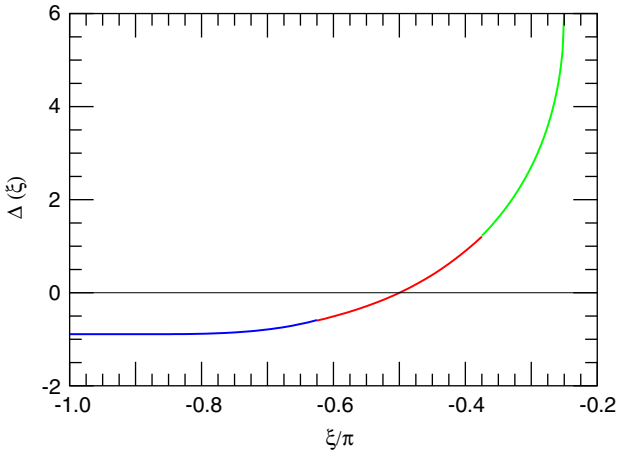

Fig. 25. The universal function $\Delta(\xi)$ for $-\pi < \xi < -\frac{1}{4}\pi$.

The function $\Delta(\xi)$ is shown in Fig. 25. The parametrizations deviate from the numerical results for $\Delta(\xi)$ by less than 0.013. The discontinuities at $\xi = -\frac{3}{8}\pi$ and $\xi = -\frac{5}{8}\pi$ are less than 0.016. The expansion variable x defined in Eq. (198a) has a square-root singularity at $\xi = -\frac{1}{4}\pi$, which corresponds to the atom–dimer threshold. Near this threshold, the 3-body bound state reduces to a 2-body bound state consisting of an atom and dimer, and the square-root singularity follows from the known analytic behavior of the 2-body problem. The expansion variable z defined in Eq. (198c) has an essential singularity at $\xi = -\pi$, which corresponds to the 3-atom threshold. An essential singularity seems to be necessary to reproduce the numerical results in this region of ξ, but the precise form of the essential singularity in Eq. (198c) is simply empirical. If an analytic understanding of the form of the 3-atom threshold were available, it could be used to construct a better parametrization.

Efimov's universal function $\Delta(\xi)$ has recently been calculated with a precision of about 12 digits for $a > 0$, which corresponds to the range $-\frac{1}{2}\pi < \xi < -\frac{1}{4}\pi$ [88]. The calculation of Ref. [88] provides a check on the accuracy of the parameterizations in Eqs. (197). The errors in the parameterization of $\Delta(\xi)$ increase slowly from less than 0.002 near $\xi = -\frac{1}{2}\pi$ to about 0.004 at $\xi = -(1.007)\frac{1}{4}\pi$, and then increase to about 0.012 at $\xi = -\frac{1}{4}\pi$. The precise result for the value of $\Delta(\xi)$ at the point that corresponds to the atom–dimer threshold is [89]

$$\Delta(-\tfrac{1}{4}\pi) = 6.02730678199. \tag{199}$$

The corresponding result from the parameterization in Eq. (197a) is 6.04, which is too large by 0.2%.

The results for $\Delta(\xi)$ can be used to determine the critical values of the scattering length at which Efimov trimers disappear through the atom–dimer threshold or the 3-atom threshold. For the branch of Efimov trimers labelled by $n = n_*$, whose binding energy in the resonant limit is $E_{\rm T}^{(n_*)} = \hbar^2\kappa_*^2/m$, the critical values a_* and a_*' are illustrated in Fig. 24. The precise result for $\Delta(-\frac{1}{4}\pi)$ in Eq. (199) can be used to determine the positive critical values of a for which there is an Efimov trimer at the atom–dimer threshold. For the branch of Efimov trimers labelled by $n = n_*$, the critical value at which $E_{\rm T}^{(n_*)} = E_{\rm D}$ is

$$a_* = 0.0707645086901\kappa_*^{-1}. \tag{200}$$

The other critical values are $(e^{\pi/s_0})^n a_*$, where n is an integer. The value $\Delta(-\pi) \approx -0.89$ given in Eq. (197c) can be used to determine the negative critical values of a for which there is an Efimov trimer at the 3-atom threshold. For the branch of Efimov trimers labelled by $n = n_*$, the critical value at which $E_{\rm T}^{(n_*)} = 0$ is

$$a_*' = -1.56(5)\kappa_*^{-1}. \tag{201}$$

The other critical values are $(e^{\pi/s_0})^n a_*'$, where n is an integer. The error estimate in Eq. (201) is obtained using an independent determination of a_*' from the poles in the 3-particle elastic scattering amplitude. In contrast to a_*

in Eq. (200), only a few of digits of precision are currently available for a'_*. Comparing Eqs. (200) and (201), we see that $a'_* \approx -22.0\ a_*$.

There is a common misconception in the literature that Efimov states must have binding energies that differ by multiplicative factors of 515.03. However, this ratio applies only in the resonant limit $a \to \pm\infty$. The ratio $E_{\rm T}^{(n-1)}/E_{\rm T}^{(n)}$ of the binding energies of adjacent Efimov trimers can be much smaller than 515 if $a > 0$ and much larger than 515 if $a < 0$. The smallest ratios occur at the critical values $(e^{\pi/s_0})^n a_*$, where a_* is given in Eq. (200). The accurate results of Ref. [88] for the binding energies $E_{\rm T}$ of the first few Efimov states in units of $E_{\rm D} = \hbar^2/ma^2$ are

$$E_{\rm T}^{(N)} = E_{\rm D}, \tag{202a}$$
$$E_{\rm T}^{(N-1)} = 6.75029015026 E_{\rm D}, \tag{202b}$$
$$E_{\rm T}^{(N-2)} = 1406.13039320 E_{\rm D}. \tag{202c}$$

Thus, if $a > 0$, the ratio $E_{\rm T}^{(N-1)}/E_{\rm T}^{(N)}$ of the binding energies for the two shallowest Efimov trimers can range from about 6.75 to about 208. The largest ratios occur at the critical values $(e^{\pi/s_0})^n a'_*$, where a'_* is given in Eq. (201). The binding energies $E_{\rm T}$ of the first few Efimov states can be obtained by solving Eq. (194) using the parameterization in Eq. (197a) [87]:

$$E_{\rm T}^{(N)} = 0, \tag{203a}$$
$$E_{\rm T}^{(N-1)} = 1.09 \times 10^3\ \hbar^2/ma^2, \tag{203b}$$
$$E_{\rm T}^{(N-2)} = 5.97 \times 10^5\ \hbar^2/ma^2. \tag{203c}$$

Thus, if $a < 0$, the ratio $E_{\rm T}^{(N-1)}/E_{\rm T}^{(N)}$ of the binding energies for the two shallowest Efimov states can range from about 550 to ∞.

For any nonzero value of a, the binding energy equation (194) has a shallowest solution $E_{\rm T}^{(N)}$ and infinitely many deeper solutions $E_{\rm T}^{(n)}$ corresponding to all integers $n < N$. Thus it predicts that there are infinitely many Efimov states. However, this prediction is an artifact of the scaling limit $\ell \to 0$. For a system with natural low-energy length scale ℓ, the only states of physical relevance are those whose binding energies are less than the natural ultraviolet cutoff of order $\hbar^2/m\ell^2$. The deeper bound states predicted by Eq. (194) are artifacts of the scaling limit.

It is useful to have analytic approximations for the Efimov binding energies for limited ranges of the scattering length. One such range is the region of a just above the value a_* at which there is an Efimov state at the atom–dimer threshold. A simple approximation for the binding energy $E_{\rm T}^{(N)}$ of the shallowest Efimov state in this region can be obtained by exploiting the fact that the atom–dimer scattering length $a_{\rm AD}$ diverges at $a = a_*$. The universal result for the binding energy in the limit $a_{\rm AD} \gg a$ is given in Eq. (166). The errors in this approximation scale as $(a - a_*)^3$. Efimov's universal formula for $a_{\rm AD}$ is given in Eq. (39). The values of the real numerical constants b_0, b_1, and β are given in Section 6.4 in Eq. (216). One can derive an alternative approximation that also has errors of order $(a - a_*)^3$ by inserting Efimov's universal formula for $a_{\rm AD}$ into Eq. (39) and expanding in powers of $\ln(a/a_*)$:

$$E_{\rm T}^{(N)} \approx E_{\rm D}[1 + 0.164 \ln^2(a/a_*)]. \tag{204}$$

In Fig. 26, we compare the analytic approximations Eqs. (166) and (204) to the numerical solution for the binding energy of the shallowest Efimov state over the range $a_* < a < e^{\pi/s_0} a_*$. The large-$a_{\rm AD}$ approximation in Eq. (166) has pathological behavior as a approaches at $8.62a_*$, because $a_{\rm AD}$ vanishes at that point. The approximation in Eq. (204) has comparable accuracy as $a \to a_*$, and it is better behaved at larger a.

Another region in which an analytic approximation for the binding energies of the Efimov states can be given is the resonant region $a \to \pm\infty$. The binding energies in the resonant limit are given in Eq. (158). The leading correction for finite a can be obtained by expanding $\Delta(\xi)$ in Eq. (194) to first order around $\xi = -\frac{1}{2}\pi$:

$$E_{\rm T}^{(n)} = (e^{-2\pi/s_0})^{n-n_*} \frac{\hbar^2\kappa_*^2}{m} \left(1 + 2.11 \frac{(e^{\pi/s_0})^{n-n_*}}{\kappa_* a}\right), \tag{205}$$

where we have used $\Delta'(-\frac{1}{2}\pi) \approx 2.12$ from the parameterization in Eq. (197b).

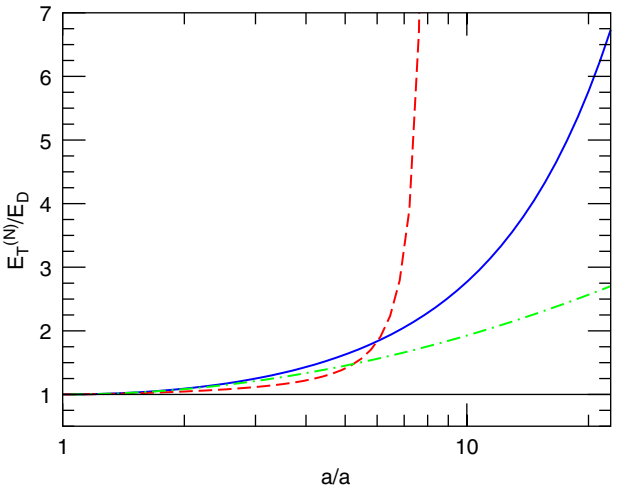

Fig. 26. Comparison of the analytic approximations in Eqs. (166) (dashed line) and (204) (dash-dotted line) to the numerical solution for the binding energy of the shallowest Efimov state (solid line) over the range $a_* < a < e^{\pi/s_0}a_*$.

It would also be valuable to have an analytic approximation for the binding energy of the shallowest Efimov states near the negative value a'_* where the Efimov state disappears into the 3-atom continuum. This would require understanding the analytic behavior of the function $\Delta(\xi)$ near the point $\xi = -\pi$.

6.4. Atom–dimer elastic scattering

The simplest scattering states in the 3-atom sector are atom–dimer scattering states, which we denote by AD. As indicated in Fig. 23, these states are possible only if $a > 0$. The total energy for an atom and dimer in the center-of-mass frame with wave vectors $\pm\boldsymbol{k}$ is

$$E = -E_{\rm D} + \frac{3\hbar^2 k^2}{4m}, \tag{206}$$

where $E_{\rm D} = \hbar^2/ma^2$ is the atom–dimer binding energy. The threshold for atom–dimer scattering is $E = -E_{\rm D}$ or $k = 0$. The scattering is elastic up to the dimer-breakup threshold $E = 0$ or $k = 2/(\sqrt{3}a)$. Above that threshold, the inelastic channel AD $\to$ AAA opens up.

The expression for the differential cross section for atom–dimer scattering in terms of the elastic scattering amplitude $f_k^{\rm AD}(\theta)$ is

$$\frac{{\rm d}\sigma_{\rm AD}}{{\rm d}\Omega} = |f_k^{\rm AD}(\theta)|^2. \tag{207}$$

The elastic cross section $\sigma_{\rm AD}(E)$ is obtained by integrating over the solid angle of 4π. The partial wave expansion for the elastic scattering amplitude has the form

$$f_k^{\rm AD}(\theta) = \sum_{L=0}^{\infty} \frac{2L+1}{k\cot\delta_L^{\rm AD}(k) - {\rm i}k} P_L(\cos\theta). \tag{208}$$

The phase shifts $\delta_L^{\rm AD}(k)$ are real-valued below the dimer-breakup threshold, but they become complex-valued above that threshold. The expression for the elastic cross section obtained by integrating over the scattering angle is

$$\sigma_{\rm AD}(E) = \frac{4\pi}{k^2}\sum_{L=0}^{\infty}(2L+1){\rm e}^{-2\,{\rm Im}\,\delta_L^{\rm AD}(k)}|\sin\delta_L^{\rm AD}(k)|^2. \tag{209}$$

Near the atom–dimer threshold, the $L = 0$ term in the partial-wave expansion can be expanded in powers of k. The expansion is conventionally expressed in the form

$$k \cot \delta_0^{\rm AD}(k) = -1/a_{\rm AD} + \tfrac{1}{2} r_{s,{\rm AD}} k^2 + \cdots, \tag{210}$$

which defines the atom–dimer scattering length $a_{\rm AD}$ and effective range $r_{s,{\rm AD}}$. The optical theorem relates the total cross section, which is the sum of the elastic cross section in Eq. (209) and the inelastic cross section, to the $\theta \to 0$ limit of the elastic scattering amplitude in Eq. (208):

$$\sigma_{\rm AD}^{\rm (total)}(E) = \frac{4\pi}{k} \,{\rm Im}\, f_k^{\rm AD}(\theta = 0). \tag{211}$$

Since the phase shifts $\delta_L^{\rm AD}(k)$ are dimensionless, they can depend only on the dimensionless combinations ka and $a\kappa_*$. For $L \geqslant 1$, the phase shifts are insensitive to 3-body interactions at short distances, and they are therefore universal functions of ka only. The $L = 0$ phase shift is sensitive to 3-body interactions at short distances. The universal expression for $\delta_0^{\rm AD}(k)$ therefore depends on $a\kappa_*$ as well as on ka, although the dependence on $a\kappa_*$ is strongly constrained by Efimov's radial law in Eq. (190a). For S-wave atom–dimer scattering states, the S-matrix element $S_{\rm AD,AD}$ can be expressed in terms of the phase shift $\delta_0^{\rm AD}(k)$:

$$S_{\rm AD,AD} = {\rm e}^{2{\rm i}\delta_0^{\rm AD}(k)}. \tag{212}$$

Below the dimer-breakup threshold, the phase shift is real-valued. In this region, the 2×2 submatrix with entries s_{11}, $s_{12} = s_{21}$, and s_{22} is a unitary matrix. Using the unitarity of this submatrix, we can eliminate s_{22} from the radial law in Eq. (190a) and express it in the form given by Efimov [42]:

$${\rm e}^{2{\rm i}\delta_0^{\rm AD}(k)} = \frac{s_{12}}{s_{12}^*} \frac{{\rm e}^{2{\rm i}\theta_*} - s_{11}^*}{1 - s_{11}{\rm e}^{2{\rm i}\theta_*}}. \tag{213}$$

Efimov used his radial law to derive analytically the dependence of the atom–dimer scattering length $a_{\rm AD}$ on a and κ_*. He showed that $a_{\rm AD}$ must have the form in Eq. (39) where b_0, b_1, and β are universal constants [42]. This expression diverges at the critical values of a given by Eq. (200) for which there is an Efimov trimer at the atom–dimer threshold. The expression in Eq. (39) is also consistent with the discrete scaling symmetry in Eq. (173), because the dimensionless combination $a_{\rm AD}/a$ is a periodic function of $\ln(a)$ with period π/s_0. We proceed to derive Efimov's formula for $a_{\rm AD}$. We need the behavior of the matrix s as $k \to 0$. At $k = 0$, we must have $s_{12} = 0$ and we can set $s_{22} = 1$ by a choice of the overall phase of the matrix s. By the unitarity of s, s_{11} must be a pure phase at $k = 0$: $s_{11} = -{\rm e}^{2{\rm i}\beta'}$ for some angle β'. For small k, the most general form for the nontrivial entries of s allowed by unitarity is

$$s_{11} = -{\rm e}^{2{\rm i}\beta'}[1 - 2(b_0 + {\rm i}b_2)ak + \cdots], \tag{214a}$$

$$s_{12} = (4b_0 ak)^{1/2}{\rm e}^{{\rm i}\beta'}[1 - (2b_3 + {\rm i}b_1 + {\rm i}b_2)ak + \cdots], \tag{214b}$$

$$s_{22} = 1 - 2(b_0 + {\rm i}b_1)ak + \cdots, \tag{214c}$$

where b_0, b_1, b_2, b_3, and β' are real constants and $b_0 > 0$. Inserting these expressions for s_{ij} into the radial law in Eq. (190a), we find that the S-matrix element for atom–dimer scattering near the atom–dimer threshold is

$$S_{\rm AD,AD} \longrightarrow 1 - 2{\rm i}[b_1 - b_0 \tan(\theta_* + \beta')]ak \quad \text{as } E \to -E_{\rm D}. \tag{215}$$

Identifying this expression with $1 - 2{\rm i}a_{\rm AD}k$, using the expression for θ_* in Eq. (187), and setting $H = \sqrt{2}/a$, we obtain Efimov's expression in Eq. (39) with $\beta = \beta' - s_0 \ln(\sqrt{2}\, c\kappa_*/\Lambda_0)$. The real numerical constants b_1 and b_0 in Eq. (39) were first calculated by Simenog and Sinitchenko [43]. They were also calculated by Bedaque, Hammer, and van Kolck using an effective field theory [61,62]. A more accurate determination of these constants is given in Ref. [90]. The explicit expression for the atom–dimer scattering length is

$$a_{\rm AD} = (1.46 - 2.15 \tan[s_0 \ln(a\Lambda_*) + 0.09])a, \tag{216}$$

where Λ_* is a 3-body parameter that arises naturally in the renormalization of the effective field theory. It differs from the parameter κ_* defined by the Efimov spectrum in the resonant limit by a multiplicative factor that is known to only

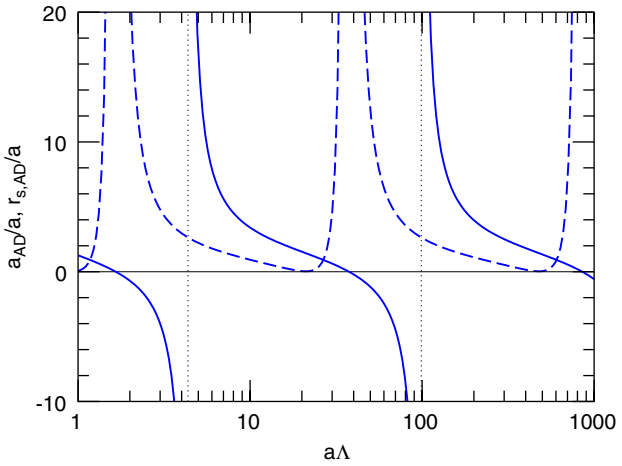

Fig. 27. The atom–dimer scattering length $a_{\rm AD}$ (solid line) and the effective range $r_{s,{\rm AD}}$ (dashed line) as functions of $a\Lambda_*$. The vertical dotted lines indicate the location of the poles in $a_{\rm AD}$.

a few digits of accuracy and is given in Eq. (196). Since most of the phases of the log-periodic functions that appear in 3-body observables in the scaling limit have been calculated using effective field theory, we will express them in terms of Λ_*. The corresponding results in terms of κ_* can be obtained by making the substitution

$$s_0 \ln(a\Lambda_*) = s_0 \ln(a\kappa_*) + 0.97 \quad \mod \pi. \tag{217}$$

Efimov's radial law can also be used to deduce the functional form of the effective range $r_{s,{\rm AD}}$. The expansions in Eq. (214) must be extended to third order in ak. After inserting these expansions into Eq. (213), the expression for $k \cot \delta_0^{\rm AD}(k)$ can be expanded in powers of k and compared to Eq. (210). After taking into account the constraints from the unitarity of s, there is still a linear term in k as well as a quadratic term. The coefficients of these terms depend on b_0, b_1, b_2, b_3, β', and 4 additional constants. However, $k \cot \delta_0^{\rm AD}(k)$ must be an analytic function of k^2, so the coefficients of the odd powers of k must vanish. This implies, for example, that $b_2 = 0$ and $b_3 = b_0/2$. After taking into account the constraints of analyticity, we obtain an expression for $r_{s,{\rm AD}}$ that involves β', b_0, b_1, and three additional constants. Simenog et al. have calculated $a_{\rm AD}^2 r_{s,{\rm AD}}$ by solving the Faddeev equation for an interaction with a small but finite range [43,91]. Hammer and Mehen have calculated $r_{s,{\rm AD}}/a$ as a function of $a\Lambda_*$ [92] using the effective field theory of Refs. [61,62]. Both calculations agree qualitatively. A more accurate expression can be obtained by fitting the calculated atom–dimer scattering phase shifts up to the dimer-breakup threshold (see below) and deriving $r_{s,{\rm AD}}$ from this fit. The resulting expression for $r_{s,{\rm AD}}$ is [90]

$$r_{s,{\rm AD}} = (1.30 - 1.64 \tan[s_0 \ln(a\Lambda_*) + 1.07] + 0.53 \tan^2[s_0 \ln(a\Lambda_*) + 1.07])a. \tag{218}$$

In Fig. 27, we plot the atom–dimer scattering length $a_{\rm AD}$ and effective range $r_{s,{\rm AD}}$ as functions of $a\Lambda_*$ from 1 to 1000, which corresponds to a little more than two periods in $\ln(a)$. The scattering length $a_{\rm AD}$ diverges at the critical values $a_*^{(n)}$ of the scattering length given in Eq. (200) for which there is an Efimov trimer at the atom–dimer threshold. The atom–dimer effective range $r_{s,{\rm AD}}$ behaves smoothly at these points. The atom–dimer scattering length $a_{\rm AD}$ also has zeroes at $a = (e^{\pi/s_0})^n 1.65/\Lambda_*$. The effective range $r_{s,{\rm AD}}$ diverges at this points, but $r_{s,{\rm AD}} a_{\rm AD}^2$ behaves smoothly. The atom–dimer effective range achieves its minimum value at the points $a = (e^{\pi/s_0})^n 0.94/\Lambda_*$. Its value at the minimum is consistent with zero to within the numerical accuracy. If it really is zero, it would indicate that the coefficient of a in Eq. (218) is the square of an expression that is linear in $\tan[s_0 \ln(a\Lambda_*) + 1.07]$. This would require an additional constraint on the expansion coefficients of the matrix s in Eq. (214) beyond those that follow from unitarity and analyticity. If we assume that there is such a constraint, our best fit to the expression for $r_{s,{\rm AD}}$ is

$$r_{s,{\rm AD}} = (1.13 - 0.73 \tan[s_0 \ln(a\Lambda_*) + 1.07])^2 a. \tag{219}$$

Macek et al. [93] have derived an analytic expression for the atom–dimer S-wave phase shift $\delta_0^{\rm AD}(k)$ at the dimer-breakup threshold $k = k_0$, where $k_0 a = 2/\sqrt{3}$:

$$\delta_0^{\rm AD}(k_0) = s_0 \ln(a\kappa_*) - \delta_0 + \delta_\infty + \arctan \frac{\sin[2s_0 \ln(a\kappa_*) - 2\delta_0]}{e^{2\pi s_0} - \cos[2s_0 \ln(a\kappa_*) - 2\delta_0]}, \tag{220}$$

where δ_0 and δ_∞ are real numerical constants.[8] Using Eq. (209), we can get an analytic expression for the S-wave contribution to the atom–dimer elastic scattering cross section at the dimer-breakup threshold. Because $e^{2\pi s_0} \approx 557$ is large, the phase shift in Eq. (220) is well approximated by the much simpler expression

$$\delta_0^{\rm AD}(k_0) \approx s_0 \ln(a\kappa_*) - \delta_0 + \delta_\infty. \tag{221}$$

The corresponding approximation for the $L = 0$ term in the atom–dimer cross section at the dimer-breakup threshold is

$$\sigma_{\rm AD}^{(L=0)}(E = 0) \approx 3\pi \sin^2[s_0 \ln(a\kappa_*) - \delta_0 + \delta_\infty]\, a^2. \tag{222}$$

For a complete parameterization of the S-wave phase shift $\delta_0^{\rm AD}(k)$ in the region $ka < 2/\sqrt{3}$ below the dimer-breakup threshold, we start from the expression for $\cot \delta_0^{\rm AD}(k)$ in Eq. (213). Multiplying it by ka and using trigonometric identities, it can be written in the form

$$ka \cot \delta_0^{\rm AD}(k) = c_1(ka) + c_2(ka) \cot[s_0 \ln(a\Lambda_*) + \phi(ka)]. \tag{223}$$

The simple approximation in Eq. (221) for the S-wave phase shift at the dimer-breakup threshold requires the functions $c_1(ka)$ and $c_2(ka)$ to have specific values at $k_0 a = 2/\sqrt{3}$:

$$c_1(k_0 a) \approx 0, \quad c_2(k_0 a) \approx 2/\sqrt{3}. \tag{224}$$

The functions $c_1(ka)$, $c_2(ka)$, and $\phi(ka)$ have been determined over the entire range $0 < ka < 2/\sqrt{3}$ [90] by calculating the phase shifts $\delta_0^{\rm AD}(k)$ numerically using the effective field theory of Refs. [61,62]. The results can be parametrized as [90]

$$c_1(ka) = -0.22 + 0.39\, k^2a^2 - 0.17\, k^4a^4, \tag{225a}$$
$$c_2(ka) = 0.32 + 0.82\, k^2a^2 - 0.14\, k^4a^4, \tag{225b}$$
$$\phi(ka) = 2.64 - 0.83\, k^2a^2 + 0.23\, k^4a^4. \tag{225c}$$

The approximate constraints in Eqs. (224) have been incorporated into these parameterizations.

We now discuss the qualitative behavior of the expression for $k \cot \delta_0^{\rm AD}(k)$ in Eq. (223). As $a\Lambda_*$ varies with ξ fixed, the cotangent ranges from $-\infty$ to $+\infty$. Thus for fixed ka, $k \cot \delta_0^{\rm AD}(k)$ ranges over all possible value from $-\infty$ to $+\infty$. A divergence in $k \cot \delta_0^{\rm AD}(k)$ implies a zero in the S-wave contribution to the differential cross section. At those values of k, the cross section is dominated by the higher partial waves. The S-wave contribution vanishes at the atom–dimer threshold $k = 0$ if $a\Lambda_* = (e^{\pi/s_0})^n \times 1.65$ and it vanishes at the dimer-breakup threshold $ka = 2/\sqrt{3}$ if $a\Lambda_* = (e^{\pi/s_0})^n \times 0.15$. A zero in $k \cot \delta_0^{\rm AD}(k)$ implies that the S-wave contribution to the differential cross section $d\sigma/d\Omega$ saturates its unitary bound of $1/k^2$. The unitarity bound is saturated in the limit $k \to 0$ if $a\Lambda_* = (e^{\pi/s_0})^n \times 4.34$, which corresponds to the critical values where there is an Efimov state at the atom–dimer threshold. The unitarity bound is saturated at the dimer-breakup threshold $ka = 2/\sqrt{3}$ if $a\Lambda_* = (e^{\pi/s_0})^n \times 15.7$.

In Fig. 28, we plot the S-wave contribution to the differential cross section for atom–dimer scattering as a function of ka for the four special values $a\Lambda_* = 0.15$, 1.65, 4.34, and 15.7 described above. The heavy solid line is the unitarity bound $1/k^2$. Note that the shape of the differential cross section varies dramatically with $a\Lambda_*$.

Using their result in Eq. (220) for the atom–dimer S-wave phase shift at the dimer-breakup threshold, Macek et al. [93] have deduced the 3×3 matrix s whose entries appear in Efimov's radial laws in Eq. (190). At $E = 0$,

[8] For later convenience, we have chosen a phase δ_0 that differs from that in Ref. [93] by $\frac{1}{2}\pi$.

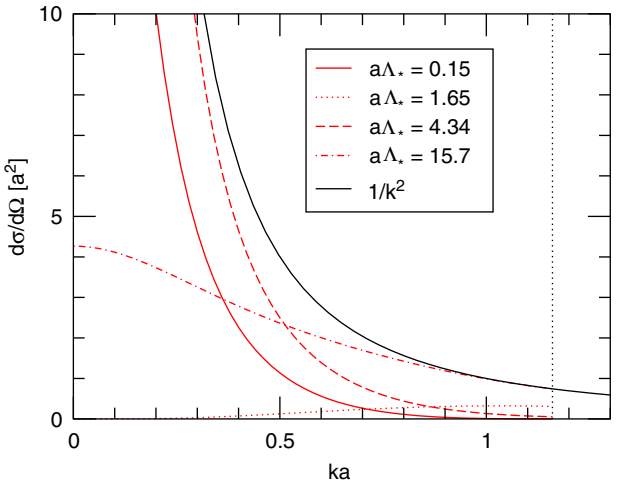

Fig. 28. The S-wave contribution to the differential cross section for atom–dimer scattering in units of a^2 as a function of ka for $a\Lambda_*=0.15$, 1.65, 4.34, and 15.7. The black solid line is the unitarity bound $1/k^2$. The vertical dotted line is the dimer-breakup threshold.

the nonzero entries of the matrix are

$$s_{11} = e^{-2\pi s_0} e^{-2i\delta_0}, \tag{226a}$$

$$s_{12} = \sqrt{1 - e^{-4\pi s_0}}\, e^{i(\delta_\infty - \delta_0)}, \tag{226b}$$

$$s_{22} = -e^{-2\pi s_0} e^{2i\delta_\infty}, \tag{226c}$$

$$s_{33} = 1. \tag{226d}$$

We have set $s_{33} = 1$ by the choice of an overall phase in the matrix s. Since $e^{2\pi s_0} \approx 557$ is large, the diagonal entries s_{11} and s_{22} are very small. This implies that the lowest hyperspherical potential $V_0(R)$ is almost *reflectionless* at $E = 0$. If it were exactly reflectionless, an incoming atom–dimer scattering state with $E = 0$ would be almost completely transmitted through the long-distance region $R \sim a$ into an incoming hyperradial wave in the scale-invariant region. Similarly, an outgoing hyperradial wave would be almost completely transmitted through the long-distance region into an atom–dimer scattering state.

6.5. Three-body recombination

Three-body recombination is a process in which three atoms collide to form a diatomic molecule and an atom. The energy released by the binding energy of the molecule goes into the kinetic energies of the molecule and the recoiling atom. If the scattering length a is negative, the molecule can only be a deep (tightly-bound) diatomic molecule with binding energy of order $\hbar^2/m\ell^2$ or larger. However, if a is positive and unnaturally large ($a \gg \ell$), the molecule can be the shallow dimer with binding energy $E_D = \hbar^2/ma^2$. Three-body recombination into deep molecules will be discussed in Section 7. In this section, we assume there are no deep molecules. We therefore assume $a > 0$ and focus on 3-body recombination into the shallow dimer.

The 3-body recombination rate depends on the momenta of the three incoming atoms. If their momenta are sufficiently small, the dependence on the momenta can be neglected, and the recombination rate reduces to a constant. The *recombination event rate constant* α is defined such that the number of recombination events per time and per volume in a gas of cold atoms with number density n_A is αn_A^3. The resulting rate of decrease in the number of atoms with energies small compared to $\hbar^2/ma^2$ depends on whether the three atoms are in a gas or a Bose–Einstein condensate:

$$\frac{d}{dt} n_A = -3\alpha n_A^3 \quad \text{(gas)}, \tag{227a}$$

$$= -\tfrac{1}{2}\alpha n_A^3 \quad \text{(BEC)}. \tag{227b}$$

In Eq. (227a), the factor of 3 accounts for the three low-energy atoms lost per recombination event. In a Bose–Einstein condensate, the three atoms must all be in the same quantum state, so the coefficient of n_A^3 in Eq. (227a) must be multiplied by 1/3! to account for the symmetrization of the wave functions of the three identical particles [94]. The decrease in the 3-body recombination rate by a factor of 6 when a cold gas condenses into a Bose–Einstein condensate was first observed in experiments on ^{85}Rb atoms [95].

We now restrict our attention to the case of large scattering length and 3-body recombination into the shallow dimer. The condition that the recombination rate be independent of the momenta of the three atoms is that their energies are small compared to $\hbar^2/ma^2$. In this case, we might as well set them all equal to zero. Energy and momentum conservation then imply that the atom and dimer will emerge with wave numbers $k_f = 2/(\sqrt{3}a)$.

We denote the contribution to the rate constant α from 3-body recombination into the shallow dimer by $\alpha_{\rm shallow}$. By dimensional analysis, it is proportional to $\hbar a^4/m$ with a coefficient that depends only on $a\kappa_*$. Petrov has derived a remarkable analytic expression for $\alpha_{\rm shallow}$ [96]:

$$\alpha_{\rm shallow} = \frac{128\pi^2(4\pi - 3\sqrt{3})}{\sinh^2(\pi s_0) + \cosh^2(\pi s_0)\tan^2[s_0\ln(a\kappa_*) + \gamma]}\,\frac{\hbar a^4}{m}, \tag{228}$$

where γ is a real numerical constant. The maximum value of the coefficient of $\hbar a^4/m$ is

$$C_{\rm max} = \frac{128\pi^2(4\pi - 3\sqrt{3})}{\sinh^2(\pi s_0)}. \tag{229}$$

Its numerical value is $C_{\rm max} = 67.1177$. We can exploit the fact that $e^{2\pi s_0} \approx 557$ is large to simplify the expression in Eq. (228). It can be approximated with an error of less than 1% by

$$\alpha_{\rm shallow} \approx C_{\rm max}\sin^2[s_0\ln(a\kappa_*) + \gamma]\,\frac{\hbar a^4}{m}. \tag{230}$$

This approximate functional form of the rate constant was first deduced by Nielsen and Macek [97] and by Esry et al. [98].[9] The constants C and γ were first calculated accurately by Bedaque et al. [99] using the effective field theory of Refs. [61,62]. A more accurate determination of the phase γ was given in Ref. [90]. The resulting expression is

$$\alpha_{\rm shallow} \approx 67.1\sin^2[s_0\ln(a\Lambda_*) + 0.19]\,\frac{\hbar a^4}{m}. \tag{231}$$

The relation between Λ_* and κ_* is given in Eq. (217). The coefficient of $\hbar a^4/m$ is shown as a function of $\ln(a\Lambda_*)$ in Fig. 29. The most remarkable feature of the analytic expression in Eq. (228) and the approximate expression in Eq. (231) is that the coefficient of $\hbar a^4/m$ oscillates between 0 and 67.1 as a function of a. In particular, $\alpha_{\rm shallow}$ has zeroes at values of a that differ by multiplicative factors of $e^{\pi/s_0} \approx 22.7$. Using Eq. (217), the locations of the zeroes can be expressed as

$$a = (e^{\pi/s_0})^n 0.32\,\kappa_*^{-1}, \tag{232}$$

where n is an integer. The maxima of α/a^4 occur near the values of the scattering length for which there is an Efimov trimer at the atom–dimer threshold: $a = (e^{\pi/s_0})^n a_*$, where n is an integer and a_* is given in Eq. (200).

The oscillations in the coefficient of $\hbar a^4/m$ in the recombination rate constant arise from interference effects that were first derived within the hyperspherical framework by Nielsen and Macek and by Esry et al. [97,98]. The 3-body recombination process involves the transition from an incoming 3-atom scattering state on the second lowest hyperspherical potential $V_1(R)$ in Fig. 21 to an outgoing atom–dimer scattering state on the lowest hyperspherical potential $V_0(R)$. These two potentials, which correspond to the lowest two solid lines in Fig. 21, asymptote to $E = 0$ and $E = -E_{\rm D}$, respectively. The 3-body recombination process involves a nonadiabatic transition between these two adiabatic potentials that takes place in the long-distance region $R \sim a$. The process begins with an incoming 3-atom scattering state approaching the long-distance region. The state that emerges from the long-distance region is a superposition of an outgoing atom–dimer scattering state and an incoming hyperradial wave. The incoming hyperradial

[9] In the formula for $\alpha_{\rm shallow}$ in Ref. [98], $s_0 \approx 1.00624$ is replaced by 1.

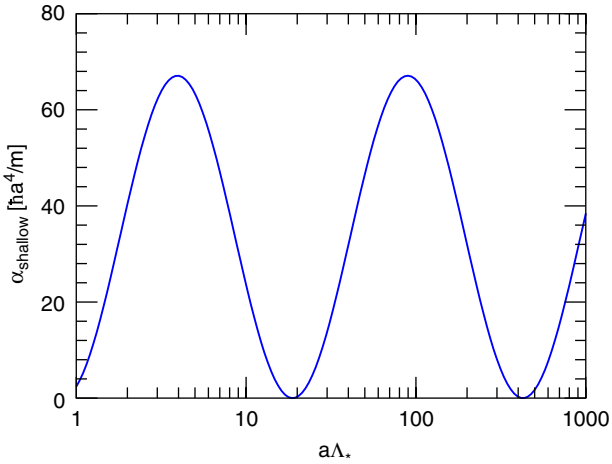

Fig. 29. The 3-body recombination rate constant $\alpha_{\rm shallow}$ in units of $\hbar a^4/m$ as a function of $a\Lambda_*$.

wave flows to short-distances, where it is completely reflected into an outgoing hyperradial wave. It is then almost completely transmitted through the $R \sim a$ region into an atom–dimer scattering state, because the lowest hyperspherical potential is almost reflectionless at $E = 0$. The resulting atom–dimer scattering state can interfere with the atom–dimer scattering state that emerges directly from the nonadiabatic transition, and this interference gives rise to the oscillations of the coefficient of $\hbar a^4/m$ in Eq. (228) as a function of $\ln(a)$. The zeroes in the recombination rate constant indicate that the interference is totally destructive. Such exact zeroes are a well-known phenomenon in the Landau–Zener–Stueckelberg problem of the nonadiabatic transition between two adiabatic energy levels with an avoided crossing.

Nielsen and Macek [97] obtained their result for $\alpha_{\rm shallow}$ by applying *hidden crossing theory*. The adiabatic hyperspherical potentials $V_n(R)$ in Eq. (113) involve the functions $\lambda_n(R)$ that are solutions to Eq. (129). If this equation is used to define the functions $\lambda_n(R)$ for complex values of R, the channel potentials $V_n(R)$ become sheets in the complex R plane that are connected at square-root branch points. For example, if $a > 0$ one can go continuously from the lowest adiabatic potential $V_0(R)$ to the second lowest one $V_1(R)$ by following a path that goes around a square-root branch point at $R = (2.59 + 2.97i)a$. In the analysis of Nielsen and Macek, the two interfering amplitudes that contribute to $\alpha_{\rm shallow}$ correspond to two WKB integration contours. Both contours begin with real-valued R in the asymptotic region of the $n = 1$ adiabatic potential, go continuously around the branch point in the complex R plane to the $n = 0$ adiabatic potential, and eventually end with real-valued R in the asymptotic region of the $n = 0$ adiabatic potential. However, after having made the transition to the $n = 0$ adiabatic potential, the first contour goes immediately out to asymptotic R, while the second contour first goes to the short-distance region of R and then returns through the region $R \sim a$ to the asymptotic R. Along the path to the short-distance region and back, the second contour picks up an additional WKB phase. Thus the two amplitudes have the same magnitude and differ only by a phase that is determined by the short-distance region of the lowest adiabatic potential.

Esry et al. [98] obtained their result for $\alpha_{\rm shallow}$ by solving the 3-body Schrödinger equation in hyperspherical coordinates. They attributed the $\sin^2$ factor in Eq. (230) to Stückelberg oscillations associated with a broad avoided crossing between the $n = 0$ and $n = 1$ adiabatic potentials for R around $3a$.

The a^4 scaling behavior of $\alpha_{\rm shallow}$ was first obtained in Ref. [100]. However, the coefficient of a^4 was claimed to be a constant independent of a: $\alpha_{\rm shallow} = 3.9\hbar a^4/m$. Several independent groups using completely different methods have shown that the coefficient is actually a log-periodic function of a. We conclude that there was an error in the analysis of Ref. [100].

The power-law scaling behavior $\alpha_{\rm shallow} \sim a^4$ has been verified in experiments with ^{133}Cs atoms [101]. The logarithmic scaling violations associated with the log-periodic dependence on a of the coefficient in Eq. (228) have not yet been observed in experiments.

Since the zeroes in $\alpha_{\rm shallow}$ are so remarkable, it is worth enumerating some of the effects that will tend to fill in the zeroes, turning them into local minima of $\alpha_{\rm shallow}/a^4$. First, all universal predictions for the 2-body and 3-body sectors

hold only up to corrections suppressed by powers of ℓ/a. Thus the zeroes in $\alpha_{\rm shallow}$ really mean that the coefficient of $\hbar a^4/m$ goes to zero like ℓ/a as $\ell \to 0$. The zeroes in $\alpha_{\rm shallow}$ are also exact only at threshold. If the recombining atoms have wave numbers of order k, the zeroes indicate that $\alpha_{\rm shallow}/a^4$ goes to zero like ka as $k \to 0$. Thus thermal effects that give nonzero momentum to the atoms could tend to fill in the zeroes. Finally, if the 2-body potential supports deep diatomic molecules, their effects will tend to fill in the zeros of $\alpha_{\rm shallow}$ as described in Section 7.4. Furthermore, 3-body recombination into those deep molecules gives an additive contribution $\alpha_{\rm deep}$ to the rate constant that will be determined in Section 7.5. The range of validity of the universal expression in Eq. (228) has been studied by D'Incao et al. [102]. They showed that it is a good approximation only for collision energy E in the threshold region $E \lesssim E_{\rm D}$. However, their conclusion that "universal behavior is limited to the threshold region" is a misinterpretation. Universality predicts that 3-body observables are determined by a and κ_* only not only in the threshold region but at all energies satisfying $E \ll \hbar^2/(mr_s^2)$. Thus far, the predictions of universality for the recombination rate have been calculated only at the threshold $E = 0$. They have not yet been calculated as a function of E.

We now proceed to show how the analytic dependence of the 3-body recombination rate constant $\alpha_{\rm shallow}$ on a and κ_* in Eq. (228) can be derived from Efimov's radial law. The radial law for the S-matrix element $S_{\rm AD,AAA}$ is given in Eq. (190b). The recombination rate constant α is determined by the behavior of s_{11}, s_{12}, s_{13}, and s_{23} just above the dimer-breakup threshold. The values of s_{11} and s_{12} at the threshold $E = 0$ are given in Eq. (226). The entries s_{13} and s_{23} vanish at $E = 0$. The leading dependence of these entries on the energy $E = \hbar^2 K^2/m$ can be deduced from threshold laws for 3-body reaction rates [77]. They require s_{13} and s_{23} to scale like K^2:

$$s_{13} = -c_1 e^{-i\gamma_0} a^2 K^2 [1 + \cdots], \tag{233a}$$

$$s_{23} = -c_2 e^{+i\gamma_1} a^2 K^2 [1 + \cdots], \tag{233b}$$

where c_1, c_2, γ_0, and γ_1 are real numerical constants and c_1 and c_2 are positive. The entries of s have expansions in powers of K. The unitarity of s imposes constraints on the numerical constants in these expansions. For example, it implies $c_2 = [\tanh(\pi s_0)]^{1/2} c_1$. Expanding the S-matrix element for 3-body recombination in Eq. (190b) to leading order in K, we find

$$S_{\rm AD,AAA} \longrightarrow -c_2 e^{i\gamma_1} a^2 K^2 \, \frac{1 + e^{2i(\theta_* - \delta_0)}}{1 - e^{-2\pi s_0} e^{2i(\theta_* - \delta_0)}} \quad \text{as } E \to 0^+. \tag{234}$$

The 3-body recombination rate constant α is proportional to $|S_{\rm AD,AAA}|^2$. Squaring the expression in Eq. (234) and setting $\theta_* = s_0 \ln(a\kappa_*)$, we find that the dependence on a and κ_* agrees with the analytic expression for $\alpha_{\rm shallow}$ in Eq. (228).

6.6. Three-atom elastic scattering

The physical region for 3-atom scattering states is $E > 0$, where E is the total energy of the three atoms. We expect nontrivial 3-body effects to be most dramatic in the threshold region $E \to 0$, so we will only consider this limit. In the standard plane-wave basis, the T-matrix element for 3-body elastic scattering diverges as $E \to 0$ [103]. The most singular term comes from two successive 2-body scatterings that involve all three particles, and it is proportional to a^2/E. There are also singular terms proportional to $a^3/\sqrt{E}$ and $a^4 \ln E$. To obtain the 3-body elastic scattering rate, the effects of 2-body elastic collisions, with the third particle infinitely far away, must be subtracted [7].

The T-matrix element $\mathscr{T}$ for 3-atom elastic scattering depends on the three wave vectors of the incoming atoms and the three wave vectors of the outgoing atoms. The contribution to $\mathscr{T}$ from total orbital angular momentum quantum number $L = 0$ depends only on the total energy $E = \hbar^2 K^2/m$ of the three particles. Its limiting behavior as $E \to 0$ is

$$\mathscr{T}^{(L=0)} \longrightarrow \left(\frac{A}{K^2 a^2} + \frac{B}{Ka} + C \ln(K|a|) + D_\pm \right) \frac{\hbar a^4}{m} \quad \text{as } E \to 0. \tag{235}$$

The coefficients A, B, and C are numerical constants. The sensitivity to Efimov physics resides only in the coefficient $D_\pm$, which depends on the sign $\pm$ of a and is a function of $a\kappa_*$. The coefficient D_- for the case $a < 0$ is real-valued. The coefficient D_+ for the case $a > 0$ is complex-valued. Its imaginary part is related to the 3-body recombination rate constant $\alpha_{\rm shallow}$ given in Eq. (228) by the unitarity condition

$$\mathrm{Im}\, \mathscr{T} = 3\alpha_{\rm shallow}. \tag{236}$$

The numerical constants A, B, and C can be calculated from the terms of orders a^2, a^3, and a^4, respectively, in the perturbative expansion of $\mathscr{T}$, which are given explicitly in Section 8.5. The coefficients A and B have not been calculated. The coefficient C is known analytically [104]:

$$C = 384\pi(4\pi - 3\sqrt{3}). \tag{237}$$

The coefficient $D_\pm$ in Eq. (235) can only be obtained by a nonperturbative calculation. One might expect that $D_\pm$ could be obtained from the order-a^4 term in the perturbative expansion of $\mathscr{T}$, but the perturbative contribution to $D_\pm$ is ultraviolet divergent. The perturbative approximation can be expressed in the form

$$D_\pm \approx D_\pm^{(\mathrm{pert})} - C\ln(|a|\Lambda), \tag{238}$$

where Λ is the ultraviolent cutoff and $D_\pm^{(\mathrm{pert})}$ is a numerical constant that depends on how the ultraviolet cutoff is implemented. The difference between the coefficient $D_\pm$ and its perturbative approximation can be determined by a nonperturbative 3-body calculation. The coefficient $D_\pm$ can be expressed as the sum of the perturbative and nonperturbative contributions:

$$D_\pm = \Big[D_\pm^{(\mathrm{pert})} - C\ln(|a|\Lambda)\Big] + \Big[D_\pm^{(\mathrm{nonpert})} + C\ln(|a|\Lambda)\Big], \tag{239}$$

where $D_\pm^{(\mathrm{nonpert})}$ depends on $|a|\kappa_*$. The dependence on the ultraviolet cutoff cancels in the sum of the two contributions in Eq. (239).

The nonperturbative contributions to the coefficients $D_\pm$ were calculated in Ref. [105] for a specific regularization of the perturbative T-matrix element: *dimensional regularization* and *minimal subtraction*. In dimensional regularization, momentum integrals are analytically continued from 3 dimensions to D dimensions, in which case logarithmic ultraviolet divergences appear as poles in $D-3$. In minimal subtraction, the ultraviolet divergences are removed simply by subtracting the poles in $D-3$. In the case $a<0$, the functional form of the dependence of D_- on $|a|\kappa_*$ was deduced by Efimov [42]. In Ref. [105], the calculated result for $D_-^{(\mathrm{nonpert})}$ was fit to that functional form, with the result

$$D_-^{(\mathrm{nonpert})} = C(1.23 + 3.16\cot[s_0\ln(|a|\Lambda_*) - 1.38]), \tag{240}$$

where C is given in Eq. (237). The coefficient $D_-^{(\mathrm{nonpert})}$ diverges at those negative values of the scattering length for which there is an Efimov trimer at the 3-atom threshold: $a = (e^{\pi/s_0})^n a'_*$, where n is an integer and a'_* is given in Eq. (201).

The nonperturbative contribution to the complex-valued coefficient D_+ was also calculated in Ref. [105]. The calculated result for $D_+^{(\mathrm{nonpert})}$ was found empirically to be an oscillatory function of $\ln(a\Lambda_*)$. Its real and imaginary parts were fit by the expressions

$$\mathrm{Re}\, D_+^{(\mathrm{nonpert})} \approx C(1.22 + 0.021\sin^2[s_0\ln(a\Lambda_*) - 0.6]), \tag{241a}$$

$$\mathrm{Im}\, D_+^{(\mathrm{nonpert})} \approx C(0.022\sin^2[s_0\ln(a\Lambda_*) + 0.19]). \tag{241b}$$

The imaginary part in Eq. (241b) is consistent with the unitarity constraint in Eq. (236) if we use the approximate expression for α in Eq. (231). Note that the oscillatory term of the real part in Eq. (241a) has approximately the same amplitude as the imaginary part but a different phase.

We proceed to derive the dependence of the coefficients $D_\pm$ in Eq. (235) on $a\kappa_*$ using Efimov's radial law. The radial law for the $L=0$ contribution to the S-matrix element for 3-atom elastic scattering is given in Eq. (190c). It involves the entries s_{11}, s_{13} and s_{33} of the 3×3 matrix s. We first consider the case $a<0$. We need the behavior of the entries of s as a function of the energy $E = \hbar^2K^2/m$ near the threshold. At $K=0$, we must have $s_{13}=0$ and we can set $s_{33}=1$ by a choice of the overall phase of the matrix s. By the unitarity of s, s_{11} must be a pure phase at $K=0$: $s_{11} = -\mathrm{e}^{2\mathrm{i}\delta}$ for some angle δ. All the entries have expansions in powers of aK. The coefficients are constrained by the unitarity of the 3×3 matrix s. The expansion of the off-diagonal entry s_{13} must begin at order a^2K^2 for the dependence of $S_{\mathrm{AAA,AAA}}$ on κ_* to enter only at order a^4K^4. There is an additional constraint on the coefficients from the fact that

the expansion of $S_{\rm AAA,AAA} - 1$ begins at order a^2K^2. The resulting expansions for the entries of s that contribute to $S_{\rm AAA,AAA}$ are

$$s_{11} = -e^{2i\delta}[1 - id_1aK - (\tfrac{1}{2}d_2^2 + id_6)a^2K^2 + \cdots], \tag{242a}$$

$$s_{13} = d_0 e^{i\delta}a^2K^2[1 - (d_5 + i\tfrac{1}{2}d_1)aK + \cdots], \tag{242b}$$

$$s_{33} = 1 - id_2a^2K^2 - id_3a^3K^3 - (\tfrac{1}{2}d_0^2 + \tfrac{1}{2}d_2^2 + id_4)a^4K^4 + \cdots, \tag{242c}$$

where d_0, d_1, d_2, d_3, d_4, d_5, d_6, and δ are real constants and $d_0 > 0$. Inserting the expressions for s_{ij} in Eqs. (242) into the radial law in Eq. (190c), we obtain

$$S_{\rm AAA,AAA} \longrightarrow 1 - id_2a^2K^2 - id_3a^3K^3 - \left[\tfrac{1}{2}d_2^2 + id_4 - \tfrac{1}{2}d_0^2\cot(\theta_* + \delta)\right]a^4K^4 \quad \text{as } E \to 0. \tag{243}$$

The elements of the S-matrix and the T-matrix are related by $S = 1 + iT$. Note that the coefficient of the a^4K^4 term has the same functional dependence on $a\kappa_*$ as the empirical coefficient $D_-^{(\rm nonpert)}$ in Eq. (240), which is the nonperturbative part of the coefficient of a^4 in the T-matrix element in Eq. (235).

We next consider the case $a > 0$. The radial law for $S_{\rm AAA,AAA}$ in Eq. (190c) involves the entries s_{11}, s_{13} and s_{33} of the 3×3 matrix s. The values of s_{11}, s_{12}, s_{22}, and s_{33} at $E = 0$ are given in Eqs. (226). The leading terms in the entries s_{13} and s_{23} are of order a^2K^2 and are given in Eq. (233a). The entries all have expansions in powers of K. The coefficients are constrained by the unitarity of the 3×3 matrix s. There is an additional constraint from the fact that the expansion of $S_{\rm AAA,AAA} - 1$ begins at order a^2K^2. That expansion includes a term of order a^3K^3 with a constant coefficient and then a term of order a^4K^4 whose coefficient iD depends on $a\kappa_*$. The coefficient D has the form

$$D = c_3 + ic_1^2 - ic_1^2\frac{e^{2i(\theta_* - \delta_0)}}{1 - e^{-2\pi s_0}e^{2i(\theta_* - \delta_0)}}, \tag{244}$$

where c_1 is the numerical constant in Eq. (233a) and c_3 is another numerical constant. The relation between the S-matrix and the T-matrix is $S = 1 + iT$. Thus the coefficient D_+ of the a^4 term in the T-matrix element in Eq. (235) must have the same dependence on $a\kappa_*$ as in Eq. (244). We can exploit the fact that $e^{2\pi s_0} \approx 557$ is large to simplify the coefficient in Eq. (244). It can be approximated with an error of less than 1% by

$$D \approx c_3 - ic_1^2(e^{2i(\theta_* - \delta_0)} - 1) \tag{245a}$$

$$= c_3 - c_1^2 + 2c_1^2\sin^2(\theta_* - \delta_0 + \tfrac{1}{4}\pi) + 2ic_1^2\sin^2(\theta_* - \delta_0). \tag{245b}$$

The dependence of this approximate expression on $a\kappa_*$ is compatible with that of the empirically determined coefficient $D_+^{(\rm nonpert)}$ given by Eqs. (241). In particular, the amplitudes of the oscillatory terms in Eqs. (241a) and (241b) are equal to within the numerical accuracy and the phase difference between the oscillations is close to the value $\frac{1}{4}\pi \approx 0.79$ predicted by Eq. (245b). More precise results for the coefficients in Eq. (241) could have been obtained if the constraints from Efimov's radial law had been imposed on the fit.

For a dilute homogeneous Bose gas composed of particles with a positive scattering length a and number density n, the leading term in the low-density expansion of the energy per particle is given in Eq. (1). The low-density expansion is an expansion in powers of the diluteness variable $(na^3)^{1/2}$. Despite the fractional powers of a, this is a perturbative expansion in powers of a. The dimensionless expansion parameter is the ratio a/ξ of the scattering length and the coherence length $\xi = (16\pi na)^{-1/2}$. The first few terms in the low-density expansion have the form

$$\frac{\mathscr{E}}{n} = \frac{2\pi\hbar^2}{m}an\left(1 + \frac{128}{15\sqrt{\pi}}(na^3)^{1/2} + \frac{8(4\pi - 3\sqrt{3})}{3}\left[\ln(na^3) + 2d\right]na^3\right). \tag{246}$$

The $(na^3)^{1/2}$ correction was first calculated by Lee and Yang in 1957 for the case of particles interacting through a hard-sphere potential of radius a [106]. This correction is universal: it applies equally well to any potential with a positive scattering length a. The $na^3\ln(na^3)$ correction, which was first calculated in 1959 [107–109], is also universal in the sense that it depends only on a. The na^3 correction is not universal, according to the definition traditionally used in the theory of the homogeneous Bose gas, because it depends on few-body parameters other than a. Specifically, it

depends on the coefficient D_+ in the low-energy expansion of the T-matrix element for 3-body elastic scattering given in Eq. (235) [104]. In the special case of a large scattering length, this correction is universal by our definition, which we argue is more appropriate for this strongly interacting problem. The coefficient of na^3 in Eq. (246) has a well-defined scaling limit as the range of the interaction is tuned to zero. It is a log-periodic function of $a\kappa_*$ [105]:

$$d = D_+^{(\text{nonpert})}/C + 2.36, \tag{247}$$

where $D_+^{(\text{nonpert})}$ is given in Eqs. (241). The imaginary part of the coefficient reflects the loss of mean-field energy due to 3-body recombination into the shallow dimer.

6.7. Helium atoms

Helium atoms provide a beautiful illustration of universality in the 3-body system [90]. The binding energies of the ^{4}He trimers have been calculated accurately for a number of different model potentials for the interaction between two ^{4}He atoms. For the purposes of illustration, we will use the TTY potential [19]. The scattering length for the TTY potential is $a = 188.99a_0$. This is much larger than its effective range $r_s = 13.85a_0$, which is comparable to the van der Waals length scale $\ell_{\text{vdw}} = 10.2a_0$. The TTY potential supports a single 2-body bound state, the ^{4}He dimer whose binding energy is $E_2 = 1.30962\,\text{mK}$. The conversion factor to the atomic energy unit is given in Eq. (33). The ^{4}He dimer was first observed in 1992 [110]. The TTY potential has exactly two 3-body bound states: the ground-state trimer, which we label $n = 0$, and the excited trimer, which we label $n = 1$. There have been several accurate calculations of the binding energies $E_3^{(0)}$ and $E_3^{(1)}$ for the TTY potential [111–113]. The results agree to within 0.5% for both $E_3^{(0)}$ and $E_3^{(1)}$. The results of Ref. [113] are $E_3^{(0)} = 125.8\,\text{mK}$ and $E_3^{(1)} = 2.28\,\text{mK}$. The ground state trimer was first observed in 1994 [114]. The excited state has not yet been observed.

Lim, Duffy, and Damert proposed in 1977 that the excited state of the ^{4}He trimer is an Efimov state [115]. This interpretation is almost universally accepted. Some researchers have proposed that the ground state trimer is also an Efimov state [61,62,44]. This raises an obvious question: what is the definition of an Efimov state? The most commonly used definition is based on rescaling the depth of the 2-body potential: $V(\mathbf{r}) \longrightarrow \lambda V(\mathbf{r})$. A trimer is defined to be an Efimov state if its binding energy as a function of the scaling parameter λ has the qualitative behavior illustrated in Fig. 24. As λ is decreased below 1, the trimer eventually disappears through the 3-atom threshold. As λ is increased above 1, the trimer eventually disappears through the atom–dimer threshold. Calculations of the trimer binding energies [116] using a modern helium potential show that the excited trimer satisfies this definition of an Efimov state but the ground state trimer does not. The excited trimer disappears through the 3-atom threshold when λ is decreased to about 0.97, and it disappears through the atom–dimer threshold when λ is increased to about 1.1. The ground state trimer disappears through the 3-atom threshold when λ is about 0.9. However, as λ is increased above 1, its binding energy relative to the atom–dimer threshold continues to increase. Thus is does not qualify as an Efimov state by the definition given above.

The traditional definition of an Efimov state described above is not natural from the point of view of universality. The essence of universality concerns the behavior of a system when the scattering length becomes increasingly large. The focus of the traditional definition is on the endpoints of the binding energy curve in Fig. 24, which concerns the behavior of the system as the scattering length decreases in magnitude. The problem is that the rescaling of the potential can move the system outside the large-scattering-length region $|a| \gg r_s$ before the trimer reaches the endpoint of the binding energy curve. We therefore propose a definition of an Efimov state that is more natural from the universality perspective. A trimer is defined to be an Efimov state if a deformation that tunes the scattering length to $\pm\infty$ moves its binding energy along the universal curve illustrated in Fig. 24. The focus of this definition is on the resonant limit where the binding energy crosses the $1/a = 0$ axis. In particular, the binding energy at this point should be larger than that of the next shallowest trimer by about a factor of 515. In the case of helium, the resonant limit can be reached by rescaling the 2-body potential by a factor $\lambda \approx 0.97$ [116]. At this point, the binding energy of the ground state trimer is larger than that of the excited trimer by about a factor of 570. The closeness of this ratio to the asymptotic value 515 supports the hypothesis that the properties of the ground state trimer are largely determined by universality. Further evidence in support of this hypothesis will be presented below.

In order to apply the universal predictions for low-energy 3-body observables to the case of ^{4}He atoms, we need a 2-body input and a 3-body input to determine the parameters a and κ_*. The scattering length $a = 188.99a_0$ itself can

Table 2
Binding energies $E_3^{(n)}$ of the ^{4}He trimers for the TTY potential (row 1) compared to the universality predictions using as the inputs either E_2 and $E_3^{(1)}$ (row 2) or a and $E_3^{(1)}$ (row 3). Energies are given in mK and lengths are given in å. The trimer binding energies for the TTY potential are from Ref. [113]. (Note that $\hbar^2/m = 12.1194\,\mathrm{K\AA}^2$ for ^{4}He atoms.)

Potential	a	a_D	$E_3^{(1)}$	$E_3^{(0)}$	$E_3^{(-1)}$
TTY	100.0	96.2	2.28	125.8	—
		Input	Input	129.1	5.38×10^4
	Input		Input	146.4	6.23×10^4

be taken as the 2-body input. An alternative 2-body input is the dimer binding energy E_2. A scattering length a_D can be determined by identifying E_2 with the universal binding energy of the shallow dimer: $E_2 = \hbar^2/ma_D^2$. The result is $a_D = 181.79a_0$. The 3.8% difference between a and a_D is a measure of how close the system is to the scaling limit. To minimize errors associated with the deviations of the system from the scaling limit, it is best to take the shallowest 3-body binding energy available as the input for determining κ_*. In the case of ^{4}He atoms, this is the binding energy $E_3^{(1)}$ of the excited trimer.

We proceed to consider the universal predictions for the trimer binding energies. Having identified $E_3^{(1)}$ with the universal trimer binding energy $E_T^{(1)}$, we can use Efimov's binding energy equation (194) with $n_* = 1$ to calculate κ_* up to multiplicative factors of $e^{\pi/s_0} \approx 22.7$ [90]. The result is $\kappa_* = 0.00215a_0^{-1}$ or $\kappa_* = 0.00232a_0^{-1}$, depending on whether $E_2 = 1.31$ mK or $a = 189.0a_0$ is used as the 2-body input. The intuitive interpretation of κ_* is that if a parameter in the short-distance potential is adjusted to tune a to $+\infty$, the binding energy $E_3^{(1)}$ should approach a limiting value of approximately $\hbar^2\kappa_*^2/m$, which is 0.201 mK or 0.233 mK depending on the 2-body input.

Once κ_* has been calculated, we can solve Eq. (194) for the binding energies of the deeper Efimov states. The prediction for the next two binding energies are shown in Table 2. The prediction for $E_3^{(0)}$ differs from the binding energy of the ground-state trimer by 2.6% or 16.4%, depending on whether E_2 or a is taken as the 2-body input. The expected error is comparable to the maximum of $\ell_{vdW}/a = 5.4\%$ and $(E_3^{(0)}/E_{vdW})^{1/2} \approx 50\%$, where $E_{vdW} = \hbar^2/m\ell_{vdW}^2 \approx 420$ mK is the natural ultraviolet cutoff for ^{4}He atoms. The errors are much smaller than expected, suggesting that the scaling limit is more robust than one might naively expect.

Efimov's equation (194) also predicts infinitely many deeper 3-body bound states. The prediction for the next deepest state is given in Table 2: $E_3^{(-1)} \approx 5 \times 10^4$ mK. This is more than two orders of magnitude larger than the natural ultraviolet cutoff for ^{4}He atoms, which is about 420 mK. We conclude that this state and all the deeper bound states are artifacts of the scaling limit.

Using the above values of κ_* for the TTY potential, we can immediately predict the atom–dimer scattering length a_{AD}. If a is used as the 2-body input, we find $a_{AD} \approx 0.94a$, corresponding to $a_{AD} \approx 178a_0$. If E_2 is used as the 2-body input, we find $a_{AD} \approx 1.19a_D$, corresponding to $a_{AD} \approx 216a_0$. These values are in reasonable agreement with the calculation of Ref. [113], which gave $a_{AD} = 248(10)a_0$. Since $r_s/a = 7.3\%$ for the TTY potential, much of the remaining discrepancy can perhaps be attributed to effective-range corrections.

We can also predict the 3-body recombination rate constant for ^{4}He atoms interacting through the TTY potential. The prediction for $\alpha_{shallow}$ is $2.9\hbar a_D^4/m$ or $6.9\hbar a^4/m$, depending on whether the dimer binding energy E_2 or the scattering length a is used as the 2-body input. In either case, the coefficient of $\hbar a^4/m$ is much smaller than the maximum possible value 67.1. Thus ^{4}He atoms are fortuitously close to a combination of a and κ_* for which $\alpha_{shallow}$ is zero. The 3-body recombination rate constant has not yet been calculated for the TTY potential, so the prediction of universality cannot be tested.

Similar comparisons can be made for other modern ^{4}He potentials. In Table 3, we have collected the available 3-body results and universality predictions for the HFDHE2 [117], HFD-B [118], LM2M2 [18], TTY [19], and HFD-B3-FCI1 [119] potentials. The 3-body results for the HFDHE2, HFD-B, LM2M2, and TTY potentials are from Ref. [113], while the 3-body results for the HFD-B3-FCI1 potential are from Refs. [120,121]. The universality predictions are given for the case where a_D and $E_3^{(1)}$ are used as the inputs and for the case where a and $E_3^{(1)}$ are used as the inputs. Where a comparison can be made, we find reasonably good agreement between the universality predictions and the direct calculations.

Table 3
Three-body results for various model potentials for ^{4}He compared to the universality predictions using either a_D and $E_3^{(1)}$ or a and $E_3^{(1)}$ as the inputs

Potential	a	a_D	$E_3^{(1)}$	$E_3^{(0)}$	a_{AD}	α
HFDHE2	124.6	120.8	1.67	116.7	—	—
		Input	Input	118.5	87.9	3.79
	Input		Input	129.1	65.8	5.95
HFD-B	88.5	84.8	2.74	132.5	135(5)	—
		Input	Input	137.5	120.2	0.064
	Input		Input	159.7	100.4	0.37
LM2M2	100.2	96.4	2.28	125.9	131(5)	—
		Input	Input	130.3	113.1	0.45
	Input		Input	147.4	92.8	1.16
TTY	100.0	96.2	2.28	125.8	131(5)	—
		Input	Input	129.1	114.5	0.41
	Input		Input	146.4	94.0	1.11
HFD-B3-FCI1	91.0	87.0	2.62	131.3	—	0.12
		Input	Input	133.8	123.0	0.090
	Input		Input	156.1	101.5	0.48

All energies are given in mK, all lengths are given in å, and α is given in 10^{-27} cm^6/s. The 3-body results for the HFDHE2, HFD-B, LM2M2, and TTY potentials are from Ref. [113], while the 3-body results for the HFD-B3-FCI1 potential are from Refs. [120,121]. (Note that $\hbar^2/m = 12.1194$ KÅ^2 for ^{4}He atoms.)

6.8. Universal scaling curves

The logarithmic scaling violations associated with the Efimov effect imply that low-energy observables in the scaling limit depend not only on the scattering length a, but also on the 3-body parameter κ_*. A dimensionless combination of observables is called a *scaling variable*. Examples are ratios of binding energies, such as $E_T^{(N)}/E_D$, or ratios of scattering lengths, such as a_{AD}/a. Since they are dimensionless, 3-body scaling variables must be a function of the dimensionless combination $a\kappa_*$ only. By eliminating κ_*, we can express one scaling variable as a function of another. Equivalently, in the plane defined by two scaling variables, the variation of κ_* generates a curve. Such a curve is called a *universal scaling curve*.

The universal scaling curve relating the binding energies $E_T^{(n+1)}$ and $E_T^{(n)}$ of two successive Efimov states was calculated in Ref. [44] using the renormalized zero-range model [122,123]. The scaling variables in Ref. [44] were $[(E_T^{(n+1)} - E_a)/E_T^{(n)}]^{1/2}$ and $[E_T^{(n)}/E_a]^{-1/2}$, where $E_a = \hbar^2/ma^2$. The scaling curve was calculated over the entire range of $E_T^{(n+1)}$, which includes the resonant limit where $a \to \pm\infty$. A more useful pair of scaling variables that contains much of the same information is $E_T^{(N)}/E_a$ and $E_T^{(N-1)}/E_a$, where $E_T^{(N)}$ and $E_T^{(N-1)}$ are the binding energies of the two shallowest Efimov states. The universal scaling curves for $a > 0$ and < 0 were calculated in Ref. [90] using the effective field theory of Ref. [61,62]. They are shown in Figs. 30(a) and (b). For $a > 0$, the ranges of $E_T^{(N)}/E_a$ and $E_T^{(N-1)}/E_a$ are 1 to 6.75 and 6.75 to 1406, respectively. For $a < 0$, their ranges are 0 to 1.1×10^3 and 1.1×10^3 to 6.0×10^5, respectively. If a and $E_T^{(N)}$ are known, these universal scaling curves can be used to predict the binding energy $E_T^{(N-1)}$ of the second shallowest Efimov state.

The availability of accurate numerical calculations of the 3-body binding energies for various potential models for ^{4}He atoms allows for a dramatic illustration of the universal scaling curves. The first fully-converged calculation for a ^{4}He potential was carried out by Cornelius and Glöckle in 1986 [124]. Fully-converged calculations for more modern ^{4}He potentials have recently become available [111–113]. The potentials for which fully-converged calculations are available have scattering lengths a that range widely from 167.2 a_0 to 235.6 a_0. If we use the dimer binding energy E_D and the excited trimer binding energy $E_T^{(1)}$ as inputs, Λ_* ranges from $0.922\, a_D^{-1}$ to $1.258\, a_D^{-1}$, where $a_D = (mE_D/\hbar^2)^{1/2}$. Thus $\ln \Lambda_*$ ranges over 10% of its complete period of π/s_0, which is enough to trace out a significant fraction of the universal scaling curve. In Fig. 31, the scaling variables $E_T^{(1)}/E_D$ and $E_T^{(0)}/E_D$ from the fully converged calculations are shown along with the appropriate part of the universal scaling curve from Fig. 30(a). The numerical results all lie

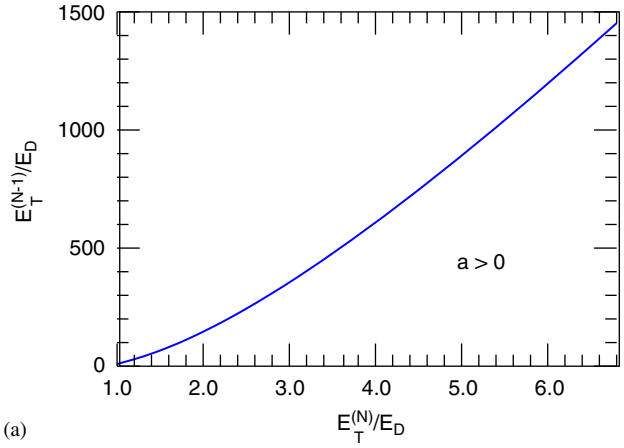

(a)

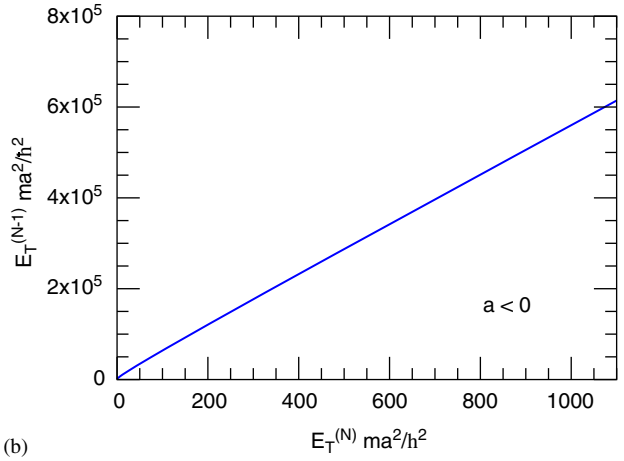

(b)

Fig. 30. Universal scaling curves for $E_{\mathrm{T}}^{(N-1)}ma^2/\hbar^2$ vs. $E_{\mathrm{T}}^{(N)}ma^2/\hbar^2$ for (a) $a>0$ and (b) $a<0$. $E_{\mathrm{T}}^{(N)}$ and $E_{\mathrm{T}}^{(N-1)}$ are the binding energies of the shallowest and second shallowest Efimov states.

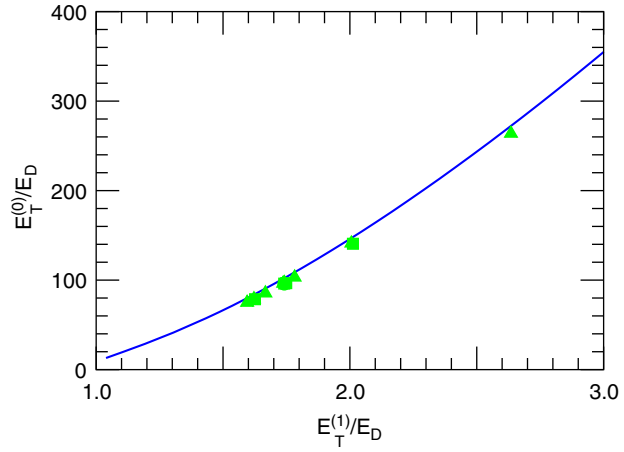

Fig. 31. The universal scaling curve in Fig. 30(a) in the region relevant for ^{4}He atoms. The data points are fully-converged calculations for various ^{4}He potentials.

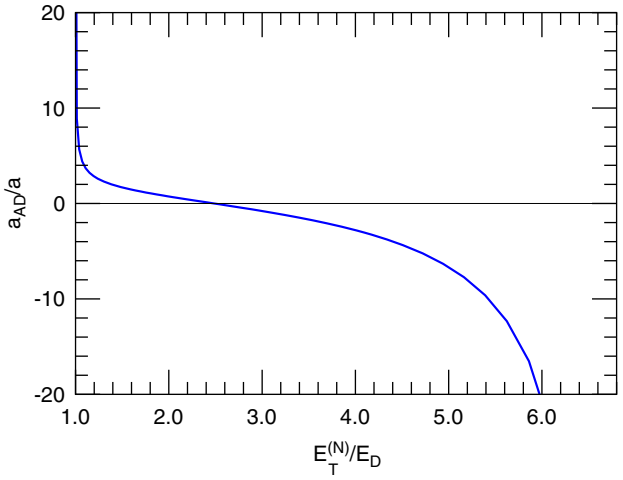

Fig. 32. Universal scaling curve for $a_{\rm AD}/a$ vs. $E_{\rm T}^{(N)}/E_{\rm D}$, where $E_{\rm T}^{(N)}$ is the binding energy of the shallowest Efimov state.

very close to the universal scaling curve. Thus the correlation between $E_{\rm T}^{(1)}$ and $E_{\rm T}^{(0)}$ is very close to that predicted by the scaling limit. This is somewhat surprising, because the ground-state binding energy $E_{\rm T}^{(0)}$, which ranges from 117 to 133 mK depending on the potential, is not much smaller than the natural ultraviolet cutoff $\hbar^2/m\ell_{\rm vdW}^2 = 420\,{\rm mK}$. This suggests that the scaling limit is surprisingly robust.

The numerical results in Fig. 31 all lie systematically below the universal scaling curve. This can be explained by the fact that the effective ranges r_s for the potentials for which fully converged calculations are available all lie in the narrow range between 13.75 a_0 and 13.98 a_0. Much of the discrepancies between the calculated results and the universal scaling curve can perhaps be explained by the leading power-law scaling violations, which are first-order in r_s/a.

The universal scaling curve for the scaling variables $E_{\rm T}^{(1)}/E_{\rm D}$ and $a_{\rm AD}/a$ was calculated in Ref. [90] using the effective field theory of Ref. [61,62] and is shown in Fig. 32. The ratio $a_{\rm AD}/a$ diverges to $+\infty$ at $E_{\rm T}^{(1)}/E_{\rm D} = 1$ and to $-\infty$ at $E_{\rm T}^{(1)}/E_{\rm D} = 6.75$. An approximate expression for this scaling curve in the resonant region $a \to +\infty$ can be obtained by using Eqs. (205), (216), (217) and eliminating $\kappa_* a$.

Several other universal scaling curves have been calculated using the renormalized zero-range model [122,123]. One is the scaling curve relating $E_{\rm T'}^{(N+1)}/E_{\rm D}$ and $E_{\rm T'}^{(N)}/E_{\rm D}$, where $E_{\rm T'}^{(n)}$ is the energy of the virtual state that appears when the nth Efimov state disappears through the atom–dimer threshold [125]. The scaling curves relating $E_{\rm T}^{(n)}{\rm ma}^2/\hbar^2$ and $\langle R^2\rangle^{(n)} E_{\rm T}^{(n)}{\rm m}/\hbar^2$, where $\langle R^2\rangle^{(n)}$ is the mean-square hyperradius of the nth Efimov state, have been calculated for $n = N$ and $N-1$ [126]. Finally the scaling curve relating $\alpha m/\hbar a^4$ and $E_{\rm D}/E_{\rm T}^{(N)}$, where α is the 3-body recombination rate constant, has also been calculated [127].

7. Effects of deep two-body bound states

In Section 6, we assumed implicitly that there are no deep (tightly-bound) diatomic molecules. In this section, we deduce the effects of deep molecules on the universal aspects of the 3-body problem.

7.1. Extension of Efimov's radial law

In Efimov's derivation of his radial law, he assumed implicitly that the effects of deep 2-body bound states were negligible. This assumption implies that all the probability in an incoming hyperradial wave is reflected back from the short-distance region $R \sim \ell$ into an outgoing hyperradial wave. The resulting expression for the hyperradial wave function in the scale-invariant region $\ell \ll R \ll |a|$ is Eq. (185). If there are deep 2-body bound states, this assumption is

not true. Some of the probability in the incoming hyperradial wave that flows into the short-distance region emerges in the form of scattering states that consist of an atom and a deep diatomic molecule with large kinetic energy but small total energy. We will refer to these states as *high-energy atom–molecule scattering states*.

The 2-body potentials for the alkali atoms other than hydrogen have many 2-body bound states. If it was necessary to take into account each of the bound states explicitly, the problem would be hopelessly difficult. Fortunately the cumulative effect of all the deep 2-body bound states on low-energy 3-body observables can be taken into account by a simple extension of Efimov theory. This extension introduces one additional low-energy parameter: an inelasticity parameter η_* that determines the widths of the Efimov states. In the scaling limit, the low-energy 3-body observables are completely determined by a, κ_*, and η_*.

The reason the cumulative effects of the deep 2-body bound states can be described by a single number η_* is that all pathways from a low-energy 3-body state with $|E| \ll \hbar^2/m\ell^2$ to a high-energy atom–molecule scattering state must flow through the lowest hyperspherical potential, which in the scale-invariant region has the form given in Eq. (142). The reason for this is that in order to reach a high-energy atom–molecule scattering state, the system must pass through an intermediate configuration in which all three atoms are simultaneously close together with a hyperradius R of order ℓ or smaller. It is obvious that the two atoms that form the bound state must approach to within a distance of order ℓ, since the size of the bound state is of order ℓ or smaller. However, the third atom must also approach the pair to within a distance of order ℓ. Let $E_{\rm deep}$ be the binding energy of the 2-body bound state, with $E_{\rm deep} \gtrsim \hbar^2/m\ell^2$. Energy and momentum conservation then require that the molecule and the recoiling atom emerge with equal and opposite momenta $(4mE_{\rm deep}/3)^{1/2}$, which is of order $\hbar/\ell$ or greater. The third atom and the pair can deliver the necessary momentum kicks only if they approach to within short distances of order ℓ or smaller. Thus any path from a low-energy 3-body state to a high-energy atom–molecule scattering state must pass through a configuration with small hyperradius R of order ℓ. Such small values of R are accessible to a low-energy 3-body state only through the lowest hyperspherical potential.

Efimov's radial law was based on combining the analytic solution to the hyperradial equation in the scale-invariant region $\ell \ll R \ll |a|$ in Eq. (182) with conservation of probability in the short-distance region $R \sim \ell$ and in the long-distance region $R \sim |a|$. If there are deep diatomic molecules, the only aspect that must be treated differently is the short-distance region. Efimov assumed that a hyperradial wave that flows to short distances is totally reflected back to the scale-invariant region. The amplitude A of the outgoing wave in Eq. (182) then differs from the amplitude B of the incoming wave by a phase as in Eq. (184). If there are deep molecules, some of the probability in a hyperradial wave that flows to short distances emerges in the form of atom–molecule scattering states. The fraction of the probability that is reflected back to long distances through the lowest adiabatic hyperspherical potential is less than 1. We will denote this fraction by $e^{-4\eta_*}$ and refer to η_* as the inelasticity parameter. The corresponding boundary condition on the amplitudes of the hyperradial waves in Eq. (182) is

$$A = -\mathrm{e}^{-2\eta_* + 2\mathrm{i}\theta_*} B. \tag{248}$$

We can now write down the extensions of Efimov's radial laws in Eqs. (190) to the case in which there are deep 2-body bound states. All that is required is to replace the phase factor $\mathrm{e}^{2\mathrm{i}\theta_*}$ associated with reflection from the short-distance region by the factor $\mathrm{e}^{-2\eta_* + 2\mathrm{i}\theta_*}$:

$$S_{\rm AD,AD} = s_{22} + \frac{s_{21}\mathrm{e}^{-2\eta_* + 2\mathrm{i}\theta_*} s_{12}}{1 - \mathrm{e}^{-2\eta_* + 2\mathrm{i}\theta_*} s_{11}}, \tag{249a}$$

$$S_{\rm AD,AAA} = s_{23} + \frac{s_{21}\mathrm{e}^{-2\eta_* + 2\mathrm{i}\theta_*} s_{13}}{1 - \mathrm{e}^{-2\eta_* + 2\mathrm{i}\theta_*} s_{11}}, \tag{249b}$$

$$S_{\rm AAA,AAA} = s_{33} + \frac{s_{31}\mathrm{e}^{-2\eta_* + 2\mathrm{i}\theta_*} s_{13}}{1 - \mathrm{e}^{-2\eta_* + 2\mathrm{i}\theta_*} s_{11}}. \tag{249c}$$

All dependence on the radial variable H is contained in the angle θ_*, which is still given by Eq. (187). The symmetric unitary 3×3 matrix s is the same universal function of the angular variable ξ as before. The only difference in the radial law is that the S-matrix elements now depend also on the inelasticity parameter η_*. The remarkable conclusion is that if the universal expressions for the S-matrix elements are known in the case $\eta_* = 0$, all the effects of deep 2-body bound states in the scaling limit can be deduced by the simple substitution $\theta_* \to \theta_* + \mathrm{i}\eta_*$.

The radial laws can also be generalized to the S-matrix elements for transitions from low-energy 3-body scattering states to high-energy scattering states consisting of an atom and a deep diatomic molecule with large kinetic energy but small total energy. The transitions from low-energy scattering states to these high-energy atom–molecule scattering states involve the wave function in the short-distance region $R \sim \ell$. This wave function may be very complicated, but it must conserve probability. We can therefore treat this region in the same way Efimov treated the scale-invariant region $R \sim a$. If we identify the appropriate asymptotic states, the evolution of the wave function between those states will be described by a unitary matrix t. In the scale-invariant region, the asymptotic states as far as the short-distance region is concerned are the outgoing and incoming hyperradial waves represented by the first and second terms on the right side of Eq. (182). We denote them by $|1\ \text{out}\rangle$ and $|1\ \text{in}\rangle$, respectively. Note that the outgoing hyperradial wave is an outgoing asymptotic state $|1\ \text{out}\rangle$ as far as the short-distance region $R \sim \ell$ is concerned, while it is an incoming asymptotic state $|1\ \text{in}\rangle$ as far as the long-distance region $R \sim |a|$ is concerned. In the asymptotic region $R \gg |a|$, the asymptotic states whose probability can flow directly into or out of the short-distance region are incoming or outgoing high-energy atom–molecule scattering states. We denote them by $|X\ \text{in}\rangle$ and $|X\ \text{out}\rangle$, where X ranges over all the high-energy atom–molecule scattering states. The amplitudes for the incoming asymptotic states to evolve into the outgoing asymptotic states is described by a unitary matrix t:

$$t_{ij} = \langle \text{i out}|\hat{U}|j\ \text{in}\rangle, \tag{250}$$

where $\hat{U}$ is the evolution operator that evolves a wave function through the short-distance region over an arbitrarily long time interval.

We already know one element of the unitary matrix t that describes the evolution of the wave function between these asymptotic states. The entry of the matrix that gives the amplitude of the incoming hyperradial wave $|1\ \text{in}\rangle$ to be reflected into the outgoing hyperradial wave $|1\ \text{out}\rangle$ is

$$t_{11} = \exp(-2\eta_* + 2\mathrm{i}\theta_*). \tag{251}$$

The unitarity of the matrix t then determines that the total probability for an incoming hyperradial wave to emerge as a high-energy atom–molecule scattering state:

$$\sum_X |t_{X1}|^2 = 1 - e^{-4\eta_*}. \tag{252}$$

We can now write down the radial laws for the S-matrix elements for the transitions from low-energy scattering states AAA and AD to a high-energy atom–molecule scattering state X:

$$S_{X,\mathrm{AD}} = t_{X1}s_{12} + t_{X1}\frac{s_{11}\mathrm{e}^{-2\eta_*+2\mathrm{i}\theta_*}s_{12}}{1-\mathrm{e}^{-2\eta_*+2\mathrm{i}\theta_*}s_{11}}, \tag{253a}$$

$$S_{X,\mathrm{AAA}} = t_{X1}s_{13} + t_{X1}\frac{s_{11}\mathrm{e}^{-2\eta_*+2\mathrm{i}\theta_*}s_{13}}{1-\mathrm{e}^{-2\eta_*+2\mathrm{i}\theta_*}s_{11}}. \tag{253b}$$

The first terms in Eqs. (253a) and (253b) are the contributions from transmission through the long-distance region followed by transmission through the short-distance region to the asymptotic state X. The second terms include the contributions from arbitrarily many reflections of hyperradial waves from the short-distance region with amplitude $\mathrm{e}^{2\mathrm{i}\theta_*-2\eta_*}$ and from the long-distance region with amplitude s_{11}.

The S-matrix elements in Eq. (253) have a factor t_{X1} that depends strongly on the short-distance behavior of the interaction potential. However, the corresponding rates summed over all high-energy atom–molecule scattering states X are much less sensitive to short distances. Squaring the S-matrix elements, summing over the high-energy states X, and using the unitarity relation in Eq. (252), we obtain

$$\sum_X |S_{X,\mathrm{AD}}|^2 = \frac{(1-e^{-4\eta_*})|s_{12}|^2}{|1-\mathrm{e}^{-2\eta_*+2\mathrm{i}\theta_*}s_{11}|^2}, \tag{254a}$$

$$\sum_X |S_{X,\mathrm{AAA}}|^2 = \frac{(1-e^{-4\eta_*})|s_{13}|^2}{|1-\mathrm{e}^{-2\eta_*+2\mathrm{i}\theta_*}s_{11}|^2}. \tag{254b}$$

These are the radial laws for the inclusive transitions from low-energy scattering states into states that include deep molecules. These inclusive rates are sensitive to short-distances only through the parameters a, κ_*, and η_*.

7.2. Widths of Efimov states

One obvious consequence of the existence of deep diatomic molecules is that the Efimov states are no longer sharp states. They have widths, because they can decay into an atom and a deep molecule. Thus, the Efimov states are really just resonances in the scattering of an atom and a deep molecule.

The binding energy $E_{\rm T}$ and width $\Gamma_{\rm T}$ of an Efimov resonance can be obtained as a complex eigenvalue $E = -(E_{\rm T} + {\rm i}\Gamma_{\rm T}/2)$ of the 3-body Schrödinger equation. If the width is small compared to the binding energy, the line shape of the resonance can be approximated by a Breit–Wigner resonance centered at the energy $-E_{\rm T}$ and with full width at half maximum $\Gamma_{\rm T}$. The cross section for the scattering of an atom and a deep molecule with total energy E near $-E_{\rm T}$ is

$$\sigma(E) \approx \frac{\Gamma_{\rm T}^2/4}{(E+E_{\rm T})^2 + \Gamma_{\rm T}^2/4}\sigma_{\rm max}. \tag{255}$$

In the absence of deep molecules, the binding energies of Efimov states satisfy Eq. (194), where $\Delta(\xi)/2$ is the phase shift of a hyperradial wave that is reflected from the long-distance region $R \sim |a|$. To obtain the corresponding equation in the case of deep bound states, we need only make the substitution $\theta_* \to \theta_* + {\rm i}\eta_*$ in Eq. (193):

$$2(\theta_* + {\rm i}\eta_*) + \Delta(\xi) = 0 \mod 2\pi. \tag{256}$$

This can be satisfied only if we allow complex values of ξ in the argument of Δ. Using the expression for θ_* in Eq. (187) and inserting the definition of H in Eq. (70), we obtain the equation

$$E_{\rm T} + \frac{\rm i}{2}\Gamma_{\rm T} + \frac{\hbar^2}{ma^2} = (e^{-2\pi/s_0})^{n-n_*} \exp\left[\frac{\Delta(\xi) + 2{\rm i}\eta_*}{s_0}\right]\frac{\hbar^2\kappa_*^2}{m}, \tag{257}$$

where the complex-valued angle ξ is defined by

$$\tan\xi = -(m(E_{\rm T} + {\rm i}\Gamma_{\rm T}/2)/\hbar^2)^{1/2}a. \tag{258}$$

To solve this equation for $E_{\rm T}$ and $\Gamma_{\rm T}$, we need the analytic continuation of $\Delta(\xi)$ to complex values of ξ. The parametrizations for $\Delta(\xi)$ in Eqs. (197) should be accurate for complex values of ξ with sufficiently small imaginary parts, except near $\xi = -\pi$ where the empirical expansion parameter z defined in Eq. (198c) has an essential singularity. If the analytic continuation of $\Delta(\xi)$ were known, the binding energy and width of one Efimov state could be used to determine κ_* and η_*. The remaining Efimov states and their widths could then be calculated by solving Eq. (257).

If the inelasticity η_* parameter is extremely small, the right side of Eq. (257) can be expanded to first order in η_*. The resulting expression for the width is

$$\Gamma_{\rm T} \approx \frac{4\eta_*}{s_0}\left(E_{\rm T} + \frac{\hbar^2}{ma^2}\right). \tag{259}$$

For the shallowest Efimov states, the order of magnitude of the width is simply $\eta_*\hbar^2/ma^2$. The widths of the deeper Efimov states are proportional to their binding energies, which behave asymptotically like Eq. (38). This geometric decrease in the widths of shallower Efimov states has been observed in calculations of the elastic scattering of atoms with deeply bound molecules [128].

7.3. Atom–dimer elastic scattering

The effects of deep diatomic molecules modify the universal expressions for low-energy 3-body scattering observables derived in Section 6. The radial laws in Eqs. (249) for the case in which there are deep molecules can be obtained from Efimov's radial laws in Eqs. (190) simply by substituting $\theta_* \to \theta_* + {\rm i}\eta_*$. Thus if the universal expression for

a scattering amplitude for the case of no deep molecules is expressed as an analytic function of $\ln(\kappa_*)$, the corresponding universal expression for the case in which there are deep molecules can be obtained simply by substituting $\ln(a\kappa_*) \to \ln(a\kappa_*) + i\eta_*/s_0$.

Just above the atom–dimer threshold, the S-wave phase shift $\delta_0^{\rm AD}(k)$ for atom–dimer scattering can be approximated accurately by keeping the first two terms in the expansion in Eq. (210). The universal expressions for the atom–dimer scattering length $a_{\rm AD}$ and for the effective range $r_{s,\rm AD}$ if there are no deep molecules are given in Eqs. (216) and (219). The corresponding expressions for the case in which there are deep molecules can be obtained by replacing $s_0 \ln(a\Lambda_*)$ by $s_0 \ln(a\Lambda_*) + i\eta_*$. The resulting expressions can be written in the form

$$a_{\rm AD} = (1.46 + 2.15 \cot[s_0 \ln(a/a_*) + i\eta_*])a, \tag{260a}$$

$$r_{s,\rm AD} = (1.13 + 0.73 \cot[s_0 \ln(a/a_*) + 0.98 + i\eta_*])^2 a, \tag{260b}$$

where a_* is a value of the scattering length for which the peak of an Efimov resonance is at the atom–dimer threshold. The relation between a_* and Λ_* can be obtained by combining Eqs. (200) and (217):

$$s_0 \ln(a/a_*) = s_0 \ln(a\Lambda_*) + 1.66 \mod \pi. \tag{261}$$

The expressions in Eqs. (260) are complex-valued, because there are inelastic channels in which the scattering produces high-energy atom–molecule scattering states.

Near the atom–dimer threshold, the cross section for elastic atom–dimer scattering is dominated by S-wave scattering. At the threshold $E = -E_{\rm D}$, the differential cross section is simply $|a_{\rm AD}|^2$. Inserting the expression for the atom–dimer scattering length in Eq. (260a) and multiplying by the 4π solid angle, the cross section has the form

$$\sigma_{\rm AD}(E = -E_{\rm D}) = 84.9 \, \frac{\sin^2[s_0 \ln(a/a_*) - 0.97] + \sinh^2 \eta_*}{\sin^2[s_0 \ln(a/a_*)] + \sinh^2 \eta_*} \, a^2. \tag{262}$$

This expression has maxima near the values $a = (e^{\pi/s_0})^n a_*$ for which the peak of an Efimov resonance is at the atom–dimer threshold. In the strongly inelastic limit $\eta_* \to \infty$, the cross section reduces simply to $84.9a^2$.

We next consider the effect of deep molecules on the cross section for atom–dimer scattering below the dimer-breakup threshold. The S-wave contribution to the cross section is obtained by inserting the S-wave phase shift $\delta_0^{\rm AD}(k)$ into Eq. (209). The universal expression for the cotangent of the phase shift at $ka < 2/\sqrt{3}$ in the case of no deep molecules is given by Eq. (223). Explicit parameterizations of the universal functions $c_1(ka)$, $c_2(ka)$, and $\phi(ka)$ are given in Eqs. (225). The phase shift in the case where there are deep molecules can be obtained by making the substitution $s_0 \ln(a\Lambda_*) \to s_0 \ln(a\Lambda_*) + i\eta_*$ in Eq. (223):

$$ka \cot \delta_0^{\rm AD}(k) = c_1(ka) + c_2(ka) \cot[s_0 \ln(a\Lambda_*) + \phi(ka) + i\eta_*]. \tag{263}$$

The resulting differential cross section is shown in Fig. 33 for inelasticity parameter $\eta_* = 0.1$ and $a\Lambda_* = 0.15$, 1.65, 4.34, and 15.7. Comparing with Fig. 28 which shows the differential cross section for the same four values of $a\Lambda_*$ but with $\eta_* = 0$, we see that the effects of deep 2-body bound states fill in the zeroes and prevent the cross section from saturating the unitarity bound.

7.4. Three-body recombination into the shallow dimer

If there are no deep molecules, the rate constant $\alpha_{\rm shallow}$ for 3-body recombination into the shallow dimer has the remarkable form given in Eq. (228), which has zeroes at values a that differ by multiples of $e^{\pi/s_0} \approx 22.7$. One of the effects of deep molecules is to fill in these zeroes.

If there are deep molecules, the radial law for the S-matrix element for 3-body recombination into the shallow dimer is given in Eq. (249b). For energies $E = \hbar^2\kappa^2/m$ just above the dimer-breakup threshold, the entries of the matrix s_{ij} have the expansions given in Eqs. (233). The limiting behavior of the S-matrix element as $E \to 0^+$ is obtained by substituting $\theta_* \to \theta_* + i\eta_*$ into Eq. (234):

$$S_{\rm AD,AAA} \longrightarrow -c_2 e^{i\gamma_1} a^2 K^2 \frac{1 + e^{2i(\theta_* - \delta_0) - 2\eta_*}}{1 - e^{-2\pi s_0} e^{2i(\theta_* - \delta_0) - 2\eta_*}} \quad \text{as } E \to 0^+. \tag{264}$$

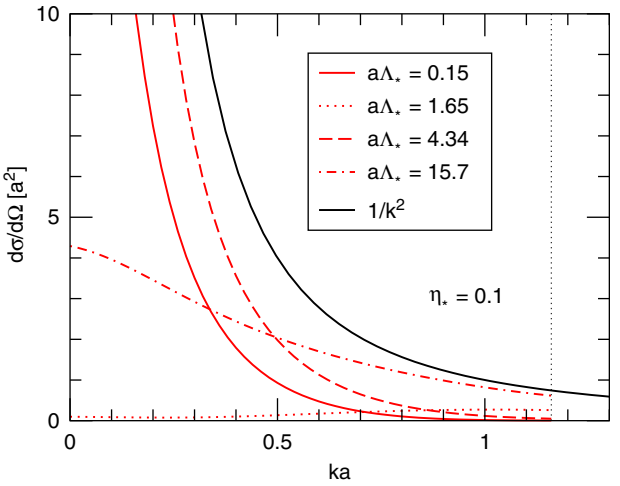

Fig. 33. The S-wave contribution to the differential cross section for atom–dimer scattering in units of a^2 as a function of ka for $a\Lambda_* = 0.15, 1.65, 4.34, 15.7$ and inelasticity parameter $\eta = 0.1$. The black solid line is the unitarity bound $1/k^2$. The vertical dotted line is the dimer-breakup threshold.

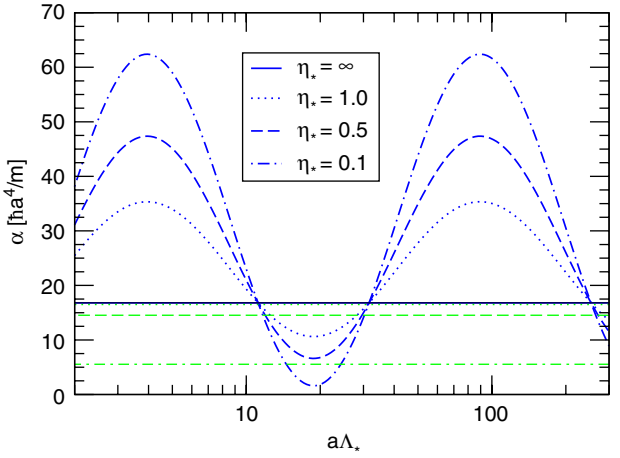

Fig. 34. The 3-body recombination rate constants $\alpha_{\rm shallow}$ (with large-amplitude oscillations) and $\alpha_{\rm deep}$ (with small-amplitude oscillations) in units of $\hbar a^4/m$ as functions of $a\Lambda_*$ for $a > 0$ and different values of η_*.

The corresponding modification of the analytic expression for the rate constant $\alpha_{\rm shallow}$ in Eq. (228) is

$$\alpha_{\rm shallow} = \frac{128\pi^2(4\pi - 3\sqrt{3})(\cos^2[s_0\ln(a\kappa_*) + \gamma] + \sinh^2\eta_*)}{\sinh^2(\pi s_0 + \eta_*) + \sin^2[s_0\ln(a\kappa_*) + \gamma]}\,\frac{\hbar a^4}{m}. \tag{265}$$

We can exploit the fact that $e^{2\pi s_0} \approx 557$ is large to simplify the expression in Eq. (265). It can be approximated with an error of less than 1% by

$$\alpha_{\rm shallow} \approx 67.1e^{-2\eta_*}(\sin^2[s_0\ln(a/a_*) + 1.67] + \sinh^2\eta_*)\frac{\hbar a^4}{m}. \tag{266}$$

The relation between a_* and Λ_* is given in Eq. (261). The coefficient of $\hbar a^4/m$ is shown as a function of $a\Lambda_*$ in Fig. 34 for several values of η_*. As a varies, the coefficient of $\hbar a^4/m$ oscillates between about $67.1e^{-2\eta_*}\sinh^2\eta_*$ and about $67.1e^{-2\eta_*}\cosh^2\eta_*$. Thus one effect of the deep molecules is to eliminate the zeros in the rate constant for

3-body recombination into the shallow dimer. Note that the depth of the minimum is quadratic in η_* as $\eta_* \to 0$, so the coefficient of $\hbar a^4/m$ can be very small if the inelasticity parameter η_* is small.

In the strongly inelastic limit $\eta_* \to \infty$, the coefficient of $\hbar a^4/m$ in Eq. (265) approaches a constant 16.719 that is extremely close to $\frac{1}{4}$ of the maximum coefficient when $\eta_* = 0$, which is $C = 67.1177$. This can be understood from the fact that $|s_{32}|^2/|s_{31}|^2 \to \tanh(\pi s_0)$ as $E \to 0$. Since $\tanh(\pi s_0) \approx 0.996$, the amplitude for an incoming 3-atom scattering state to be reflected from the long-distance region into an outgoing atom–dimer scattering state is nearly equal in magnitude to the amplitude for it to be transmitted through the long-distance region to an incoming hyperspherical wave. If $\eta_* = \infty$, the incoming hyperspherical wave is completely absorbed at short distances and only the first amplitude contributes to the recombination rate into the shallow dimer. If $\eta_* = 0$, the hyperspherical wave is completely reflected at short distances and totally transmitted into an outgoing atom–dimer scattering state. At special values of a, there is constructive interference between the two amplitudes and the recombination rate is approximately 4 times larger than the contribution from the first amplitude alone.

7.5. Three-body recombination into deep molecules

The existence of deep diatomic molecules opens up additional channels for 3-body recombination. If there are no deep molecules, 3-body recombination can only produce the shallow dimer if $a > 0$ and it cannot proceed at all if $a < 0$. If there are deep molecules, they can be produced by 3-body recombination regardless of the sign of a. The rate constant α for 3-body recombination is defined in Eq. (227). We will denote the inclusive contribution to this rate constant from 3-body recombination into all the deep molecules by $\alpha_{\rm deep}$.

The radial law for inclusive 3-body recombination into deep molecules is given in Eq. (254b). We first consider the case of positive scattering length $a > 0$. As the energy $E = \hbar^2 K^2/m$ approaches the dimer-breakup threshold, the limiting behaviors of s_{11} and s_{13} are given in Eqs. (226a) and (233a). Thus the limiting behavior of the sum of the squares of S-matrix elements in Eq. (254b) as $K \to 0$ is

$$\sum_X |S_{X,\rm AAA}|^2 \longrightarrow \frac{c_1^2 a^4 K^4 (1 - e^{-4\eta_*})}{|1 - e^{-2\pi s_0} e^{2i(\theta_* - \delta_0) - 2\eta_*}|^2} \quad \text{as } E \to 0. \tag{267}$$

An analytic expression for $\alpha_{\rm deep}$ can be obtained from Eqs. (264), (265), and (267) by using the facts that $\alpha_{\rm deep}/\alpha_{\rm shallow}$ is equal to the ratio of $\sum_X |S_{X,\rm AAA}|^2$ to $|S_{\rm AD,AAA}|^2$ and that $c_2^2/c_1^2 = \tanh(\pi s_0)$:

$$\alpha_{\rm deep} = \frac{C_{\max} \cosh(\pi s_0) \sinh(\pi s_0) \cosh\eta_* \sinh\eta_*}{\sinh^2(\pi s_0 + \eta_*) + \sin^2[s_0 \ln(a\kappa_*) + \gamma]} \frac{\hbar a^4}{m}. \tag{268}$$

The coefficient of $\hbar a^4/m$ has very weak log-periodic dependence on $a\kappa_*$. We can exploit the fact that $e^{2\pi s_0} \approx 557$ is large to simplify the expression in Eq. (268). It can be approximated with an error of less than 1% by

$$\alpha_{\rm deep} \approx 16.7(1 - e^{-4\eta_*}) \frac{\hbar a^4}{m} \quad (a > 0). \tag{269}$$

The fact that the coefficient of $\hbar a^4/m$ is very nearly constant is a consequence of the nearly reflectionless character of the lowest adiabatic hyperspherical potential at $E = 0$. The extremely weak dependence on $a\Lambda_*$ was first observed in numerical calculations using an effective field theory for the case of infinitesimal η_* [129]. The numerical result for the coefficient in Eq. (269) was first derived in Ref. [130]. The coefficient of $\hbar a^4/m$, which is independent of $a\kappa_*$, is shown in Fig. 34 for several values of η_*.

In the strongly inelastic limit $\eta_* \to \infty$, the coefficient of $\hbar a^4/m$ in Eq. (268) approaches the constant 16.779. This is extremely close to the coefficient of $\hbar a^4/m$ in $\alpha_{\rm shallow}$ in Eq. (266) in the limit $\eta_* \to \infty$. This can be understood from the fact that $|s_{32}|/|s_{31}| \to \tanh(\pi s_0)$ as $E \to 0$. Since $\tanh(\pi s_0) \approx 0.997$, the amplitude for an incoming 3-atom scattering state to be reflected from the long-distance region into an outgoing atom–dimer scattering state is almost equal in magnitude to the amplitude for it to be transmitted through the scaling region to an incoming hyperspherical wave. If $\eta = \infty$, the incoming hyperspherical wave is completely absorbed at short distances and emerges as high-energy atom–molecule scattering states. The approximate equality of $|s_{32}|^2$ and $|s_{31}|^2$ as $E \to 0$ implies the approximate equality of the 3-body recombination rate into the shallow dimer and the inclusive 3-body recombination rate into deep molecules.

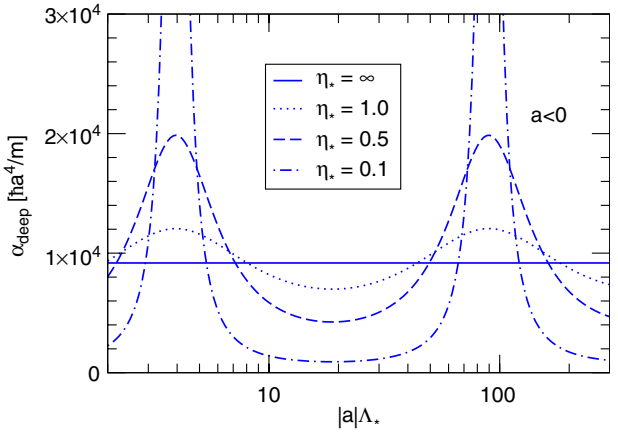

Fig. 35. The 3-body recombination rate constant $\alpha_{\rm deep}$ in units of $\hbar a^4/m$ as a function of $|a|\Lambda_*$ for $a<0$ and different values of η_*.

We now consider the consequences of the radial law in Eq. (254b) for 3-body recombination into deep molecules in the case of negative scattering length $a<0$. As the energy $E=\hbar^2K^2/m$ approaches the 3-atom threshold $E=0$, the limiting behavior of the entries of the matrix s are given in (242). Thus the limiting behavior of the sum of the squares of the S-matrix elements in Eq. (254b) is

$$\sum_X |S_{X,\rm AAA}|^2 \longrightarrow 2d_0 aK\,\frac{\sinh(2\eta_*)}{\sin^2(\theta_*+\gamma)+\sinh^2\eta_*} \quad \text{as } E\to 0. \tag{270}$$

The resulting 3-body recombination constant for $a<0$ is

$$\alpha_{\rm deep} = \frac{4590\sinh(2\eta_*)}{\sin^2[s_0\ln(a/a_*')]+\sinh^2\eta_*}\,\frac{\hbar a^4}{m} \quad (a<0), \tag{271}$$

where a_*' is a negative value of the scattering length for which the peak of an Efimov resonance is at the 3-atom threshold. The relation between a_*' and Λ_* can be obtained by combining Eqs. (201) and (217):

$$s_0\ln(a/a_*') = s_0\ln(|a|\Lambda_*) + 1.72(3) \mod \pi. \tag{272}$$

The coefficient of $\hbar a^4/m$ is shown as a function of $a\Lambda_*$ in Fig. 35 for several values of η_*. It displays resonant behavior with maxima when the scattering length has one of the values $(e^{\pi/s_0})^n a_*'$ for which the peak of an Efimov resonance is at the 3-atom threshold. The maximum value $9180\coth\eta_*$ diverges in the limit $\eta_*\to 0$. In the limit $\eta_*\to\infty$, the coefficient of $\hbar a^4/m$ in Eq. (271) approaches the constant 9180 independent of $a\Lambda_*$. Thus, the resonant effects associated with Efimov states disappear in the limit of strong inelasticity.

The scaling of $\alpha_{\rm deep}$ with a^4 was first predicted by Nielsen and Macek and by Esry et al. [97,98]. The existence of a log-periodic sequence of resonances related to Efimov states was pointed out by Esry et al. [98]. The explicit formula for $\alpha_{\rm deep}$ in Eq. (271) was first derived in Ref. [130].

7.6. Dimer relaxation into deep molecules

If there are no deep diatomic molecules, atom–dimer scattering is completely elastic below the dimer-breakup threshold $ka=2/\sqrt{3}$. The existence of deep molecules opens up an inelastic channel in which an atom and a shallow dimer with low energy collide to form an atom and a deep molecule. The large binding energy of the molecule is released through the large kinetic energies of the recoiling atom and molecule. This process is called *dimer relaxation*.

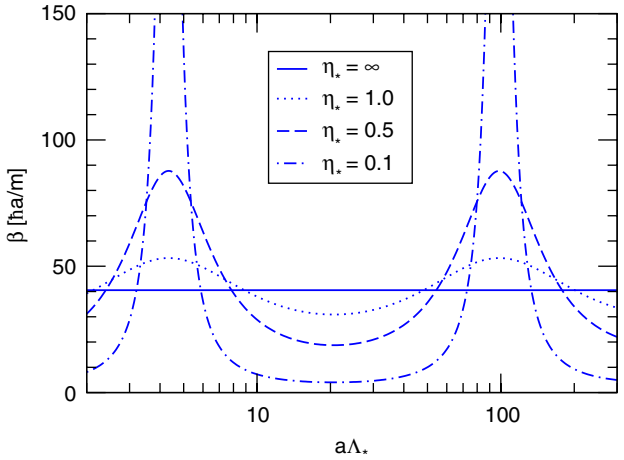

Fig. 36. The dimer relaxation rate constant β in units of $\hbar a/m$ for different values of η_* as a function of $a\Lambda_*$.

The relaxation rate depends on the momenta of the incoming atom and dimer. If the momenta are small enough, the relaxation rate reduces to a constant. The *relaxation event rate constant* β is defined so that the number of relaxation events per time and per volume in a gas of very cold atoms with number density $n_{\rm A}$ and very cold dimers with number density $n_{\rm D}$ is $\beta n_{\rm A} n_{\rm D}$. The resulting decrease in the number densities is given by

$$\frac{\mathrm{d}}{\mathrm{d}t} n_{\rm A} = \frac{\mathrm{d}}{\mathrm{d}t} n_{\rm D} = -\beta n_{\rm A} n_{\rm D}. \tag{273}$$

These equations apply equally well if either the atoms or the dimers or both are in Bose–Einstein condensates.

The radial law for the inclusive dimer relaxation rate is given in Eq. (254a). The total energy of the atom and dimer is expressed in terms of the common wave number k of the atom and dimer in Eq. (206). Just above the atom–dimer threshold, the nonzero entries of the unitary matrix s have the form given in Eq. (214). The resulting expression for the sum of the squares of the S-matrix elements in Eq. (254a) reduces to

$$\sum_X |S_{X,\rm AD}|^2 \longrightarrow 2b_0 ak \frac{\sinh(2\eta_*)}{\sin^2(\theta_* + \beta') + \sinh^2 \eta_*} \quad \text{as } E \to -E_{\rm D}. \tag{274}$$

The constants b_0 and β' are calculated in Ref. [130]. The resulting expression for the dimer relaxation constant β defined by Eq. (273) is given by

$$\beta = \frac{20.3 \sinh(2\eta_*)}{\sin^2[s_0 \ln(a/a_*)] + \sinh^2 \eta_*} \frac{\hbar a}{m}. \tag{275}$$

This result was first obtained in Ref. [130]. The relation between a_* and Λ_* is given in Eq. (261). The coefficient of $\hbar a/m$ is shown as a function of $a\Lambda_*$ in Fig. 36 for several values of η_*. It displays resonant behavior with maxima when the scattering length has one of the values $(e^{\pi/s_0})^n a_*$ for which the peak of an Efimov resonance is at the atom–dimer threshold. The maximum value $40.6 \coth \eta_*$ diverges in the limit $\eta_* \to 0$. In the limit $\eta_* \to \infty$, the coefficient of $\hbar a^4/m$ approaches the constant 40.6 independent of $a\Lambda_*$. Thus, the resonant effects associated with Efimov states disappear in the limit of strong inelasticity.

The result for the dimer relaxation rate constant in Eq. (275) could also have been obtained from the expression for the atom–dimer scattering length in Eq. (260a) using unitarity:

$$\beta = -\frac{6\pi\hbar}{m} \operatorname{Im} a_{\rm AD}. \tag{276}$$

The optical theorem then implies that the cross section for inelastic atom–dimer scattering at threshold is

$$\sigma_{\rm AD}^{\rm (inelastic)}(E) \longrightarrow \frac{2m}{3\hbar k}\beta \quad \text{as } E \to -E_{\rm D}. \tag{277}$$

8. Effective field theory

Effective field theory has proved to be a very powerful tool for quantitative calculations of the predictions of universality. In this section, we give an introduction to effective field theory and describe how it can be applied to the problem of identical bosons with large scattering length in the scaling limit.

8.1. Effective field theories

Effective theory is a general approach to understanding the low-energy behavior of a physical system that has deep roots in several areas of physics. Some of these roots are described implicitly in Ken Wilson's Nobel lecture on the Renormalization Group [48]. Effective field theory is the application of this general method to a field theory. In elementary particle physics, the roots of effective field theory have two main branches. One branch is concerned with making intuitive sense of the renormalization procedure for *quantum electrodynamics* (QED) [131]. The other main branch came from trying to understand the low-energy behavior of strongly interacting particles like pions and nucleons.

In perturbative calculations in QED, intermediate steps are plagued by *ultraviolet divergences* that indicate strong sensitivity to physics at extremely short distances. Yet the renormalization procedure allows extremely accurate predictions of low-energy properties of electrons, positrons, and photons in terms of two fundamental parameters: the fine structure constant α and the electron mass m_e. If one tries to introduce any additional parameters into the theory, there are ultraviolet divergences that cannot be eliminated and the renormalization procedure breaks down. This would not be a problem if QED with electrons and photons was a complete theory. But in the real world, there are also other heavier charged particles, such as muons and pions. There are effects from such particles that cannot be absorbed into the definitions of α and m_e. Adding interaction terms to QED to take these effects into account destroys the renormalizability of the theory.

Let us focus specifically on the effects of muons, whose mass m_μ is about 200 times larger than that of the electron. The effects of muons can be described with arbitrary accuracy by the extension of QED to a quantum field theory that has a muon field in addition to the photon and electron fields. However, the effects of virtual muons on electrons, positrons, and photons with energies small compared to m_μ can also be described with arbitrary accuracy by an effective field theory that has only photon and electron fields. More specifically, the effective field theory approach involves the construction of a sequence of field theories that take into account the effects of muons with increasing accuracy. QED is simply the first theory in this sequence. If the electrons and photons have momenta of order p, the QED predictions for their scattering amplitudes have errors that are 2nd order in $x = p/m_\mu$ and $y = m_e/m_\mu$. However, the errors can be reduced to 4th order in x and y by using an effective field theory with an additional magnetic moment interaction. The additional parameter can be calculated as a function of α, m_e, and m_μ. The errors can be reduced further to 6th order in x and y by adding three additional interaction terms whose coefficients are calculable as functions α, m_e, and m_μ. Proceeding in this manner, one can take into account the effects of muons on electrons, positrons, and photons with momenta small compared to m_μ with arbitrarily high accuracy.

The fundamental quantum field theory that describes *hadrons*, the particles that feel the strong force, is *quantum chromodynamics* (QCD). It describes the strong interactions between hadrons in terms of gauge interactions between their constituents: quarks, antiquarks and gluons. The lightest hadrons are the pions: π^+, π^0, and π^-. Because the QCD interaction is strong, the direct calculation of the behavior of pions from QCD is very difficult. However, effective field theory can provide a systematically improvable description of the low-energy behavior of pions without using any information about QCD other than its symmetries [132]. In addition to the space–time symmetries, QCD has a global symmetry called *chiral symmetry*. The simplest effective field theory for pions is called the *nonlinear sigma model*. It has two parameters that can be determined by taking the pion mass $m_\pi = 140\,\text{MeV}$ and the pion decay constant $f_\pi = 93\,\text{MeV}$ as input. Predictions for the scattering amplitudes of low-energy pions with momenta of order p have errors that are 4th order in $x \sim p/(4\pi f_\pi)$ and $y \sim m_\pi/(4\pi f_\pi)$. However, the errors can be decreased systematically to 6th order in x and y by using an effective field theory with 10 additional parameters, thus requiring 10 additional

low-energy measurements as input. The error can be decreased even further to 8th order in x and y by adding even more parameters, and so on. The systematic expansion in x and y generated by this sequence of effective field theories is called *chiral perturbation theory*.[10]

Starting from these two main roots, effective field theory has developed into a universal language for modern elementary particle physics [134–136]. It has two main classes of applications. One class involves the systematic development of various low-energy approximations to the Standard Model of elementary particle physics. The other class of applications involves treating the Standard Model itself as a low-energy approximation to a more fundamental theory, such as a unified field theory or string theory.

Effective field theory also has many applications in condensed matter physics [137,138]. Examples include the Landau theory of Fermi liquids [139], phonons [140], spin waves [141], the weakly-interacting Fermi gas [142], and the weakly-interacting Bose gas [1].

8.2. *Effective theories in quantum mechanics*

Most of the applications of effective theories to date have been carried out within the context of quantum field theory. However, as pointed out by Lepage [143], the principles of effective theory apply equally well to problems in quantum mechanics, such as two particles interacting through a potential $V(r)$. Suppose we are interested only in the low-energy observables of the system, where "low energy" refers to energy E close to the scattering threshold $E=0$. The low-energy observables include bound-state energy levels close to threshold and low-energy scattering cross sections. Suppose also that the potential $V(r)$ is known accurately at long distances $r > r_0$, but that its short-distance behavior is not known accurately enough to calculate the low-energy observables. For example, if it is a short-range potential with range smaller than r_0, then $V(r)=0$ for $r > r_0$. If the particles are real atoms interacting at long distances through a van der Waals potential, then $V(r) \approx -C_6/r^6$ for $r > r_0$. Given more and more information about some of the low-energy observables, effective theories allow all other low-energy observables to be calculated with increasingly high accuracy without having any information about the short-distance potential.

The basic idea is very simple. Simply replace $V(r)$ by an effective potential $V_{\rm eff}(r; c_1)$ that is identical for $r > r_0$ and whose form for $r < r_0$ involves an adjustable parameter c_1. For $r < r_0$, the effective potential need not bear any resemblance to the original potential $V(r)$ as long as it has an adjustable parameter. Tune the value of this parameter c_1 so that the scattering amplitude at threshold is reproduced exactly. Then the Schrödinger equation with $V_{\rm eff}(r; c_1)$ will reproduce all the low-energy observables with errors that are linear in E. There is typically some energy scale E_0 at which the errors become roughly 100%. We can describe the errors at energies $|E| < E_0$ as being of order E/E_0. To achieve higher accuracy than order E/E_0, use an effective potential $V_{\rm eff}(r; c_1, c_2)$ with two adjustable parameters c_1 and c_2, and tune them to reproduce the scattering amplitude at threshold and the linear term in its expansion in powers of the energy E. Using this effective potential, all low-energy observables involving energies $|E| \ll E_0$ will be reproduced with errors of order $(E/E_0)^2$. If one tunes N parameters, the errors in the S-wave scattering amplitude can be reduced to order $(E/E_0)^N$, and the errors in other low-energy S-wave observables will also scale like $(E/E_0)^N$. Thus a low-energy observable can be calculated to increasingly high accuracy by tuning more and more parameters in the effective potential. Note that the rate of decrease of the error depends on the energy. The improvement is very rapid if $|E| \ll E_0$, but there may be no improvement if $|E| \sim E_0$.

It is well-known in the atomic physics community that the determination of low-energy observables like the scattering length can be improved by tuning short-distance parameters to fit other low-energy observables. For example, low-energy 2-body observables are known to be extremely sensitive to the inner wall of the interatomic potential. By fine-tuning the inner wall to fit some low-energy 2-body observables, one can significantly improve the predictions for others. This method has been used to improve the determination of the scattering length for ^{23}Na atoms [144]. The new insight from effective theory is that tuning more and more short-distance parameters can give systematically improvable determinations of low-energy observables with errors that scale as increasingly high powers of the energy.

It is easy to prove that by tuning N short-distance parameters, the errors in S-wave scattering amplitudes can be made to scale like E^N. Let $V_{\rm eff}(r; c)$ be the effective potential that depends on N short-distance tuning parameters $c_1, c_2, \ldots, c_N$ that we denote collectively by c. Let $u_k(r)/r$ be the radial wave function for S-wave scattering with energy $E=\hbar^2k^2/m$ for the true potential $V(r)$, and let $\delta_0(k)$ be the phase shift for S-wave scattering. Let $w_k(r; c)/r$ and

[10] See, e.g., Ref. [133] for a textbook treatment of this effective field theory.

$\delta_0(k;c)$ be the corresponding quantities for the effective potential. Since $V_{\rm eff}(r;c) = V(r)$ for $r > r_0$, the Wronskian $u_k(r)w_k'(r;c) - u_k'(r)w_k(r;c)$ must be independent of r in that region. In the asymptotic region $r \to \infty$, these functions behave like

$$u_k(r) \longrightarrow A\sin[kr + \delta_0(k)], \tag{278a}$$

$$w_k(r;c) \longrightarrow B\sin[kr + \delta_0(k;c)], \tag{278b}$$

where A and B are irrelevant constants. Setting the Wronskian at $r = r_0$ equal to the Wronskian of these asymptotic solutions, we have

$$u_k(r_0)w_k'(r_0;c) - u_k'(r_0;c)w_k(r_0) = kAB\sin[\delta_0(k) - \delta_0(k;c)]. \tag{279}$$

The left side is an analytic function of $E = \hbar^2k^2/m$, because $u_k(r_0)$ and $w_k(r_0;c)$ are obtained by integrating the Schrödinger equation with parameter E over the finite interval from $r = 0$ to $r = r_0$. This implies that, up to an overall factor of k, $\delta_0(k) - \delta_0(k;c)$ must be an analytic function of k^2. Note that the phase shifts $\delta_0(k)$ and $\delta_0(k;c)$ need not separately be analytic functions of k^2, but the difference between the phase shifts must be analytic. Both sides of Eq. (279) therefore have power series expansion in E whose coefficients depend on the short-distance parameters $c_1, \ldots, c_N$. If those parameters are tuned so that the first N coefficients in the expansion of the left side of Eq. (279) in powers of k^2 vanish, then the differences between the phase shifts $\delta_0(k)$ and $\delta_0(k;c)$ will be of order k^{2N-1}. This demonstrates that by tuning short-distance parameters that affect the effective potential only in the region $r < r_0$, we can decrease the error in the phase shifts to higher and higher order in E.

The systematic decrease of the errors in the scattering amplitudes leads to systematic decrease of the errors in other low-energy observables. For example, the binding energies $E^{(n)}$ of S-wave bound states can be determined from the S-wave phase shifts by solving Eq. (17). Thus the sequence of effective potentials that give phase shifts with errors that scale as $(E/E_0)^N$ will also give binding energies with errors that scale as $(E^{(n)}/E_0)^N$.

As an illustration of the application of effective theory in quantum mechanics, we consider a particle in a spherically-symmetric potential $V(r)$ that is attractive and proportional to $1/r^2$ for r greater than some radius r_0:

$$V(r) = -\left(\frac{1}{4} + s_0^2\right)\frac{\hbar^2}{2mr^2}, \quad r > r_0, \tag{280a}$$

$$= V_{\rm short}(r), \quad r < r_0, \tag{280b}$$

where s_0 is a positive parameter. The coefficient of the $1/r^2$ potential is written as $\frac{1}{4} + s_0^2$ because $s_0^2 = 0$ is the critical value above which the potential is too singular for the problem to be well-behaved in the limit $r_0 \to 0$. For example, the spectrum of the Hamiltonian is unbounded from below if $s_0^2 > 0$. We imagine that the short-distance potential $V_{\rm short}(r)$ is unknown, but that the energies of bound states can be measured. The potential $V(r)$ has infinitely many arbitrarily-shallow S-wave bound states whose binding energies $E^{(n)}$ have an accumulation point at the scattering threshold $E = 0$. As the threshold is approached, the ratio of the binding energies of successive states approaches $e^{2\pi/s_0}$. The asymptotic spectrum near the threshold therefore has the form

$$E^{(n)} \longrightarrow (e^{-2\pi/s_0})^{n-n_*}\hbar^2\kappa_*^2/m \quad \text{as } n \to +\infty, \tag{281}$$

where n_* is an integer that can be chosen for convenience and κ_* is determined up to a multiplicative factor of e^{π/s_0} by the short-distance potential. This geometric spectrum reflects an asymptotic discrete scaling symmetry in which the distance from the origin is rescaled by the discrete scaling factor e^{π/s_0}.

The effective theory strategy can be implemented in this problem by replacing the potential $V(r)$ by an effective potential $V_{\rm eff}(r;\lambda)$ that is identical to $V(r)$ in the region $r > r_0$ but whose behavior in the short-distance region $r < r_0$ depends on a tuning parameter λ. One of the simplest choices for the short-distance potential is a spherical delta-shell potential concentrated on a shell with radius infinitesimally close to but smaller than r_0 [145]:

$$V_{\rm eff}(r) = -\left(\frac{1}{4} + s_0^2\right)\frac{\hbar^2}{2mr^2}, \quad r > r_0, \tag{282a}$$

$$= -\lambda\frac{\hbar^2}{2mr_0}\,\delta(r - r_0), \quad r \leqslant r_0. \tag{282b}$$

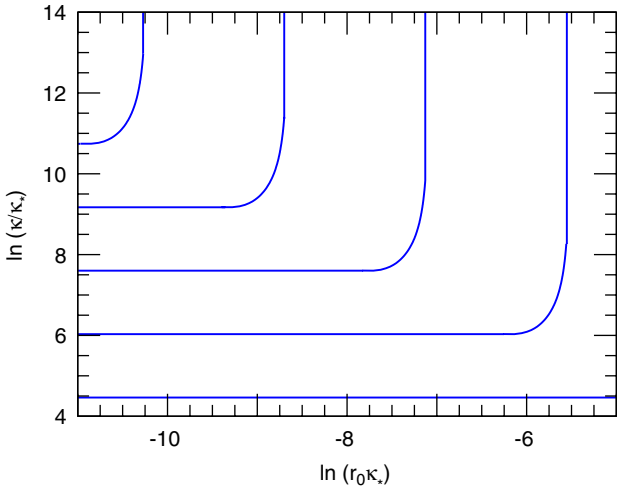

Fig. 37. The binding wave numbers κ for the deepest bound states as a function of $\ln(r_0\kappa_*)$ for $s_0 = 2$ and the delta-shell regularization potential.

We will call the dimensionless coefficient λ the *coupling constant*. Some quantity involving low energies $|E| \ll \hbar^2/mr_0^2$ is selected as a matching quantity, and the coupling constant is then tuned so that the effective potential $V_{\rm eff}(r)$ reproduces the value of the matching quantity for the true potential $V(r)$. A convenient choice for the matching quantity is the bound-state parameter κ_* defined by Eq. (281). The resulting value of the coupling constant depends on r_0:

$$\lambda(r_0) = \frac{1}{2} - s_0 \cot\left[s_0 \ln \frac{\kappa_* r_0}{2} - \arg\Gamma(1 + \mathrm{i}s_0)\right]. \tag{283}$$

We now consider the bound-state spectrum. In the effective potential, the equation for the binding wave number κ defined by $E = -\hbar^2\kappa^2/2m$ is

$$\frac{1}{2} + \kappa r_0 \frac{K'_{\mathrm{i}s_0}(\kappa r_0)}{K_{\mathrm{i}s_0}(\kappa r_0)} - \kappa r_0 \coth(\kappa r_0) = -\lambda(r_0). \tag{284}$$

The spectrum of very shallow bound states has the form (281). The spectrum for the deepest bound states is illustrated in Fig. 37. At critical values of r_0 that differ by multiples of $e^{-\pi/s_0}$, a new bound state with infinitely large binding energy appears. As r_0 decreases further, that binding energy rapidly approaches its asymptotic value given by (281).

The binding energies for the true potential $V(r)$ are guaranteed to differ from those for the effective potential by errors that scale like $E^{(n)}/E_0$, where $E_0 = \hbar^2/mr_0^2$ is the energy scale at which the effective potential begins to differ significantly from the true potential. By tuning a second short-distance parameter in the effective potential, one could decrease the errors so that they scale like $(E^{(n)}/E_0)^2$.

We can interpret r_0 as a short-distance cutoff and $\hbar^2/mr_0^2$ as the corresponding ultraviolet energy cutoff. The tuning of $\lambda(r_0)$ can be interpreted as the renormalization of the coupling constant. As shown in Fig. 38, $\lambda(r_0)$ is a log-periodic function of r_0 with infinite discontinuities. It jumps discontinuously from $+\infty$ to $-\infty$ as r_0 decreases through the critical values at which a bound state appears in the spectrum. The log-periodic behavior of $\lambda(r_0)$ indicates that the renormalization is governed by an RG limit cycle. One of the signatures of the RG limit cycle is the discrete scaling symmetry of the bound state spectrum for the effective potential. Another simple choice for the effective potential at short distances is a spherical square-well potential [146,147]. In this case, the matching condition for the coupling constant $\lambda(r_0)$ has infinitely many solutions. It can be chosen to be a log-periodic function of r_0 corresponding to an RG limit cycle, but such a choice is not required. Alternatively, the $1/r^2$ potential can be regularized by a cutoff Λ in momentum space and renormalized by a momentum-independent counterterm. In this case, the counterterm is necessarily a log-periodic function of Λ corresponding to an RG limit cycle [148].

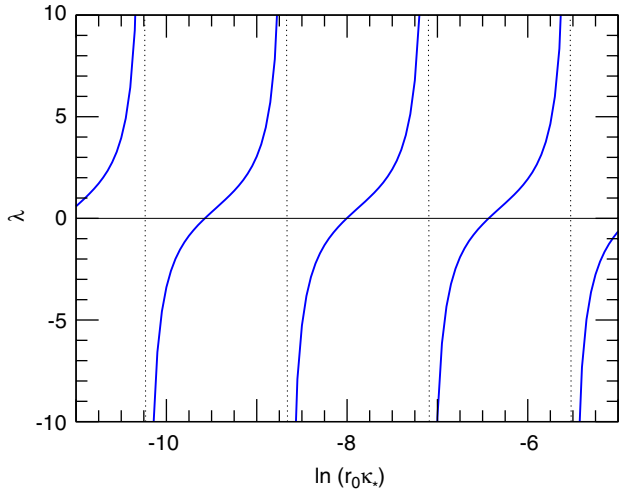

Fig. 38. The coupling constant $\lambda(r_0)$ for the delta-shell regularization potential as a function of $\ln(r_0\kappa_*)$ for $s_0 = 2$.

8.3. *Effective field theories for atoms*

Effective theories can also be used to describe low-energy atoms. For purposes of illustration, we take the fundamental interaction between the atoms to be governed by a 2-body potential $V(r)$. The Hamiltonian that describes the N-atom system is then

$$\hat{H}^{(N)} = \sum_{i=1}^{N} \frac{1}{2m}\boldsymbol{p}_i^2 + \sum_{i<j} V(r_{ij}), \tag{285}$$

where $r_{ij} = |\boldsymbol{r}_{ij}|$ and $\boldsymbol{r}_{ij} = \boldsymbol{r}_i - \boldsymbol{r}_j$. There is some natural low-energy length scale ℓ associated with the potential $V(r)$. We are interested only in the low-energy behavior of this system, where low energy means energy close to the N-atom scattering threshold. More specifically, we require each atom to have kinetic energy small compared to the natural low-energy scale $\hbar^2/m\ell^2$ and we also require each pair of atoms to have potential energy small compared to $\hbar^2/m\ell^2$.

We can describe the low-energy behavior by using an effective theory. The simplest possibility is an effective theory defined by a short-ranged 2-body potential $V_{\rm eff}(r)$ that depends on a set of short-distance tuning parameters $c = (c_1, c_2, \ldots)$:

$$\hat{H}^{(N)}_{\rm eff} = \sum_{i=1}^{N} \frac{1}{2m}\boldsymbol{p}_i^2 + \sum_{i<j} V_{\rm eff}(r_{ij}). \tag{286}$$

One tuning parameter is required to reproduce the scattering length a. Additional tuning parameters may be required to reproduce the 2-body scattering amplitude to higher orders in the expansion in powers of the energy or to reproduce 3-body or higher n-body scattering amplitudes to the desired accuracy.

An equivalent formulation of the quantum mechanics of the N-atom system is in terms of a *quantum field theory* through the "second quantization" formalism. Instead of coordinate and momentum operators $\boldsymbol{r}_i$ and $\boldsymbol{p}_i$, the theory is formulated in terms of a quantum field operator $\psi(\boldsymbol{r})$ that annihilates an atom at the point $\boldsymbol{r}$. If the atoms are bosons, the field operator satisfies the equal-time commutation relations

$$[\psi(\boldsymbol{r}, t), \psi(\boldsymbol{r}', t)] = 0, \quad [\psi(\boldsymbol{r}, t), \psi^\dagger(\boldsymbol{r}', t)] = \delta^3(\boldsymbol{r} - \boldsymbol{r}'). \tag{287}$$

The time evolution of the quantum field is generated by the Hamiltonian

$$\hat{H} = \int \mathrm{d}^3 r \frac{\hbar^2}{2m}\nabla\psi^\dagger \cdot \nabla\psi + \frac{1}{2}\int \mathrm{d}^3 r \int \mathrm{d}^3 r' \; \psi^\dagger\psi(\boldsymbol{r}) V(|\boldsymbol{r} - \boldsymbol{r}'|)\psi^\dagger\psi(\boldsymbol{r}'). \tag{288}$$

The constraint that there be N particles in the system is implemented through a number operator defined by

$$\hat{N} = \int \mathrm{d}^3 r \psi^\dagger \psi(\boldsymbol{r}). \tag{289}$$

A quantum state $|X\rangle$ containing precisely N particles is an eigenstate of $\hat{N}$:

$$\hat{N}|X\rangle = N|X\rangle. \tag{290}$$

The quantum field theory problem defined by the Hamiltonian in Eq. (288), the commutation relations in Eqs. (287), and,and the constraint in Eq. (290) is completely equivalent to the N-body quantum mechanics problem defined by the Hamiltonian in Eq. (285) with canonical commutation relations for the coordinate and momentum operators. The effective theory defined by the effective Hamiltonian in Eq. (286) can also be formulated as a quantum field theory by replacing $V(|\boldsymbol{r}-\boldsymbol{r}'|)$ in Eq. (288) with $V_{\rm eff}(|\boldsymbol{r}-\boldsymbol{r}'|)$.

A class of effective theories that is particularly useful for studying universal aspects of low-energy physics are those that can be formulated as *local quantum field theories*. The Hamiltonian for such a theory can be expressed as the integral of a Hamiltonian density that depends only on the quantum field ψ and its gradients at the same point:

$$\hat{H}_{\rm eff} = \int \mathrm{d}^3 r \mathscr{H}_{\rm eff}. \tag{291}$$

There are infinitely many terms that can appear in $H_{\rm eff}$, so we will write down only a few of them explicitly:[11]

$$\mathscr{H}_{\rm eff} = \frac{\hbar^2}{2m}\nabla\psi^\dagger\cdot\nabla\psi + \mu\psi^\dagger\psi + \frac{g_2}{4}(\psi^\dagger\psi)^2 + \frac{h_2}{4}\nabla(\psi^\dagger\psi)\cdot\nabla(\psi^\dagger\psi) + \frac{g_3}{36}(\psi^\dagger\psi)^3 + \cdots. \tag{292}$$

There are several principles that can be used to reduce the number of possible terms in $\mathscr{H}_{\rm eff}$. If the fundamental Hamiltonian in Eq. (288) has a symmetry, this symmetry can be imposed on the effective Hamiltonian. A simple example is the phase symmetry $\psi \to \mathrm{e}^{\mathrm{i}\alpha}\psi$, which guarantees conservation of particle number. It requires that each term in $\mathscr{H}_{\rm eff}$ have an equal number of factors of ψ and $\psi^\dagger$. We will refer to a term with n factors of both ψ and $\psi^\dagger$ as an n-body term. Galilean symmetry imposes particularly powerful constraints on $\mathscr{H}_{\rm eff}$. It forbids any 2-body terms besides the two terms on the first line of Eq. (292). The constraints of Galilean symmetry on higher n-body terms are more complicated and will not be given here. Terms in $\mathscr{H}_{\rm eff}$ that differ by integration by parts are equivalent, because their difference integrates to a boundary term. Thus the term $\psi^\dagger\psi\nabla^2(\psi^\dagger\psi)$ can be omitted, because it is equivalent to the term $\nabla(\psi^\dagger\psi)\cdot\nabla(\psi^\dagger\psi)$ in Eq. (292). Terms with n factors of ψ (and n factors of $\psi^\dagger$) affect only systems with n or more particles. Thus if we are considering the 3-body problem, we need only consider 2-body and 3-body terms in $\mathscr{H}_{\rm eff}$. Terms with additional factors of ∇ have effects that are suppressed by additional powers of the energy E. Thus if we are trying to reproduce the predictions of the fundamental Hamiltonian only up to errors that scale like E^{n+1}, we need only consider terms with up to $2n$ factors of ∇. The terms shown explicitly in Eq. (292) are sufficient to describe 2-body observables up to errors that scale as E^2 and 3-body observables up to errors that scale as E.

The coefficients of the terms in the effective Hamiltonian density in Eq. (292) are called *coupling constants*. They can be used as tuning parameters to reproduce low-energy observables. The coupling constant g_2 for the 2-body contact interaction can be tuned to reproduce the scattering length. The coupling constants g_2 and h_2 can be tuned simultaneously to reproduce the scattering length and the effective range associated with the 2-body potential. It may also be necessary to tune the coupling constant g_3 for the 3-body contact interaction to reproduce low-energy 3-body scattering amplitudes. For a theory with short-range interactions, it is possible to reproduce the low-energy N-body scattering amplitudes to any desired order in the energy by tuning the coupling constants of a local quantum field theory. This guarantees that the low-energy behavior of an N-atom system can be described by a local quantum field theory.

One complication of using a local quantum field theory is that it is ill-defined without an ultraviolet cutoff. We will usually take the ultraviolet cutoff to be a cutoff on the wave numbers of atoms that can appear in virtual states: $|\boldsymbol{k}| < \Lambda$. The values of the coefficients will of course depend on the cutoff Λ. With an ultraviolet cutoff in place, we do not need to be careful about specifying the ordering of the quantum field operators in the Hamiltonian density (292). A difference

[11] The fundamental Hamiltonian in Eq. (285) or (288) is invariant under Galilean transformations. This symmetry can be used to constrain the terms in the effective Hamiltonian density.

in operator-ordering can be compensated by a change in the coupling constants. In practice, it may be convenient to use normal-ordered operators, but we will not bother to specify any operator ordering explicitly.

A local quantum field theory is particularly convenient for describing the scaling limit of a few-atom system with a large scattering length $|a| \gg \ell$. The scaling limit involves taking the range of the interaction to zero, but such a limit is built into a local quantum field theory. One complication is that the large scattering length implies strong interactions between the atoms, so the field theory must be solved nonperturbatively. The minimal quantum field theory required to describe the 2-atom system in the scaling limit has only a 2-body contact interaction. Its coupling constant g_2 can be tuned to give the desired value of the scattering length a. The minimal quantum field theory required to describe the 3-atom system in the scaling limit has also a 3-body contact interaction. Its coupling constant g_3 can be tuned to give the desired value of the 3-body parameter κ_*. It would also be possible to reproduce both a and κ_* by simultaneously tuning g_2 and the coupling constant for a second 2-body interaction term. The advantage of using g_2 and g_3 is that g_3 has no effect on the 2-body sector. Thus one can first tune g_2 to get the desired value of a by calculating a 2-body observable, and then tune g_3 to get the desired value of κ_* by calculating a 3-body observable.

An important open question is whether additional tuning parameters would be required to reproduce the low-energy observables in the N-body sectors, $N = 4, 5, 6, \ldots$ to leading order in ℓ/a. This issue will be addressed in Section 10.1.

8.4. Two-body problem

We will now use our local effective field theory to solve the 2-body problem. Although the solution is very simple, it illustrates many aspects of the solution to the 3-body problem.

The problem of two identical bosons with large scattering length a in the scaling limit can be described by a local quantum field theory whose only interaction term is a 2-body contact interaction. For practical calculations, it is more convenient to use the Lagrangian formulation of the effective field theory instead of the Hamiltonian one from the previous section. The Lagrangian and Hamiltonian densities are simply related by a Legendre transformation. The Lagrangian density is

$$\mathscr{L} = \psi^\dagger \left(\mathrm{i}\,\frac{\partial}{\partial t} + \frac{1}{2}\nabla^2 \right) \psi - \frac{g_2}{4} (\psi^\dagger \psi)^2. \tag{293}$$

For simplicity of notation, we set $\hbar = 1$ and $m = 1$ here and in the remainder of this section. The coupling constant g_2 must be adjusted as a function of the ultraviolet cutoff Λ so that the field theory describes atoms with scattering length a.

If the effects of the interaction term in Eq. (293) are calculated as a power series in g_2 using perturbation theory, the effective field theory describes scattering states of two atoms. After renormalization, the scattering amplitude coincides with the expansion of the universal scattering amplitude in Eq. (58) in powers of ka. If the effects of the interaction term are calculated nonperturbatively, we not only obtain the complete universal expression for the scattering amplitude in Eq. (58) but we find that the effective field theory also describes bound states with binding energy given by Eq. (62). Thus this effective field theory reproduces all the universal low-energy observables of the 2-body problem with large scattering length.

All information about the physical observables in the 2-body sector is encoded in the 4-point Green's function $\langle 0|\mathrm{T}(\psi\psi\psi^\dagger\psi^\dagger)|0\rangle$, where $|0\rangle$ is the vacuum state, T represents time-ordering, and we have suppressed the time and space coordinates of the four field operators. The physical information is encoded more succinctly in the truncated connected Green's function in momentum space which we denote by $\mathrm{i}\mathscr{A}$. It is obtained by subtracting the disconnected terms that have the factored form $\langle 0|\mathrm{T}(\psi\psi^\dagger)|0\rangle\langle 0|\mathrm{T}(\psi\psi^\dagger)|0\rangle$, Fourier transforming in all coordinates, factoring out an overall energy-momentum conserving delta function, and also factoring out propagators associated with each of the four external legs. We will refer to $\mathscr{A}$ as the $2 \to 2$ off-shell amplitude.

The amplitude $\mathrm{i}\mathscr{A}$ can be expressed as the sum of connected Feynman diagrams constructed out of the propagator in Fig. 39(a) and the vertex in Fig. 39(b). The first three diagrams in the perturbative expansion of $\mathrm{i}\mathscr{A}$ in powers of g_2 are shown in Fig. 40(a). Energy and momentum are both conserved at every vertex of the Feynman diagrams. For every closed loop, there is an energy p_0 and a momentum $\boldsymbol{p}$ that are not determined by the external energies and momenta. They must be integrated over with the measure $d^4p/(2\pi)^4$. There are also symmetry factors of $1/n!$ associated with subdiagrams that are invariant under the permutation of n internal lines. For example, the second diagram in Fig. 40(a) has a symmetry factor of $1/2$ and the third diagram has a symmetry factor of 1/4.

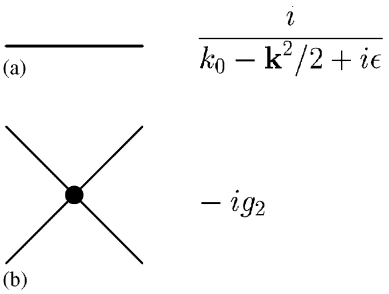

Fig. 39. Feynman rules for the Lagrangian in Eq. (293): (a) the propagator for an atom with energy k_0 and momentum $\boldsymbol{k}$, (b) the vertex for the 2-body contact interaction.

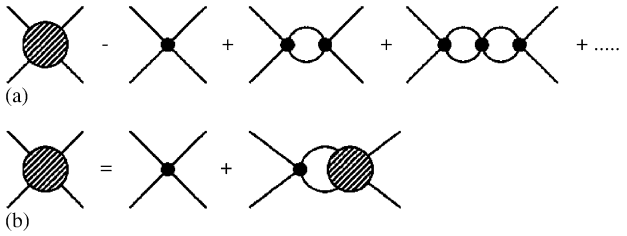

Fig. 40. Diagrammatic equations for the $2 \to 2$ off-shell amplitude: (a) the perturbative expansion in g_2, and (b) the integral equation.

In general, the amplitude $\mathscr{A}$ depends on the energies and momenta of the four external lines. It is called an *off-shell* amplitude, because the energy p_0 of an external line with momentum $\boldsymbol{p}$ need not be equal to its physical value $p^2/2$. The T-matrix element $\mathscr{T}$ for a $2 \to 2$ scattering process is obtained by evaluating $\mathscr{A}$ at the *on-shell point* where p_0 is set equal to $p^2/2$ for every external momentum $\boldsymbol{p}$. In the center-of-mass frame, we can take the 2 incoming momenta to be $+\boldsymbol{k}$ and $-\boldsymbol{k}$ and the two outgoing momenta to be $+\boldsymbol{p}$ and $-\boldsymbol{p}$. The amplitude $\mathscr{A}$ then depends on $\boldsymbol{k}, \boldsymbol{p}$, and the 4 off-shell energies. When the only interaction is the 2-body contact interaction in Fig. 39(b), the amplitude simplifies enormously because it can depend only on the total momentum and the total off-shell energy E. In the center-of-mass frame, it is a function of E only, so we will denote it by $\mathscr{A}(E)$. The on-shell point corresponds to setting $E = 2(k^2/2) = 2(p^2/2)$, which requires $p = k$. The off-shell $2 \to 2$ amplitude $\mathscr{A}(E)$ encodes all physical information about the 2-body system at low energies. For example, the T-matrix element for atoms of momenta $\pm\boldsymbol{k}$ to scatter into atoms of momenta $\pm\boldsymbol{k}'$ with $|\boldsymbol{k}'| = |\boldsymbol{k}| = k$ is

$$\mathscr{T}(k) = \mathscr{A}(E = k^2). \tag{294}$$

The conventional scattering amplitude $f_k(\theta)$ for atoms with momenta $\pm\boldsymbol{k}$ to scatter through an angle θ is proportional to $\mathscr{A}(E)$ evaluated at the on-shell point:

$$f_k(\theta) = \frac{1}{8\pi}\mathscr{A}(E = k^2). \tag{295}$$

The limit of the scattering amplitude as $k \to 0$ determines the scattering length:

$$a = -\frac{1}{8\pi}\mathscr{A}(0). \tag{296}$$

The contact interaction in Eq. (293) is ill-defined unless an ultraviolet cutoff is imposed on the momenta in loop diagrams. This can be seen by writing down the off-shell amplitude for 2-body scattering at second order in perturbation theory:

$$\mathscr{A}(E) \approx -g_2 - \frac{\mathrm{i}}{2}g_2^2 \int \frac{\mathrm{d}^3 q}{(2\pi)^3} \int \frac{\mathrm{d}q_0}{2\pi} \frac{1}{q_0 - q^2/2 + \mathrm{i}\epsilon} \frac{1}{E - q_0 - q^2/2 + \mathrm{i}\epsilon} + \cdots. \tag{297}$$

The two terms correspond to the first two diagrams in Fig. 40(a). The intermediate lines have momenta $\pm\boldsymbol{q}$. The integral over q_0 in Eq. (297) is easily evaluated using contour integration:

$$\mathscr{A}(E) \approx -g_2 - \frac{1}{2}g_2^2 \int \frac{\mathrm{d}^3 q}{(2\pi)^3} \frac{1}{E - q^2 + \mathrm{i}\epsilon} + \cdots. \tag{298}$$

The integral over $\boldsymbol{q}$ diverges. It can be regularized by imposing an ultraviolet cutoff $|\boldsymbol{q}| < \Lambda$. Taking the limit $\Lambda \gg |E|^{1/2}$, the amplitude reduces to[12]

$$\mathscr{A}(E) \approx -g_2 + \frac{g_2^2}{4\pi^2}\left(\Lambda - \frac{\pi}{2}\sqrt{-E - \mathrm{i}\epsilon}\right) + \cdots. \tag{299}$$

The dependence on the ultraviolet cutoff Λ can be consistently eliminated by a perturbative renormalization procedure. A simple choice is to eliminate the parameter g_2 in favor of the scattering length a, which is given by Eq. (296):

$$a \approx \frac{g_2}{8\pi}\left(1 - \frac{g_2\Lambda}{4\pi^2} + \cdots\right). \tag{300}$$

Inverting this expression to obtain g_2 as a function of a we obtain

$$g_2 \approx 8\pi a\left(1 + \frac{2a\Lambda}{\pi} + \cdots\right), \tag{301}$$

where we have truncated at second order in a. Inserting the expression for g_2 into Eq. (299) and expanding to second order in a, we obtain the renormalized expression for the amplitude:

$$\mathscr{A}(E) \approx -8\pi a(1 + a\sqrt{-E - \mathrm{i}\epsilon} + \cdots). \tag{302}$$

If we evaluate this at the on-shell point $E = k^2$ and insert it into Eq. (295), we find that it reproduces the first two terms in the expansion of the universal scattering amplitude in Eq. (58) in powers of ka. By calculating $\mathscr{A}(E)$ to higher order in perturbation theory, we can reproduce the low-momentum expansion of Eq. (58) to higher order in ka. Thus a perturbative treatment of the effective field theory reproduces the low-momentum expansion of the 2-body scattering amplitude. The perturbative approximation is valid only if the energy satisfies $E \ll 1/a^2$.

If we are interested in observables involving energy $E \sim 1/a^2$, then we must solve the problem nonperturbatively [69,149]. This is most easily accomplished by realizing that the Feynman diagrams in Fig. 40(a) form a geometric series. Summing the geometric series, the exact expression for the amplitude is

$$\mathscr{A}(E) = -g_2\left[1 + \frac{g_2}{4\pi^2}\left(\Lambda - \frac{\pi}{2}\sqrt{-E - \mathrm{i}\epsilon}\right)\right]^{-1}. \tag{303}$$

Alternatively, we can use the fact that summing the diagrams in Fig. 40(a) is equivalent to solving the following integral equation:

$$\mathscr{A}(E) = -g_2 - \frac{\mathrm{i}}{2}g_2 \int \frac{\mathrm{d}^3 q}{(2\pi)^3} \int \frac{\mathrm{d}q_0}{2\pi} \frac{1}{q_0 - q^2/2 + \mathrm{i}\epsilon} \frac{1}{E - q_0 - q^2/2 + \mathrm{i}\epsilon} \mathscr{A}(E). \tag{304}$$

The integral equation is expressed diagrammatically in Fig. 40(b). Since the function $\mathscr{A}(E)$ is independent of $\boldsymbol{q}$ and q_0, it can be pulled outside of the integral in Eq. (304). The integral can be regularized by imposing an ultraviolet cutoff Λ. The integral equation is now trivial to solve and the solution is given in Eq. (303).

The expression for the nonperturbative $2 \to 2$ off-shell amplitude in Eq. (303) depends on the parameter g_2 in the Lagrangian and on the ultraviolet cutoff Λ. Renormalization can be implemented by eliminating g_2 in favor of a low-energy observable, such as the scattering length a. Using Eq. (295), the nonperturbative expression for the scattering length is

$$a = \frac{g_2}{8\pi}\left(1 + \frac{g_2\Lambda}{4\pi^2}\right)^{-1}. \tag{305}$$

[12] If the calculation was carried out in a frame in which the total momentum of the two scattering particles was nonzero, the simple cutoff $|\boldsymbol{q}| < \Lambda$ would give a result that does not respect Galilean invariance. To obtain a Galilean-invariant result requires either using a more sophisticated cutoff or else imposing the cutoff $|\boldsymbol{q}| < \Lambda$ only after an appropriate shift in the integration variable $\boldsymbol{q}$.

Solving for g_2, we obtain

$$g_2 = 8\pi a\left(1 - \frac{2a\Lambda}{\pi}\right)^{-1}. \tag{306}$$

Given a fixed ultraviolet cutoff Λ, this equation prescribes how the parameter g_2 must be tuned in order to give the correct scattering length a. Note that for $\Lambda \gg 1/|a|$, the coupling constant g_2 is always negative regardless of the sign of a. Eliminating g_2 in Eq. (303) in favor of a, we find that the nonperturbative off-shell amplitude reduces to

$$\mathscr{A}(E) = \frac{8\pi}{-1/a + \sqrt{-E - \mathrm{i}\epsilon}}. \tag{307}$$

In this simple case, we find that our renormalization prescription eliminates the dependence on Λ completely. In general, we should expect it to only be suppressed by powers of $1/(a\Lambda)$ or E/Λ^2. A final step of taking the limit $\Lambda \to \infty$ would then be required to obtain results that are completely independent of Λ.

Evaluating the off-shell amplitude in Eq. (307) at the on-shell point $E = k^2$ and inserting it into the expression for the scattering amplitude in Eq. (295), we recover the universal expression in Eq. (58). The differential cross section is therefore given by Eq. (59). The nonperturbative off-shell amplitude in Eq. (307) also encodes information about bound states. It is an analytic function of the complex energy E except for a branch cut along the positive real axis and possibly a pole on the negative real axis. The branch cut is associated with 2-particle scattering states. A pole on the negative real axis corresponds to a bound state. If $a > 0$, the amplitude in Eq. (307) has a pole at $E = -1/a^2$. This pole indicates that there is a 2-body bound state with binding energy given by Eq. (62). If $a < 0$, the pole in the off-shell amplitude is located at $E = \mathrm{e}^{3\pi\mathrm{i}}/a^2$, which is on the second sheet of the complex energy E. Such a state is called a virtual state. Therefore there is no 2-body bound state when $a < 0$.

The formula for the scattering length in Eq. (305) illustrates an important basic principle of effective theories. Nonanalytic behavior in long-distance observables generally arises from completely analytic behavior in short-distance parameters. In this case, the long-distance observable is the scattering length a, and the short-distance parameter is the strength g_2 of the 2-body contact interaction. We should think of the ultraviolet cutoff Λ as some fixed momentum scale that is large compared to the wave numbers of interest. Particles with wave numbers less than Λ are taken into account explicitly in the field theory. Particles with wave numbers greater than Λ are excluded by this cutoff. The effects of virtual 2-body states with such wave numbers are taken into account through the strength g_2 of the 2-body contact interaction. According to Eq. (305), the scattering length diverges when g_2 is tuned to the critical value $-4\pi^2/\Lambda$. There is nothing particularly remarkable about this value as far as short-distance physics is concerned. The divergence in a arises from the iteration of quantum fluctuations involving virtual particles with wave numbers less than Λ, which generates the term $g_2\Lambda/4\pi$ in the denominator of Eq. (305). The scattering length a is not an analytic function of g_2 at the critical point: a small change in the short-distance parameter g_2 can produce an enormous change in a.

The formula in Eq. (306) illustrates that an arbitrarily large coupling constant is not necessarily pathological in a nonperturbative field theory. The expression for g_2 diverges as $\Lambda \to \pi/2a$. However, physical observables are independent of Λ. Thus the effects of the arbitrarily large coupling constant g_2 must be compensated by equally large effects from the iteration of quantum fluctuations involving virtual particles.

We now discuss the renormalization of this field theory from a renormalization group perspective. We consider a dimensionless combination of the coupling constant g_2 and the ultraviolet cutoff Λ:

$$\hat{g}_2(\Lambda) = \frac{\Lambda g_2}{4\pi^2}. \tag{308}$$

Using Eq. (306), the dimensionless coupling constant can be written as

$$\hat{g}_2(\Lambda) = -\frac{a\Lambda}{a\Lambda - \pi/2}. \tag{309}$$

As Λ is varied with a fixed, the expression for $\hat{g}_2$ in Eq. (308) maps out a renormalization group (RG) trajectory. The RG trajectories for various values of a are illustrated in Fig. 41. All the points on a given trajectory represent the same physical theory with a given scattering length a. As Λ increases, the dimensionless coupling constant

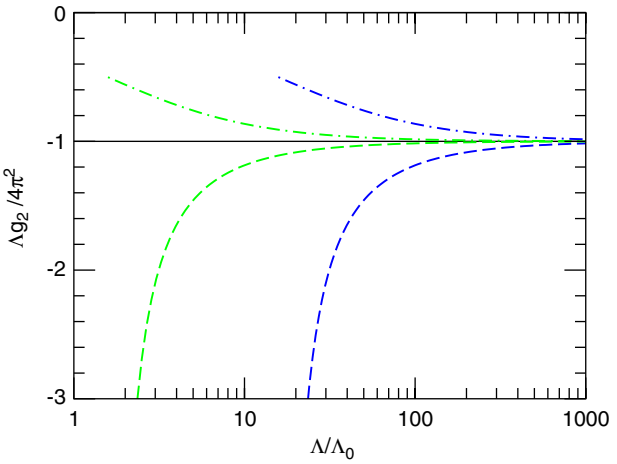

Fig. 41. The dimensionless 2-body coupling constant $\hat{g}_2 = \Lambda g_2/4\pi^2$ as a function of the ultraviolet cutoff Λ for several values of the scattering length a. As $\Lambda \to \infty$, Λg_2 asymptotically approaches an RG fixed point.

in Eq. (309) flows towards an ultraviolet fixed point:

$$\hat{g}_2(\Lambda) \longrightarrow -1 \quad \text{as } \Lambda \to \infty. \tag{310}$$

Using (305), we can identify the fixed-point theory as the 2-body problem in the resonant limit $a \to \pm\infty$. The scaling limit $\ell \to 0$ is implicit in our formulation of the problem in terms of a local quantum field theory, so the fixed point corresponds to taking the resonant and scaling limits simultaneously. All the RG trajectories in Fig. 41 are focused towards this fixed point as $\Lambda \to \infty$. The focusing of the RG trajectories indicates that as the energy scale becomes larger and larger compared to $1/a^2$, the system with fixed scattering length a behaves more and more like the resonant limit. For a physical system, there is a natural ultraviolet cutoff $\Lambda \sim 1/\ell$ beyond which the physics can no longer be reproduced by a 2-body contact interaction. For $\Lambda > 1/\ell$, the behavior of the system becomes more complicated and it no longer flows toward the fixed point corresponding to the resonant and scaling limits.

Further insight into this problem can be achieved by expressing the renormalization group flow in terms of a differential equation for the Λ-dependence of $\hat{g}_2$. By differentiating both sides of Eq. (309), one can derive the differential RG equation [149]

$$\Lambda \frac{\mathrm{d}}{\mathrm{d}\Lambda}\hat{g}_2 = \hat{g}_2(1 + \hat{g}_2). \tag{311}$$

It is clear from this equation that the RG flow of $\hat{g}_2$ has two fixed points: $\hat{g}_2 = -1$ and $\hat{g}_2 = 0$. The fixed point $\hat{g}_2 = -1$ corresponds to the resonant limit $a \to \pm\infty$ discussed above. The second fixed point $\hat{g}_2 = 0$ corresponds to the noninteracting system with $a = 0$. The perturbative expansion for the scattering amplitude in Eq. (302) corresponds to an expansion about this fixed point. In the theory of the homogeneous Bose gas, the expansion in powers of the diluteness parameter $(na^3)^{1/2}$ [1] provides another example of an expansion around this noninteracting fixed point.

At the two fixed points, the 2-body system is scale invariant. In general, the continuous scaling symmetry defined by Eqs. (66) is a mapping of the theory onto another theory with a different scattering length. At the fixed points $a = \pm\infty$ and 0, the continuous scaling symmetry maps the theory onto itself. For the $a = 0$ fixed point, the scale invariance is trivial because there are no interactions. The $a = \pm\infty$ fixed point has nontrivial scale invariance. The 2-body system at this fixed point is actually invariant under a larger group of conformal symmetry transformations [150].

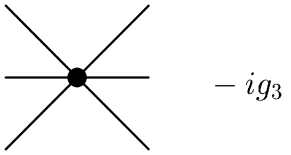

Fig. 42. Feynman rule for the 3-body contact interaction.

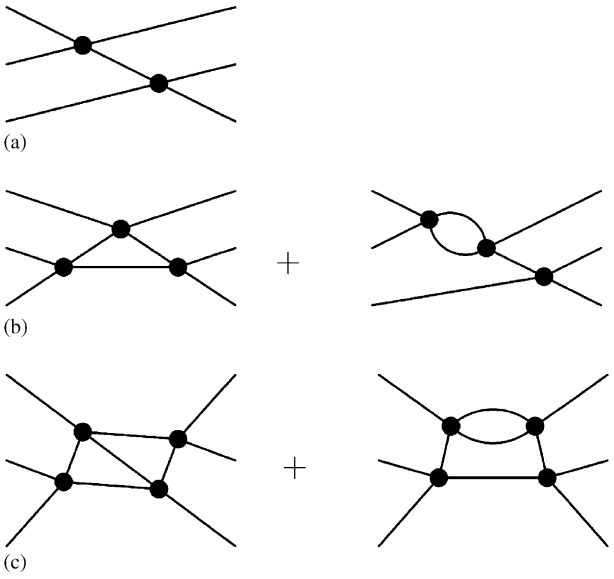

Fig. 43. Feynman diagrams for the $3 \to 3$ elastic scattering amplitude: (a) a tree diagram that contributes to the E^{-1} term, (b) one-loop diagrams that contribute to the $E^{-1/2}$ term, (c) two-loop diagrams that contribute to the $\ln(E)$ term.

8.5. Three-body problem

We now formulate the 3-body problem in the language of effective field theory. The problem of three identical bosons with large scattering length in the scaling limit can be described by a local quantum field theory whose only interaction terms are 2-body and 3-body contact interactions. The Lagrangian density is

$$\mathscr{L} = \psi^\dagger \left(\mathrm{i}\frac{\partial}{\partial t} + \frac{1}{2}\nabla^2 \right) \psi - \frac{g_2}{4}\left(\psi^\dagger\psi\right)^2 - \frac{g_3}{36}\left(\psi^\dagger\psi\right)^3. \tag{312}$$

In addition to the Feynman rules in Fig. 39, there is the additional Feynman rule for the 3-body contact interaction in Fig. 42.

If the interaction terms in Eq. (312) are treated perturbatively, the 3-body sector of the quantum field theory describes 3-atom scattering states. The perturbative expansion in powers of g_2 and g_3 coincides after renormalization with an expansion in powers of the energies of the scattering atoms. The renormalization associated with g_2 can be implemented by making the substitution in Eq. (306) and expanding in powers of a. If we take all the atoms to have energies proportional to E, then the T-matrix element can be expanded in powers of E. The expansion contains singular terms proportional to E^{-1}, $E^{-1/2}$, and $\ln(E)$ [103]. At the leading order g_2^2 of the perturbation expansion in g_2, the E^{-1} term comes from tree diagrams such as the one in Fig. 43(a). There are higher order contributions to the E^{-1} term from the insertion of the string of one-loop bubble diagrams shown in Fig. 40 in place of the vertices in Fig. 43(a). Their effect is simply to renormalize the coupling constant, $g_2 \to 8\pi a$, so that the E^{-1} term is proportional to a^2. There are two classes of contributions to the $E^{-1/2}$ term in the T-matrix element for 3-atom elastic scattering. At the leading order g_2^3, the $E^{-1/2}$ term comes from the 1-particle-irreducible 1-loop diagram in Fig. 43(b) and from the insertion of a 1-loop

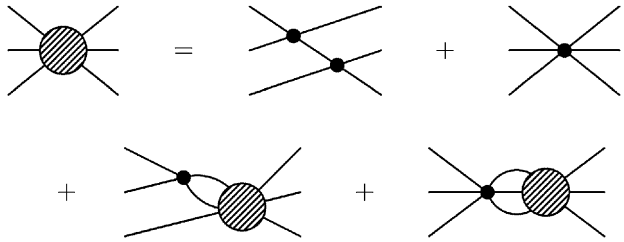

Fig. 44. Simple integral equation for the truncated connected 3-body amplitude. The first and third diagrams should be summed over the three pairs of atoms that interact first.

bubble diagram in place of either of the vertices in Fig. 43(a). Again the contributions from higher order diagrams is simply to renormalize the coupling constant, so that the $E^{-1/2}$ term is proportional to a^3. Terms with the logarithmic singularity $\ln(E)$ arise first at order g_2^4 from the 1-particle-irreducible 2-loop diagrams with the two topologies shown in Fig. 43(c). The effects of higher-order diagrams in which the vertices in Fig. 43(c) are replaced by strings of the one-loop bubble diagrams in Fig. 40 is to renormalize the coupling constant, so that the coefficient of the $\ln(E)$ term is proportional to a^4.

The logarithm of E in the T-matrix element arises from a scale-invariant region of the 2-loop integral for the diagrams in Fig. 43(c) that extends from the momentum scale $E^{1/2}$ to the ultraviolet cutoff Λ. Thus the logarithmic term is proportional to $a^4 \ln(E/\Lambda^2)$. This logarithmic dependence on the ultraviolet cutoff is not removed by renormalization of the 2-body coupling constant g_2. The logarithmic dependence on Λ comes from the region of the loop integrals in which all the virtual particles in the diagrams in Fig. 43(c) have large momenta of order Λ. In coordinate space, this corresponds to all the particles having small separations of order $1/\Lambda$. The dependence on Λ can therefore be cancelled by the 3-body contact interaction in the Lagrangian in Eq. (312) with a coefficient $g_3(\Lambda)$ that depends on the ultraviolet cutoff Λ. The required cutoff-dependence of the 3-body coupling constant is described by the differential RG equation [151]

$$\Lambda \frac{\mathrm{d}}{\mathrm{d}\Lambda} g_3 = 384(4\pi - 3\sqrt{3})a^4. \tag{313}$$

If the cutoff Λ is increased, the strength of the 3-body contact interaction must be increased in accordance with Eq. (313) to cancel the additional short-distance contributions from four successive 2-body scatterings.

In order to calculate observables involving energies E of order $1/ma^2$, it is necessary to solve the quantum field theory nonperturbatively. All information about physical observables in the 3-body sector is encoded in the 6-point Green's function $\langle 0|\mathrm{T}(\psi\psi\psi\psi^\dagger\psi^\dagger\psi^\dagger)|0\rangle$, where we have suppressed the time and space coordinates of the 6 field operators. It is encoded even more succinctly in the truncated connected 6-point Green's function in momentum space which we will denote by $\mathscr{A}$.[13] In the center-of-mass frame, $\mathscr{A}$ is a function of 4 momentum vectors and 5 off-shell energies. One can in principle solve the quantum field theory by solving an integral equation for $\mathscr{A}$. The simplest integral equation for $\mathscr{A}$ is illustrated in Fig. 44. It simply states that the Feynman diagrams that contribute to the amplitude are either tree diagrams or they involve at least one loop. For those diagrams that involve a loop, the first interaction is either a 2-body contact interaction or a 3-body contact interaction. The various possibilities are represented by the diagrams on the right side of the integral equation in Fig. 44. The first two diagrams are tree diagrams and they constitute the inhomogeneous term in the integral equation. In the third diagram, the first interaction is a 2-body constant interaction and it involves a one-loop integral over the amplitude $\mathscr{A}$. In the fourth diagram, the first interaction is a 3-body contact interaction and it involves a 2-loop integral over the amplitude $\mathscr{A}$.

Integral equations in many variables are very difficult to solve numerically, so the integral equation in Fig. 44 is not very useful in practice. However, from our understanding of universality in the 3-body problem, we can anticipate some of the features that would appear in the nonperturbative solution. In addition to 3-atom scattering states, there must be scattering states consisting of an atom and a dimer whose binding energy is $E_\mathrm{D} = 1/a^2$. There must also be a sequence of 3-body bound states with binding energies that range from order $1/a^2$ to order Λ^2. The number of these Efimov

[13] The 3-atom amplitude $\mathscr{A}$ should not be confused with the atom–atom amplitude in Section 8.4, which was denoted by the same symbol.

states will depend on the ultraviolet cutoff Λ imposed on the loop momenta, but it should be roughly $\ln(|a|\Lambda)/\pi$ for asymptotically large Λ. These bound states must all emerge dynamically from the nonperturbative effects encoded in the simple Lagrangian in Eq. (312).

We conclude this subsection by giving the perturbative expansion for the T-matrix element for elastic 3-atom scattering through 4th order in the scattering length a. Three atoms with momenta $\boldsymbol{k}_1$, $\boldsymbol{k}_2$ and $\boldsymbol{k}_3$ can scatter into states with momenta $\boldsymbol{k}'_1$, $\boldsymbol{k}'_2$ and $\boldsymbol{k}'_3$ that are allowed by conservation of energy and momentum. The probability amplitude for $3 \to 3$ scattering processes in which all three atoms participate is given by the connected T-matrix element, which we denote by $\mathcal{T}(\boldsymbol{k}_1, \boldsymbol{k}_2, \boldsymbol{k}_3; \boldsymbol{k}'_1, \boldsymbol{k}'_2, \boldsymbol{k}'_3)$. For simplicity, we consider only the center-of-mass frame, in which $\boldsymbol{k}_1+\boldsymbol{k}_2+\boldsymbol{k}_3=0$, and we introduce the shorthand

$$\mathcal{T}(123 \to 1'2'3') \equiv \mathcal{T}(\boldsymbol{k}_1, \boldsymbol{k}_2, \boldsymbol{k}_3; \boldsymbol{k}'_1, \boldsymbol{k}'_2, \boldsymbol{k}'_3). \tag{314}$$

The connected T-matrix element for $3 \to 3$ scattering can be separated into the terms that involve a single virtual particle in the intermediate state, which are called *one-particle-reducible* (1PR), and the remaining terms, which are called *one-particle-irreducible* (1PI):

$$\mathcal{T}(123 \to 1'2'3') = \mathcal{T}^{\rm 1PR}(123 \to 1'2'3') + \mathcal{T}^{\rm 1PI}(123 \to 1'2'3'), \tag{315}$$

The 1PR terms can be written down in closed form [104]:

$$\mathcal{T}^{\rm 1PR}(123 \to 1'2'3') = \sum_{(123)} \sum_{(1'2'3')} \frac{\mathcal{A}(q_{12}^2/4)\mathcal{A}(q_{1'2'}^2/4)}{\boldsymbol{k}_1 \cdot \boldsymbol{k}_2 - (\boldsymbol{k}_1+\boldsymbol{k}_2)\cdot \boldsymbol{k}'_3 + k_3'^2 - {\rm i}\epsilon}, \tag{316}$$

where $q_{12} = |\boldsymbol{k}_1 - \boldsymbol{k}_2|$, $q_{1'2'} = |\boldsymbol{k}'_1 - \boldsymbol{k}'_2|$, and $\mathcal{A}(E)$ is the amplitude for atom–atom scattering given in Eq. (307). The sums in Eq. (316) are over cyclic permutations of $\boldsymbol{k}_1$, $\boldsymbol{k}_2$, and $\boldsymbol{k}_3$ and over cyclic permutations of $\boldsymbol{k}'_1$, $\boldsymbol{k}'_2$, and $\boldsymbol{k}'_3$. The summand that is given explicitly in Eq. (316) corresponds to the $2 \to 2$ scattering of particles 1 and 2 to produce particle $3'$ and a virtual particle. A subsequent $2 \to 2$ scattering of the virtual particle and particle 3 produces particles $1'$ and $2'$. Examples of diagrams that contribute to the sum are the tree diagram in Fig. 43(a) and the second diagram in Fig. 43(b). The 1PR term in Eq. (316) can be expanded as a power series in a simply by expanding the amplitudes $\mathcal{A}(E)$ as power series in a using Eq. (302).

The 1PI terms in the T-matrix element cannot be expressed in closed form, but we will give explicit expressions for the terms of order a^3 and a^4 in its perturbative expansion. The term of order a^3 comes from one-loop diagrams like the first diagram in Fig. 43(b). It can be expressed as [104]

$$\mathcal{T}_3^{\rm 1PI}(123 \to 1'2'3') = -512\pi^3 a^3 \sum_{(123)} \sum_{(1'2'3')} \mathcal{I}(123 \to 1'2'3'), \tag{317}$$

where the integral $\mathcal{I}$ is a function of the wave vectors $\boldsymbol{k}_i$ and $\boldsymbol{k}'_i$:

$$\mathcal{I}(123 \to 1'2'3') = \int \frac{{\rm d}^3 p}{(2\pi)^3} \frac{1}{p^2 + \boldsymbol{p}\cdot\boldsymbol{k}_3 + \boldsymbol{k}_1\cdot\boldsymbol{k}_2 - {\rm i}\epsilon} \frac{1}{p^2 + \boldsymbol{p}\cdot\boldsymbol{k}'_3 + \boldsymbol{k}'_1\cdot\boldsymbol{k}'_2 - {\rm i}\epsilon}. \tag{318}$$

The terms of order a^4 in the perturbative expansion of the 1PI T-matrix element come from adding a one-loop bubble to the first one-loop diagram in Fig. 43(b) and from the two-loop diagrams in Fig. 43(c). The three terms can be expressed in the form [104]

$$\mathcal{T}_{4a}^{\rm 1PI}(123 \to 1'2'3') = 256{\rm i}\pi^3 a^4 \sum_{(123)} \sum_{(1'2'3')} (q_{12} + q_{1'2'})\mathcal{I}(123 \to 1'2'3'), \tag{319a}$$

$$\mathcal{T}_{4b}^{\rm 1PI}(123 \to 1'2'3') = 8192\pi^4 a^4 \sum_{(123)} \sum_{(1'2'3')} \mathcal{J}(123 \to 1'2'3'), \tag{319b}$$

$$\mathcal{T}_{4c}^{\rm 1PI}(123 \to 1'2'3') = 4096\pi^4 a^4 \sum_{(123)} \sum_{(1'2'3')} \mathcal{J}'(123 \to 1'2'3'). \tag{319c}$$

The integrals inside the sums in Eqs. (319b) and (319c) are given by

$$\mathscr{J}(123 \to 1'2'3') = \int \frac{\mathrm{d}^3p}{(2\pi)^3} \int \frac{\mathrm{d}^3q}{(2\pi)^3} \frac{1}{p^2+q^2+r^2-2mE-\mathrm{i}\epsilon} \times \frac{1}{p^2+\boldsymbol{p}\cdot\boldsymbol{k}_3+\boldsymbol{k}_1\cdot\boldsymbol{k}_2-\mathrm{i}\epsilon} \frac{1}{q^2+\boldsymbol{q}\cdot\boldsymbol{k}_3'+\boldsymbol{k}_1'\cdot\boldsymbol{k}_2'-\mathrm{i}\epsilon}, \tag{320a}$$

$$\mathscr{J}'(123 \to 1'2'3') = \int \frac{\mathrm{d}^3p}{(2\pi)^3} \int \frac{\mathrm{d}^3q}{(2\pi)^3} \left(\frac{1}{p^2+q^2+r^2-2mE-\mathrm{i}\epsilon} - \frac{1}{2q^2} \right) \times \frac{1}{p^2+\boldsymbol{p}\cdot\boldsymbol{k}_3+\boldsymbol{k}_1\cdot\boldsymbol{k}_2-\mathrm{i}\epsilon} \frac{1}{p^2+\boldsymbol{p}\cdot\boldsymbol{k}_3'+\boldsymbol{k}_1'\cdot\boldsymbol{k}_2'-\mathrm{i}\epsilon}, \tag{320b}$$

where $r = |\boldsymbol{p}+\boldsymbol{q}|$ and $E = (k_1^2+k_2^2+k_3^2)/2m$ is the total energy. These two-loop integrals are logarithmically ultraviolet divergent. The divergence can be isolated in a term that is momentum-independent by subtracting and adding the following integrals:

$$\mathscr{J}_{\log}(\kappa) = \int \frac{\mathrm{d}^3p}{(2\pi)^3} \int \frac{\mathrm{d}^3q}{(2\pi)^3} \frac{1}{p^2+q^2+r^2+2\kappa^2} \frac{1}{(p^2+\kappa^2)(q^2+\kappa^2)}, \tag{321a}$$

$$\mathscr{J}'_{\log}(\kappa) = \int \frac{\mathrm{d}^3p}{(2\pi)^3} \int \frac{\mathrm{d}^3q}{(2\pi)^3} \left(\frac{1}{p^2+q^2+r^2+2\kappa^2} - \frac{1}{2(q^2+\kappa^2)} \right) \frac{1}{(p^2+\kappa^2)^2}. \tag{321b}$$

Dimensional regularization can be applied to these integrals by changing the integrals over three-dimensional vectors to integrals over D-dimensional vectors with the following prescription for the integration measure:

$$\int \frac{\mathrm{d}^3p}{(2\pi)^3} \longrightarrow \Lambda^{3-D} \int \frac{\mathrm{d}^Dp}{(2\pi)^D}, \tag{322}$$

where Λ, which has dimensions of momentum, is called the *renormalization scale*. The factor of Λ^{3-D} ensures that dimensional analysis appropriate to 3 dimensions is respected. The logarithmic ultraviolet divergences then appear as poles in $D-3$. The results for these integrals with dimensional regularization reduce in the limit $D \to 3$ to

$$\mathscr{J}_{\log}(\kappa) = -\frac{1}{96\pi^3} \left(\frac{1}{D-3} - 0.82735 \right) \left(\frac{\kappa}{\Lambda} \right)^{2(D-3)}, \tag{323a}$$

$$\mathscr{J}'_{\log}(\kappa) = -\frac{\sqrt{3}}{64\pi^3} \left(\frac{1}{D-3} - 0.39157 \right) \left(\frac{\kappa}{\Lambda} \right)^{2(D-3)}. \tag{323b}$$

In the minimal subtraction renormalization prescription, the poles in ϵ are subtracted from the Laurent expansion of the integral in $D-3$. In the integrals in Eqs. (323a) and (323a), this is equivalent to replacing $1/(D-3)$ by $2\ln(\kappa/\Lambda)$ and then setting $D=3$.

8.6. The diatom field trick

A significant breakthrough in applying effective field theory to the 3-body problem with a large scattering length was made by Bedaque, Hammer, and van Kolck [61,62]. They introduced a new effective field theory that has been used to calculate many new universal results for 3-body observables. This effective field theory makes manifest the connection between the 3-body problem with a large scattering length and renormalization group limit cycles.

Using the effective field theory of Bedaque, Hammer, and van Kolck, it is very easy to derive the Skorniakov–Ter-Martirosian (STM) equation, a simple integral equation for the 3-body problem in the scaling limit. It is not surprising that many of the universal aspects of the 3-body problem can be captured in an integral equation simpler than that in Fig. 44. First, the most interesting and subtle aspects of this problem appear in the sector with total angular momentum quantum number $L=0$. Second, the integral equation in Fig. 44 does not exploit the fact that the 2-body problem for this quantum field theory can be solved analytically. Bedaque, Hammer, and van Kolck found a way to exploit both of these features.

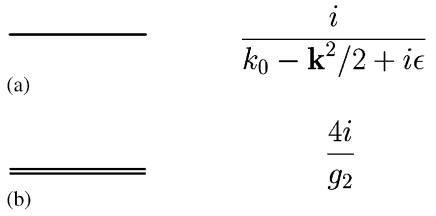

Fig. 45. Feynman rules for the Lagrangian in Eq. (324): (a) the propagator for an atom with energy k_0 and momentum $\boldsymbol{k}$, (b) the bare propagator for a diatom. Energy and momentum are always flowing to the right.

The STM integral equation is not an equation for the 6-point Green's function $\langle 0|\mathrm{T}(\psi\psi\psi\psi^\dagger\psi^\dagger\psi^\dagger)|0\rangle$ discussed in the previous section. Instead it is an equation for the 4-point Green's function $\langle 0|\mathrm{T}(d\psi d^\dagger\psi^\dagger)|0\rangle$, where the *diatom field* d is a local operator that annihilates two atoms at a point. The diatom field is essentially just the composite quantum field operator ψ^2. In order to obtain the simplest possible integral equation, it is useful to construct a new formulation of the quantum field theory that involves the field d explicitly.[14] The Lagrangian for the three-boson system used by Bedaque, Hammer, and van Kolck can be expressed in the form

$$\mathscr{L}_{\mathrm{BHvK}} = \psi^\dagger\left(\mathrm{i}\frac{\partial}{\partial t} + \frac{1}{2}\nabla^2\right)\psi + \frac{g_2}{4}\,d^\dagger d - \frac{g_2}{4}\left(d^\dagger\psi^2 + \psi^{\dagger 2}d\right) - \frac{g_3}{36}\,d^\dagger d\psi^\dagger\psi. \tag{324}$$

One important feature of this Lagrangian is that there is no direct 2-body contact interaction term $(\psi^\dagger\psi)^2$. Another important feature is that there are also no time derivatives acting on the diatom field d, so d is not a dynamical field independent from ψ. Furthermore, the Lagrangian has only linear and quadratic terms in d. The physics of this quantum field theory is therefore identical to that of the quantum field theory whose Lagrangian is obtained by eliminating d from the Lagrangian in Eq. (324) by using its equation of motion. The equation obtained by varying $d^\dagger$ is

$$d - \psi^2 - (g_3/9g_2)d\psi^\dagger\psi = 0, \tag{325}$$

leading to the solution

$$d = \frac{\psi^2}{1 - (g_3/9g_2)\psi^\dagger\psi}. \tag{326}$$

The Lagrangian obtained by eliminating d from Eq. (324) is

$$\mathscr{L} = \psi^\dagger\left(\mathrm{i}\frac{\partial}{\partial t} + \frac{1}{2}\nabla^2\right)\psi - \frac{g_2}{4}\,\frac{(\psi^\dagger\psi)^2}{1 - (g_3/9g_2)\psi^\dagger\psi}. \tag{327}$$

If we expand the interaction term in powers of $\psi^\dagger\psi$, and truncate after the $(\psi^\dagger\psi)^3$ term, we recover the Lagrangian in Eq. (312). Thus in the 2-body and 3-body sectors, the quantum field theory with the Lagrangian in Eq. (324) is completely equivalent to the quantum field theory with the Lagrangian in Eq. (312). The Lagrangian in Eq. (324) also has N-body contact interaction terms $(\psi^\dagger\psi)^N$ for $N \geqslant 4$, but they affect only the N-body sectors with $N \geqslant 4$.

The Feynman rules for the Lagrangian in Eq. (324) are shown in Figs. 45 and 46. The bare propagator for the diatom field is simply the constant $4i/g_2$, which corresponds to no propagation in space or time. However, there are corrections to the diatom propagator from the diagrams in Fig. 47(a) which allow the diatom to propagate. In Feynman diagrams, we represent the complete diatom propagator $\mathrm{i}D(P_0, P)$ by a thick solid line. We can calculate the complete diatom propagator by solving the simple integral equation shown in Fig. 47(b). The loop on the right side is just the integral in Eq. (297), with E replaced by $P_0 - P^2/4$, where P_0 and $\boldsymbol{P}$ are the energy and momentum of the diatom. The solution for the complete diatom propagator is

$$D(P_0, P) = \frac{4}{g_2}\left[1 + \frac{g_2}{4\pi^2}\left(\Lambda - \frac{\pi}{2}\sqrt{-P_0 + P^2/4 - \mathrm{i}\epsilon}\right)\right]^{-1}, \tag{328}$$

[14] This trick has been used in many other contexts. A pedagogical treatment in the context of the O(N) version of ϕ^4 theory can be found in the Erice lectures by Coleman [152]. For early applications in nuclear few-body systems, see e.g. Refs. [153,154].

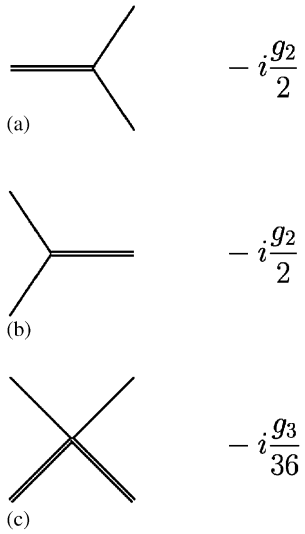

Fig. 46. Feynman rules for the Lagrangian in Eq. (324): interaction vertices.

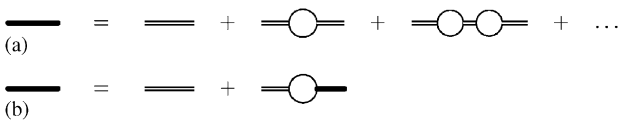

Fig. 47. Diagrammatic equations for the complete diatom propagator $\mathrm{i}D(P_0, P)$: (a) perturbative expansion in powers of g_2, (b) integral equation.

where Λ is a cutoff on the loop momentum in the bubbles. After making the substitution given in Eq. (306), the expression for the complete diatom propagator is

$$D(P_0, P) = \frac{32\pi}{g_2^2}\left[1/a - \sqrt{-P_0 + P^2/4 - \mathrm{i}\epsilon}\right]^{-1}. \tag{329}$$

Note that all the dependence on the ultraviolet cutoff is now in the multiplicative factor $1/g_2^2$. The complete diatom propagator differs from the off-shell 2-body amplitude $\mathscr{A}$ in Eq. (307) only by a multiplicative constant. For $a > 0$, it has a pole at $P_0 = -1/a^2 + P^2/4$ corresponding to a dimer of momentum $\boldsymbol{P}$ and binding energy $E_{\mathrm{D}} = 1/a^2$. As P_0 approaches the dimer pole, the limiting behavior of the propagator is

$$D(P_0, P) \longrightarrow \frac{Z_{\mathrm{D}}}{P_0 - (-1/a^2 + P^2/4) + \mathrm{i}\epsilon}, \tag{330}$$

where the residue factor is

$$Z_{\mathrm{D}} = 64\pi/(ag_2^2). \tag{331}$$

If we regard the composite operator d as a quantum field that annihilates and creates dimers, then Z_{D} is the wave function renormalization constant for that field. The renormalized propagator $Z_{\mathrm{D}}^{-1} D(P_0, P)$ is completely independent of the ultraviolet cutoff.

8.7. STM integral equation

The first derivation of the Skorniakov–Ter-Martirosian (STM) equation using Feynman diagrams was carried out in Ref. [155]. The derivation is particularly simple in the effective field theory introduced by Bedaque, Hammer, and

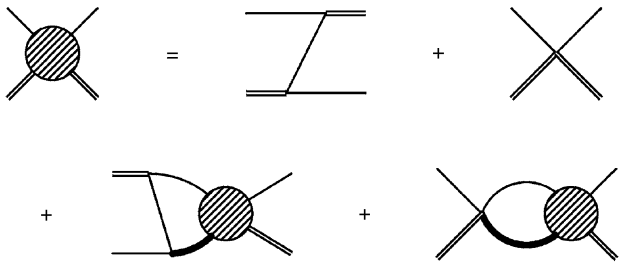

Fig. 48. The integral equation for the 3-body amplitude $\mathscr{A}$.

van Kolck. The STM equation is an integral equation for the Fourier transform of the amputated connected part of the Green's function $\langle 0|\mathrm{T}(d\psi d^\dagger \psi^\dagger)|0\rangle$, which we will denote by $\mathscr{A}$.[15] The integral equation is shown diagrammatically in Fig. 48. It simply states that the Feynman diagrams that contribute to $\mathscr{A}$ are either tree diagrams or they involve at least one loop. For those diagrams that involve a loop, the first interaction must be one of the vertices in Fig. 46. The two tree diagrams on the right side of Fig. 48 constitute the inhomogeneous term in the integral equation. The two loop diagrams involve 1-loop integrals over the same amplitude $\mathscr{A}$. Note that the thick black lines in Fig. 48 represent the complete diatom propagator given in Eq. (329).

In the center-of-mass frame, we can take the external momenta of the atom and diatom to be $-\boldsymbol{p}$ and $+\boldsymbol{p}$ for the incoming lines and $-\boldsymbol{k}$ and $+\boldsymbol{k}$ for the outgoing lines. We take their energies to be $E_{\rm A}$ and $E - E_{\rm A}$ for the incoming lines and $E'_{\rm A}$ and $E - E'_{\rm A}$ for the outgoing lines. The amplitude $\mathscr{A}$ is then a function of the momenta $\boldsymbol{p}$ and $\boldsymbol{k}$ and the energies E, $E_{\rm A}$ and $E'_{\rm A}$. The integral equation involves a loop over the momentum $-\boldsymbol{q}$ and energy q_0 of a virtual atom. Using the Feynman rules from Figs. 45 and 46, we obtain

$$\begin{aligned}\mathscr{A}(\boldsymbol{p},\boldsymbol{k};\,E,\,E_{\rm A},\,E'_{\rm A}) = &-\left[\frac{g_2^2/4}{E-E_{\rm A}-E'_{\rm A}-(\boldsymbol{p}+\boldsymbol{k})^2/2+\mathrm{i}\epsilon}+\frac{g_3}{36}\right]\\ &+\frac{32\pi\mathrm{i}}{g_2^2}\int\frac{\mathrm{d}q_0}{2\pi}\int\frac{\mathrm{d}^3q}{(2\pi)^3}\left[\frac{g_2^2/4}{E-E_{\rm A}-q_0-(\boldsymbol{p}+\boldsymbol{q})^2/2+\mathrm{i}\epsilon}+\frac{g_3}{36}\right]\\ &\times\frac{1}{q_0-q^2/2+\mathrm{i}\epsilon}\,\frac{\mathscr{A}(\boldsymbol{q},\boldsymbol{k};\,E,\,q_0,\,E'_{\rm A})}{1/a-\sqrt{-(E-q_0)+q^2/4-\mathrm{i}\epsilon}}.\end{aligned}\tag{332}$$

The integral over q_0 can be evaluated by contour integration. This sets $q_0 = q^2/2$, so the amplitude $\mathscr{A}$ inside the integral has the incoming atom on-shell.

We obtain a simpler integral equation if we also set the energies of both the initial and final atoms in $\mathscr{A}$ on-shell: $E_{\rm A} = p^2/2$, $E'_{\rm A} = k^2/2$. Thus only the diatom lines have energies that are off-shell.[16] The resulting integral equation is

$$\begin{aligned}\mathscr{A}(\boldsymbol{p},\boldsymbol{k};\,E,\,p^2/2,k^2/2) = &-\frac{g_2^2}{4}\left[\frac{1}{E-(p^2+\boldsymbol{p}\cdot\boldsymbol{k}+k^2)+\mathrm{i}\epsilon}+\frac{g_3}{9g_2^2}\right]\\ &-8\pi\int\frac{d^3q}{(2\pi)^3}\left[\frac{1}{E-(p^2+\boldsymbol{p}\cdot\boldsymbol{q}+q^2)+\mathrm{i}\epsilon}+\frac{g_3}{9g_2^2}\right]\frac{\mathscr{A}(\boldsymbol{q},\boldsymbol{k};\,E,\,q^2/2,k^2/2)}{-1/a+\sqrt{-E+3q^2/4-\mathrm{i}\epsilon}}.\end{aligned}\tag{333}$$

[15] The atom–diatom amplitude $\mathscr{A}$ should not be confused with the atom–atom amplitude in Section 8.4 or the 3-atom amplitude in Section 8.5, which were denoted by the same symbol.

[16] This trick of putting one leg on-shell has also been used to simplify integral equations for relativistic bound states, such as positronium in QED [156].

This is an integral equation with three integration variables for an amplitude $\mathscr{A}$ that depends explicitly on seven independent variables. There is also an additional implicit variable provided by an ultraviolet cutoff $|\boldsymbol{q}| < \Lambda$ on the loop momentum. If we set $g_3 = 0$ and ignore the ultraviolet cutoff, the integral equation in Eq. (333) is equivalent to the Skorniakov–Ter-Martirosian (STM) equation, an integral equation for three particles interacting via zero-range 2-body forces derived by Skorniakov and Ter-Martirosian in 1957 [5]. In the following, we will refer to the generalization of the STM equation with a nonzero 3-body coupling g_3 simply as the *STM3 equation*.

It was shown by Danilov that the STM equation has no unique solution in the case of identical bosons [6]. He also pointed out that a unique solution could be obtained if one 3-body binding energy is fixed. Kharchenko was the first to solve the STM equation with a finite ultraviolet cutoff that was tuned to fit observed 3-body data. Thus the cutoff was treated as an additional parameter [157]. Below we will show that this ad hoc procedure is indeed justified and emerges naturally when the STM3 equation is renormalized.

If we restrict our attention to the sector of the 3-body problem with total orbital angular momentum $L = 0$, we can further simplify the integral equation. The projection onto $L = 0$ can be accomplished by averaging the integral equation over the cosine of the angle between $\boldsymbol{p}$ and $\boldsymbol{k}$: $x = \boldsymbol{p} \cdot \boldsymbol{k}/(pk)$. It is also convenient to multiply the amplitude $\mathscr{A}$ by the wave function renormalization factor $Z_{\rm D}$ given in Eq. (331). We will denote the resulting amplitude by $\mathscr{A}_S$:

$$\mathscr{A}_S(p, k; E) \equiv Z_{\rm D} \int_{-1}^{1} \frac{{\rm d}x}{2}\, \mathscr{A}(\boldsymbol{p}, \boldsymbol{k}; E, p^2/2, k^2/2). \tag{334}$$

Furthermore, it is convenient to express the 3-body coupling constant in the form

$$g_3 = -\frac{9g_2^2}{\Lambda^2}\, H(\Lambda). \tag{335}$$

Since H is dimensionless, it can only be a function of the dimensionless variables $a\Lambda$ and Λ/κ_*, where κ_* is the 3-body parameter defined by the spectrum of Efimov states in the resonant limit, Eq. (164). We will find that H is a function of Λ/κ_* only.

The resulting equation is the STM3 integral equation in its simplest form:

$$\begin{aligned}\mathscr{A}_S(p, k; E) = {} & \frac{16\pi}{a}\left[\frac{1}{2pk}\ln\frac{p^2 + pk + k^2 - E - {\rm i}\epsilon}{p^2 - pk + k^2 - E - {\rm i}\epsilon} + \frac{H(\Lambda)}{\Lambda^2}\right] \\ & + \frac{4}{\pi}\int_0^{\Lambda} {\rm d}q\, q^2 \left[\frac{1}{2pq}\ln\frac{p^2 + pq + q^2 - E - {\rm i}\epsilon}{p^2 - pq + q^2 - E - {\rm i}\epsilon} + \frac{H(\Lambda)}{\Lambda^2}\right] \frac{\mathscr{A}_S(q, k; E)}{-1/a + \sqrt{3q^2/4 - E - {\rm i}\epsilon}}.\end{aligned} \tag{336}$$

Note that the ultraviolet cutoff Λ on the integral over q has been made explicit. A change in the endpoint Λ of the loop integral should be compensated by the Λ-dependence of the function H in Eq. (336). More specifically, H must be tuned as a function of Λ so that the cutoff dependence of the solution $\mathscr{A}_S(p, k; E)$ of Eq. (336) decreases as a power of Λ. This will guarantee that $\mathscr{A}_S(p, k; E)$ has a well-behaved limit as $\Lambda \to \infty$. Note that the H/Λ^2 term in the inhomogeneous term of Eq. (336) can be omitted, since it goes to zero in the limit $\Lambda \to \infty$.

We will see in Section 8.9 that the function H in Eq. (336) must have the form

$$H(\Lambda) = \frac{\cos[s_0 \ln(\Lambda/\Lambda_*) + \arctan s_0]}{\cos[s_0 \ln(\Lambda/\Lambda_*) - \arctan s_0]}. \tag{337}$$

This equation defines a 3-body scaling-violation parameter Λ_* with dimensions of momentum. Note that H is a periodic function of Λ/Λ_*, so Λ_* is defined only up to a multiplicative factor of $(e^{\pi/s_0})^n$, where n is an integer. The relation between Λ_* and the 3-body parameter κ_* defined by the spectrum of Efimov states in the resonant limit, which is given in Eq. (164), can be expressed as

$$s_0 \ln(\kappa_*) \approx s_0 \ln(0.381\, \Lambda_*) \mod \pi. \tag{338}$$

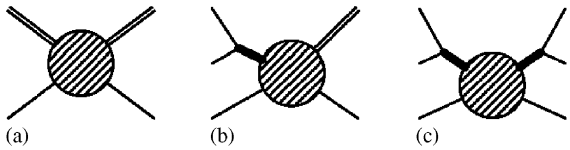

Fig. 49. Amplitudes for (a) atom–dimer scattering, (b) 3-body recombination, and (c) $3 \to 3$ scattering. Diagrams (b) and (c) should be summed over the three pairs of atoms that can interact first. Diagram (c) should also be summed over the three pairs of atoms that can interact last.

This relation can be obtained by using the STM3 integral equation in Eq. (336) to calculate the binding energy of the Efimov trimers in the resonant limit $a = \pm\infty$.

8.8. Three-body observables

The solution $\mathscr{A}_S(p, k; E)$ to the STM3 integral equation in Eq. (336) encodes all information about 3-body observables in the sector with total orbital angular momentum quantum number $L = 0$. In particular, it contains information about the binding energies $E_{\rm T}^{(n)}$ of the Efimov states. For a given ultraviolet cutoff Λ, the amplitude $\mathscr{A}_S(p, k; E)$ has a finite number of poles in E corresponding to the Efimov trimers whose binding energies are less than about Λ^2. As Λ increases, new poles emerge corresponding to deeper Efimov trimers. In the limit $\Lambda \to \infty$, the locations of these poles approach the energies $-E_{\rm T}^{(n)}$ of the Efimov trimers. The residues of the poles of $\mathscr{A}_S(p, k; E)$ factor into functions of p and functions of k:

$$\mathscr{A}_S(p, k; E) \longrightarrow \frac{\mathscr{B}^{(n)}(p)\mathscr{B}^{(n)}(k)}{E + E_{\rm T}^{(n)}} \quad \text{as } E \to -E_{\rm T}^{(n)}. \tag{339}$$

Matching the residues of the poles on both sides of Eq. (336), we obtain the bound-state equation

$$\mathscr{B}^{(n)}(p) = \frac{4}{\pi}\int_0^\Lambda \mathrm{d}q\, q^2 \left[\frac{1}{2pq}\ln\frac{p^2+pq+q^2-E-\mathrm{i}\epsilon}{p^2-pq+q^2-E-\mathrm{i}\epsilon} + \frac{H(\Lambda)}{\Lambda^2}\right]\left[-1/a + \sqrt{3q^2/4 - E - \mathrm{i}\epsilon}\right]^{-1}\mathscr{B}^{(n)}(q). \tag{340}$$

The values of E for which this homogeneous integral equation has solutions are the energies $-E_{\rm T}^{(n)}$ of the Efimov states. For a finite ultraviolet cutoff Λ, the spectrum of $E_{\rm T}^{(n)}$ is cut off around Λ^2, so the number of Efimov states is roughly $\ln(|a|\Lambda)/\pi$. To find deeper Efimov states, one simply needs to increase the cutoff. Most of the results on the binding energies of Efimov states in Section 6.3 were obtained by solving the homogeneous integral equation in Eq. (340).

The S-wave phase shifts for atom–dimer scattering can be determined from the solution $\mathscr{A}_S(p, k; E)$ to the STM3 integral equation in Eq. (336). The T-matrix element for the elastic scattering of an atom and a dimer with momenta k is given by the amplitude $\mathscr{A}$ evaluated at the on-shell point $p = k$ and $E = -E_{\rm D} + 3k^2/4$ and multiplied by a wave function renormalization factor $Z_{\rm D}^{1/2}$ for each dimer in the initial or final state. It can be represented by the Feynman diagram in Fig. 49(a). The blob represents the amplitude $\mathscr{A}$ or equivalently $Z_{\rm D}^{-1}\mathscr{A}_S$. The external double lines correspond to asymptotic dimers and are associated with factors $Z_{\rm D}^{1/2}$. The S-wave contribution to the T-matrix element is

$$\mathscr{T}^{(L=0)}_{\rm AD\to AD} = \mathscr{A}_S(k, k; 3k^2/4 - 1/a^2). \tag{341}$$

Note that the factors of $Z_{\rm D}$ multiplying $\mathscr{A}_S$ cancel. The differential cross section for elastic atom–dimer scattering is

$$d\sigma_{\rm AD\to AD} = \frac{2}{3k}\,|\mathscr{T}_{\rm AD\to AD}(k)|^2\,\frac{k}{6\pi^2}\,\mathrm{d}\Omega. \tag{342}$$

The flux factor $2/(3k)$ is the inverse of the relative velocity of the atom and the dimer. The phase space factor $k\,\mathrm{d}\Omega/(6\pi^2)$ takes into account energy and momentum conservation and the standard normalization of momentum eigenstates:

$$\int \frac{\mathrm{d}^3p_{\rm A}}{(2\pi)^3}\frac{\mathrm{d}^3p_{\rm D}}{(2\pi)^3}(2\pi)^4\delta^3(\boldsymbol{p}_{\rm A}+\boldsymbol{p}_{\rm D})\delta\left(\frac{1}{2}p_{\rm A}^2 + \frac{1}{4}p_{\rm D}^2 - E\right) = \frac{1}{6\pi^2}(4E/3)^{1/2}\int \mathrm{d}\Omega. \tag{343}$$

Comparing the expressions for the differential cross section in Eqs. (342) and (207),), we see that the T-matrix element differs from the scattering amplitude $f_k(\theta)$ by a factor of 3π. Using the expression for the S-wave term in the scattering amplitude from Eq. (208), the S-wave phase shift is given by

$$\frac{1}{k\cot\delta_0^{\rm AD}(k)-{\rm i}k}=\frac{1}{3\pi}\,\mathscr{A}_S(k,k;3k^2/4-1/a^2). \tag{344}$$

In particular, the atom–dimer scattering length is given by

$$a_{\rm AD}=-\frac{1}{3\pi}\,\mathscr{A}_S(0,0;-1/a^2). \tag{345}$$

The results on atom–dimer elastic scattering in Section 6.4 were obtained from the expression in Eq. (344).

The threshold 3-body recombination rate can also be obtained from the solution $\mathscr{A}_S(p,k;E)$ to the STM3 integral equation in Eq. (336). This is possible only at threshold, because a 3-atom scattering state becomes pure $L=0$ only in the limit that the energies of the atoms go to zero. The T-matrix element for the recombination process can be represented by the Feynman diagram in Fig. 49(b) summed over the three pairs of atom lines that can attach to the diatom line. The blob represents the amplitude $Z_{\rm D}^{-1}\mathscr{A}_S$ evaluated at the on-shell point $p=0$, $k=2/(\sqrt{3}\,a)$, and $E=0$. The solid line represents the diatom propagator ${\rm i}D(0,0)$ evaluated at zero energy and momentum, which is given by Eq. (328). The factor for the atom–diatom vertex is $-{\rm i}g_2/2$. The wave function renormalization factor $Z_{\rm D}^{1/2}$ for the final-state dimer is given by Eq. (331). In the product of factors multiplying $\mathscr{A}_S$, the dependence on g_2 and Λ can be eliminated in favor of the scattering length a given in Eq. (305). Taking into account a factor of 3 from the three Feynman diagrams, the T-matrix element is

$$\mathscr{T}_{\rm AAA\to AD}=6\sqrt{\pi a^3}\,\mathscr{A}_S(0,2/(\sqrt{3}a);0). \tag{346}$$

The differential rate ${\rm d}R$ for the recombination of three atoms with energies small compared to the dimer binding energy can be expressed as

$${\rm d}R=|\mathscr{T}_{\rm AAA\to AD}|^2\,\frac{k}{6\pi^2}\,{\rm d}\Omega, \tag{347}$$

where $k=2/(\sqrt{3}a)$. The time rate of change of the number density $n_{\rm A}$ of low-energy atoms is obtained by integrating Eq. (347) over the 4π solid angle and multiplying by the number density per volume-cubed of triples in the gas, which is $n_{\rm A}^3/3!$. Thus the recombination rate constant α on the right side of Eq. (227a) is

$$\alpha=\frac{8a^2}{\sqrt{3}}\,|\mathscr{A}_S(0,2/(\sqrt{3}a);0)|^2. \tag{348}$$

This expression was used to calculate the approximate expression for the 3-body recombination constant given in Eq. (231). The expression for α in Eq. (348) gives the recombination rate for three atoms with distinct momenta in the limit in which they all approach zero. If the atoms are all in exactly the same state, which is the case if they are in a Bose–Einstein condensate, the rate must be divided by 3! to account for the symmetrization of the wave function of the identical particles.

The T-matrix element for 3-atom elastic scattering can be represented by a sum of Feynman diagrams like the one shown in Fig. 49(c). The T-matrix element has not yet been calculated. However, in Ref. [105], the 4-point Green's function $\langle 0|{\rm T}(\psi d\psi^\dagger d^\dagger)|0\rangle$, which is related to the $3\to 3$ scattering amplitude, was calculated at the three-atom threshold. That calculation was used to extract the results for the nonperturbative constants given in Eqs. (240) and (241).

8.9. Renormalization group limit cycle

The form of the exact renormalized diatom propagator in Eq. (329) is consistent with the continuous scaling symmetry given in Eqs. (66). In the integral (336), this scaling symmetry is broken by the ultraviolet cutoff on the integral and by the 3-body terms proportional to H/Λ^2. To see that the cutoff and the 3-body terms are essential, we can try setting $H=0$ and taking $\Lambda\to\infty$. The resulting integral equation has exact scaling symmetry. We should therefore expect

its solution $\mathscr{A}_S(p,k;E)$ to behave asymptotically as $p\to\infty$ like a pure power of p. Neglecting the inhomogeneous term, neglecting E and $1/a^2$ compared to q^2, and setting $\mathscr{A}_S\approx p^{s-1}$, the integral equation reduces to [6,45,46,158]

$$p^{s-1}=\frac{4}{\sqrt{3}\pi p}\int_0^\infty \mathrm{d}q\, q^{s-1}\ln\frac{p^2+pq+q^2}{p^2-pq+q^2}. \tag{349}$$

Making the change of variables $q=xp$, the dependence on p drops out, and we obtain

$$1=\frac{4}{\sqrt{3}\pi}\int_0^\infty \mathrm{d}x\, x^{s-1}\ln\frac{1+x+x^2}{1-x+x^2}. \tag{350}$$

The integral is a Mellin transform that can be evaluated analytically. The resulting equation for s is

$$1=\frac{8}{\sqrt{3}s}\frac{\sin(\pi s/6)}{\cos(\pi s/2)}. \tag{351}$$

This is identical to the angular eigenvalue (129) in the limit $R\gg|a|$ in the adiabatic hyperspherical representation of the 3-body Schrödinger equation. The solutions with the lowest values of $|s|$ are purely imaginary: $s=\pm\mathrm{i}s_0$, where $s_0\approx 1.00624$. The most general asymptotic solution therefore has two arbitrary constants:

$$\mathscr{A}_S(p,k;E)\longrightarrow A_+\,p^{-1+\mathrm{i}s_0}+A_-\,p^{-1-\mathrm{i}s_0}\quad\text{as } p\to\infty. \tag{352}$$

The inhomogeneous term in the integral (336) will determine one of the constants. The role of the 3-body term in the integral equation is to determine the other constant, thus giving the integral equation a unique solution.

By demanding that the solution of the integral (336) has a well-defined limit as $\Lambda\to\infty$, Bedaque, Hammer, and van Kolck deduced the Λ-dependence of H and therefore of g_3 [61,62]. The leading dependence on Λ on the right side of the STM3 integral equation in Eq. (336) as $\Lambda\to\infty$ is a log-periodic term of order Λ^0 that comes from the region $q\sim\Lambda$. There are also contributions of order $1/\Lambda$ from the region $|a|^{-1}, k, |E|^{1/2}\ll q\ll\Lambda$, which have the form

$$\frac{8}{\pi\sqrt{3}}\int^\Lambda \mathrm{d}q\,\left(\frac{1}{q^2}+\frac{H}{\Lambda^2}\right)(A_+\,q^{+\mathrm{i}s_0}+A_-q^{-\mathrm{i}s_0}). \tag{353}$$

The sum of the two terms will decrease even faster as $1/\Lambda^2$ if we choose the function H to have the form

$$H(\Lambda)=\frac{A_+\Lambda^{\mathrm{i}s_0}/(1-\mathrm{i}s_0)+A_-\Lambda^{-\mathrm{i}s_0}/(1+\mathrm{i}s_0)}{A_+\Lambda^{\mathrm{i}s_0}/(1+\mathrm{i}s_0)+A_-\Lambda^{-\mathrm{i}s_0}/(1-\mathrm{i}s_0)}. \tag{354}$$

The tuning of H that makes the term in Eq. (353) decrease like $1/\Lambda^2$ also suppresses the contribution from the region $q\sim\Lambda$ by a power of $1/\Lambda$ so that it goes to 0 in the limit $\Lambda\to\infty$ [61,62]. By choosing $A_\pm=(1+s_0^2)^{1/2}\Lambda_*^{\mp\mathrm{i}s_0}/2$ in Eq. (354), we obtain the expression for H in Eq. (337).

The dimensionless 2-body coupling constant $\hat{g}_2$ is introduced in Eq. (309). It is convenient to also introduce a dimensionless 3-body coupling constant $\hat{g}_3$ by

$$\hat{g}_3(\Lambda)=\frac{\Lambda^4 g_3}{144\pi^4}. \tag{355}$$

Using Eqs. (335) and (306), the dimensionless 3-body coupling constant can be written as

$$\hat{g}_3(\Lambda)=-\left(\frac{a\Lambda}{a\Lambda-\pi/2}\right)^2 H(\Lambda). \tag{356}$$

As Λ is varied with a and Λ_* fixed, the expression for $\hat{g}_3$ in Eq. (355) maps out RG trajectory. The RG trajectories for a fixed value of Λ_* and various values of a are illustrated in Fig. 41. All the points on a given trajectory represent the same physical theory with given values of a and Λ_*. As Λ increases, the dimensionless coupling constant in Eq. (356) flows towards an ultraviolet limit cycle:

$$\hat{g}_3(\Lambda)\longrightarrow-\frac{\cos[s_0\ln(\Lambda/\Lambda_*)+\arctan s_0]}{\cos[s_0\ln(\Lambda/\Lambda_*)-\arctan s_0]}\quad\text{as } \Lambda\to\infty. \tag{357}$$

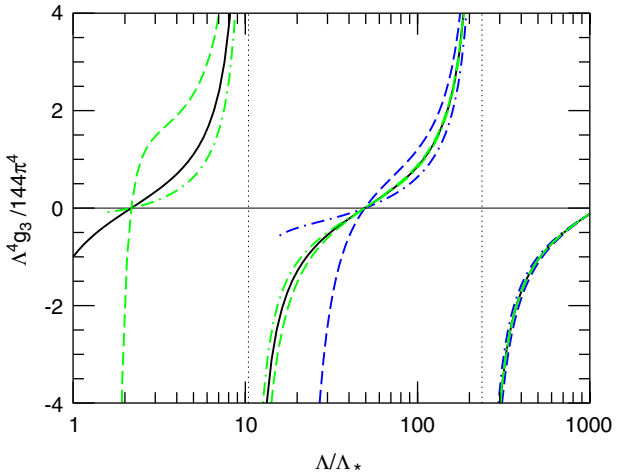

Fig. 50. The dimensionless 3-body coupling constant $\hat{g}_3 = \Lambda^4 g_3/144\pi^4$ as a function of the ultraviolet cutoff Λ for a fixed value of Λ_* and several values of the scattering length a. As $\Lambda \to \infty$, $\hat{g}_3$ asymptotically approaches the RG limit cycle shown as a heavy solid line.

This limit cycle corresponds to the theory in the resonant limit $a = \pm\infty$. In Fig. 50, the dimensionless 3-body coupling constant $\hat{g}_3$ is shown as a function of Λ for several different values of the scattering lengths. The RG trajectories for finite a are rapidly focused to the limit cycle.

Further insight into this problem can be achieved by expressing the renormalization group flow in terms of a differential equation for the Λ-dependence of $\hat{g}_3$. By differentiating both sides of Eq. (356), one can derive the differential RG equation

$$\Lambda \frac{\mathrm{d}}{\mathrm{d}\Lambda} \hat{g}_3 = \frac{1+s_0^2}{2} \left(\hat{g}_2^2 + \frac{\hat{g}_3^2}{\hat{g}_2^2} \right) + (3 - s_0^2 + 2\hat{g}_2)\hat{g}_3. \tag{358}$$

At the fixed point $\hat{g}_2 = -1$, the right side of Eq. (358) has no real roots for $\hat{g}_3$, so there is no ultraviolet fixed point. Instead the ultraviolet behavior is governed by the fixed point $\hat{g}_2 = -1$ and the limit cycle in Eq. (357) for $\hat{g}_3$.

One might expect to be able to derive the perturbative differential RG equation for g_3 in Eq. (313) from the nonperturbative differential RG equation in Eq. (358). However, the connection between these equations is obscured by a fundamental difference in renormalization schemes. The perturbative RG equation in Eq. (313) is derived within a renormalization scheme in which power ultraviolet divergences are subtracted from Green's functions, so that renormalization of the coupling constants is only required to remove residual logarithmic divergences. For example, in this renormalization scheme, all the loop corrections in the expression for g_2 in Eq. (306) are subtracted away and the expression reduces to $g_2 = 8\pi a$. In the nonperturbative renormalization scheme corresponding to the differential RG equations for $\hat{g}_2$ in Eq. (311) and $\hat{g}_3$ in Eq. (358), power ultraviolet divergences are removed by renormalization of the coupling constants. The renormalization of $\hat{g}_3$ also removes from 3-body amplitudes cutoff-dependent effects that remain bounded as $\Lambda \to \infty$, but have log-periodic dependence on Λ.

One remarkable feature of the renormalization of g_3 is that there are values of the ultraviolet cutoff for which the dimensionless coupling constant $\Lambda^4 g_3$ diverges. The divergences occur as Λ approaches the values

$$\Lambda_n' = (e^{\pi/s_0})^n \exp([\tfrac{1}{2}\pi + \arctan s_0]/s_0)\Lambda_*, \tag{359}$$

where n is an integer. At these points, $\Lambda^4 g_3$ increases to ∞, jumps discontinuously to $-\infty$, and then continues to increase. There is a simple intuitive explanation for this remarkable behavior. The ultraviolet cutoff Λ excludes Efimov states with binding energies greater than about Λ^2. As Λ increases, the strength of the 3-body contact interaction must increase in order to keep low-energy observables invariant. This 3-body contact interaction takes into account the effects of short-distance 3-body configurations that are excluded by the cutoff, including the excluded Efimov states.

When Λ reaches a critical value, $\Lambda^4 g_3$ becomes infinite. At this critical value, a new Efimov state with binding energy of order Λ^2 appears in the spectrum and $\Lambda^4 g_3$ jumps discontinuously to $-\infty$, because the 3-body contact interaction no longer needs to take into account the virtual effects of that Efimov state.

Another interesting feature of the renormalization of g_3 is that there are values of the ultraviolet cutoff for which g_3 vanishes. The zeros occur as Λ approaches the values

$$\Lambda_n = (e^{\pi/s_0})^n \exp([\tfrac{1}{2}\pi - \arctan s_0]/s_0)\Lambda_*. \tag{360}$$

At these discrete values of Λ, there is no need for a 3-body contact interaction. One can therefore simplify the generalized STM integral equation in Eq. (336) by setting $H = 0$ and $\Lambda = \Lambda_n$ [92]. One can take the limit $\Lambda \to \infty$ by increasing the integer n. However, one must choose n large enough that corrections suppressed by $1/(a\Lambda_n)$ and k/Λ_n are negligible. In practice, $n = 1$ or 2 is often large enough to get a few digits of accuracy. This simple trick turns out to be very useful for practical calculations. It justifies Kharchenko's ad hoc procedure of fitting the cutoff in the STM equation to a 3-body datum and then using the same cutoff to predict other data [157].

8.10. Effects of deep 2-body bound states

Effective field theory can also be used to take into account the effects of deep 2-body bound states. The coefficient g_3 of the 3-body contact interaction in Eq. (324) must be generalized to a complex-valued coupling constant. The real and imaginary parts of g_3 can then be tuned simultaneously as functions of the ultraviolet cutoff to reproduce the correct values for the two 3-body parameters κ_* and η_* that together with a determine the low-energy 3-body observables.

In the absence of deep 2-body bound states, a sufficient condition for solutions to the STM3 integral equation in Eq. (336) to have a well-behaved limit as $\Lambda \to \infty$ is that the 3-body coupling constant g_3 must have the form given by Eqs. (335) and (337). Since the function $H(\Lambda)$ in Eq. (337) is an analytic function of $\ln \Lambda_*$, the integral equation defines the amplitude $\mathscr{A}_s(q, k; E)$ as an analytic function of $\ln \Lambda_*$. The STM3 integral equation continues to have a well-behaved limit as $\Lambda \to \infty$ if Λ_* in the expression for $H(\Lambda)$ in Eq. (337) is replaced by the complex variable $\Lambda_* e^{i\eta_*/s_0}$:

$$H(\Lambda) = \frac{\cos[s_0 \ln(\Lambda/\Lambda_*) + \arctan s_0 - i\eta_*]}{\cos[s_0 \ln(\Lambda/\Lambda_*) - \arctan s_0 - i\eta_*]}. \tag{361}$$

If the dependence of the amplitude $\mathscr{A}_s(q, k; E)$ on Λ_* is known analytically, the effect of the parameter η_* can be obtained simply by the substitution $\ln \Lambda_* \to \ln \Lambda_* + i\eta_*/s_0$. The bound-state equation in Eq. (340) also defines the energy eigenvalues for the Efimov states as analytic functions of $\ln \Lambda_*$. If analytic expressions for the binding energies as functions of Λ_* were known, the effects of the parameter η_* could again be determined by simple substitution. One limit in which the analytic expression is known is the resonant limit $a = \pm\infty$. In this case, the Efimov binding energies in the absence of deep 2-body bound states satisfy Eq. (164). Since κ_* differs from Λ_* only by a multiplicative constant, the effect of the parameter η_* can be determined by the substitution $\kappa_* \to \kappa_* e^{i\eta_*/s_0}$. If there are deep 2-body bound states, the resonance energies $E_{\rm T}^{(n)}$ of the trimers and their widths $\Gamma_{\rm T}^{(n)}$ in the resonance limit must satisfy

$$E_{\rm T}^{(n)} + \frac{i}{2}\Gamma_{\rm T}^{(n)} \longrightarrow (e^{-2\pi/s_0})^{n-n_*} e^{2i\eta_*/s_0} \frac{\hbar^2\kappa_*^2}{m} \quad \text{as } n \to \infty \text{ with } a = \pm\infty. \tag{362}$$

The ratios of the widths and the resonance energies approach a constant as the 3-atom threshold is approached:

$$\Gamma_{\rm T}^{(n)}/E_{\rm T}^{(n)} \longrightarrow 2\tan(2\eta_*/s_0) \quad \text{as } n \to \infty \text{ with } a = \pm\infty. \tag{363}$$

This equation, which involves only physical observables, provides an operational definition of the parameter η_*. It can be used to determine η_* for any system that can be tuned to the resonant limit $a = \pm\infty$.

The effects of deep 2-body bound states are particularly simple if the inelasticity parameter η_* is infinitesimally small. For example, the rate constants for 3-body recombination into deep molecules are given with an accuracy of better than 1% by Eqs. (269) and (271). Their expansions to first order in η_* are

$$\alpha_{\rm deep} \approx 67.1\eta_* \frac{\hbar a^4}{m} \quad (a > 0), \tag{364a}$$

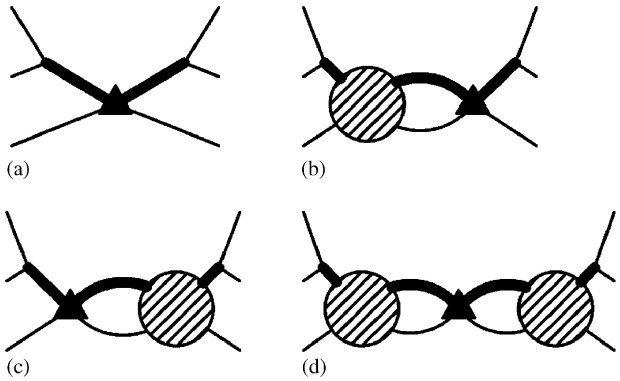

Fig. 51. Feynman diagrams with a single insertion of the $d^\dagger d\psi^\dagger\psi$ vertex proportional to h_3 represented by the triangle. Diagram (d) dominates in the limit $\Lambda \to \infty$.

$$\alpha_{\rm deep} \approx \frac{9180\,\eta_*}{\sin^2[s_0 \ln(a/a'_*)]}\,\frac{\hbar a^4}{m} \quad (a<0). \tag{364b}$$

Note that the expression for $\alpha_{\rm deep}$ in Eq. (364b) diverges at values of a that differ from a'_* by multiples of e^{π/s_0}. These divergences are cut off in Eq. (271) by summing corrections of higher order in η_* to all orders.

Calculations of the effects of deep 2-body bound states have been carried out using effective field theory for the case in which the inelasticity parameter η_* is infinitesimally small. In this case, the imaginary part of the coupling constant g_3 is also infinitesimally small and can be treated as a perturbation. At leading order in Im g_3, the tuning of Re g_3 is unaffected and is given by Eq. (335). An integral equation for the first-order change in the amplitude $\mathscr{A}$ can be obtained by substituting $\mathscr{A} \to \mathscr{A} + \delta\mathscr{A}$ and $g_3 \to g_3 + {\rm i}\,{\rm Im}\,g_3$ into the integral equation in Eq. (333) and expanding to first order in $\delta\mathscr{A}$ and Im g_3. However, it is simpler to express the first-order change $\delta\mathscr{A}$ as the sum of all amputated connected Feynman diagrams with a single insertion of a $d^\dagger d\psi^\dagger\psi$ vertex with the Feynman rule Im $g_3/36$. The resulting set of diagrams is shown in Fig. 51, where the triangle represents the $d^\dagger d\psi^\dagger\psi$ vertex and the blob represents the amplitude $\mathscr{A}$. One can easily show that the S-wave amplitude can be expressed in the factored form

$$\delta\mathscr{A}_S(p,k;E) = -{\rm i}\,{\rm Im}\,g_3\,\frac{64\pi^2 a^2}{g_2^2}(1+\mathscr{C}_S(p;E))(1+\mathscr{C}_S(k;E)), \tag{365}$$

where $\mathscr{C}_S(p;E)$ is given by an integral of $\mathscr{A}_S$ over one of its arguments:

$$\mathscr{C}_S(p;E) = \frac{a}{4\pi^2}\int_0^\Lambda \frac{{\rm d}q\,q^2\mathscr{A}_S(p,q;E)}{-1/a+\sqrt{3q^2/4-E-{\rm i}\epsilon}}. \tag{366}$$

Since $\mathscr{A}_S$ scales like q^{-1} as $q \to \infty$, the integral is linearly divergent. Thus the 1 in the factors $(1+\mathscr{C}_S)$ in Eq. (365) can be neglected as $\Lambda \to \infty$. To obtain a finite limit for $\delta\mathscr{A}_S$ as $\Lambda \to \infty$, Im g_3/g_2^2 must be proportional to $1/\Lambda^2$. The function $\mathscr{C}_S(p;E)$ can be obtained by solving the integral equation for $\mathscr{A}_S(p,q;E)$ for all values of q and inserting the solution into the integral in Eq. (366). This method was used in Ref. [129] to calculate the rate constants $\alpha_{\rm deep}$ for $a>0$ and $a<0$ to first order in Im g_3. The functional dependence of the results on a and Λ_* were found to have the forms shown in Eq. (364). For the special cutoff values Λ_n at which Re $g_3 = 0$ (cf. Eq. (360)), the relation between the infinitesimal parameters Im g_3 and η_* were found to be[17]

$${\rm Im}\,g_3 \approx -23.3\,\eta_*\,g_2^2/\Lambda_n^2. \tag{367}$$

[17] Note that a factor of $1/(32\pi^2)$ was omitted from the expression for $h' = -{\rm Im}\,g_3/(9g_2)$ in Ref. [129].

The dependence on a of the rate constants $\alpha_{\rm deep}$ in Eqs. (364) was derived using the generalization of Efimov's radial laws to the case in which there are deep 2-body bound states. The fact that these results can be reproduced using a purely numerical method based on effective field theory increases our confidence in the generalization of the radial laws.

If the expression for the complex-valued 3-body coupling constant g_3 given by Eqs. (335) and (361) is expanded to first order in η_*, the result is

$$\mathrm{Im}\, g_3 = -\frac{9\sin[2\arctan s_0]}{\cos^2[s_0\ln(\Lambda/\Lambda_*)-\arctan s_0]}\,\eta_*\,\frac{g_2^2}{\Lambda^2}\,. \tag{368}$$

There is a factor 2.6 discrepancy between the analytic result for Im g_3 in Eq. (368) at $\Lambda=\Lambda_n$ and the numerical result in Eq. (367).

9. Universality in other three-body systems

In this section, we summarize the universal information that is known about 3-body systems with large scattering lengths other than three identical bosons in 3 space dimensions.

9.1. Unequal scattering lengths

There are 3-body systems in which the three particles all have the same mass, but the three pairs of particles need not all have the same scattering lengths. For example, different hyperfine spin states of the same atom have the same mass, but the scattering lengths a_{ij} can be different for each pair ij of hyperfine states. As another example, different isotopes of a heavy atom have nearly the same masses. Finally, the proton and neutron have nearly equal masses. It is therefore worthwhile to consider the universal behavior of systems with equal masses and scattering lengths that are large but not all equal. Note that a multiple fine-tuning of the interactions might be required to make more than one scattering length large simultaneously.

One of the most basic questions for a 3-body system is whether the Efimov effect occurs in that system. This question can be answered by determining the channel eigenvalue $\lambda_0(R)$ for the lowest hyperspherical potential in the scaling limit. The Efimov effect occurs if $\lambda_0(R)$ is negative at $R=0$. If $\lambda_0(0)=-s_0^2$, the discrete scaling factor in the Efimov effect is e^{π/s_0}. The Efimov effect in general 3-body systems was first discussed by Amado and Noble [39] and by Efimov [159,160]. A summary of their results is as follows. If only one of the three scattering lengths is large, the Efimov effect does not occur. If two of the scattering lengths are large, the Efimov effect occurs with a discrete scaling factor of about 1986.1 unless two of the three particles are identical fermions, in which case the Efimov effect does not occur. If all three scattering lengths are large, the Efimov effect occurs with a discrete scaling factor of about 22.7.

To derive these results, we first consider the case of three distinguishable atoms with equal masses and large scattering lengths a_{12}, a_{23}, and a_{31}. The other cases can be obtained from this one by taking appropriate limits. If three atoms are distinguishable, the Schrödinger wave function need not be symmetric under interchange of the atoms. We restrict our attention to total angular momentum $L=0$ and assume that for each Faddeev component $\psi^{(i)}(\boldsymbol{r}_{jk},\boldsymbol{r}_{i,jk})$, there is no orbital angular momentum associated with either the jk or i, jk subsystems. In this case, the Schrödinger wave function can be expressed in the form

$$\Psi(\boldsymbol{r}_1,\boldsymbol{r}_2,\boldsymbol{r}_3)=\psi^{(1)}(R,\alpha_1)+\psi^{(2)}(R,\alpha_2)+\psi^{(3)}(R,\alpha_3). \tag{369}$$

If $R\sin\alpha_i$ is large enough that the 2-body potential $V(R\sin\alpha_i)$ can be neglected, the ith Faddeev wave function must have the form

$$\psi^{(i)}(R,\alpha_i)\approx F^{(i)}(R)\,\frac{\sin[\lambda^{1/2}(R)((\pi/2)-\alpha_i)]}{\sin(2\alpha_i)}. \tag{370}$$

The Faddeev equations can also be solved approximately in the region $\alpha_i \ll 1$. The matching equations for these solutions are [76]

$$\left[\cos\left(\lambda^{1/2}\frac{\pi}{2}\right)\begin{pmatrix}1&0&0\\0&1&0\\0&0&1\end{pmatrix} - \frac{4}{\sqrt{3}}\lambda^{-1/2}\sin\left(\lambda^{1/2}\frac{\pi}{6}\right)\begin{pmatrix}0&1&1\\1&0&1\\1&1&0\end{pmatrix} - \sqrt{2}\lambda^{-1/2}\sin\left(\lambda^{1/2}\frac{\pi}{2}\right)\begin{pmatrix}R/a_{23}&0&0\\0&R/a_{31}&0\\0&0&R/a_{12}\end{pmatrix}\right]\times\begin{pmatrix}F^{(1)}\\F^{(2)}\\F^{(3)}\end{pmatrix} = 0. \tag{371}$$

The consistency condition for a nontrivial solution is that the determinant of the 3×3 matrix on the left side of Eq. (371) vanishes. The solutions to this equation are the possible hyperangular eigenvalues $\lambda_n(R)$. If atoms 2 and 3 are identical bosons, then $a_{12} = a_{31}$ and we must impose the constraint $F^{(2)} = F^{(3)}$. The matching equations then reduce to

$$\left[\cos\left(\lambda^{1/2}\frac{\pi}{2}\right)\begin{pmatrix}1&0\\0&1\end{pmatrix} - \frac{4}{\sqrt{3}}\lambda^{-1/2}\sin\left(\lambda^{1/2}\frac{\pi}{6}\right)\begin{pmatrix}0&2\\1&1\end{pmatrix} - \sqrt{2}\lambda^{-1/2}\sin\left(\lambda^{1/2}\frac{\pi}{2}\right)\begin{pmatrix}R/a_{23}&0\\0&R/a_{31}\end{pmatrix}\right]\times\begin{pmatrix}F^{(1)}\\F^{(2)}\end{pmatrix} = 0. \tag{372}$$

The consistency condition that determines the eigenvalues $\lambda_n(R)$ is that the determinant of the 2×2 matrix on the left side of Eq. (372) vanishes. If atoms 1, 2, and 3 are all identical bosons, then $a_{23} = a_{23} = a_{31}$ and we must impose the constraints $F^{(1)} = F^{(2)} = F^{(3)}$. In this case, the matching equation reduces to Eq. (129).

We next consider the case of two large scattering lengths a_{23} and a_{31}, with the third scattering length a_{12} having a natural size of order ℓ. In the scaling limit, we can set $a_{12} = 0$. The matching condition for $\psi^{(3)}$ requires $F^{(3)} = 0$. The matching equations for $\psi^{(1)}$ and $\psi^{(2)}$ then reduce to

$$\left[\cos\left(\lambda^{1/2}\frac{\pi}{2}\right)\begin{pmatrix}1&0\\0&1\end{pmatrix} - \frac{4}{\sqrt{3}}\lambda^{-1/2}\sin\left(\lambda^{1/2}\frac{\pi}{6}\right)\begin{pmatrix}0&1\\1&0\end{pmatrix} - \sqrt{2}\lambda^{-1/2}\sin\left(\lambda^{1/2}\frac{\pi}{2}\right)\begin{pmatrix}R/a_{23}&0\\0&R/a_{31}\end{pmatrix}\right]\times\begin{pmatrix}F^{(1)}\\F^{(2)}\end{pmatrix} = 0. \tag{373}$$

The consistency condition that determines the eigenvalues $\lambda_n(R)$ is that the determinant of the 2×2 matrix on the left side of Eq. (373) vanishes. If atoms 1 and 2 are identical bosons, we must impose the constraint $F^{(1)} = F^{(2)}$. Setting $a_{23} = a_{31} = a$, the matching equation is

$$\cos\left(\lambda^{1/2}\frac{\pi}{2}\right) - \frac{4}{\sqrt{3}}\lambda^{-1/2}\sin\left(\lambda^{1/2}\frac{\pi}{6}\right) = \sqrt{2}\lambda^{-1/2}\sin\left(\lambda^{1/2}\frac{\pi}{2}\right)\frac{R}{a}. \tag{374}$$

If atoms 1 and 2 are identical fermions, then a_{12} must be exactly 0 and we must impose the constraint $F^{(1)} = -F^{(2)}$. Setting $a_{23} = a_{31} = a$, the matching equation is

$$\cos\left(\lambda^{1/2}\frac{\pi}{2}\right) + \frac{4}{\sqrt{3}}\lambda^{-1/2}\sin\left(\lambda^{1/2}\frac{\pi}{6}\right) = \sqrt{2}\lambda^{-1/2}\sin\left(\lambda^{1/2}\frac{\pi}{2}\right)\frac{R}{a}. \tag{375}$$

Finally, we consider the case of a single large scattering length $a_{23} = a$, with the other two scattering lengths having natural sizes of order ℓ. In the scaling limit, we can set $a_{12} = a_{31} = 0$. The matching conditions for $\psi^{(2)}$ and $\psi^{(3)}$ then require $F^{(2)} = F^{(3)} = 0$. The matching equation for $\psi^{(1)}$ is

$$\cos\left(\lambda^{1/2}\frac{\pi}{2}\right) = \sqrt{2}\,\lambda^{-1/2}\sin\left(\lambda^{1/2}\frac{\pi}{2}\right)\frac{R}{a}. \tag{376}$$

We now ask whether the Efimov effect occurs and if so, what the discrete scaling factor is. We first consider the case of three distinguishable atoms with large scattering lengths a_{12}, a_{23}, and a_{31}. The matching equations are given in Eq. (371). At $R = 0$, the consistency condition reduces to

$$\left[\cos\left(\lambda^{1/2}\frac{\pi}{2}\right) + \frac{4}{\sqrt{3}}\lambda^{-1/2}\sin\left(\lambda^{1/2}\frac{\pi}{6}\right)\right]^2\left[\cos\left(\lambda^{1/2}\frac{\pi}{2}\right) - \frac{8}{\sqrt{3}}\lambda^{-1/2}\sin\left(\lambda^{1/2}\frac{\pi}{6}\right)\right] = 0. \tag{377}$$

If atoms 2 and 3 are identical bosons, the matching equations are given in Eq. (372). At $R=0$, the consistency condition is the same as Eq. (377) except that the first factor on the left side is not squared. The possible values of $\lambda(0)$ are identical. A negative value of $\lambda(0)$ comes only from the vanishing of the second factor on the left side of Eq. (377). This condition is identical to the matching equation for three identical bosons in Eq. (129). It has the negative solution $\lambda=-s_0^2$, with $s_0\approx 1.00624$. Thus there is an Efimov effect with discrete scaling factor $e^{\pi/s_0}\approx 22.7$.

We now consider the case of two large scattering lengths a_{13} and a_{23}. If the three atoms are distinguishable, the matching equations are given in Eq. (373). At $R=0$, the consistency condition reduces to

$$\left[\cos\left(\lambda^{1/2}\frac{\pi}{2}\right)+\frac{4}{\sqrt{3}}\lambda^{-1/2}\sin\left(\lambda^{1/2}\frac{\pi}{6}\right)\right]\left[\cos\left(\lambda^{1/2}\frac{\pi}{2}\right)-\frac{4}{\sqrt{3}}\lambda^{-1/2}\sin\left(\lambda^{1/2}\frac{\pi}{6}\right)\right]=0. \tag{378}$$

If atoms 1 and 2 are identical bosons, the matching equation is given in Eq. (374). At $R=0$, this implies the vanishing of the second factor on the left side of Eq. (378). This equation has a single negative solution $\lambda_0=-s_0^2$, with $s_0\approx 0.4137$. Thus there is an Efimov effect with discrete scaling factor $e^{\pi/s_0}\approx 1986.1$. If atoms 1 and 2 are identical fermions, the consistency equation is given in Eq. (375). At $R=0$, this implies the vanishing of the first factor on the left side of Eq. (378). This equation has no negative solutions, so there is no Efimov effect.

Finally we consider the case of a single large scattering length $a_{23}=a$. The matching equation is given in Eq. (376). At $R=0$, there are no negative solutions for λ, so there is no Efimov effect.

9.2. Unequal masses

In the 2-body sector, the universal results for particles of unequal masses are only a little more complicated than those for the equal-mass case in Sections 4.1 and 4.2. Let the atoms 1 and 2 have a large scattering length a_{12} and unequal masses m_1 and m_2. The 2-body reduced mass is defined by

$$m_{12}=\frac{m_1m_2}{m_1+m_2}. \tag{379}$$

It approaches m_1 in the limit $m_1\to 0$ and m_2 in the limit $m_1\to\infty$. In the case of equal masses m, it reduces to $m_{12}=m/2$. If the momenta of the two atoms are $\pm\hbar\boldsymbol{k}$, their total kinetic energy is $E=\hbar^2k^2/(2m_{12})$. The differential cross section for elastic scattering is

$$\frac{\mathrm{d}\sigma}{\mathrm{d}\Omega}=\frac{a_{12}^2}{1+a_{12}^2k^2}. \tag{380}$$

The cross section is obtained by integrating over the total solid angle of 4π. If a_{12} is large and positive, the atoms 1 and 2 form a shallow dimer with binding energy

$$E_{\mathrm{D}}=\frac{\hbar^2}{2m_{12}a_{12}^2}. \tag{381}$$

In the general 3-body system, the three masses can be unequal and any combination of the three scattering lengths can be large. The Efimov effect in general 3-body systems was first discussed by Amado and Noble [39] and by Efimov [159,160]. The special case in which two of the three particles have the same mass was also discussed by Ovchinnikov and Sigal [161]. The conditions for the existence of the Efimov effect and the value of the discrete scaling factor depend on the ratios of the masses. We summarize briefly the results for the extreme cases in which two masses are equal and the third mass is either much larger or much smaller. In the case of two heavy particles and one light particle, the Efimov effect occurs provided the heavy-light scattering length is large. In the case of one heavy particle and two light particles, the Efimov effect occurs only if all three pairs of particles have large scattering lengths.

In the 3-body problem with unequal masses m_1, m_2, and m_3, it is convenient to introduce a 3-body reduced mass:

$$m_{123}=\frac{m_1m_2m_3}{m_1m_2+m_2m_3+m_3m_1}. \tag{382}$$

It approaches m_1 in the limit $m_1\to 0$ and m_{23} in the limit $m_1\to\infty$. In the case of equal masses m, it reduces to $m_{123}=m/3$.

The hyperspherical coordinates defined for equal-mass particles in Section 5.1 can be generalized to the case of unequal masses. A set of Jacobi coordinates consists of the separation vector $\boldsymbol{r}_{ij}$ between a pair of atoms, which is defined in Eq. (83), and the separation vector of atom k from the center-of-mass coordinate of atoms i and j:

$$\boldsymbol{r}_{k,ij} = \boldsymbol{r}_k - \frac{m_i \boldsymbol{r}_i + m_j \boldsymbol{r}_j}{m_i + m_j}. \tag{383}$$

The hyperradius is the square root of a weighted average of the separations of the pairs of atoms:

$$R^2 = \frac{m_1 m_2 r_{12}^2 + m_2 m_3 r_{23}^2 + m_3 m_1 r_{31}^2}{m_1 m_2 + m_2 m_3 + m_3 m_1}. \tag{384}$$

The hyperangles α_k are defined by

$$\tan \alpha_k = \left(\frac{m_{ij}^2 (m_1 + m_2 + m_3)}{m_1 m_2 m_3} \right)^{1/2} \frac{r_{ij}}{r_{k,ij}}. \tag{385}$$

The magnitudes of the separation vectors are

$$r_{ij} = \left(\frac{m_1 m_2 m_3}{m_{ij} m_{123} (m_1 + m_2 + m_3)} \right)^{1/2} R \sin \alpha_k, \tag{386a}$$

$$r_{k,ij} = \left(\frac{m_{ij}}{m_{123}} \right)^{1/2} R \cos \alpha_k. \tag{386b}$$

In Ref. [76], the authors used a definition of the hyperradius ρ that depends on an arbitrary mass parameter μ:

$$\rho^2 = \frac{m_1 m_2 + m_2 m_3 + m_3 m_1}{\mu (m_1 + m_2 + m_3)} R^2. \tag{387}$$

Thus our definition in Eq. (384) corresponds to a specific choice for μ.

By introducing hyperspherical coordinates in the Faddeev equation for the 3-body system, the hyperangular variables can be separated from the hyperradius R. The hyperangular eigenvalue equations determine the channel eigenvalues $\lambda_n(R)$. The channel potentials that appear in the coupled set of differential equations for the hyperradial functions can be written as[18]

$$V_n(R) = -\frac{(\lambda_n(R) - \frac{1}{4})\hbar^2 (m_1 + m_2 + m_3)}{2(m_1 m_2 + m_2 m_3 + m_3 m_1) R^2}. \tag{388}$$

The question of whether the Efimov effect occurs in a 3-body system can be answered by determining the channel eigenvalue $\lambda_0(R)$ for the lowest hyperspherical potential in the scaling limit. In the absence of subsystem orbital angular momenta, the Schrödinger wave function can be expressed as the sum of three Faddeev wave functions as in Eq. (369). If $R \sin \alpha_i$ is large enough, the Faddeev wave functions must have the form given in Eq. (370). The approximate solutions of the Faddeev equations in the region $\alpha_i \ll 1$ leads to the matching conditions [76]

$$\begin{aligned} &\left[\cos\left(\lambda^{1/2} \frac{\pi}{2}\right) - \left(\frac{m_1 m_2 m_3}{m_{jk} m_{123} (m_1 + m_2 + m_3)} \right)^{1/2} \lambda^{-1/2} \sin\left(\lambda^{1/2} \frac{\pi}{2}\right) \frac{R}{a_{jk}} \right] F^{(i)} \\ &\quad - 2\lambda^{-1/2} \left[\frac{\sin[\lambda^{1/2}((\pi/2) - \gamma_{ij})]}{\sin(2\gamma_{ij})} F^{(j)} + \frac{\sin[\lambda^{1/2}((\pi/2) - \gamma_{ik})]}{\sin(2\gamma_{ik})} F^{(k)} \right] = 0, \end{aligned} \tag{389}$$

where i, j, k is a permutation of 1, 2, 3 and the angle γ_{ij} satisfies

$$\tan \gamma_{ij} = \left(\frac{m_k (m_1 + m_2 + m_3)}{m_i m_j} \right)^{1/2}. \tag{390}$$

[18] Our channel eigenvalues λ_n corresponds to $\lambda_n + 4$ in the notation of Ref. [76].

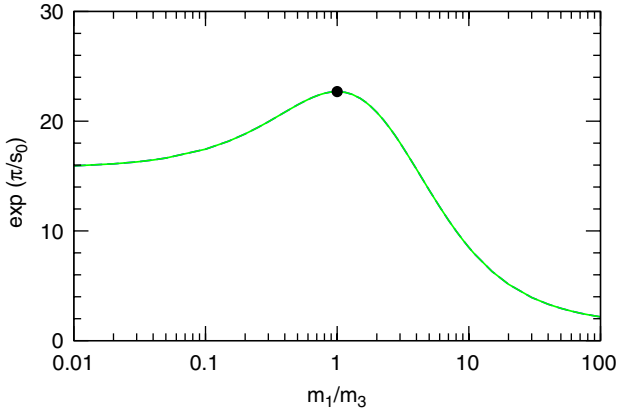

Fig. 52. Discrete scaling factor e^{π/s_0} for two particles of equal mass $m_1 = m_2$ as a function of the mass ratio m_1/m_3 for the case in which all three pairs have large scattering lengths. The particles 1 and 2 can be either identical bosons or distinguishable. The dot indicates the case of three identical bosons.

This angle is in the range $0 < \gamma_{ij} < \frac{1}{2}\pi$. The three angles satisfy

$$\gamma_{12} + \gamma_{23} + \gamma_{31} = \pi. \tag{391}$$

The three equations corresponding to cyclic permutations of i, j, k in Eq. (389) can be expressed as a homogeneous matrix equation for the 3-component vector $(F^{(1)}, F^{(2)}, F^{(3)})$. The consistency condition that there be a nontrivial solution is that the determinant of the 3×3 coefficient matrix be zero. The $R \to 0$ limit of this equation was first deduced by Efimov [159,160]. The solutions to this equation are the channel eigenvalues $\lambda_n(R)$. If particles i and j are identical bosons, then we must impose the constraint $F^{(i)} = F^{(j)}$. If particles i and j are identical fermions, then we must impose the constraint $F^{(i)} = -F^{(j)}$. In either case, the consistency condition reduces to the vanishing of the determinant of a 2×2 matrix.

We first consider the case in which all three pairs have a large scattering length. This excludes the possibility of any pair of particles being identical fermions. The Efimov effect occurs if the lowest channel eigenvalue $\lambda_0(R)$ in the scaling limit has a negative value at $R = 0$. The consistency condition at $R = 0$ does not depend on the scattering lengths. For any values of the masses, there is a single channel eigenvalue with a negative value $\lambda_0(0) = -s_0^2$ at $R = 0$. The Efimov effect therefore occurs with a discrete scaling factor e^{π/s_0}. The discrete scaling factor is largest if all three masses are equal. It has the same value $e^{\pi/s_0} \approx 22.7$ as for three identical bosons. In the case of two equal-mass particles, the discrete scaling factor is the same whether the equal-mass particles are identical bosons or distinguishable. The discrete scaling factor for $m_1 = m_2$ is shown in Fig. 52 as a function of the mass ratio $m_1/m_3 = m_2/m_3$. In the limit $m_1 = m_2 \ll m_3$, the discrete scaling factor approaches 15.7. In the limit $m_1 = m_2 \gg m_3$, it approaches 1.

We now consider the case in which only two pairs have large scattering lengths. If a_{31} and a_{23} are large, the equation for $F^{(3)}$ in Eq. (389) should be ignored and $F^{(3)}$ should be set to zero in the equations for $F^{(1)}$ and $F^{(2)}$. If the particles 1 and 2 are distinguishable, the resulting consistency condition reduces at $R = 0$ to

$$\left[\cos\left(\lambda^{1/2}\frac{\pi}{2}\right) + \frac{2\lambda^{-1/2}\sin\left[\lambda^{1/2}\left(\frac{\pi}{2} - \gamma_{12}\right)\right]}{\sin(2\gamma_{12})}\right]\left[\cos\left(\lambda^{1/2}\frac{\pi}{2}\right) - \frac{2\lambda^{-1/2}\sin\left[\lambda^{1/2}\left(\frac{\pi}{2} - \gamma_{12}\right)\right]}{\sin(2\gamma_{12})}\right] = 0. \tag{392}$$

There is a single negative eigenvalue $\lambda_0 = -s_0^2$ for any values of the masses. It comes from the vanishing of the second factor on the left side of Eq. (392). The discrete scaling factor e^{π/s_0} depends on the masses only through the angle γ_{12} defined in Eq. (390). If particles 1 and 2 are identical bosons, the matching condition reduces at $R = 0$ to the vanishing of the second factor on the left side of Eq. (392). Thus there is an Efimov effect with the same discrete scaling factor as in the case in which the two equal mass particles are distinguishable. If particles 1 and 2 are identical fermions, the matching equation reduces at $R = 0$ to the vanishing of the first factor on the left side of Eq. (392). This equation has no negative solutions for λ. Thus there is no Efimov effect associated with hyperangular channels with no

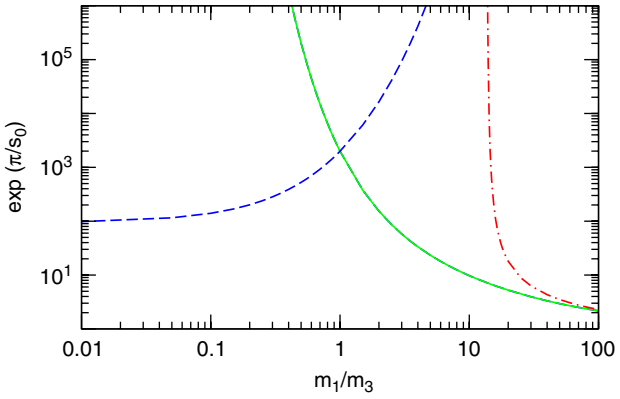

Fig. 53. Discrete scaling factor e^{π/s_0} for two particles of equal mass $m_1 = m_2$ as a function of the mass ratio m_1/m_3 for the cases in which two pairs have large scattering lengths. If a_{23} and a_{31} are large, particles 1 and 2 can be either identical bosons or distinguishable particles (solid line) or else identical fermions (dash-dotted line). If a_{12} and a_{31} (or a_{12} and a_{23}) are large, particles 1 and 2 must be distinguishable particles (dashed line).

subsystem angular momentum. However, as will be discussed in Section 9.3, there is an Efimov effect associated with hyperangular channels with nonzero subsystem angular momentum if the mass ratio m_3/m_1 exceeds a critical value.

The discrete scaling factor for the cases in which only two pairs have large scattering lengths are illustrated in Fig. 53. We consider only the special case in which particles 1 and 2 have the same masses $m_1 = m_2$, and we plot the discrete scaling factor as a function of the mass ratio m_1/m_3. If the large scattering lengths are a_{23} and a_{31} and if particles 1 and 2 are either identical bosons or distinguishable, the discrete scaling factor is e^{π/s_0}, where $\lambda = -s_0^2$ is a negative solution to Eq. (392). As m_1/m_3 increases from 0 to 1 to ∞, e^{π/s_0} decreases monotonically from ∞ to 1986.1 to 1 as shown in Fig. 53. The case in which particles 1 and 2 are identical fermions, for which the discrete scaling factor is also shown in Fig. 53, is discussed in Section 9.3. If the large scattering lengths are either a_{12} and a_{31} or a_{12} and a_{23}, particles 1 and 2 must be distinguishable. The equation that determines the discrete scaling factor is Eq. (392), with γ_{12} replaced by $\gamma_{23} = \gamma_{31}$. As m_1/m_3 increases from 0 to 1 to ∞, e^{π/s_0} increases monotonically from 94.36 to 1986.1 to ∞ as shown in Fig. 53.

In the case of two heavy atoms and a third atom that is much lighter, the Efimov effect can be understood intuitively using the Born–Oppenheimer approximation [162]. We take the heavy masses to be $m_1 = m_2 = M$ and the light mass to be $m_3 = m$ with $m \ll M$. The hyperradius R defined in Eq. (384) can be identified with the separation r_{12} of the two heavy atoms. We take the coordinates of the three particles in the center-of-mass frame to be $\boldsymbol{r}_1 = +\frac{1}{2}\boldsymbol{R}$, $\boldsymbol{r}_2 = -\frac{1}{2}\boldsymbol{R}$, and $\boldsymbol{r}_3 = \boldsymbol{r}$. We assume that the potential between the heavy atoms can be neglected, so that the 3-body potential $V(\boldsymbol{r}_1, \boldsymbol{r}_2, \boldsymbol{r}_3)$ can be expressed as the sum of two pairwise potentials $V(r_{23})$ and $V(r_{31})$. In this case, the 3-body Schrödinger equation in the center-of-mass frame can be reduced to

$$\left[-\frac{\hbar^2}{M}\nabla_R^2 - \frac{\hbar^2}{2m}\nabla_r^2 + V\left(\left|\boldsymbol{r} + \frac{1}{2}\boldsymbol{R}\right|\right) + V\left(\left|\boldsymbol{r} - \frac{1}{2}\boldsymbol{R}\right|\right)\right] \Psi = E\,\Psi. \tag{393}$$

In the Born–Oppenheimer approximation, which becomes exact in the limit $M/m \to \infty$, the wave function is expressed in the factored form

$$\Psi(\boldsymbol{r}, \boldsymbol{R}) = \psi(\boldsymbol{r}, \boldsymbol{R})\,\phi(\boldsymbol{R}), \tag{394}$$

where $\psi(\boldsymbol{r}, \boldsymbol{R})$ can be interpreted as the wave function for the light particle in the presence of the two heavy particles with fixed positions $\pm\frac{1}{2}\mathbf{R}$. The 3-body Schrödinger equation in Eq. (393) can be separated into two coupled equations. The first is the Schrödinger equation for ψ:

$$\left[-\frac{\hbar^2}{2m}\nabla_r^2 + V\left(\left|\boldsymbol{r} + \frac{1}{2}\boldsymbol{R}\right|\right) + V\left(\left|\boldsymbol{r} - \frac{1}{2}\boldsymbol{R}\right|\right)\right] \psi = \epsilon(R)\,\psi. \tag{395}$$

The second is the Schrödinger equation for the heavy particles in an effective potential that is determined by the eigenvalue in Eq. (395):

$$\left[-\frac{\hbar^2}{M}\nabla_R^2 + \epsilon(R)\right]\phi = E\,\phi. \tag{396}$$

Fonseca, Redish and Stanley applied the Born–Oppenheimer approach to the problem of a potential $V(r)$ for which an analytic equation could be obtained for the Born–Oppenheimer potential $\epsilon(R)$ [162]. The potential was tuned to give a large positive scattering length a in the heavy-light system. Thus the heavy and light particles form a shallow bound state with binding energy $E_2 = \hbar^2/(2ma^2)$. The Born–Oppenheimer potential can be expressed in the form

$$\epsilon(R) = -\frac{\hbar^2}{2m}\kappa^2(R). \tag{397}$$

In the scaling limit, the equation for $\kappa(R)$ reduces to [162]

$$(\kappa - 1/a)R = e^{-\kappa R}. \tag{398}$$

The solution interpolates between a $1/R^2$ potential for $R \ll a$ and a Yukawa potential for $R \gg a$:

$$\epsilon(R) \longrightarrow -x_0^2\,\frac{\hbar^2}{2mR^2} \quad \text{as } R \to 0, \tag{399a}$$

$$\longrightarrow -\frac{\hbar^2}{2ma^2} - \frac{\hbar^2}{maR}e^{-R/a} \quad \text{as } R \to \infty. \tag{399b}$$

In Eq. (399a), the number $x_0 = 0.567143$ in the prefactor of $\hbar^2/2mR^2$ is the solution to the equation $x = e^{-x}$. Expressing the asymptotic potential in Eq. (399a) in the form in Eq. (142) with m replaced by M, we find that s_0 is

$$s_0 \approx 0.567143\,(M/m)^{1/2}. \tag{400}$$

In the limit $M/m \to \infty$, s_0 approaches ∞ and the discrete scaling factor e^{π/s_0} approaches 1. In Eq. (399b), the first term is just the binding energy of the shallow dimer. The second term is a Yukawa potential that arises from the exchange of the light particle between the two heavy particles.

If we apply the hyperspherical formalism to this problem, the matching condition given in Eq. (389) reduces to

$$\cos\left(\lambda^{1/2}\frac{\pi}{2}\right) - (2m\lambda/M)^{-1/2}\sin\left[\lambda^{1/2}\frac{\pi}{2} - (2m\lambda/M)^{1/2}\right] = (2m\lambda/M)^{-1/2}\sin\left(\lambda^{1/2}\frac{\pi}{2}\right)\frac{R}{a}. \tag{401}$$

For negative λ, the cosines and sines in Eq. (401) become hyperbolic functions with real arguments. Keeping only the leading exponentials in the hyperbolic functions, the matching equation in Eq. (401) reduces to Eq. (398) for the Born–Oppenheimer potential with $\kappa = (2m\lambda/M)^{1/2}R^{-1}$. The matching equation Eq. (401) is more general, because it also applies for negative values of the scattering length.

The widths of Efimov resonances composed of two heavy atoms and one light atom (or electron) have been calculated by Pen'kov [163]. He considered a model in which the two identical heavy bosonic atoms with mass M form a deep S-wave bound state with binding energy $E_{\rm deep}$ and the interaction between a heavy atom and the light atom of mass m is tuned to the resonant limit $a = \pm\infty$. The Efimov trimers appear as resonances in the scattering of the light atom and the deep diatomic molecule composed of the two heavy atoms. Pen'kov obtained an analytic expression for the widths $\Gamma_{\rm T}^{(n)}$ of the Efimov trimers. In the limit $M \gg m$, Pen'kov's result approaches [163]

$$\frac{\Gamma_{\rm T}^{(n)}}{E_{\rm T}^{(n)}} \longrightarrow 103.0\,\exp\left(-1.260\sqrt{M/m}\right)\sin^2\left[\frac{1}{2}s_0\ln(4E_{\rm deep}/E_{\rm T}^{(n)})\right] \quad \text{as } n \to \infty \quad \text{with } a = \pm\infty. \tag{402}$$

where s_0 is given in Eq. (400). Note that in spite of the appearance of the binding energy $E_{\rm T}^{(n)}$ on the right side of Eq. (402), the ratio of the width to the binding energy is the same for all Efimov states. This follows from the fact that the binding energies $E_{\rm T}^{(n)}$ differ by integral powers of the discrete scaling factor $e^{2\pi/s_0}$. Thus Pen'kov's result is consistent with an exact discrete scaling symmetry in the resonant limit.

9.3. Two identical fermions

If two atoms are identical fermions, their S-wave scattering length must vanish. However, the fermions can have a nonzero scattering length with another atom. If that scattering length is large, 3-body systems consisting of two fermions and the third atom have universal properties. We will first describe the universal results that have been calculated and then discuss the conditions for the Efimov effect in this system.

We first give some universal results for the special case in which the identical fermions and the third atom have the same mass m. We take the third atom to be an orthogonal spin state of the same atom, and we label the spin states $\uparrow$ and $\downarrow$. The large scattering length is $a_{\uparrow\downarrow} = a$. If $a > 0$, the two spin states form a shallow dimer with binding energy $E_{\rm D} = \hbar^2/(ma^2)$ that we label D. The Efimov effect does not occur in this case, so the universal 3-body predictions are completely determined by a. The atom–dimer scattering length was first calculated by Skorniakov and Ter–Martirosian in 1956 [5]:

$$a_{\uparrow D} = a_{\downarrow D} = 1.2\, a. \tag{403}$$

The 3-body recombination rate constant has been calculated by Petrov [164]. The rate of decrease in the number density $n_\uparrow$ of low-energy atoms with spin $\uparrow$ from the 3-body recombination processes $\uparrow\uparrow\downarrow \longrightarrow \uparrow\, D$ and $\uparrow\downarrow\downarrow \longrightarrow \downarrow\, D$ has the form

$$\frac{\mathrm{d}}{\mathrm{d}t} n_\uparrow = -2\alpha \langle \epsilon_\uparrow \rangle n_\uparrow^2 n_\downarrow - \alpha \langle \epsilon_\downarrow \rangle n_\uparrow n_\downarrow^2, \tag{404}$$

where $\langle \epsilon_\uparrow \rangle$ and $\langle \epsilon_\downarrow \rangle$ are the average kinetic energies of the atoms in the spin states $\uparrow$ and $\downarrow$, respectively. The 3-body recombination event rate constant α defined by Eq. (404) is [164]

$$\alpha = 148\, a^6/\hbar. \tag{405}$$

If the fermions with spins $\uparrow$ and $\downarrow$ also form deep diatomic molecules, low energy atoms and dimers can be lost from a system through atom–dimer collisions via dimer relaxation. In the limit $a \gg \ell$, where ℓ is the natural low-energy length scale, the rate constant for this process scales like a power of a:

$$\beta_{\rm AD} = B\, (a/\ell)^{-2-2v} \hbar a/m. \tag{406}$$

The coefficient B depends on the details at short distances, but the exponent of a is universal. The relaxation process requires all three atoms to approach within a distance of order ℓ. Since two of these three atoms are identical fermions, we might expect the prefactor of $\hbar a/m$ in Eq. (406) to be suppressed by $(\ell/a)^2$. However, it actually scales like a^{-2-2v}, where $v = 1.166$ is an anomalous dimension [165,166]. This anomalous scaling behavior dramatically suppresses the relaxation rate when a is large.

Some universal results have been calculated explicitly for the case of two identical fermions with mass $m_1 = m_2$ and a third particle with mass m_3. As discussed below, the Efimov effect occurs in this system only if the mass ratio m_1/m_3 exceeds a critical value [159,160]. If $m_1/m_3 < 13.6$, there is no Efimov effect and universal results for 3-body observables depend only on a and the masses. We label the identical fermions A_1 and the third particle A_3. The large scattering length is $a_{13} = a$. If $a > 0$, the particles A_1 and A_3 form a shallow dimer labelled D with binding energy $\hbar^2/(2m_{13}a^2)$. The atom–dimer scattering length $a_{A_1 D}$ has been calculated as a function of m_1/m_3 by Petrov [164]. The ratio $a_{A_1 D}/a$ is a monotonically increasing function of m_1/m_3. For $m_1 \ll m_3$, the ratio seems to approach 1. For equal masses $m_1 = m_3$, its value is 1.2, in agreement with Eq. (403). It increases to about 2.3 for $m_1/m_3 = 13.6$. In Ref. [164], the result for $a_{A_1 D}/a$ was given as a function of the mass ratio m_1/m_3, even for $m_1/m_3 > 13.6$. When the mass ratio exceeds this critical value for the Efimov effect, one would expect $a_{A_1 D}$ to also depend on a 3-body parameter.

Petrov has also calculated the 3-body recombination rate constants associated with the process $A_1 A_1 A_3 \to A_1 D$ for mass ratios in the range $0 < m_1/m_3 < 13.6$ [164]. The equation analogous to Eq. (404) for the time-derivative of the number density n_1 of the atoms A_1 includes the term $-2\alpha \langle \epsilon_1 \rangle n_1^2 n_3$, where $\langle \epsilon_1 \rangle$ is the average kinetic energy of the atoms A_1. The event rate constant α vanishes at the endpoints of the range $0 < m_1/m_3 < 13.6$ and also at the intermediate value $m_1/m_3 = 8.62$. These zeros are the results of interference effects and are analogous to the zeros in the 3-body recombination rate constant for identical bosons given in Eq. (228). The dimensionless ratio $\alpha_1 \hbar/a^6$ has local maxima of about 60 near $m_1/m_3 = 4$ and about 3 near $m_1/m_3 = 12$. If $m_1/m_3 = 1$, its value is 148, as given in Eq. (405). For $m_1/m_3 > 13.6$, α presumably depends also on a 3-body parameter.

We proceed to consider the conditions for the Efimov effect in the system consisting of two identical fermions of mass m_1 and a third atom of mass m_3. The Efimov effect occurs if there is a hyperangular channel eigenvalue $\lambda(R)$ that in the scaling limit is negative as $R \to 0$. The matching equation for the case in which particles 1 and 2 are identical fermions and there is no subsystem orbital angular momentum was deduced in Section 9.2. The matching equation at $R=0$ is that the first factor on the left side of Eq. (392) must vanish. This equation has no negative solutions for $\lambda(0)$, so no Efimov effect arises from this angular momentum channel. However, if m_1/m_3 is sufficiently large, there is a lower eigenvalue in a channel with one unit of angular momentum in the subsystem consisting of a pair and a third atom. This corresponds to the $l_x = 0, l_y = 1$ term in the angular momentum decomposition of the Faddeev wave function in Eq. (106). The matching equation for the hyperangular eigenvalue for this component of the wave function is [76]

$$\sin\left(\lambda^{1/2}\frac{\pi}{2}\right) - \frac{1}{3}\lambda^{1/2}\cos(\gamma_{12})\,{}_2F_1\left(\frac{1}{2}(3+\lambda^{1/2}), \frac{1}{2}(3-\lambda^{1/2}), \frac{5}{2}; \cos^2\gamma_{12}\right) = -\sqrt{2}\frac{\lambda^{1/2}}{\lambda-1}\cos\left(\lambda^{1/2}\frac{\pi}{2}\right)\frac{R}{a}, \tag{407}$$

where γ_{12} is given by Eq. (390). The lowest eigenvalue has a negative value $\lambda(0) = -s_0^2$ at $R = 0$ if m_1/m_3 exceeds the critical value 13.607. The discrete scaling factor is shown as a function of m_1/m_3 in Fig. 53. As m_1/m_3 increases from the critical value to ∞, e^{π/s_0} decreases monotonically from ∞ to 1.

9.4. Particles with a spin symmetry

We now turn to the case of particles with distinct states that are related by a symmetry. We will refer to these states as spin states, although they could equally well be states associated with some internal symmetry such as isospin. A general treatment of this case was given by Bulgac and Efimov in Ref. [167]. It is more complex than the previously considered cases for several reasons:

(1) There can be more than one spin configuration leading to a given total spin of the three-particle system under consideration.
(2) The level spectrum does not in general show the same simple regularities as in the spinless case. A typical spectrum looks like a superposition of several, strongly interacting spectra for the spinless case.
(3) The magnitude of the attraction between the particles depends on a number of factors: the particle masses and spins, the total spin of the state considered, the number of channels with large scattering lengths and their spins, and the strength of the coupling between the spin configurations of different particle pairs.

In the following, we will illustrate some of these new features in more detail. For a more complete treatment, we refer the reader to Ref. [167].

For a state of total spin σ, the Schrödinger wave function can be decomposed in the form

$$\Psi_\sigma(\boldsymbol{r}_1, \boldsymbol{r}_2, \boldsymbol{r}_3) = \sum_{\sigma_{23}} \psi^{(1)}_{\sigma_{23}}(R, \alpha_1)\chi_{\sigma,\sigma_{23}} + \sum_{\sigma_{31}} \psi^{(2)}_{\sigma_{31}}(R, \alpha_2)\chi_{\sigma,\sigma_{31}} + \sum_{\sigma_{12}} \psi^{(3)}_{\sigma_{12}}(R, \alpha_3)\chi_{\sigma,\sigma_{12}}, \tag{408}$$

which is a generalization of the decomposition in Eq. (369). In each of the terms, the sum is over the spin quantum number σ_{ij} of the pair ij. Only channels with large scattering length will contribute to Eq. (408). The symbol $\chi_{\sigma,\sigma_{ij}}$ denotes the spin function for the total spin σ and the spin σ_{ij} for the pair ij. The number of terms in the sum is equal to the number of ways the total spin σ can be obtained by first coupling the spins of the pair ij to the spin σ_{ij} and then coupling σ_{ij} and the spin of the third particle σ_k to the total spin σ. We assume that the orbital angular momenta are all zero.

Using Eq. (408), one can obtain a matching equation analogous to Eq. (372). A new feature of the matching equation is that there can be several negative hyperangular eigenvalues λ. This is related to the fact that, in general, there is no unique way of obtaining a given total spin of the three particles from coupling the single particle spins. These different spin configurations are mixed by the interaction, and as a result some configurations may lead to attraction while others lead to repulsion. As a consequence, the number of negative eigenvalues cannot be larger than the number of ways the total spin can be obtained by coupling the individual spins of the particles.

An example that will be discussed in the next subsection is the triton channel in the case of three nucleons. There are two ways to obtain the total isospin $\frac{1}{2}$ and spin $\frac{1}{2}$ of the triton from nucleons which also have isospin $\frac{1}{2}$ and spin $\frac{1}{2}$. The consistency condition at $R = 0$ becomes

$$\left[\cos\left(\lambda^{1/2}\frac{\pi}{2}\right) + \frac{4}{\sqrt{3}}\lambda^{-1/2}\sin\left(\lambda^{1/2}\frac{\pi}{6}\right)\right]\left[\cos\left(\lambda^{1/2}\frac{\pi}{2}\right) - \frac{8}{\sqrt{3}}\lambda^{-1/2}\sin\left(\lambda^{1/2}\frac{\pi}{6}\right)\right] = 0. \tag{409}$$

Only the vanishing of the second factor on the right side can lead to a negative solution for the eigenvalue λ. This condition is identical to the matching equation for three identical bosons in Eq. (129). It has the negative solution $\lambda = -s_0^2$, with $s_0 \approx 1.00624$. Thus there is an Efimov effect with discrete scaling factor $e^{\pi/s_0} \approx 22.7$. This is a consequence of the Pauli principle which relates the symmetry in the spin–isospin and coordinate-space wave functions of the triton. A negative eigenvalue corresponding to attraction is possible only in the channel yielding a totally symmetric coordinate-space wave function and a totally antisymmetric spin–isospin wave function. As a consequence, the triton system has the same discrete scaling factor as identical bosons.

If there is more than one negative eigenvalue, the Efimov spectrum ceases to be geometric in the resonant limit in which all large scattering lengths are tuned to $\pm\infty$. For n negative eigenvalues, one can think of this as arising from superimposing n independent geometric spectra. If one allows mixing from the coupling between different spin configurations, the levels interact. Close levels repel each other, but the total number of levels does not change. For explicit examples of configurations with more than one negative eigenvalue, we refer the reader to Ref. [167].

9.5. Dimensions other than 3

The hyperspherical expansion can be generalized to a continuous number of spacial dimensions d. A completely general discussion of the dependence of the Efimov effect on d is given in Ref. [76]. We will simplify the discussion by considering only the case of identical bosons. The hyperangular eigenvalue equation has a more complicated form than the equation for $d = 3$ in Eq. (112). One can choose conventions for the eigenvalues $\lambda_n(R)$ so that the hyperradial equation in the adiabatic hyperspherical approximation has the same form as in 3 dimensions:[19]

$$\frac{\hbar^2}{2m}\left(-\frac{\partial^2}{\partial R^2} + \frac{\lambda_n(R) - \frac{1}{4}}{R^2}\right) f_n(R) \approx E f_n(R). \tag{410}$$

In the neighborhood of $d = 3$, the consistency equation that determines the eigenvalue $\lambda_n(R)$ reduces in the limit $R \to 0$ to

$$\cos\left(\lambda^{1/2}\frac{\pi}{2}\right) + 2\,\sin\left(d\frac{\pi}{2}\right)\,{}_2F_1\left(\frac{1}{2}(d-1+\lambda^{1/2}), \frac{1}{2}(d-1-\lambda^{1/2}); \frac{1}{2}d; \frac{1}{4}\right) = 0. \tag{411}$$

In the scale-invariant region where the energy E can be ignored and $\lambda_n(R)$ can be approximated by $\lambda_n(0)$, the radial equation in Eq. (410) has the power-law solutions $f_n(R) = R^p$, where the power p satisfies

$$p(p-1) = \lambda_n(0) - \tfrac{1}{4}. \tag{412}$$

The Efimov effect occurs if p is imaginary, which requires $\lambda_n(0) < 0$. The Efimov effect occurs only for a narrow range of dimensions:

$$2.30 < d < 3.76. \tag{413}$$

The only integer dimension for which the Efimov effect occurs is $d = 3$. In particular, the Efimov cannot occur in $d = 2$ dimensions [168].

Since there is no Efimov effect in two dimensions, the universal predictions are completely determined by the masses and scattering lengths of the particles. As an illustration, we describe the spectrum of shallow bound states for the case of identical bosons with mass m and large scattering length a. We denote the binding energies of N-body bound states by E_N. Shallow few-body bound states exist only if $a > 0$. There are various conventions for the effective-range expansion

[19] Our channel eigenvalue λ_n corresponds to $\lambda_n + (d-1)^2$ in the notation of Ref. [76].

in 2 dimensions. We follow the conventions of Ref. [169] in which the scattering length a and the effective range r_s are defined by

$$\tfrac{1}{2}\pi \cot \delta_0(k) = \gamma + \ln(\tfrac{1}{2}ka) + \tfrac{1}{4}r_s^2 k^2 + \mathcal{O}(k^4), \tag{414}$$

where $\gamma \simeq 0.577216$ is Euler's constant. The binding energy of the shallow dimer in the scaling limit is given by

$$E_2 = 4e^{-2\gamma}\frac{\hbar^2}{ma^2}. \tag{415}$$

The leading correction is second order in r_s/a. In the scaling limit, there are two shallow 3-body bound states with binding energies [170,168,171]

$$E_3^{(1)} = 1.2704091(1)\, E_2, \tag{416a}$$

$$E_3^{(0)} = 16.522688(1)\, E_2. \tag{416b}$$

The 4-body system in two dimensions also has exactly two bound states with binding energies [172]

$$E_4^{(1)} = 25.5(1)\, E_2, \tag{417a}$$

$$E_4^{(0)} = 197.3(1)\, E_2. \tag{417b}$$

In the case of weakly interacting bosons in two dimensions, one can derive a number of interesting properties of shallow N-body bound states in the scaling limit [171]. For each N, we will refer to the deepest of the shallow bound states as the N-boson droplet. The properties of N-boson droplets with N large compared to 1 are universal and quite remarkable. The size R_N of the N-boson droplet satisfies

$$\frac{R_{N+1}}{R_N} \approx 0.3417, \quad N \gg 1. \tag{418}$$

The size decreases geometrically with N: adding an additional boson into an existing N-boson droplet reduces the size of the droplet by almost a factor of three. Correspondingly, the binding energy E_N of the N-boson droplet increases geometrically with N:

$$\frac{E_{N+1}}{E_N} \approx 8.567, \quad N \gg 1. \tag{419}$$

Thus the separation energy for one particle is approximately 88% of the total binding energy. This is in contrast to most other physical systems, where the ratio of the single-particle separation energy to the total binding energy decreases to zero as the number of particles increases. The numbers $E_3^{(0)}/E_2 = 16.5$ and $E_4^{(0)}/E_3^{(0)} = 11.9$ obtained from the exact 3-body and 4-body results in Eqs. (416b) and (417b) appear to be converging toward the universal prediction for large N in Eq. (419).

The origin of the peculiar behavior of N-boson droplets for large N lies in the asymptotic freedom of bosons in two dimensions with a zero-range potential. As the separation r of two bosons decreases, their interaction strength decreases asymptotically to zero as $1/\ln(r)$. For a potential with a small but nonzero effective range r_s, Eqs. (418) and (419) are valid for N large compared to 1 but small compared to a critical value given by

$$N_{\rm crit} \approx 0.931 \ln \frac{R_2}{r_s} + \mathcal{O}(N^0), \tag{420}$$

where R_2 is the size of the dimer. For $N \sim N_{\rm crit}$, the size R_N of the droplet is comparable to the range of the potential and universality is lost. If the ratio of R_2 to r_s is exponentially large, then $N_{\rm crit}$ is much larger than one.

9.6. Few-nucleon problem

The concept of universality in few-body systems with large scattering length was originally developed in nuclear physics. It is therefore worthwhile to describe the nuclear physics context in some detail.

Since the nuclear force is short range, nucleon–nucleon interactions at low energy should be dominated by S-waves. As discussed in Section 2.4, isospin symmetry implies that there are two independent S-wave nucleon–nucleon scattering channels. The scattering lengths a_s and a_t for these two channels are both relatively large compared to the natural low-energy length scale $\ell = \hbar/m_\pi c$. The effective-range expansion for S-wave phase shifts in Eq. (15) is an expansion in powers of the energy. *Effective-range theory*, which goes back to Schwinger, Blatt, and Bethe [11,67,68], is defined by the truncation of this expansion after the effective-range term as in Eq. (71). Effective-range theory gives a remarkably good description of the 2-nucleon system. It reproduces the S-wave *np* phase shifts to better than 5% out to a momentum of about 150 MeV/c in the center-of-mass frame. It reproduces the binding energy of the deuteron to an accuracy of 0.2%.

The *zero-range model* is defined by the more severe truncation of the effective-range expansion after the scattering length term, as in Eq. (40). It is equivalent to approximating the nuclear forces by zero-range potentials whose depths are tuned to reproduce the 2-body scattering lengths a_s and a_t. Considering its simplicity, the zero-range model gives a surprisingly good description of the 2-nucleon system. It reproduces the S-wave *np* phase shifts to better than 20% out to center-of-mass momenta of about 40 MeV. It gives the binding energy of the deuteron with an error of 37%. This modest success of the zero-range model motivates an approach in which the effective range and other coefficients in the low-energy expansion of the phase shifts are treated as perturbations. If the first-order corrections in the effective ranges are included in the S-wave phase shifts, they are accurate to better than 6% out to kinetic energies as high as 70 MeV. If the first-order corrections in the effective ranges are included in the cotangents of the S-wave phase shifts, it is equivalent to effective-range theory, which is much more accurate, as described above. The error in the deuteron binding energy decreases to 16% and then to 8% upon including the first- and second-order corrections in Eq. (78). Thus this approach works reasonably well in the 2-nucleon system.

Pioneering work in applying the zero-range model to the 3-nucleon system was carried out by Skorniakov and Ter-Martirosian in 1957 [5] and by Danilov and Lebedev in 1963 [158]. In 1981, Efimov proposed a new approach to the low-energy few-nucleon problem in nuclear physics that was based on perturbation theory around the zero-range model [173]. Efimov described it as a "qualitative approach," but it can more accurately be described as "semi-quantitative," because its goal was the understanding of few-body observables at about the 10% level. The traditional nuclear physics community, on the other hand, was accustomed to reproducing the observed binding energies of the light nuclei to several digits of accuracy using nuclear forces described by phenomenological potentials with a large number of adjustable parameters.

Remarkably, Efimov's program also works reasonably well in the 3-nucleon system at momenta small compared to m_π. The only 3-nucleon bound states are the *triton* and the ^{3}He nucleus, which are *pnn* and *ppn* bound states, respectively. These nuclei have no excited states. The *ppn* system is complicated by the Coulomb interaction between the two protons, so we focus on the *pnn* system. The Efimov effect makes it necessary to impose a boundary condition on the wave function at short distances [173]. The boundary condition can be fixed by using either the spin-doublet neutron–deuteron scattering length or the triton binding energy as input. If the deuteron binding energy is used as the 2-body input and if the boundary condition is fixed by using the spin-doublet neutron–deuteron scattering length as input, the triton binding energy is predicted with an accuracy of 6%. The accuracy of the predictions can be further improved by taking into account the effective range as a first-order perturbation [174]. Thus the triton can be identified as an Efimov state associated with the deuteron being a *pn* bound state with large scattering length [173].

Efimov's program was implemented within an effective field theory framework by Bedaque, Hammer, and van Kolck [154,175,176]. In Ref. [176], they found that the renormalization of the effective field theory requires a SU(4)-symmetric 3-body interaction with an ultraviolet limit cycle. SU(4)-symmetry was introduced by Wigner in 1937 as generalization of the SU(2) × SU(2) spin–isospin symmetry, allowing for a mixing of spin and isospin degrees of freedom in symmetry transformations [177]. It is satisfied to a high degree in the energy spectra of atomic nuclei. Exact Wigner symmetry requires the 2-body scattering lengths a_s and a_t to be equal. However, if the two body scattering lengths are large, it is a very good approximation even if they are different since the symmetry-breaking terms are proportional to the inverse scattering lengths.[20] The 3-body force introduced by Bedaque, Hammer, and van Kolck depends on a parameter Λ_* that is determined through a renormalization condition that plays the same role as Efimov's boundary condition. In addition to the triton, the effective field theory of Ref. [176] also predicts infinitely many deeper bound states in the triton channel, with the ratio of the binding energies of successive states approaching the universal

[20] See Ref. [178] for a discussion of Wigner's SU(4) symmetry in the two-nucleon system.

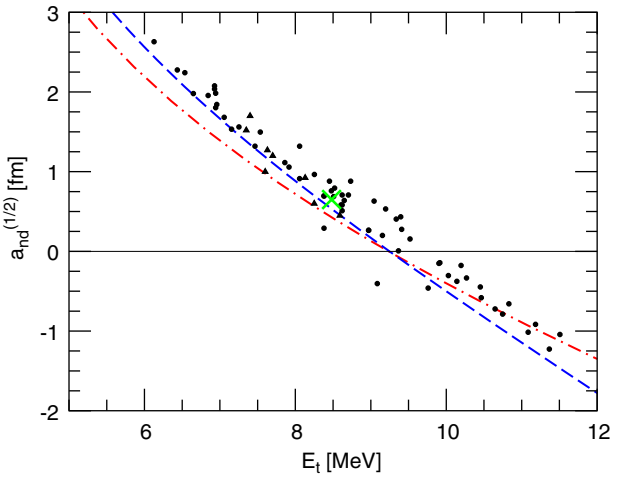

Fig. 54. The Phillips line at leading order (dash–dotted line) and next-to-leading order (dashed line) from the EFT calculation of Ref. [180]. The dots correspond to the predictions for the triton binding energy and doublet scattering length in different models with the same 2-body scattering lengths and effective ranges as inputs. The cross is the experimental result. (Figure taken from Ref. [180].)

constant $\lambda_0^2 \approx 515$, but they are artifacts of the scaling limit. The effective field theory is ideally suited to calculating corrections to the universal results in the scaling limit. The leading corrections come from the effective range and are discussed in subsection 10.2. The effective field theory also allows for a straightforward treatment of electroweak interactions of the nucleons (see Refs. [74,75] and references therein).

A peculiar universal feature of the three-nucleon system is the Phillips line [179]. If the predictions of different nucleon–nucleon potentials for the triton binding energy E_t and the spin-doublet neutron–deuteron scattering length $a_{\rm nd}^{(1/2)}$ are plotted against each other, they fall close to a straight line.[21] This correlation between E_t and $a_{\rm nd}^{(1/2)}$ is called the Phillips line and cannot be understood in conventional potential models. The Phillips line is shown in Fig. 54. The dots correspond to the potential model predictions while the cross marks the experimental value.

The Phillips line can easily be understood within Efimov's program [181–183] and its effective field theory implementation [176]. If corrections to the *scaling limit* are neglected, all low-energy 3-body observables depend only on the singlet and triplet S-wave scattering lengths a_s and a_t and the 3-body parameter Λ_*. Since the nucleon–nucleon potentials reproduce the nucleon–nucleon phase shifts, they all have the same scattering lengths. The short distance part of the potentials which is encoded in the 3-body parameter Λ_*, however, is not constrained by the phase shifts and in general is different for each potential. The different potential model calculations must therefore fall close to a line that can be parametrized by the parameter Λ_*. Due to the uncertainty from higher order corrections in the expansion in $\ell/|a|$, the Phillips line becomes a band of finite width. For an estimate of the error band for the Phillips line, see Ref. [184]. In Fig. 54, we show the Phillips line from the effective field theory calculation of Ref. [180] at leading order and including the first-order effective-range correction. The leading-order curve already agrees reasonably well with the predictions from potential models. Including the linear effective-range correction improves the agreement with potential models and also moves the curve closer to the experimental value. The Phillips line for the proton–deuteron system where the Coulomb interaction is present was discussed in Refs. [185,186]. A similar correlation between the triton charge radius and binding energy has been traced back to the variation of the parameter Λ_* as well [187].

The success of Efimov's program for the few-nucleon problem can be explained by the fact that QCD is close to the critical trajectory for an infrared limit cycle in the 3-nucleon sector [52]. The parameters of QCD include the masses m_u and m_d of the up and down quarks. The inverse scattering lengths $1/a_s$ and $1/a_t$ for the 2-nucleon system depend strongly on $m_u + m_d$, with the dependence on the mass difference $m_u - m_d$ entering only at second order. Effective field theories with nucleon and pion fields have been used to extrapolate a_s and a_t in the variable $m_u + m_d$ [188–191]. The physical observable most sensitive to $m_u + m_d$ is the pion mass, whose physical value is $m_\pi = 138\,\text{MeV}$. The

[21] A similar correlation exists between the binding energy of the ^{3}He nucleus and the spin-doublet proton–deuteron scattering length.

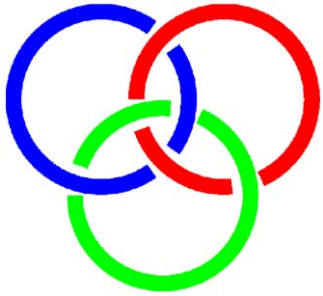

Fig. 55. Borromean rings.

extrapolation in $m_u + m_d$ can therefore be interpreted as an extrapolation in m_π. These extrapolations in $m_u + m_d$ suggest that $1/a_s$ and $1/a_t$ vanish at points $m_{\pi,s}$ and $m_{\pi,t}$ that are not too much larger than the physical pion mass. The quark mass difference $m_u - m_d$ provides an additional tuning parameter that could be used to make $1/a_s$ and $1/a_t$ vanish at the same point: $m_{\pi,s} = m_{\pi,t}$. This is the critical point for an infrared limit cycle. At this critical point, the binding energy of the deuteron is exactly zero and there is also a bound state at threshold in the spin-singlet iso-triplet channel. The triton has infinitely many excited states with an accumulation point at the 3-nucleon threshold. The ratio of the binding energies of successive bound states rapidly approaches the universal constant $\lambda_0^2 \approx 515.03$. Thus tuning the quark masses m_u and m_d to the critical point puts QCD on a critical trajectory for an infrared limit cycle.

The natural formulation of Efimov's program for the nuclear few-body problem is in terms of an effective field theory in which nucleons interact through contact interactions. There are other nuclear physics applications in which higher partial waves play a more important role.These systems can also be described using effective field theory [65,192]. Due to the absence of the Efimov effect, 3-body forces are suppressed in these systems. For calculations of neutron–deuteron scattering phase shifts in higher partial waves using effective field theory, see Refs. [184,193]. The nuclear few-body problem has also been studied using effective field theories with explicit pion fields. For the current status of these calculations, see Refs. [74,75,194,195] and references therein.

9.7. *Halo nuclei*

A special class of nuclear systems exhibiting universal behavior are *halo nuclei* [196–199]. A halo nucleus is one that consists of a tightly bound core surrounded by one or more loosely bound valence nucleons. The valence nucleons are characterized by a very low separation energy compared to those in the core. As a consequence, the radius of the halo nucleus is large compared to the radius of the core. A trivial example is the deuteron, which can be considered a 2-body halo nucleus. The RMS radius of the deuteron $\langle r^2 \rangle^{1/2} \approx 3\,\text{fm}$ is about four times larger than the size of the constituent nucleons. Halo nuclei with two valence nucleons are particularly interesting examples of 3-body systems. If none of the 2-body subsystems are bound, they are called *Borromean* halo nuclei. This name is derived from the heraldic symbol of the Borromeo family of Italy, which consists of three rings interlocked in such way that if any one of the rings is removed the other two separate. Fig. 55 shows an illustration of the Borromean rings.

The separation of scales in halo nuclei leads to universal properties that are insensitive to the structure of the core (see, e.g., Refs. [200–203]). The most carefully studied Borromean halo nuclei are ^{6}He and ^{11}Li, which have two weakly bound valence neutrons [198,199]. In the case of ^{6}He, the core is a ^{4}He nucleus, which is also known as an α particle. The two-neutron separation energy for ^{6}He is about 1 MeV, small compared to the binding energy of the α particle which is about 28 MeV. The $n\alpha$ system has no bound states, because the ^{5}He nucleus is unstable. The ^{6}He nucleus is therefore Borromean. There is, however, a strong P-wave resonance in the $J = 3/2$ channel of $n\alpha$ scattering, and this leads to the binding of ^{6}He. Thus ^{6}He can be interpreted as a bound state of an α-particle and two neutrons, both of which are in $P_{3/2}$ configurations.[22] The structure of ^{11}Li is somewhat more complicated because a larger number of partial waves contribute.

[22] For an effective field theory treatment of $n\alpha$-scattering, see Refs. [204,205].

Halo nuclei with two valence nucleons in S-wave states are candidates for Efimov states. Such a state would also be a Borromean halo nucleus if all three pairs have negative scattering lengths and no deep 2-body bound states. Among the possible candidates for Efimov states are ^{18}C and ^{20}C, which both consist of a core nucleus with spin and parity quantum numbers $J^P = 0^+$ and two valence neutrons. The nuclei ^{17}C and ^{19}C are both expected to have $\frac{1}{2}^+$ states near threshold, implying a shallow neutron-core bound state and therefore a large neutron-core scattering length [206].

The simplest strange halo nucleus is the hypertriton, a 3-body bound state of a proton, neutron, and a strange particle called the Λ. The total binding energy is only about 2.4 MeV. The hypertriton is not Borromean, because the proton–neutron subsystem has a bound state, the deuteron. The separation energy for the Λ, $E_\Lambda = 0.13 \pm 0.05$ MeV [207,208], is tiny compared to the binding energy $E_d = 2.225$ MeV of the deuteron. The hypertriton can therefore also be considered a 2-body halo nucleus. It has been studied in both 2-body and 3-body approaches. See, e.g. Refs. [209–211] and references therein. The hypertriton has also been studied in the effective field theory for short-range interactions [212]. The scattering lengths in the $^3S_1$ NN channel and in the $^1S_0$ $N\Lambda$ channel were both assumed to be large. As in the case of the triton, the renormalization requires a 3-body parameter and involves a limit cycle. The discrete scaling factor for this case is only 10.2, roughly a factor two smaller than in the triton case.

10. Frontiers of universality

In this section, we discuss some problems at the frontiers of universality: the N-body problem for $N \geqslant 4$, higher-order effective-range corrections, and the case of a large P-wave scattering length.

10.1. The N-body problem for $N \geqslant 4$

Amado and Greenwood wrote a paper in 1972 entitled "There is no Efimov effect for four or more particles" [213]. They showed that, for $N \geqslant 4$, the tuning of the binding energy of an $(N-1)$-body bound state to zero cannot produce an infinite number of N-body bound states with an accumulation point at $E = 0$. We will refer to this result as the *Amado–Greenwood theorem*. Note that the Amado–Greenwood theorem does not forbid an infinite number of N-body bound states with an accumulation point at some energy other than zero.

The example of four identical bosons is instructive. First consider a negative scattering length at the value $a'_* < 0$ for which there is an Efimov trimer at the 3-atom threshold. The Amado–Greenwood theorem implies that there cannot be an infinite sequence of tetramers with an accumulation point at the threshold $E = 0$. Next consider a positive scattering length at the value a_* for which there is an Efimov trimer at the atom–dimer threshold and assume there are no deeper dimers or trimers. Then there is an infinite sequence of 4-body bound states with an accumulation point at the atom–dimer threshold $E = -E_{\rm D}$. This is a simple consequence of the Efimov effect and the fact that the atom–dimer scattering length $a_{\rm AD}$ diverges at $a = a_*$. If a is just a little larger than a_*, then $a_{\rm AD} \gg a$ and an Efimov trimer is essentially a 2-body bound state consisting of a dimer of size a_* and a third atom separated by a distance of order $a_{\rm AD}$. In the atom–atom–dimer system, two of the three pairs have a resonant interaction with large scattering length $a_{\rm AD}$. The atom–atom–dimer system consists of two identical bosons with mass m and a third particle with mass $2m$. Thus at the critical point where $a_{\rm AD} \to \pm\infty$, the Efimov effect produces infinitely many tetramers with discrete scaling factor 2.016×10^5. This value can be read off from Fig. 53.

Adhikari and Fonseca used the Born–Oppenheimer approximation to study the possibility of an Efimov effect in the 4-body system consisting of three identical heavy particles and one light particle with a large scattering length a between the heavy particles and the light particle [214]. They concluded that, in the resonant limit $a \to \infty$, there can be at most a finite number of 4-body bound states near the scattering threshold. This result is consistent with the Amado–Greenwood theorem.

In the 3-body problem, exact numerical solutions are facilitated by the Faddeev equations. The generalization of the Faddeev equations to the N-body problem with $N \geqslant 4$ was given by Yakubovsky [215]. He set up a system of coupled integral equations which are in unique correspondence to the N-body Schrödinger equation and have a kernel which gets connected after a finite number of iterations. An equivalent set of equations was given independently by Grassberger and Sandhas [216]. Due to the complexity of these equations, exact numerical solutions for $N = 4$ have only recently been obtained.

In nuclear physics, exact numerical solutions of the bound state problem for four nucleons interacting through a potential are now standard. (See [217,218] and references therein for more details.) The 4-nucleon scattering problem

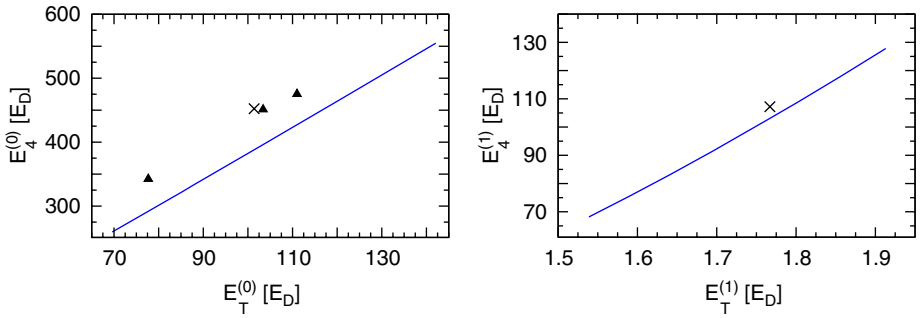

Fig. 56. Universal scaling curves for the binding energies of the ground states (left panel) and excited states (right panel) of the ^{4}He trimer and the ^{4}He tetramer. The crosses are the results for the LM2M2 potential [223]. The triangles are the results for the TTY, HFD-B, and HFDHE2 potentials [222,227]. (Figure taken from Ref. [226].)

is much more complicated and no exact numerical solution is available to date. The binding energies of the ground and excited states for nuclei up to atomic mass number $A = 10$ have been calculated using quantum Monte Carlo methods and the no-core shell model [219–221].

In molecular physics, the only numerically exact N-atom calculations for $N \geqslant 4$ that we are aware of are for ground-state binding energies. There has been a large interest in the calculation of the properties of clusters of helium atoms. The ground-state binding energies for the N-body clusters $(^4\mathrm{He})_N$ up to $N = 10$ have been calculated using the diffusion Monte Carlo method [222]. Using an approximate numerical method that combines Monte Carlo methods with the hyperspherical expansion, Blume and Greene have also calculated the binding energies of the ground state and excited states for $(^4\mathrm{He})_N$, as well as the scattering lengths for elastic $^4\mathrm{He} + (^4\mathrm{He})_{N-1}$ scattering, up to $N = 10$ [223].

An important issue in the 4-body system with a large 2-body scattering length is how many parameters are required to describe the system in the scaling limit, that is, up to corrections that decrease like $l/|a|$ as $a \to \pm\infty$. In the case of identical bosons, low-energy 4-body observables necessarily depend on the 2-body parameter a and the 3-body parameter κ_*. But are any additional 4-body parameters required? There are theoretical arguments in support of both answers to this question. There is a renormalization argument for zero-range 2-body potentials that indicates that an additional N-body parameter is required to calculate N-body binding energies for all $N \geqslant 3$ [122]. On the other hand, a power-counting argument within the effective field theory framework suggests that no additional parameters should be necessary to calculate N-body observables for $N > 3$ [224]. There is some circumstantial evidence in favor of this later possibility from the 4-body problem in nuclear physics. There is a correlation called the "Tjon line" between the binding energy E_t of the triton and the binding energy E_α of the α particle [225]. Calculations of these binding energies using modern nucleon–nucleon interaction potentials give results that underestimate both binding energies but cluster along a line in the E_t–E_α plane. By adding a 3-nucleon potential whose strength is adjusted to get the correct value for E_t, one also gets an accurate result for E_α. (See Ref. [217] for some recent calculations with modern nuclear forces.)

Platter, Hammer, and Meißner have recently studied the universal properties of the four-boson system with short-range interactions in an effective quantum mechanics approach [226]. They constructed the effective interaction potential at leading order in the large scattering length and computed the 4-body binding energies using the Yakubovsky equations. They found that cutoff independence of the 4-body binding energies does not require the introduction of a 4-body force. This suggests that 2-body and 3-body interactions are sufficient to renormalize the 4-body system. They have applied their equations to ^{4}He atoms and calculated the binding energies of the ground state and the excited state of the ^{4}He tetramer. Using the binding energy E_2 of the ^{4}He dimer as the 2-body input and the binding energy $E_3^{(1)}$ of the excited state of the ^{4}He trimer as the 3-body input, they found good agreement with the results of Blume and Greene [223].

The authors of Ref. [226] also observed a correlation between the binding energies of the ^{4}He tetramer and the ^{4}He trimer similar to the Tjon line in nuclear physics. We denote the binding energies of 4-body bound states by $E_4^{(n)}$. The universal scaling curves for the binding energies of the ground states of $(^4\mathrm{He})_4$ and $(^4\mathrm{He})_3$ and for the binding energies of the excited states of $(^4\mathrm{He})_4$ and $(^4\mathrm{He})_3$ are shown in Fig. 56. The calculations of the binding energies for modern ^{4}He potentials fall close to the universal scaling curves from the effective theory. The crosses are the results for the ground state and the excited state of the ^{4}He tetramer for the LM2M2 potential [223]. For the ground state of the

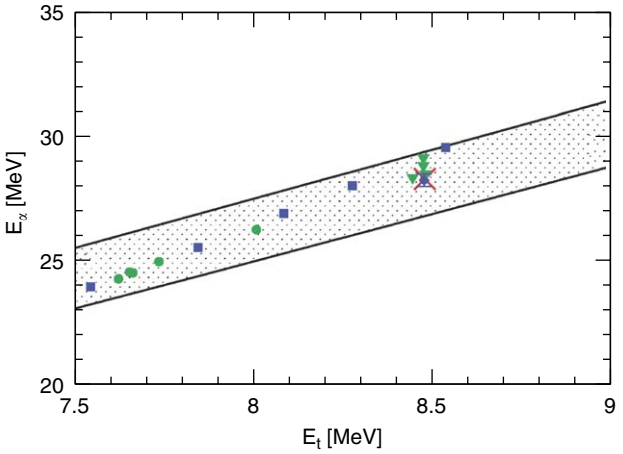

Fig. 57. The correlation between the binding energies of the triton and the α-particle. The lower (upper) line shows the leading order result using a_s and E_d (a_s and a_t) as the 2-body inputs. The data points are from calculations using various *NN* potentials with and without 3-body forces. The cross shows the experimental point. (Figure taken from Ref. [228].)

tetramer, calculations with other ^{4}He potentials are available as well. The triangles are the results for the TTY, HFD-B, and HFDHE2 potentials from Refs. [222,227]. The universal scaling curves are very close to linear over the range of binding energies relevant to ^{4}He atoms. The universal scaling curves shown in Fig. 56 are well approximated by the following linear equations [226]:

$$E_4^{(0)} \approx 4.075 E_{\rm T}^{(0)} - 24.752 E_{\rm D}, \tag{421a}$$

$$E_4^{(1)} \approx 159.4 E_{\rm T}^{(1)} - 178.0 E_{\rm D}. \tag{421b}$$

The accuracy of Eq. (421a) is better than 5% for $69 \leqslant E_{\rm T}^{(0)}/E_{\rm D} \leqslant 142$ and the accuracy of Eq. (421b) is better than 2% for $1.52 \leqslant E_{\rm T}^{(1)}/E_{\rm D} \leqslant 1.92$. These relations can be used to predict the tetramer ground and excited state energies to leading order in ℓ/a for any potential for which the dimer binding energy and one of the trimer binding energies are known.

The Tjon line for the correlation between the binding energies of the ground states of $(^4\mathrm{He})_4$ and $(^4\mathrm{He})_3$ is evident from the results of the four potentials shown in the left panel of Fig. 56. All four points are systematically above the universal scaling curve by about the same amount. If calculations of the binding energy of the excited state of $(^4\mathrm{He})_4$ were available for other potentials, they would also fall on a line parallel to the universal scaling curve for the excited states. For the LM2M2 potential, the results lie above the predictions of the universal scaling curves by 3.5% for $E_4^{(1)}$ and by 12.1% for $E_4^{(0)}$. The leading contribution to the deviations from the universal predictions are expected to come from corrections that are first order in the effective range r_s. For the shallowest 4-body bound states, the leading corrections to the universal predictions for $E_4^{(n)}$ are expected to be proportional to $E_4^{(n)} r_s/a$. The ratio of the effective-range corrections to $E_4^{(0)}$ and $E_4^{(1)}$ is then predicted to be $E_4^{(0)}/E_4^{(1)} = 3.8$. This is close to the observed ratio of the deviations from the universal predictions, which is 3.4. These results provide strong support for the hypothesis that low-energy 4-body observables in the scaling limit are completely determined by a and a single 3-body parameter.

This work was recently extended to the four-nucleon system in Ref. [228]. While the four-nucleon system is more complicated due to spin and isospin degrees of freedom, there is still only one 3-body parameter that enters at leading order in $\ell/|a|$. In Fig. 57, we show the result for the nuclear Tjon line with the spin-singlet *np* scattering length a_s and the deuteron binding energy E_d as the 2-body inputs (lower line) and the result with the *np* scattering lengths a_s and a_t as the 2-body inputs (upper line). Both lines generate a band that gives a naive estimate of higher order corrections in $\ell/|a|$. We also show some calculations using phenomenological potentials [217] and a chiral EFT potential with explicit pions [229]. The cross shows the experimental point. All calculations and the experimental point lie within the shaded area defined by the two curves. Using the triton binding energy $E_t = 8.48\,\mathrm{MeV}$ as the 3-body input, one can

obtain a prediction for the α-particle binding energy E_α. The result is $E_\alpha = 29.5\,\text{MeV}$ (26.9 MeV) if a_s and a_t (a_s and E_d) are used as 2-body input. This variation is consistent with the expected 30% accuracy of a leading order calculation in $\ell/|a|$. The results agree with the (Coulomb corrected) experimental value $E_\alpha = 29.0 \pm 0.1\,\text{MeV}$ to within 10%.

The universal result for a 4-body observable has also been calculated recently for the system consisting of a pair of identical fermions in each of two spin states. We will refer to the spin states as ↑ and ↓. If there is a large positive scattering length a between the fermions with spins ↑ and ↓, they can bind to form a shallow dimer D. The dimer is a boson and its binding energy is given by the universal formula in Eq. (62). In the low-energy limit, the scattering of a pair of these dimers is determined by the dimer–dimer scattering length a_{DD}. This 4-body observable was recently calculated independently by two different groups [165,166,230] with the result

$$a_{\text{DD}} = 0.60a. \tag{422}$$

In Ref. [165,166], the authors used the zero-range approximations and the boundary-condition method to derive an integral equation for a factor $f(\mathbf{r}, \mathbf{R})$ in the Schrödinger wave function that describes configurations in which one pair of atoms with spins ↑ and ↓ has separation $\mathbf{r}$, the other has separation $\mathbf{r}' \to 0$, and the two pairs are separated by $\mathbf{R}$. The dimer–dimer scattering length is determined by the behavior of $f(\mathbf{r}, \mathbf{R})$ as $|\mathbf{R}| \to \infty$. In Ref. [230], the authors calculated a_{DD} by solving the Yakubovsky equations for dimer–dimer scattering numerically for the system in which fermions with spins ↑ and ↓ interact through a short-range potential $V(r)$ with a large scattering length a.

If the fermions with spins ↑ and ↓ can also form deep diatomic molecules, low energy dimers can be lost from a system through dimer–dimer collisions via dimer relaxation. In the limit $a \gg \ell$, where ℓ is the natural low-energy length scale, the rate constant β_{DD} for this process scales like a power of a:

$$\beta_{\text{DD}} = B\,(a/\ell)^{-2-2v}\hbar a/m. \tag{423}$$

The coefficient B depends on the details at short distances, but the exponent of a is universal. In the dominant relaxation process, both atoms of the relaxing dimer and one of the other atoms all approach within a distance of order ℓ. Since two of these three atoms are identical fermions, we might expect the prefactor of $\hbar a/m$ in Eq. (406) to be suppressed by $(\ell/a)^2$. However, it actually scales like a^{-2-2v}, where $v = 0.773$ is an anomalous dimension [165,166]. This anomalous scaling behavior suppresses the relaxation rate when a is large.

10.2. Effective-range corrections

Corrections to the scaling limit in the 3-body system can be calculated using effective field theory. The most important correction comes from the effective range r_s. To illustrate the problems involved, we review the calculation of the range corrections to S-wave atom–dimer scattering for spinless bosons. A generalization of the STM3 integral equation in Eq. (336) that includes the effective-range correction to all orders reads

$$\begin{aligned}\mathscr{A}_S(p,k;E) = {} & 16\pi\gamma\left[\frac{1}{2pk}\ln\frac{p^2+pk+k^2-E-\mathrm{i}\epsilon}{p^2-pk+k^2-E-\mathrm{i}\epsilon}+\frac{H(\Lambda)}{\Lambda^2}\right] \\ & +\frac{4}{\pi}\int_0^\Lambda \mathrm{d}q\,q^2\left[\frac{1}{2pq}\ln\frac{p^2+pq+q^2-E-\mathrm{i}\epsilon}{p^2-pq+q^2-E-\mathrm{i}\epsilon}+\frac{H(\Lambda)}{\Lambda^2}\right] \\ & \times\left[-\gamma+\left(\frac{3}{4}q^2-E-\mathrm{i}\epsilon\right)^{1/2}-\frac{1}{2}r_s\left(\frac{3}{4}q^2-E-\gamma^2\right)\right]^{-1}\mathscr{A}_S(q,k;E),\end{aligned} \tag{424}$$

where r_s is the effective range and γ is the position of the pole in the binding momentum $(-E)^{1/2}$ of the atom–atom Green's function:

$$\gamma = \left(1-\sqrt{1-2r_s/a}\right)\frac{1}{r_s}. \tag{425}$$

If $a > 0$, γ^2 is the binding energy of the shallow dimer; if $a < 0$, $-\gamma^2$ is the energy of the shallow virtual state. In the scaling limit $r_s \to 0$, γ reduces to $1/a$. the two quantities differ if the effective range is included. We have chosen γ and r_s as our 2-body inputs instead of a and r_s, because this choice keeps the location of the dimer pole fixed which

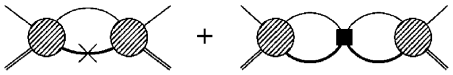

Fig. 58. Leading order range corrections. Not shown are diagrams that vanish as $\Lambda \to \infty$.

leads to a better convergence of the effective-range expansion [231]. The factor Z_D in the definition of the amplitude $\mathscr{A}_S(p,k;E)$ in Eq. (334) introduces a factor of $1-\gamma r_s$ that has been absorbed into $\mathscr{A}_S$, so that in Eq. (424) the effective range appears only in the diatom propagator. In principle one could obtain the range corrections to all orders by solving the integral equation in Eq. (424). A potential problem comes from the dimer propagator with the effective range included. In addition to the pole from the shallow dimer, it has also a deep pole. For negative effective range, the pole is on the unphysical sheet and it causes no problems. For positive effective range, the pole is on the physical sheet and it leads to problems in the solution of the integral equation.

One possible solution is to calculate the linear range correction perturbatively [62,232]. In this case, the renormalization can be carried out analytically. Writing

$$\mathscr{A}_S(q,k;E) = \mathscr{A}_{S,0}(q,k;E) + \mathscr{A}_{S,1}(q,k;E) + \cdots, \tag{426a}$$

$$H(\Lambda) = H_0(\Lambda) + H_1(\Lambda) + \cdots, \tag{426b}$$

we split the scattering amplitude into a piece of order $(\gamma r_s)^0$, a piece of order $(\gamma r_s)^1$, and higher order pieces. One can then show [232] that, up to terms that are suppressed as $\Lambda \to \infty$, $\mathscr{A}_{S,1}(q,k;E)$ is given by the diagrams shown in Fig. 58. The diagram on the left-hand side is the contribution of the effective range correction. This diagram is logarithmically divergent in the ultraviolet. Note also that the range insertion enters only on the dimer line. The second diagram is the contribution of a subleading piece of the contact 3-body force without derivatives. The 3-body force diagram is required to renormalize the ultraviolet divergence of the range correction. However, its behavior is fully determined by Λ_* as we will show in the following. Evaluation of the Feynman diagrams in Fig. 58 leads to

$$\mathscr{A}_{S,1}(k,k;E) = \frac{r_s}{4\pi^2}\int_0^\Lambda \frac{\mathrm{d}q\, q^2 \mathscr{A}_{S,0}^2(q,k;E)}{-\gamma+\sqrt{3q^2/4-E}} + \frac{1}{\pi^3\gamma}\frac{H_1(\Lambda)}{\Lambda^2}\left[\int_0^\Lambda \frac{\mathrm{d}q\, q^2 \mathscr{A}_{S,0}(q,k;E)}{-\gamma+\sqrt{3q^2/4-E}}\right]^2, \tag{427}$$

where we have set $p=k$ for simplicity. The high-q behavior of the off-shell amplitude $\mathscr{A}_{S,0}(q,k;E)$ is known exactly:

$$\mathscr{A}_{S,0}(q,k;E) \longrightarrow \frac{\mathscr{N}(k,E)}{q}\cos[s_0\ln(q/\Lambda_*)+\delta], \tag{428}$$

where δ is a phase that depends only on γ/Λ_*. The important point is that the dependences on k and E and on q factorize for large q. The ultraviolet divergent piece of the two diagrams can therefore be written as

$$\delta\mathscr{A}_{S,1}^{(\mathrm{div})} = \mathscr{N}(k,E)^2\left(\frac{r_s}{2\sqrt{3}\pi^2}\int^\Lambda \frac{\mathrm{d}q}{q}\cos^2[s_0\ln(q/\Lambda_*)+\delta] + \frac{4}{3\pi^3\gamma}\frac{H_1(\Lambda)}{\Lambda^2}\left[\int^\Lambda \mathrm{d}q\,\cos[s_0\ln(q/\Lambda_*)+\delta]\right]^2\right), \tag{429}$$

where the (hidden) lower integration bound is large compared to k but otherwise arbitrary. Since the energy dependent term $\mathscr{N}(k,E)^2$ factorizes, the linear range correction can be renormalized by adjusting $H_1(\Lambda)$ so that there is a cancellation of the terms of order Λ^0 in Eq. (429). Thus $H_1(\Lambda)$ is fully determined by the effective range r_s and the leading order parameters γ and Λ_*. The asymptotic phase δ can be extracted from the leading order solution. No new 3-body parameter enters at this order.

Another way to calculate the range corrections is to expand the dimer propagator in Eq. (424) to linear order in r_s and solve the corresponding integral equation [180]. This approach resums a selected class of (small) higher-order effective-range contributions. The renormalization can no longer be carried out analytically and a small cutoff dependence remains. However, this cutoff dependence can be used to estimate the errors from higher order corrections

by varying the cutoff over a natural range of values. Furthermore, this approach can be more easily extended to higher orders. The systematics of higher-order power corrections and 3-body forces has been discussed in Refs. [180,184] and we refer the reader to these papers for more details. A general classification of 3-body forces using renormalization group techniques has recently been given in Refs. [65,192]. Afnan and Phillips [233] have used a subtraction method suggested in Ref. [92] to obtain a renormalized equation that includes the range corrections. They first solve a subtracted integral equation for the half-off-shell amplitude $\mathscr{A}_S$ at threshold. Then they use this result to derive the full-off-shell amplitude at threshold which determines the physical scattering amplitude at all energies. Due to the subtraction, the 3-body force term drops out of the equations butt one still requires a 3-body datum to fix the subtraction constant.

To our knowledge, explicit calculations of the range corrections have to date only been carried out for nuclear systems. For the spin-quartet S-wave channel (because of the Pauli principle) and generally for channels with $L \geqslant 1$ (because of the angular momentum barrier), no 3-body parameter enters in the first three orders and the 3-body calculations are straightforward. The second-order range corrections to the scattering length [154] and the phase shift [175] in the spin-quartet S-wave neutron–deuteron channel have been calculated using effective field theory. The range corrections to the higher partial waves in neutron–deuteron scattering were calculated in Ref. [193]. The spin-doublet S-wave channel has the same structure as the case of spinless bosons discussed above. A 3-body parameter is required at leading order. The first-order range correction to the spin-doublet S-wave neutron–deuteron scattering length $a_{\rm nd}^{(1/2)}$ is naively infinite and cannot be calculated without renormalization. Efimov and Tkachenko showed that the corrections to the triton binding energy contain the same infinity and they derived the linear range correction to the Phillips line which is manifestly finite [181–183]. This correction slightly shifts the Phillips line and moves it closer to the potential model points (cf. Fig. 54). The linear range corrections have also been calculated by Efimov [174,234]. The linear range corrections for spin-doublet S-wave neutron–deuteron scattering at finite energy were first calculated perturbatively in Ref. [232]. (See Ref. [233] for a calculation using the subtraction method.) In the EFT counting, this corresponds to a next-to-leading order (NLO) calculation. No new 3-body parameter was required at this order. The first calculation to next-to-next-to-leading order ($\mathrm{N^2LO}$) was carried out in Ref. [180]. At this order both the quadratic range corrections and a second 3-body parameter contribute. Due to the second 3-body parameter there is no universal Phillips line at this order. For the linear range corrections, the methods of Refs. [232,180,233] agree very well.

A thorough analysis of the power-law corrections near the RG limit cycle has been carried out for the Glazek–Wilson model [55], a discrete Hamiltonian model described in Section 3.4. The renormalization group flow was linearized around the limit cycle, as in Eq. (50), and the complete set of eigenvectors of the linearized RG flow was deduced. The model has no relevant operators, a single marginal operator that corresponds to flow along the limit cycle, and infinitely many irrelevant operators. The critical exponents for the irrelevant operators are all integers. An important general feature of RG limit cycles was established in Ref. [55]: although the irrelevant operators may vary with the phase around the limit cycle, their critical exponents must be constants independent of that phase.

10.3. Large P-wave scattering length

The phase shifts for higher partial waves have effective-range expansions analogous to the expansion for the S-wave phase shift in Eq. (15). If the leading term in the effective-range expansion for a higher partial wave is unnaturally large, it can also lead to universal low-energy behavior. The simplest such case is a large P-wave scattering length. The $L = 1$ contribution to the atom–atom scattering amplitude in Eq. (12) can be written as

$$f_k^{L=1}(\theta) = \frac{3k^2 \cos\theta}{k^3 \cot\delta_1(k) - \mathrm{i}k^3}. \tag{430}$$

The effective-range expansion for the P-wave phase shift can be written in a form analogous to that for the S-wave phase shift in (15):

$$k^3 \cot\delta_1(k) = -1/a_p + \tfrac{1}{2} r_p k^2 + \cdots, \tag{431}$$

which defines the *P-wave scattering length* a_p and the *P-wave effective range* r_p. Dimensional analysis shows that a_p has dimensions of volume while r_p has dimensions of inverse length. For simplicity, however, we will still refer to a_p and r_p as a scattering length and an effective range.

Large P-wave scattering lengths are relevant to some halo nuclei. An example is the ^{6}He nucleus. A P-wave resonance in $n\alpha$ scattering, where n is a neutron and α is the ^{4}He nucleus, plays an important role in the binding of ^{6}He. The

resonance produces a large scattering length in the $P_{3/2}$ channel corresponding to total angular momentum quantum number $\frac{3}{2}$.

The effects of the large P-wave scattering length have been treated using two different scenarios. In one scenario, the P-wave scattering length a_p was assumed to be unnaturally large, while r_p and the coefficients of higher terms in the effective-range expansion in Eq. (431) were assumed to have natural values. In this scenario, which requires a single fine-tuning, the unitarity term ik^3 in the denominator in Eq. (430) can be neglected at leading order. This scenario has been applied to $n\alpha$ scattering close to threshold [205]. In the other scenario, both a_p and r_p were assumed to be unnaturally large [204]. In this scenario, which requires a double fine tuning, the unitarity term ik^3 in the denominator in Eq. (430) generates a rich pole structure in the complex energy plane. This scenario has also been applied to $n\alpha$ scattering [204]. Which of these scenarios is most useful for a given system with a large P-wave scattering length depends on the scales of the system under consideration. For more details, we refer the reader to Refs. [204,205].

Suno, Esry, and Greene have studied 3-body recombination in a system consisting of three identical fermions with a large P-wave scattering length [235]. The recombination was into deep molecules bound by the P-wave potential between two identical fermions. The rate of decrease in the number densities of low-energy fermions from the 3-body recombination process has the form

$$\frac{\mathrm{d}}{\mathrm{d}t}n = -3\alpha\langle\epsilon^2\rangle n^3, \tag{432}$$

where $\langle\epsilon^2\rangle$ is the average of the square of the kinetic energy of the fermions. If the event rate constant α is completely determined by the large P-wave scattering length, it should have the scaling behavior $ma_p^{8/3}/\hbar^3$. This scaling behavior was observed in some of their numerical calculations.

10.4. Scattering models

One might wish to be able to calculate N-body observables for particles with large scattering lengths from first principles. However, for $N \geqslant 3$, this is prohibitively difficult for any physical system. Even for ^{4}He atoms, where the fundamental starting point can be taken as the electrodynamics of electrons and ^{4}He nuclei, the most accurate 3-body calculations proceed through the intermediate step of constructing a potential model for the interaction between two ^{4}He atoms. Calculations from first principles in the sector consisting of two ^{4}He atoms are used as inputs in the construction of the potential. Calculations of 3-body observables are then carried out by solving the 3-body Schrödinger equation for this model potential. For more complicated particles, such as alkali atoms which have dozens of electrons, even the calculation of 2-body observables from first principles is prohibitively difficult.

Since the low-energy behavior of particles with large scattering lengths is insensitive to the details of their interactions at short distances, the potential provides an inefficient encoding of the relevant physics. The sensitivity to short distances enters primarily through the scattering length and other constants that describe low-energy scattering. This motivates a more phenomenological approach in which the interactions are described by a *scattering model*, which can be specified by a parameterization of low-energy scattering amplitudes. The parameters of the scattering model can be treated as phenomenological parameters that can be tuned to reproduce the observed low-energy observables of the 2-body system. If S-wave interactions dominate, the scattering model is conveniently expressed as a parameterization of $k\cot\delta_0(k)$, where $\delta_0(k)$ is the S-wave phase shift.

For particles that interact through a short-range potential, the effective-range expansion can be used to define a sequence of increasingly accurate scattering models. The first few models in the sequence are given by

$$k\cot\delta_0(k) = -1/a, \tag{433a}$$
$$= -1/a + \tfrac{1}{2}r_s k^2, \tag{433b}$$
$$= -1/a + \tfrac{1}{2}r_s k^2 - \tfrac{1}{4}P_s k^4. \tag{433c}$$

The model in Eq. (433a) is called the *zero-range model*. This model is a good starting point for describing the interactions between two distinguishable particles or two identical bosons. Since all higher coefficients in the effective-range expansion have been set to zero, this model is by definition the scaling limit. The model in Eq. (433b) is called *effective-range theory*. For two distinguishable particles, the leading term in the P-wave phase shift in Eq. (431) may be equally important. Effective-range theory includes effective-range corrections proportional to r_s/a. It also includes

corrections that are higher order in r_s/a to all orders. For example, if $a > 0$, the binding energy of the shallow dimer is given by Eq. (77), and if $r_s > 0$, the model includes a deep 2-body bound state whose binding energy is given approximately by Eq. (79). For particles that interact through a short-range potential, the model in Eq. (433c) provides an even more accurate description of S-wave interactions at low energies. Unfortunately this is not true for real atoms, because the potential at long distance has a van der Waals tail that falls off like $1/r^6$. As a consequence, all the higher partial waves give contributions to the scattering amplitude proportional to k^4.

Each of the models specified by Eqs. (433a)–(433c) will exhibit universal low-energy behavior as the scattering length a is tuned to $\pm\infty$. Low-energy 3-body observables in this limit will approach functions of a and the 3-body parameters κ_* and η_*. In the zero-range model, there is universal behavior for all a. The parameters κ_* and η_* enter through ambiguities in the solutions of integral equations that determine 3-body observables. In effective-range theory, universal behavior appears when $|a| \gg |r_s|$. Since r_s is the only dimensionful parameter that remains when $a = \pm\infty$, the 3-body parameter κ_* must have the form $\kappa_* = A/r_s$, where A is a numerical constant that is only defined modulo multiplicative factors of e^{π/s_0}. As described below, the constant A has been calculated for the case $r_s < 0$. In this case, the model has no deep 2-body bound states, so $\eta_* = 0$. If $r_s > 0$, the effective-range theory has a single deep 2-body bound state, so η_* is nonzero. It is expected to have the form $\eta_* = B\kappa_*/r_s$, where B is a numerical constant.

For an atom near a Feshbach resonance, the scattering length $a(B)$ as a function of the magnetic field B can be approximated by Eq. (34). The effective range $r_s(B)$ of the atoms is also a function of the magnetic field. As long as $|a(B)|$ is large compared to the natural low-energy length scale $\ell_{\rm vdW}$, the few-body system can be approximated by the zero-range model defined by (433a) with the parameter a replaced by $a(B)$. A more accurate approximation is the effective-range theory defined by Eq. (433c), with the parameters a and r_s replaced by $a(B)$ and $r_s(B)$.

An even more accurate description of atoms near a Feshbach resonance can be obtained by using a scattering model that describes more accurately the physics responsible for the Feshbach resonance. If the resonance arises from weak coupling to a closed channel in which there is a diatomic molecule extremely close to the atom–atom threshold, the interactions can be approximated by the *resonance model* [236]. This model, which has three parameters, can be defined by

$$k \cot \delta_0(k) = -\left[\lambda + \frac{g^2}{k^2 - \nu}\right]^{-1}. \tag{434}$$

The scattering length is

$$a = \lambda - g^2/\nu. \tag{435}$$

The dependence of the approximation in Eq. (34) on the magnetic field can be reproduced by taking λ and g to be independent of B and ν to be linear in $B - B_{\rm res}$. Thus λ can be identified with the off-resonant scattering length, g is the strength of the coupling to the closed channel, and ν is proportional to the detuning energy of the molecule in the closed channel with respect to the atom–atom threshold. The resonance model will exhibit universal behavior as ν is tuned to zero, which corresponds to tuning B to $B_{\rm res}$. Three-body observables will approach universal functions of a, the 3-body parameter κ_*, which is a function of λ and g, and the 3-body parameter η_*, which is a function of the dimensionless combination λg^2.

Three-body observables have been calculated in a scattering model that is a special case of the resonance model [237]. The model is defined by

$$k \cot \delta_0(k) = -1/a - R_* k^2, \tag{436}$$

where R_* is a positive parameter. Comparing with Eq. (434), we see that this is just the resonance model with the background scattering length set to 0. The parameter g and ν are given by $a = -g^2/\nu$ and $R_* = -1/g^2$. This model is also identical to the effective-range theory defined by Eq. (433b) with a negative effective range: $r_s = -2R_*$. The atom–dimer scattering length $a_{\rm AD}$ and the 3-body recombination rate constant α have been calculated in this model as functions of a and R_* [237]. For $a \gg R_*$, they have the universal behavior given in Eqs. (216) and (228). The 3-body parameter κ_* was determined in Ref. [237] to be

$$s_0 \ln(\kappa_*) = s_0 \ln(2.5/R_*) \bmod \pi. \tag{437}$$

The cross-over to the universal behavior occurs when a is comparable to R_*. The first divergence of the atom–dimer scattering length occurs when $a = 0.45R_*$. This marks the emergence of the first Efimov state below the atom–dimer threshold. The second and higher divergences of $a_{\rm AD}$ occur at values of a that are well-approximated by the universal predictions: $a = (e^{\pi/s_0})^n\, 0.64\, R_*$, $n = 1, 2, ...$, where $e^{\pi/s_0} \approx 22.7$. The first zero of the recombination rate constant occurs at $a = 3.3R_*$. The second and higher zeroes occur at values of a that are well approximated by the universal predictions: $a = (e^{\pi s_0})^n\, 2.9\, R_*$, $n = 1, 2, ...$.

Acknowledgments

We thank J.O. Andersen, P.F. Bedaque, V. Efimov, B. Esry, U. van Kolck, J. Macek, and K.G. Wilson for comments on the manuscript. E.B. is thankful for the hospitality of Nordita, Fermilab, the Aspen Center for Physics, the Kavli Institute for Theoretical Physics, and the Institute for Nuclear Theory, where parts of this review were written. H.W.H. is thankful for the hospitality of the Ohio State University, where parts of this review were written. This research was supported in part by DOE grants DE-FG02-91-ER4069, DE-FG02-00ER41132, and DE-FG02-05ER15715 and by NSF grant PHY-0098645.

References

[1] J.O. Andersen, Theory of the weakly interacting Bose gas, Rev. Mod. Phys. 76 (2004) 599 [arXiv:cond-mat/0305138].
[2] N.M. Hugenholtz, D. Pines, Ground-state energy and excitation spectrum of a system of interacting bosons, Phys. Rev. 116 (1959) 489.
[3] E. Braaten, H.-W. Hammer, S. Hermans, Nonuniversal effects in the homogeneous Bose gas, Phys. Rev. A 63 (2001) 063609 [arXiv:cond-mat/0012043].
[4] V. Efimov, Energy levels arising from resonant two-body forces in a three-body system, Phys. Lett. 33B (1970) 563.
[5] G.V. Skorniakov, K.A. Ter-Martirosian, Three body problem for short range forces 1. Scattering of low energy neutrons by deuterons, Sov. Phys. JETP 4 (1957) 648 [J. Exptl. Theoret. Phys. (U.S.S.R.) 31 (1956) 775].
[6] G.S. Danilov, On the three-body problem with short-range forces, Sov. Phys. JETP 13 (1961) 349 [J. Exptl. Theoret. Phys. (U.S.S.R.) 40 (1961) 498].
[7] R.G. Newton, Scattering Theory of Waves and Particles, Springer, Berlin, 1982.
[8] J.J. Sakurai, Modern Quantum Mechanics, Addison-Wesley, Reading, MA, 1985.
[9] J. Dalibard, Collisional dynamics of ultra-cold atomic gases, in: M. Inguscio, S. Stringari, C.E. Wieman (Eds.), Bose–Einstein Condensation in Gases, IOS Press, Amsterdam, 1999, pp. 321–349.
[10] D.J. Heinzen, Ultra-cold atomic interactions, in: M. Inguscio, S. Stringari, C.E. Wieman (Eds.), Bose–Einstein Condensation in Gases, IOS Press, Amsterdam, 1999, pp. 351–389.
[11] J. Schwinger, A variational principle for scattering problems, Phys. Rev. 72 (1947) 742.
[12] L.D. Landau, E.M. Lifshitz, Quantum Mechanics, Pergamon, New York, 1980.
[13] G.F. Gribakin, V.V. Flambaum, Calculation of the scattering length in atomic collisions using the semiclassical approximation, Phys. Rev. A 48 (1993) 546.
[14] V.V. Flambaum, G.F. Gribakin, C. Harabati, Analytic calculation of cold-atom scattering, Phys. Rev. A 59 (1999) 1998.
[15] Z.-C. Yan, J.F. Babb, A. Dalgarno, G.W.F. Drake, Variational calculations of dispersion coefficients for interactions among H, He, and Li atoms, Phys. Rev. A 54 (1996) 2824.
[16] A.R. Janzen, R.A. Aziz, Modern He–He potentials: another look at binding energy, effective range theory, retardation, and Efimov states, J. Chem. Phys. 103 (1995) 9626.
[17] R.E. Grisenti, W. Schöllkopf, J.P. Toennies, G.C. Hegerfeldt, T. Köhler, M. Stoll, Determining the bond length and binding energy of the helium dimer by diffraction from a transmission grating, Phys. Rev. Lett. 85 (2000) 2284.
[18] R.A. Aziz, M.J. Slaman, An examination of ab initio results for the helium potential energy curve, J. Chem. Phys. 94 (1991) 8047.
[19] K.T. Tang, J.P. Toennies, C.L. Yiu, Accurate analytical He–He van der Waals potential based on perturbation theory, Phys. Rev. Lett. 74 (1995) 1546.
[20] D. Blume, B.D. Esry, C.H. Greene, N.N. Klausen, G.J. Hanna, Formation of atomic tritium clusters and Bose–Einstein condensates, Phys. Rev. Lett. 89 (2002) 163402 [arXiv:physics/0207002].
[21] C.J. Williams, P.S. Julienne, Mass effects in the theoretical determination of nuclear-spin relaxation rates for atomic hydrogen and deuterium, Phys. Rev. A 47 (1993) 1524.
[22] T. Loftus, C.A. Regal, C. Ticknor, J.L. Bohn, D.S. Jin, Resonant control of elastic collisions in an optically trapped fermi gas of atoms, Phys. Rev. Lett. 88 (2002) 173201.
[23] E.G.M. van Kempen, S.J.J.M.F. Kokkelmans, D.J. Heinzen, B.J. Verhaar, Interisotope determination of ultracold rubidium interactions from three high-precision experiments, Phys. Rev. Lett. 88 (2002) 093201.
[24] P.J. Leo, C.J. Williams, P.S. Julienne, Collision properties of ultracold 133Cs atoms, Phys. Rev. Lett. 85 (2000) 2721.
[25] A. Derevianko, W.R. Johnson, M.S. Safronova, J.F. Babb, High-precision calculations of dispersion coefficients, static dipole polarizabilities, and atom–wall interaction constants for alkali–metal atoms, Phys. Rev. Lett. 82 (1999) 3589.
[26] H. Feshbach, A unified theory of nuclear reactions. II, Ann. Phys. 19 (1962) 287.

[27] E. Tiesinga, A.J. Moerdijk, B.J. Verhaar, H.T.C. Stoof, Conditions for Bose–Einstein condensation in magnetically trapped atomic cesium, Phys. Rev. A 46 (1992) R1167.
[28] E. Tiesinga, B.J. Verhaar, H.T.C. Stoof, Threshold and resonance phenomena in ultracold ground-state collisions, Phys. Rev. A 47 (1993) 4114.
[29] S. Inouye, M.R. Andrews, J. Stenger, H.-J. Miesner, D.M. Stamper-Kurn, W. Ketterle, Observation of feshbach resonances in a Bose–Einstein condensate, Nature 392 (1998) 151.
[30] Ph. Courteille, R.S. Freeland, D.J. Heinzen, F.A. van Abeelen, B.J. Verhaar, Observation of a feshbach resonance in cold atom scattering, Phys. Rev. Lett. 81 (1998) 69.
[31] J.L. Roberts, N.R. Claussen, J.P. Burke Jr., C.H. Greene, E.A. Cornell, C.E. Wieman, Resonant magnetic field control of elastic scattering in cold 85Rb, Phys. Rev. Lett. 81 (1998) 5109.
[32] V. Efimov, Is a qualitative approach to the three-body problem useful?, Comm. Nucl. Part. Phys. 19 (1990) 271.
[33] S.K. Choi, et al., [Belle Collaboration], Observation of a new narrow charmonium state in exclusive $B^{\pm} \to K^{\pm}\pi^{+}\pi^{-} J/\psi$ decays, Phys. Rev. Lett. 91 (2003) 262001 [arXiv:hep-ex/0309032].
[34] N.A. Tornqvist, Possible large deuteron—like meson meson states bound by pions, Phys. Rev. Lett. 67 (1991) 556.
[35] M.B. Voloshin, Interference and binding effects in decays of possible molecular component of X(3872), Phys. Lett. B 579 (2004) 316 [arXiv:hep-ph/0309307].
[36] E. Braaten, M. Kusunoki, Low-energy universality and the new charmonium resonance at 3870-MeV, Phys. Rev. D 69 (2004) 074005 [arXiv:hep-ph/0311147].
[37] L.H. Thomas, The interaction between a neutron and a proton and the structure of H^3, Phys. Rev. 47 (1935) 903.
[38] R.D. Amado, J.V. Noble, On Efimov's effect: a new pathology of three-particle systems, Phys. Lett. 35B (1971) 25.
[39] R.D. Amado, J.V. Noble, Efimov's effect: a new pathology of three-particle systems. II, Phys. Rev. D 5 (1972) 1992.
[40] S.K. Adhikari, A. Delfino, T. Frederico, I.D. Goldman, L. Tomio, Efimov and Thomas effects and the model dependence of three-particle observables in two and three dimensions, Phys. Rev. A 37 (1988) 3666.
[41] V. Efimov, Weakly-bound states of three resonantly-interacting particles, Sov. J. Nucl. Phys. 12 (1971) 589 [Yad. Fiz. 12 (1970) 1080].
[42] V. Efimov, Low-energy properties of three resonantly-interacting particles, Sov. J. Nucl. Phys. 29 (1979) 546 [Yad. Fiz. 29 (1979) 1058].
[43] I.V. Simenog, A.I. Sitnichenko, Effect of long-range interaction in a three-body system with short-range forces, Doklady Academy of Sciences of the Ukrainian SSR (in Russian), Ser. A, vol. 11, 1981, p. 74.
[44] T. Frederico, L. Tomio, A. Delfino, A.E.A. Amorim, Scaling limit of weakly bound triatomic states, Phys. Rev. A 60 (1999) R9.
[45] R.A. Minlos, L.D. Faddeev, On the point interaction for a three-particle system in quantum mechanics, Sov. Phys. Doklady 6 (1962) 1072 [Doklady Akademii Nauk SSR 141 (1961) 1335].
[46] R.A. Minlos, L.D. Faddeev, Comment on the problem of three particles with point interactions, Sov. Phys. JETP 14 (1962) 1315 [J. Exptl. Theoret. Phys. (U.S.S.R.) 41 (1961) 1850].
[47] M.E. Fisher, Renormalization group theory: its basis and formulation in statistical physics, Rev. Mod. Phys. 70 (1998) 653.
[48] K.G. Wilson, The renormalization group and critical phenomena, Rev. Mod. Phys. 55 (1983) 583.
[49] K.G. Wilson, The renormalization group and strong interactions, Phys. Rev. D 3 (1971) 1818.
[50] D.J. Gross, F. Wilczek, Ultraviolet behavior of non-abelian gauge theories, Phys. Rev. Lett. 30 (1973) 1343.
[51] H.D. Politzer, Reliable perturbative results for strong interactions?, Phys. Rev. Lett. 30 (1973) 1346.
[52] E. Braaten, H.-W. Hammer, An infrared renormalization group limit cycle in QCD, Phys. Rev. Lett. 91 (2003) 102002 [arXiv:nucl-th/0303038].
[53] D. Sornette, Discrete scale invariance and complex dimensions, Phys. Rep. 297 (1998) 239 [arXiv:cond-mat/9707012].
[54] S.D. Glazek, K.G. Wilson, Limit cycles in quantum theories, Phys. Rev. Lett. 89 (2002) 230401 [Erratum-ibid. 92 (2004) 139901].
[55] S.D. Glazek, K.G. Wilson, Universality, marginal operators, and limit cycles, Phys. Rev. B 69 (2004) 094304 [arXiv:cond-mat/0303297].
[56] A. Leclair, J.M. Roman, G. Sierra, Russian doll renormalization group and superconductivity, Phys. Rev. B 69 (2004) 020505 [arXiv:cond-mat/0211338].
[57] A. Leclair, J.M. Roman, G. Sierra, Russian doll renormalization group, Kosterlitz–Thouless flows, and the cyclic sine-Gordon model, Nucl. Phys. B 675 (2003) 584 [arXiv:hep-th/0301042].
[58] A. LeClair, J.M. Roman, G. Sierra, Log-periodic behavior of finite size effects in field theories with RG limit cycles, Nucl. Phys. B 700 (2004) 407 [arXiv:hep-th/0312141].
[59] A. LeClair, G. Sierra, Renormalization group limit-cycles and field theories for elliptic S-matrices, JSTAT 0408 (2004) P004 [arXiv:hep-th/0403178].
[60] S. Albeverio, R. Hoegh-Krohn, T.S. Wu, A class of exactly solvable three-body quantum mechanical problems and the universal low-energy behavior, Phys. Lett. 83A (1981) 105.
[61] P.F. Bedaque, H.-W. Hammer, U. van Kolck, Renormalization of the three-body system with short-range interactions, Phys. Rev. Lett. 82 (1999) 463 [arXiv:nucl-th/9809025].
[62] P.F. Bedaque, H.-W. Hammer, U. van Kolck, The three-boson system with short-range interactions, Nucl. Phys. A 646 (1999) 444 [arXiv:nucl-th/9811046].
[63] T. Barford, The renormalisation group and applications in few-body physics, Ph.D. Thesis, University of Manchester, 2004, [arXiv:nucl-th/0404072].
[64] T. Barford, M.C. Birse, Effective theories of scattering with an attractive inverse-square potential and the three-body problem, J. Phys. A 38 (2005) 697 [arXiv:nucl-th/0406008].
[65] H.W. Grießhammer, Naive dimensional analysis for three-body forces without pions, Nucl. Phys. A 760 (2005) 110 [arXiv:nucl-th/0502039].
[66] R.F. Mohr, R.J. Furnstahl, R.J. Perry, K.G. Wilson, H.-W. Hammer, Precise numerical results for limit cycles in the quantum three-body problem, Ann. Phys. 321 (2006) 225 [arXiv:nucl-th/0509076].

[67] J.M. Blatt, On the neutron–proton force, Phys. Rev. 74 (1948) 92.
[68] H.A. Bethe, Theory of the effective range in nuclear scattering, Phys. Rev. 76 (1949) 38.
[69] U. van Kolck, Effective field theory of short-range forces, Nucl. Phys. A 645 (1999) 273 [arXiv:nucl-th/9808007].
[70] H.A. Bethe, R. Peierls, Quantum theory of the diplon, Proc. Roy. Soc. A 148 (1935) 146.
[71] H.A. Bethe, R. Peierls, The scattering of neutrons and protons, Proc. Roy. Soc. A 149 (1935) 176.
[72] G. Breit, The scattering of slow neutrons by bound protons. I. Methods of calculation, Phys. Rev. 71 (1947) 215.
[73] K. Huang, C.N. Yang, Quantum-mechanical many-body problem with hard-sphere interaction, Phys. Rev. 105 (1957) 767.
[74] S.R. Beane, P.F. Bedaque, W.C. Haxton, D.R. Phillips, M.J. Savage, From hadrons to nuclei: crossing the border, in: M. Shifman (Ed.), At the Frontier of Particle Physics, vol. 1, World Scientific, Singapore, 2001[arXiv:nucl-th/0008064].
[75] P.F. Bedaque, U. van Kolck, Effective field theory for few-nucleon systems, Ann. Rev. Nucl. Part. Sci. 52 (2002) 339 [arXiv:nucl-th/0203055].
[76] E. Nielsen, D.V. Fedorov, A.S. Jensen, E. Garrido, The three-body problem with short-range interactions, Phys. Rep. 347 (2001) 373.
[77] L.M. Delves, Tertiary and general-order collisions. II, Nucl. Phys. 20 (1960) 275.
[78] J.H. Macek, Properties of autoionizing states of He, J. Phys. B 1 (1968) 831.
[79] A.F. Starace, G.L. Webster, Atomic hydrogen in a uniform magnetic field: low-lying energy levels for fields below 109 G, Phys. Rev. A 19 (1979) 1629.
[80] D.V. Fedorov, A.S. Jensen, Efimov effect in coordinate space Faddeev equations, Phys. Rev. Lett. 71 (1993) 4103.
[81] W. Glöckle, The quantum mechanical few-body problem, Springer, Berlin, 1983.
[82] L.D. Faddeev, Scattering theory for a three particle system, Sov. Phys. JETP 12 (1961) 1014 [Zh. Eksp. Teor. Fiz. 39 (1960) 1459].
[83] G. Gasaneo, J.H. Macek, Hyperspherical adiabatic eigenvalues for zero-range potentials, J. Phys. B 35 (2002) 2239.
[84] Z. Zhen, J. Macek, Loosely bound states of three particles, Phys. Rev. A 38 (1988) 1193.
[85] G.N.J. Ananos, H.E. Camblong, C. Gorrichategui, E. Hernadez, C.R. Ordonez, Phys. Rev. D 67 (2003) 045018 [arXiv:hep-th/0205191].
[86] J. Macek, Loosely bound states of three particles, Z. Phys. D 3 (1986) 31.
[87] E. Braaten, H.-W. Hammer, M. Kusunoki, Universal equation for Efimov states, Phys. Rev. A 67 (2003) 022505 [arXiv:cond-mat/0201281].
[88] R.F. Mohr, Quantum mechanical three-body problem with short-range interactions, Ph.D. Thesis, The Ohio State University, 2003 [arXiv:nucl-th/0306086].
[89] R.F. Mohr, unpublished.
[90] E. Braaten, H.-W. Hammer, Universality in the three-body problem for ^{4}He atoms, Phys. Rev. A 67 (2003) 042706 [arXiv:cond-mat/0203421].
[91] I.V. Simenog, D.V. Shapoval, Limiting model-independent relations between the parameters of a three-particle system, Sov. J. Nucl. Phys. 43 (1986) 352 [Yad. Fiz. 43 (1986) 554].
[92] H.-W. Hammer, T. Mehen, A renormalized equation for the three-body system with short-range interactions, Nucl. Phys. A 690 (2001) 535 [arXiv:nucl-th/0011024].
[93] J.H. Macek, S. Ovchinnikov, G. Gasaneo, Exact solution for boson–diboson elastic scattering at zero energy in the shape independent model, Phys. Rev. A 72 (2005) 032709.
[94] Yu. Kagan, B.V. Svistunov, G.V. Shlyapnikov, Effect of Bose condensation on inelastic processes in gases, JETP Lett. 42 (1985) 209.
[95] E.A. Burt, R.W. Ghrist, C.J. Myatt, M.J. Holland, E.A. Cornell, C.E. Wieman, Coherence, correlations, and collisions: what one learns about Bose–Einstein condensates from their decay, Phys. Rev. Lett. 79 (1997) 337.
[96] D. Petrov, Three-boson problem near a narrow Feshbach resonance, talk at the Workshop on Strongly Interacting Quantum Gases, Ohio State University, April 2005 (http://octs.osu.edu/images/Gases/Talks/Petrov.pdf).
[97] E. Nielsen, J.H. Macek, Low-energy recombination of identical bosons by three-body collisions, Phys. Rev. Lett. 83 (1999) 1566.
[98] B.D. Esry, C.H. Greene, J.P. Burke, Recombination of three atoms in the ultracold limit, Phys. Rev. Lett. 83 (1999) 1751.
[99] P.F. Bedaque, E. Braaten, H.-W. Hammer, Three-body recombination in Bose gases with large scattering length, Phys. Rev. Lett. 85 (2000) 908 [arXiv:cond-mat/0002365].
[100] P.O. Fedichev, M.W. Reynolds, G.V. Shlyapnikov, Three-body recombination of ultracold atoms to a weakly bound *s* level, Phys. Rev. Lett. 77 (1996) 2921.
[101] T. Weber, J. Herbig, M. Mark, H.-C. Nägerl, R. Grimm, Three-body recombination at large scattering lengths in an ultracold atomic gas, Phys. Rev. Lett. 91 (2003) 123201.
[102] J.P. D'Incao, H. Suno, B.D. Esry, Limits on universality in ultracold three-boson recombination, Phys. Rev. Lett. 93 (2004) 123201.
[103] R.D. Amado, M.H. Rubin, Low-energy expansion for elastic three-body scattering, Phys. Rev. Lett. 25 (1970) 194.
[104] E. Braaten, A. Nieto, Quantum corrections to the energy density of a homogenous Bose gas, Eur. Phys. J. B 11 (1999) 143.
[105] E. Braaten, H.-W. Hammer, T. Mehen, The dilute Bose–Einstein condensate with large scattering length, Phys. Rev. Lett. 88 (2002) 040401 [arXiv:cond-mat/0108380].
[106] T.D. Lee, C.N. Yang, Many-body problem in quantum mechanics and quantum statistical mechanics, Phys. Rev. 105 (1957) 1119.
[107] T.T. Wu, Ground state of a Bose system of hard spheres, Phys. Rev. 115 (1959) 1390.
[108] N.M. Hugenholtz, D. Pines, Ground-state energy and excitation spectrum of a system of interacting bosons, Phys. Rev. 116 (1959) 489.
[109] K. Sawada, Ground-state energy of Bose–Einstein gas with repulsive interaction, Phys. Rev. 116 (1959) 1344.
[110] F. Luo, G.C. McBane, G. Kim, C.F. Giese, W.R. Gentry, The weakest bond: experimental observation of helium dimer, J. Chem. Phys. 98 (1993) 3564–3567.
[111] E. Nielsen, D.V. Fedorov, A.S. Jensen, The structure of the atomic helium trimers: halos and Efimov states, J. Phys. B 31 (1998) 4085.
[112] V. Roudnev, S. Yakovlev, Investigation of $^4He_3$ trimer on the base of Faddeev equations in configuration space, Chem. Phys. Lett. 328 (2000) 97.
[113] A.K. Motovilov, W. Sandhas, S.A. Sofianos, E.A. Kolganova, Binding energies and scattering observables in the $^4He_3$ atomic system, Eur. Phys. J. D 13 (2001) 33.

[114] W. Schöllkopf, J.P. Toennies, The nondestructive detection of the helium dimer and trimer, J. Chem. Phys. 104 (1996) 1155.
[115] T.K. Lim, Sister K. Duffy, W.C. Damert, Efimov state in the ^{4}He trimer, Phys. Rev. Lett. 38 (1977) 341.
[116] B.D. Esry, C.D. Lin, C.H. Greene, Adiabatic hyperspherical study of the helium trimer, Phys. Rev. A 54 (1996) 394.
[117] R.A. Aziz, V.P.S. Nain, J.S. Carley, W.L. Taylor, G.T. McConville, An accurate intermolecular potential for helium, J. Chem. Phys. 70 (1979) 4330.
[118] R.A. Aziz, F.R.W. McCourt, C.C.K. Wong, A new determination of the ground state interatomic potential for He_2, Mol. Phys. 61 (1987) 1487.
[119] R.A. Aziz, A.R. Janzen, M.R. Moldover, Ab initio calculations for helium: a standard for transport property measurements, Phys. Rev. Lett. 74 (1995) 1586.
[120] H. Suno, B.D. Esry, C.H. Greene, J.P. Burke Jr., Three-body recombination of cold helium atoms, Phys. Rev. A 65 (2002) 042725.
[121] B.D. Esry, H. Suno (unpublished).
[122] S.K. Adhikari, T. Frederico, I.D. Goldman, Perturbative renormalization in quantum few-body problems, Phys. Rev. Lett. 74 (1995) 487.
[123] S.K. Adhikari, T. Frederico, Renormalization group in potential scattering, Phys. Rev. Lett. 74 (1995) 4572.
[124] Th. Cornelius, W. Glöckle, Efimov states for three ^{4}He atoms?, J. Chem. Phys. 85 (1986) 3906.
[125] M.T. Yamashita, T. Frederico, A. Delfino, L. Tomio, Scaling limit of virtual states of triatomic systems, Phys. Rev. A 66 (2002) 052702.
[126] M.T. Yamashita, R.S. Marques de Carvalho, L. Tomio, T. Frederico, Scaling predictions of radii of weakly bound triatomic molecules, Phys. Rev. A 68 (2003) 012506 [arXiv:physics/0303031].
[127] M.T. Yamashita, T. Frederico, L. Tomio, A. Delfino, Weakly bound atomic trimers in ultracold traps, Phys. Rev. A 68 (2003) 033406 [arXiv:cond-mat/0206317].
[128] E. Nielsen, H. Suno, B.D. Esry, Efimov resonances in atom–diatom scattering, Phys. Rev. A 66 (2002) 012705.
[129] E. Braaten, H.-W. Hammer, Three-body recombination into deep bound states in a Bose gas with large scattering length, Phys. Rev. Lett. 87 (2001) 160407 [arXiv:cond-mat/0103331].
[130] E. Braaten, H.-W. Hammer, Enhanced dimer relaxation in an atomic and molecular BEC, Phys. Rev. A 70 (2004) 042706 [arXiv:cond-mat/0303249].
[131] G.P. Lepage, What is renormalization?, in: T. DeGrand, D. Toussaint (Eds.), From Actions to Answers (TASI-89), World Scientific, Singapore, 1989[arXiv:hep-ph/0506330].
[132] S. Weinberg, Phenomenological Lagrangians, Physica A 96 (1979) 327.
[133] J.F. Donoghue, E. Golowich, B.R. Holstein, Dynamics of the Standard Model, Cambridge University Press, Cambridge, 1992.
[134] H. Georgi, Effective field theory, Ann. Rev. Nucl. Part. Sci. 43 (1993) 209.
[135] D.B. Kaplan, Effective field theories, arXiv:nucl-th/9506035.
[136] A.V. Manohar, Effective field theories, arXiv:hep-ph/9606222.
[137] R. Shankar, Effective field theory in condensed matter physics, arXiv:cond-mat/9703210.
[138] E.C. Marino, Field theory and condensed matter: account of a successful interaction, Braz. J. Phys. 30 (2000) 230.
[139] J. Polchinski, Effective field theory and the Fermi surface, Lectures presented at TASI 1992, arXiv:hep-th/9210046.
[140] H. Leutwyler, Phonons as goldstone bosons, Helv. Phys. Acta 70 (1997) 275 [arXiv:hep-ph/9609466].
[141] C.P. Hofmann, Spin-wave scattering in the effective Lagrangian perspective, Phys. Rev. B 60 (1999) 388 [arXiv:cond-mat/9805277].
[142] H.-W. Hammer, R.J. Furnstahl, Effective field theory for dilute fermi systems, Nucl. Phys. A 678 (2000) 277 [arXiv:nucl-th/0004043].
[143] G.P. Lepage, How to renormalize the Schrödinger equation, in: J.C.A. Barata, A.P.C. Malbouisson, S.F. Novaes (Eds.), Particles and Fields, Proceedings of the Ninth J.A. Swieca Summer School, World Scientific, Singapore, 1998[arXiv:nucl-th/9706029].
[144] E. Tiesinga, C.S. Willimas, P.S. Julienne, K.M. Jones, P.D. Lett, W.D. Phillips, A spectroscopic determination of scattering lengths for sodium atom collisions, J. Res. Natl. Inst. Stand. Technol. 101 (1996) 505.
[145] E. Braaten, D. Phillips, The renormalization group limit cycle for the $1/r^2$ potential, Phys. Rev. A 70 (2004) 052111 [arXiv:hep-th/0403168].
[146] S.R. Beane, P.F. Bedaque, L. Childress, A. Kryjevski, J. McGuire, U. van Kolck, Singular potentials and limit cycles, Phys. Rev. A 64 (2001) 042103 [arXiv:quant-ph/0010073].
[147] M. Bawin, S.A. Coon, The singular inverse square potential, limit cycles and self-adjoint extensions, Phys. Rev. A 67 (2003) 042712 [arXiv:quant-ph/0302199].
[148] H.-W. Hammer, B.G. Swingle, On the limit cycle for the $1/r^2$ potential in momentum space, Ann. Phys. 321 (2006) 306 [arXiv:quant-ph/0503074].
[149] D.B. Kaplan, M.J. Savage, M.B. Wise, Two-nucleon systems from effective field theory, Nucl. Phys. B 534 (1998) 329 [arXiv:nucl-th/9802075].
[150] T. Mehen, I.W. Stewart, M.B. Wise, Conformal invariance for non-relativistic field theory, Phys. Lett. B 474 (2000) 145 [arXiv:hep-th/9910025].
[151] E. Braaten, A. Nieto, Renormalization effects in a dilute Bose gas, Phys. Rev. B 55 (1997) 8090 [arXiv:hep-th/9609047].
[152] S. Coleman, Aspects of Symmetry, Cambridge University Press, Cambridge, 1988.
[153] D.B. Kaplan, More effective field theory for nonrelativistic scattering, Nucl. Phys. B 494 (1997) 471 [arXiv:nucl-th/9610052].
[154] P.F. Bedaque, U. van Kolck, Nucleon deuteron scattering from an effective field theory, Phys. Lett. B 428 (1998) 221 [arXiv:nucl-th/9710073].
[155] V.V. Komarov, A.M. Popova, Break-up of a deuteron by a nucleon, Nucl. Phys. 54 (1964) 278.
[156] F. Gross, Three-dimensional covariant integral equations for low-energy systems, Phys. Rev. 186 (1969) 1448.
[157] V.F. Kharchenko, Solution of the Skornyakov–Ter-Martirosian equations for three nucleons with cutoff at large momenta, Sov. J. Nucl. Phys. 16 (1973) 173 [Yad. Fiz. 16 (1972) 310].
[158] G.S. Danilov, V.I. Lebedev, Calculation of the doublet neutron–deuteron scattering length in the theory of zero range forces, Sov. Phys. JETP 17 (1963) 1015 [J. Exptl. Theoret. Phys. (U.S.S.R.) 44 (1963) 1509].
[159] V. Efimov, Level spectrum of three resonantly interacting particles, Sov. Phys. JETP Lett. 16 (1972) 34 [ZhETF Pis. Red. 16 (1972) 50].
[160] V. Efimov, Energy levels of three resonantly-interacting particles, Nucl. Phys. A 210 (1973) 157.
[161] Yu.N. Ovchinnikov, I.M. Sigal, Number of bound states of three-body systems and Efimov's effect, Ann. Phys. 123 (1979) 274.

[162] A.C. Fonseca, E.F. Redish, P.E. Shanley, Efimov effect in an analytically solvable model, Nucl. Phys. A 320 (1979) 273.
[163] F.M. Pen'kov, Lifetime of Efimov states of negative two-atom ions, Phys. Rev. A 60 (1999) 3756.
[164] D.S. Petrov, Three-body problem in fermi gases with short-range interparticle interaction, Phys. Rev. A 67 (2003) 010703(R) [arXiv:cond-mat/0209246].
[165] D.S. Petrov, C. Salomon, G.V. Shlyapnikov, Weakly bound dimers of fermionic atoms, Phys. Rev. Lett. 93 (2004) 090404 [arXiv:cond-mat/0309010].
[166] D.S. Petrov, C. Salomon, G.V. Shlyapnikov, Scattering properties of weakly bound dimers of fermionic atoms, Phys. Rev. A 71 (2005) 012708 [arXiv:cond-mat/0407579].
[167] A. Bulgac, V. Efimov, Spin dependence of the level spectrum of three resonantly interacting particles, Sov. J. Nucl. Phys. 22 (1976) 153 [Yad. Fiz. 22 (1975) 296].
[168] E. Nielsen, A.S. Jensen, D.V. Fedorov, Progress report: structure and occurrence of three-body halos in two dimensions, Few Body Systems 27 (1999) 15.
[169] B.J. Verhaar, J.P.H.W. van der Eijnde, M.A.J. Voermans, M.M.J. Schaffrath, Scattering length and effective range in two dimensions: application to adsorbed hydrogen atoms, J. Phys. A: Math. Gen. 17 (1984) 595.
[170] L.W. Bruch, J.A. Tjon, Binding of three identical bosons in two dimensions, Phys. Rev. A 19 (1979) 425.
[171] H.-W. Hammer, D.T. Son, Universal properties of two-dimensional boson droplets, Phys. Rev. Lett. 93 (2004) 250408 [arXiv:cond-mat/0405206].
[172] L. Platter, H.-W. Hammer, U.-G. Meißner, Universal properties of the four-boson system in two dimensions, Few Body Systems 35 (2004) 169 [arXiv:cond-mat/0405660].
[173] V. Efimov, Qualitative treatment of three-nucleon properties, Nucl. Phys. A 362 (1981) 45 Erratum ibid. 378 (1982) 581(E).
[174] V. Efimov, Force range correction in the three-body problem: application to three nucleon systems, Phys. Rev. C 44 (1991) 2303.
[175] P.F. Bedaque, H.-W. Hammer, U. van Kolck, Effective theory for neutron–deuteron scattering: energy dependence, Phys. Rev. C 58 (1998) 641 [arXiv:nucl-th/9802057].
[176] P.F. Bedaque, H.-W. Hammer, U. van Kolck, Effective theory of the triton, Nucl. Phys. A 676 (2000) 357 [arXiv:nucl-th/9906032].
[177] E. Wigner, On the consequences of the symmetry of the nuclear Hamiltonian on the spectroscopy of nuclei, Phys. Rev. 51 (1937) 106.
[178] T. Mehen, I.W. Stewart, M.B. Wise, Wigner symmetry in the limit of large scattering lengths, Phys. Rev. Lett. 83 (1999) 931 [arXiv:hep-ph/9902370].
[179] A.C. Phillips, Consistency of the low-energy three-nucleon observables and the separable interaction model, Nucl. Phys. A 107 (1968) 209.
[180] P.F. Bedaque, H.W. Grießhammer, H.-W. Hammer, G. Rupak, Low energy expansion in the three body system to all orders and the triton channel, Nucl. Phys. A 714 (2003) 589 [arXiv:nucl-th/0207034].
[181] V. Efimov, E.G. Tkachenko, Explanation of the Phillips-line in the three-nucleon problem, Phys. Lett. 157B (1985) 108.
[182] V. Efimov, E.G. Tkachenko, The Phillips line and the structure of few-nucleon systems, Sov. J. Nucl. Phys. 47 (1988) 17 [Yad. Fiz. 47 (1988) 29].
[183] V. Efimov, E.G. Tkachenko, On the correlation between the triton binding energy and the neutron–deuteron doublet scattering length, Few-Body Syst. 4 (1988) 71.
[184] H.W. Grießhammer, Improved convergence in the three-nucleon system at very low energies, Nucl. Phys. A 744 (2004) 192 [arXiv:nucl-th/0404073].
[185] L. Tomio, A. Delfino, S.K. Adhikari, Trinucleon system in a two-body model: Coulomb effect on bound and scattering states, Phys. Rev. C 35 (1987) 441.
[186] S.K. Adhikari, T.K. Das, Effect of polarization potential in proton-deuteron scattering, Phys. Rev. C 37 (1988) 1376.
[187] L. Platter, H.-W. Hammer, Universality in the triton charge form factor, Nucl. Phys. A 766 (2006) 132 [arXiv:nucl-th/0509045].
[188] S.R. Beane, P.F. Bedaque, M.J. Savage, U. van Kolck, Towards a perturbative theory of nuclear forces, Nucl. Phys. A 700 (2002) 377 [arXiv:nucl-th/0104030].
[189] S.R. Beane, M.J. Savage, Variation of fundamental couplings and nuclear forces, Nucl. Phys. A 713 (2003) 148 [arXiv:hep-ph/0206113].
[190] S.R. Beane, M.J. Savage, The quark mass dependence of two-nucleon systems, Nucl. Phys. A 717 (2003) 91 [arXiv:nucl-th/0208021].
[191] E. Epelbaum, U.-G. Meißner, W. Glöckle, Nuclear forces in the chiral limit, Nucl. Phys. A 714 (2003) 535 [arXiv:nucl-th/0207089].
[192] M.C. Birse, Renormalisation-group analysis of repulsive three-body systems, arXiv:nucl-th/0509031.
[193] F. Gabbiani, P.F. Bedaque, H.W. Grießhammer, Higher partial waves in an effective field theory approach to n d scattering, Nucl. Phys. A 675 (2000) 601 [arXiv:nucl-th/9911034].
[194] U.-G. Meißner, Modern theory of nuclear forces, Nucl. Phys. A 751 (2005) 149 [arXiv:nucl-th/0409028].
[195] D.R. Phillips, Building light nuclei from neutrons, protons, and pions, Czech. J. Phys. 52 (2002) B49 [arXiv:nucl-th/0203040].
[196] K. Riisager, Nuclear halo states, Rev. Mod. Phys. 66 (1994) 1105.
[197] S.M. Austin, G.F. Bertsch, Halo nuclei, Scientific American 272 (1995) 90.
[198] M.V. Zhukov, B.V. Danilin, D.V. Fedorov, J.M. Bang, I.J. Thompson, J.S. Vaagen, Bound state properties of Borromean halo nuclei: ^{6}He and ^{11}Li, Phys. Rep. 231 (1993) 151.
[199] A.S. Jensen, K. Riisager, D.V. Fedorov, E. Garrido, Structure and reactions of quantum halos, Rev. Mod. Phys. 76 (2004) 215.
[200] G.F. Bertsch, H. Esbensen, Pair correlations near the neutron drip line, Ann. Phys. 209 (1991) 327.
[201] H. Esbensen, G.F. Bertsch, K. Hencken, Application of contact interactions to Borromean halos, Phys. Rev. C 56 (1997) 3054.
[202] A.E.A. Amorim, T. Frederico, L. Tomio, Universal aspects of Efimov states and light halo nuclei, Phys. Rev. C 56 (1997) R2378 [arXiv:nucl-th/9708023].
[203] A. Delfino, T. Frederico, M.S. Hussein, L. Tomio, Virtual states of light non-Borromean halo nuclei, Phys. Rev. C 61 (2000) 051301.
[204] C.A. Bertulani, H.-W. Hammer, U. van Kolck, Effective field theory for halo nuclei: shallow P-wave states, Nucl. Phys. A 712 (2002) 37 [arXiv:nucl-th/0205063].

[205] P.F. Bedaque, H.-W. Hammer, U. van Kolck, Narrow resonances in effective field theory, Phys. Lett. B 569 (2003) 159 [arXiv:nucl-th/0304007].
[206] D.V. Federov, A.S. Jensen, K. Riisager, Efimov states in halo nuclei, Phys. Rev. Lett. 73 (1994) 2817 [arXiv:nucl-th/9409018].
[207] M. Juric, et al., A new determination of the binding-energy values of the light hypernuclei ($15 \geqslant$ A), Nucl. Phys. B 52 (1973) 1.
[208] D.H. Davis, A brief review of emulsion results on hypernuclei, in: LAMPF Workshop on (π, K) Physics, AIP Conf. Proc. 224 (1991) 38.
[209] A. Cobis, A.S. Jensen, D.V. Fedorov, Three-body halos. V. The structure of the hypertriton, J. Phys. G 23 (1997) 401 [arXiv:nucl-th/9608026].
[210] D.V. Fedorov, A.S. Jensen, Regularized zero-range model and an application to the triton and the hypertriton, Nucl. Phys. A 697 (2002) 783 [arXiv:nucl-th/0107027].
[211] J.G. Congleton, A simple model of the hypertriton, J. Phys. G 18 (1992) 339.
[212] H.-W. Hammer, The hypertriton in effective field theory, Nucl. Phys. A 705 (2002) 173 [arXiv:nucl-th/0110031].
[213] R.D. Amado, F.C. Greenwood, There is no Efimov effect for four or more particles, Phys. Rev. D 7 (1973) 2517.
[214] S.K. Adhikari, A.C. Fonseca, Four-body Efimov effect in a Born–Oppenheimer model, Phys. Rev. D 24 (1981) 416.
[215] O.A. Yakubovsky, On the integral equations in the theory of N particle scattering, Sov. J. Nucl. Phys. 5 (1967) 937 [Yad. Fiz. 5 (1967) 1312].
[216] P. Grassberger, W. Sandhas, Systematical treatment of the non-relativistic N-particle problem, Nucl. Phys. B 2 (1967) 181.
[217] A. Nogga, H. Kamada, W. Glöckle, Modern nuclear force predictions for the alpha particle, Phys. Rev. Lett. 85 (2000) 944 [arXiv:nucl-th/0004023].
[218] E. Epelbaum, A. Nogga, W. Glöckle, H. Kamada, U.-G. Meißner, H. Witala, Few nucleon systems with two-nucleon forces from chiral effective field theory, Eur. Phys. J. A 15 (2002) 543 [arXiv:nucl-th/0201064].
[219] S.C. Pieper, R.B. Wiringa, Quantum Monte Carlo calculations of light nuclei, Ann. Rev. Nucl. Part. Sci. 51 (2001) 53 [arXiv:nucl-th/0103005].
[220] S.C. Pieper, K. Varga, R.B. Wiringa, Quantum Monte Carlo calculations of $A = 9$, 10 nuclei, Phys. Rev. C 66 (2002) 044310 [arXiv:nucl-th/0206061].
[221] P. Navratil, W.E. Ormand, Ab initio shell model with a genuine three-nucleon force for the p-shell nuclei, Phys. Rev. C 68 (2003) 034305 [arXiv:nucl-th/0305090].
[222] M. Lewerenz, Structure and energetics of small helium clusters: quantum simulations using a recent perturbational pair potential, J. Chem. Phys. 106 (1997) 4596.
[223] D. Blume, C.H. Greene, Monte Carlo hyperspherical description of helium cluster excited states, J. Chem. Phys. 112 (2000) 8053.
[224] G.P. Lepage, unpublished
[225] J.A. Tjon, Bound states of ^{4}He with local interactions, Phys. Lett. B 56 (1975) 217.
[226] L. Platter, H.-W. Hammer, U.-G. Meißner, The four-boson system with short-range interactions, Phys. Rev. A 70 (2004) 052101 [arXiv:cond-mat/0404313].
[227] S. Nakaichi-Maeda, T.K. Lim, Zero-energy scattering and bound states in the ^{4}He trimer and tetramer, Phys. Rev. A 28 (1983) 692.
[228] L. Platter, H.-W. Hammer, U.-G. Meißner, On the correlation between the binding energies of the triton and the alpha-particle, Phys. Lett. B 607 (2005) 254 [arXiv:nucl-th/0409040].
[229] E. Epelbaum, A. Nogga, W. Glöckle, H. Kamada, U.-G. Meißner, H. Witala, Three-nucleon forces from chiral effective field theory, Phys. Rev. C 66 (2002) 064001 [arXiv:nucl-th/0208023].
[230] A. Bulgac, P.F. Bedaque, A.C. Fonseca, A dilute atomic Fermi system with a large positive scattering length, arXiv:cond-mat/0306302.
[231] D.R. Phillips, G. Rupak, M.J. Savage, Improving the convergence of NN effective field theory, Phys. Lett. B 473 (2000) 209 [arXiv:nucl-th/9908054].
[232] H.-W. Hammer, T. Mehen, Range corrections to doublet S-wave neutron–deuteron scattering, Phys. Lett. B 516 (2001) 353 [arXiv:nucl-th/0105072].
[233] I.R. Afnan, D.R. Phillips, The three-body problem with short-range forces: renormalized equations and regulator-independent results, Phys. Rev. C 69 (2004) 034010 [arXiv:nucl-th/0312021].
[234] V. Efimov, Effective interaction of three resonantly interacting particles and the force range, Phys. Rev. C 47 (1993) 1876.
[235] H. Suno, B.D. Esry, C.H. Greene, Recombination of three ultracold fermionic atoms, Phys. Rev. Lett. 90 (2003) 053202 [arXiv:physics/0209092].
[236] S.J.J.M.F. Kokkelmans, J.N. Milstein, M.L. Chiofalo, R. Walser, M.J. Holland, Resonance superfluidity: renormalization of resonance scattering theory, Phys. Rev. A 65 (2002) 053617 [arXiv:cond-mat/0112283].
[237] D.S. Petrov, Three-boson problem near a narrow Feshbach resonance, Phys. Rev. Lett. 93 (2004) 143201 [arXiv:cond-mat/0404036].